The *in vitro* Analysis of Metal Binding and Transfer by the Copper Metallochaperone for Cu/Zn-Superoxide Dismutase

Stephen Joseph Allen

A Thesis Submitted for the Degree of Doctor of Philosophy

September 2011

Institute for Cell and Molecular Biosciences

Newcastle University

<u>Declaration</u>

I certify that this thesis contains my own work, except where acknowledged, and that no part of this work has been submitted in support of an application for other qualifications at this or any other institution.

<u>Acknowledgements</u>

I would like to thank Prof. Christopher Dennison for his supervision and support throughout my time at Newcastle University and for providing me with the opportunity to perform this research. I would also like to thank all of the lab members, both past and present, for much assistance and encouragement. In particular thanks go to Dr. Adriana Badarau for allowing me to use her data in this thesis, providing the protein HAH1 and for her invaluable advice given in many helpful discussions. Thanks also go to Dr Katsuko Sato, Dr. Abdelnasser El Ghazouani, Dorota Kostrz and Shilpa Aggarwal for their help and encouragement. In addition, I would like to thank Andrew Thompson for his work on preliminary studies of the protein Ccs1.

I would like to thank Dr. Susan Firbank and Dr. Arnaud Basle for data collection and processing for the D1-CCS crystal structure. Thanks also to Dr. Joe Gray and Bob Liddell (Pinnacle) for analysis of proteins by mass spectrometry. I would also like to thank Prof. Nigel Robinson, Prof. Jeremy Lakey and Dr. Kevin Waldron for their help and advice over the years.

I would also like to thank the many people I have met during my time at the university that are too numerous to list here, but who have made many contributions in their own way to help me make it to the end of the project.

Last, but not least, I would like to thank my parents, my grandparents, my brother and my sister for their encouragement, support and love that has provided me with much motivation. I especially thank my parents for being there for me when I most needed them, for that I cannot thank them enough.

Abstract

The human copper metallochaperone CCS activates Cu,Zn-superoxide dismutase (SOD1) through copper transfer and formation of an intramolecular disulfide. CCS is a three domain protein with CXXC and CXC Cu(I)-binding motifs in domains 1 and 3, respectively. A detailed analysis of copper binding to CCS and variants in which the Cys residues of the CXXC and CXC motifs in domains 1 and 3, respectively, have been mutated to Ser, and also domain 1 and 3 constructs, using the chromophoric Cu(I) ligands bathocuproine disulfonate and bicinchoninic acid has been performed. Competition experiments demonstrate that CCS is able to bind a single equivalent of Cu(I) independently in both domains 1 and 3. The Cu(I) affinity of domain 1 is approximately 5 $\times 10^{17}$ M^{-1} at pH 7.5 while that of domain 3 is at least an order of magnitude weaker. The order of magnitude difference between the Cu(I) affinities of domains 1 and 3, is maintained over the pH range ~6 to 9 and therefore, at physiological pH, in the cell cytosol, where copper is limiting, the CXXC site will be preferentially occupied with Cu(I). Under such conditions the transfer of Cu(I) from domain 1 to the buried active site of SOD1 must be facilitated by the structurally flexible domain 3.

The mutation of Arg71, located on loop 5 of domain 1, to Ala results in an altered pH dependence of the Cu(I) affinity for the CXXC motif due to an increase in the pK_a of the Cu(I)-binding C-terminal Cys (Cys$_C$) residue. Therefore, lowering of the Cys$_C$ pK_a through a hydrogen bond with the Arg71 side chain that stabilises the Cys$_C$ thiolate in domain 1, observed in the crystal structure of Cu(I)-bound domain 1, modulates the nucleophilicity, and hence Cu(I)-binding affinity of this residue. In addition, high and low pK_a's for the domain 3 CXC motif Cys residues were also determined from the pH dependence of the Cu(I) affinity for this site. The relative nucleophilicities of the domain 1 and domain 3 Cu(I)-binding Cys residues, inferred from their pK_a's, suggest copper transfer from domain 1 to domain 3 is kinetically favoured. In addition, Zn(II) binding to the largest central domain of CCS was investigated to determine its role in affecting the quaternary structure of the protein. Zn(II)–binding to domain 2 was found to stabilise the dimeric form of the protein and also the CCS:SOD1 heterocomplex which orientates the Cu(I)-binding domains 1 and 3 of CCS for activation of SOD1.

Units and Abbreviations

Measurements and Techniques

M	mol dm^{-3}	OD	optical density
l	litre	A	absorbance
g	gram	λ	wavelength
μ	micro	ppm	parts per million
m	milli	nm	nanometre
^{o}C	degrees celsius	Da	Dalton
V	Volt		

ε	extinction coefficient (M^{-1} cm^{-1})
rcf	relative centrifugal force
MW	molecular weight
MWCO	molecular weight cut off
SDS-PAGE	sodium dodecyl sulphate polyacrylamide gel electrophoresis
CD	circular dichroism
UV/Vis	ultraviolet/visible
PCR	polymerase chain reaction
AAS	atomic absorption spectroscopy
MS	mass spectrometry
MALDI	matrix assisted laser desorption ionisation
TOF	time of flight
FT	fourier transform
ICR	ion cyclotron resonance

Selected Chemicals

Tris	tris(hydroxymethyl)aminoethane
Mes	2-(N-morpholino)ethanesulphonic acid
Hepes	4-(2-Hydroxyethyl)piperazine-1-ethanesulfonic acid
Taps	N-Tris(hydroxymethyl)methyl-3-aminopropanesulfonic acid
Ches	2-(Cyclohexylamino)ethanesulfonic acid
Caps	3-(cyclohexylamino)-1-propanesulfonic acid
EDTA	ethylenediaminetetraacetic acid

Units and Abbreviations (Continued)

DTT   dithiothreitol

BCS   bathocuproine disulfonic acid

BCA   bicinchoninic acid

DTNB   5,5'-dithiobis-(2-nitrobenzoic acid) (Ellman's reagent)

Selected Proteins

CCS	copper metallochaperone for Cu,Zn-superoxide dismutase
WT-CCS	wild-type CCS from *H.sapiens*
C22S/C25S-CCS	Cys to Ser CCS mutant
C244S/C246S-CCS	Cys to Ser CCS mutant
D1-CCS	CCS N-terminal domain (CCS amino acid residues 1-79)
D3-CCS	CCS C-terminal peptide (CCS amino acid residues 235-274)
SOD1	Cu,Zn-superoxide dismutase from *H.sapiens*
Ccs1	CCS from *S.cerevisae*
BACE1-CTD	β-secretase C-terminal domain (amino acid residues 478-501)
HAH1	Atx1 copper metallochaperone from *H.sapiens*

Amino Acids and Nucleic Acids

Alanine	Ala	A	Methionine	Met	M
Cysteine	Cys	C	Asparagine	Asn	N
Aspartic acid	Asp	D	Proline	Pro	P
Glutamic acid	Glu	E	Glutamine	Gln	Q
Phenylalanine	Phe	F	Arginine	Arg	R
Glycine	Gly	G	Serine	Ser	S
Histidine	His	H	Threonine	Thr	T
Isoleucine	Ile	I	Valine	Val	V
Lysine	Lys	K	Tryptophan	Trp	W
Leucine	Leu	L	Tyrosine	Tyr	Y

Adenine	a	Guanine	g
Cytosine	c	Thymine	t

Contents

Chapter 1

Introduction

1.1 Introduction

Metal ions are involved in a wide variety of roles in biological systems ranging from generating the transmembrane potential of the cell to catalyzing the disproportionation of superoxide radicals.(*1-3*) The metal copper is of particular importance and is an essential cofactor for a variety of proteins, especially in those which are involved in electron transfer, oxidoreductases activity and antioxidant defense.(*4*) Despite the usefulness of copper to organisms, however, its strict homeostasis is required in order to avoid the potential toxicity of the metal which is particularly evident when it is present at high cellular concentrations.(*5*) This has resulted in the reduction of the availability copper within the cell cytosol and therefore mechanisms for the uptake, delivery and incorporation of the metal into the copper requiring proteins are present.(*6-15*)

1.1.1 Copper Coordination Chemistry and Metalloproteins

Copper is a first row transition metal and in its ground state has an electronic valence shell composition of $4s^1\ 3d^{10}$.(*16*) It is one of the only first row metals to exhibit a stable 1+ oxidation state which occurs through the loss of the electron residing in the 4s orbital. However, in aqueous solutions, Cu(I) is unstable and quickly disproportionates to Cu(0) and Cu(II). The disproportionation reaction is fast but is slower in the absence of O_2. Cu(I) and Cu(II) form a variety of coordination complexes. Cu(I) is a soft lewis acid and prefers soft bases as ligands such as those containing sulfur donor atoms that are found in the amino acids Cys and Met. The co-ordination geometries formed by this oxidation state are predominantly tetrahedral and trigonal planar complexes.(*17*) On the other hand Cu(I), formed from the loss of an electron in a 3d orbital, is a hard lewis acid and as a result prefers hard bases as ligands such as those containing nitrogen and oxygen donor atoms such as those found in His and the carboxylate based amino acids Asp and Glu. Cu(II) complexes prefer mainly tetragonal co-ordination environments that include geometries such as square planar and axially elongated octahedral.(*17*) An axially elongated octahedron is favoured over that of a perfect octahedral geometry for the d^9 configuration of Cu(II) due to the incomplete filling of degenerate orbitals in the latter causing instability. The instability is overcome through Jahn-Teller distortions that remove the orbital degeneracy through a reduction in symmetry by forming an axially distorted octahedron.(*1*)

Copper plays a role in proteins usually as an active centre in those with functions including oxidase and oxygenase activities, electron transfer and superoxide dismutation.(*1*) The use of copper mainly relates to its redox chemistry due to the interconversion between Cu(I) (*cuprous*) and Cu(II) (*cupric*) being suitable for essential redox processes and the ability of the amino acid ligands to fine tune the relative stabilities of the two oxidation states.(*1-3,18*) The copper binding centres commonly found in metalloproteins exist as one of three main types that were originally based on their spectral properties.(*1*) The characteristics of the Type 1 to 3 copper binding sites are as follows;

Type 1

Type 1 sites consist of a copper coordinated trigonally by two His and a Cys through nitrogen and sulfur donor atoms respectively. They are characterised by an intense absorption band at 600 nm resulting from a ligand to metal charge transition (LMCT) from the bound cysteine. They exhibit an EPR spectrum as a result of an unpaired electron that is also very distinct due to a decreased hyperfine splitting compared to that of normal Cu(II) centres. Plastocyanin is an example of a protein that contains a type 1 copper site.(*19*)

Type 2

In Type 2 metal centres the copper is coordinated by mainly His residues with a square planar or pyramidal geometry. This centre also exhibits an EPR spectrum that is very different to the Type 1 centre but which is typical of Cu(II) co-ordination compounds. The copper bound to four His residues in Cu/Zn-superoxide dismutase is an example of this type of copper centre.(*20*)

Type 3

Type 3 sites consist of two copper centres which are each bound to three His residues which are antiferromagnetically coupled, and so compared to the first two types of copper centres exhibit no observable EPR spectrum. These metal centres are found in multi-copper oxidases such as ceruloplasmin that is important in iron uptake in cells through catalysis of the formation of Fe(III) from Fe(II) allowing its uptake by transporters bound within the plasma membrane.(*21*)

Other copper binding sites, which cannot be classified as Type 1,2 or 3 also exist. These include the Cu_A centre in cytochrome c oxidase (CcO) and the Cu_Z centre of nitrous oxide reductase.(*2,3*) Furthermore, the copper-binding proteins that participate in metal trafficking within the cell, discussed in the remainder of this chapter, have copper-binding sites that cannot be classified into any of the above metal centre categories.(*6-15*) One feature in common to all copper binding sites, however, is that they appear to have evolved to tune the metals chemical properties, through selection of ligating residues and co-ordination geometry allowing for the reactivity of the bound copper to be highly tuned.(*1*) For example, the reduction potentials for Type 1,2 and 3 copper containing proteins covers a wide range. The reduction potential (E_m) of the Type 1 site in plastocyanin has been measured at 370 mV while other Type 1 proteins including nitrosocyanin and rusticyanin have E_m values covering the range ~90-670 mV.(*22,23*) The Type 2 copper site of Cu,Zn-superoxide dismutase has reported E_m values between 200-400 mV, while tyrosinase that contains a Type 3 copper centre has a reported E_m value of 360 mV.(*24-26*) The large range of E_m values for the copper containing proteins resulting from the combined effect of the ligand set, coordination geometry and surrounding protein scaffold on the Cu(II)/Cu(I) redox couple.(*17,22*)

1.1.2   Copper Toxicity

The very same reasons that make copper so useful to living organisms also make it potentially dangerous. Copper in living cells has the ability to both bind adventitiously to biomolecules, causing damaging structural perturbations and preventing the correct metal cofactors binding to proteins, and mediates increased production of harmful free radical species such as superoxide which oxidise biomolecules including proteins, lipids and nucleic acids.(*27-30*) Reactions leading to the production of free radicals involve the metal shuttling between its oxidation states of 1+ and 2+ through Fenton and Haber-Weiss reactions.(*29,31*) For example reactions like those shown in equations (1.1-1.3) are possible.(*30*)

$$Cu(II) + O_2^{\cdot -} \rightleftharpoons Cu(I) + O_2 \qquad\qquad (1.1)$$

$$Cu(I) + H_2O_2 \rightleftharpoons Cu(II) + OH^- + OH^{\cdot} \quad \text{(Fenton reaction)} \qquad (1.2)$$

$$O_2^{\cdot -} + H_2O_2 \rightleftharpoons O_2 + OH^- + OH^{\cdot} \quad \text{(Haber-Weiss reaction)} \qquad (1.3)$$
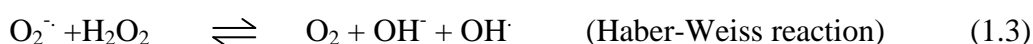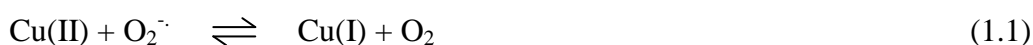
Chronic oxidative damage caused by these harmful free radicals usually results in carcinogenesis, aging and neurological disorders.(*31*) This potential for toxicity is highlighted by Wilson's disease which is characterised by copper accumulation to levels that cause damage to critical organs such as the liver and brain that is so severe that it is eventually fatal unless treated.(*32*) Therefore tight control over copper homeostasis is required so that in particular excess copper within the cell does not accumulate. Indeed, it has been discovered that the levels of 'free' copper, that is copper uncomplexed by proteins and other biomolecules, within the cytosol is extremely limited.(*6*) This high chelation capacity of the cytosol, through Cu(I) binding to glutathione (Cys containing tripeptide) and the metallothioneins (Cys rich proteins), aids in reducing the potential for copper toxicity.(*32*)

1.1.3   Mechanisms for the Specific Metallation of Proteins

A result of the low availability of 'free' copper within the eukaryotic cytosol means that mechanisms for loading the copper metalloproteins with the correct metal cofactor are required.(*6*) In general it could be thought that the specificity of a metal-binding site within a protein scaffold is determined by the availability and coordination geometry of suitable set of amino acid side chains that would have the highest metal affinity (K_b), equation (1.4), for a particular metal.(*33*)

$$K_b = \frac{[MP]}{[M] \times [P]}$$
(1.4)

Where, in equation 1.4, [M], [P] and [MP] are the concentrations of the metal, the apo-protein and metallated protein respectively. The Irving-Williams series (shown below) that refers to the relative stabilities of complexes formed by the first row divalent transition metals, however, shows that this strategy for metalloprotein metallation cannot be the primary means for metal selectivity.(*34,35*)

$$Mn(II) < Fe(II) < Co(II) < Ni(II) < Cu(II) > Zn(II)$$
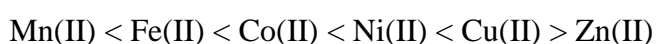
Going along the first row of the transition metals the stability constant for complex formation increases and peaks for Cu(II). This trend is found to hold irrespective of the

nature of the co-ordinating ligands and also the number of the ligands involved. Furthermore, Cu(I), which predominates in the reducing environment of the cytosol, is also highly competitive and positioned to the right of the Irving-William series together with Cu(II) and Zn(II).(*2,6*) It has been shown that a combination of covalent and electrostatic contributions to metal-ligand binding results in this observed series of complex stabilities for the divalent metals.(*36*) The ligand set and co-ordination geometry alone of proteins is therefore insufficient to achieve specific metallation when an abundance of different metals are present.(*37*)

To achieve specific metallation of proteins cells use one of two currently known mechanisms. The first takes advantage of the compartmentalisation of the cell. For example, in *Synechocystis*, the manganese and copper containing metalloproteins MncA and CucA, respectively, contain ligand sets, three His and one Glu, that populate preferentially with copper *in vitro*.(*37*) *In vivo*, however, they populate with their native metals. This was found to result from their folding in different compartments of the cell. MncA depends on incorporation of manganese in the cytosol where both copper and zinc are limiting, whereas CucA is metallated in the periplasm where copper is more available.(*37*) The secondary means for protein metallation, in contrast, involves the use of cellular components that direct or traffic the distribution of the required metal to the place of protein synthesis.(*10-13*) This mechanism is of particular importance for cellular targets for copper metallation in the eukaryotic cytosol where copper is limited.(*6*) Copper, as Cu(I), is transported to the copper requiring targets by soluble cytoplasmic proteins that shuttle the copper from the cell membrane.(*10-13*) These Cu(I)-binding proteins have been termed the copper metallochaperones and play a crucial role in the trafficking of copper within the cell.

1.1.4 Cellular Copper Trafficking

Intracellular copper trafficking is achieved mainly through a combination of the actions of membrane bound transporters and copper metallochaperones.(*10,12,13*) A simplified picture of the three major copper trafficking routes that are present a eukaryotic cell is shown in Figure 1.1. Copper is acquired from the extracellular environment by members of the copper transporter (Ctr) family.(*38,39*) These transporters bind and translocate copper across the plasma membrane of the cell. Once inside the cell the copper is then transferred to the copper metallochaperones which bind the metal in the Cu(I) state and transport it to specific cellular destinations.(*13*) In the first route the Atx1 class of

metallochaperones deliver Cu(I) to membrane-bound copper-transporting ATPases of the Golgi compartment.(*13*) In *S. cerevisiae* Atx1 transports copper to the copper-transporting ATPase Ccc2 for metallation of copper requiring proteins in the Golgi.(*40*) In humans the Atx1 homologue is HAH1 and this metallochaperone transports Cu(I) to the copper-transporting ATPases ATP7A and ATP7B for Cu(I) import to the Golgi compartment and also the secretory vesicles.(*41*) In the second route the copper chaperone for superoxide dismutase (CCS in humans and Ccs1 in *S. cerevisiae*) transports Cu(I) to the copper requiring protein Cu,Zn-superoxide dismutase (SOD1 in *H. Sapiens* and Sod1 in *S. cerevisiae*), an enzyme involved in intracellular antioxidant defence.(*42,43*) Although generally not considered a metallochaperone, as discussed in section 1.5, Cox17 is a soluble Cu(I)-binding protein that mediates delivery of the metal within the mitochondria for loading into C*c*O and is included here due to the importance of this copper trafficking route.(*44*)

Figure 1.1

The main copper trafficking pathways in a typical eukaryotic cell. The Ctr1 transporter transports across the cell membrane into the cell cytoplasm. The copper metallochaperones CCS and Atx1 then transport Cu(I) to copper requiring cellular targets SOD1, a mainly cytosolic antioxidant enzyme, and the copper-transporting ATPases (ATP7A and ATP7B), respectively. Cox17 is a small soluble protein implicated in the metallation of C*c*O.
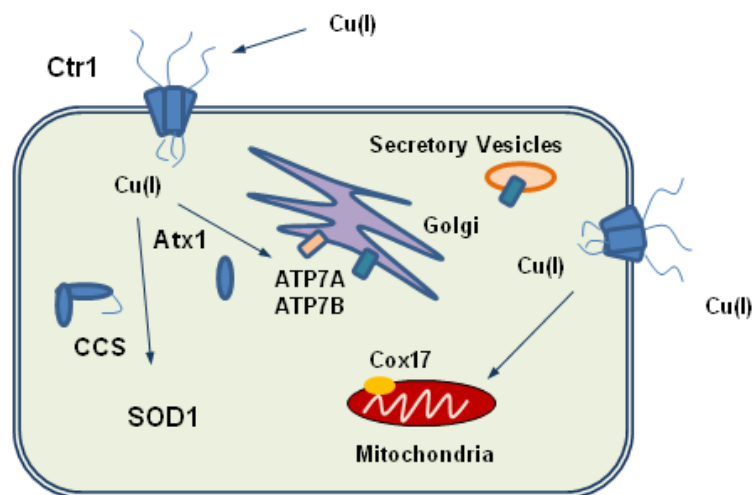
1.2   The Ctr Copper Transporters

The Ctr copper transporters are currently the only known major copper importing system in eukaryotic organisms.(*7-9*) Ctr transporters were originally identified in *S. cerevisiae*

(*45-46*) and subsequently homologues were found in humans.(*47*) Of the transporters Ctr1 and Ctr2 identified in humans only Ctr1 has been shown to be involved in cellular copper uptake.(*48*) Ctr1 is plasma cell membrane localised and has a domain structure consisting of three transmembrane domains and N-terminal extracellular and C-terminal intracellular extensions (Figure 1.2).(*49-51*)

Figure 1.2

Schematic showing the domain structure of mammalian Ctr1.
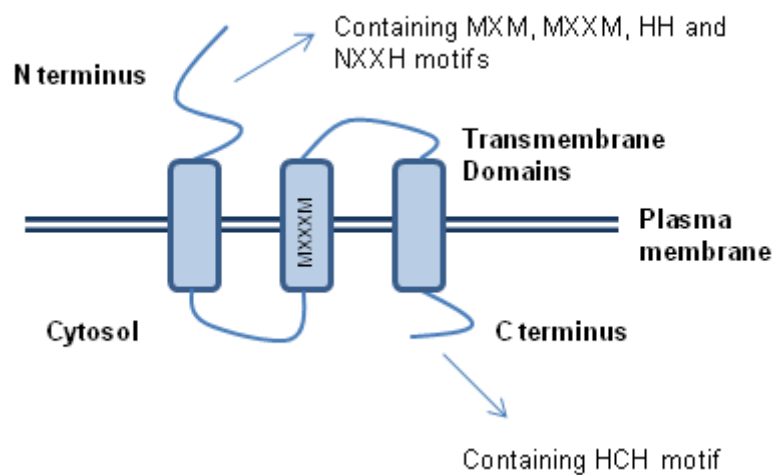
Three monomers of Ctr1 form a trimeric complex which has been found to a requirement for functioning of the transporter.(*51*) Methionine rich motifs (MXM and MXXM) in the extracellular N-terminus and a MX_3M motif located on trans-membrane helix 2 are implicated in the uptake and transport of copper by the transporter.(*52,53*) The C-terminal region also contains metal binding residues including an HCH motif.(*53*) Although the Cys residue of human Ctr1 is not required for functioning of the transporter the *S. cerevisiae* homologue contains numerous Cys residues that are implicated in homeostatic responses of the transporter to intracellular copper levels.(*54*) The structures of the transporter complex have provided insights into the mechanism of copper transport. The structures show a pore like structure through which the copper ions are thought to traverse the plasma membrane.(*49,50*) In addition, the transmembrane helix 2 which contains the MX_3M Cu(I)-binding motif lines the interior of the pore.(*49*) This together with extended X-ray absorption fine structure (EXAFS) spectroscopy which indicates the presence of two Cu(I)-binding sites involving sulphur ligand donors suggests copper transfer through Cu(I) exchange between the metal binding sites of the N-terminal and transmembrane regions.(*50*)

A metalloreductase for reduction of extracellular Cu(II) to Cu(I) for uptake by the Ctr1 transporter in *S. cerevisiae* is required although it is unknown whether this is also a requirement for the human transporter.(*54*) In either case it is likely that copper transport through the Ctr transporters is a passive process as metabolic inhibitors have no effect on their functioning.(*55*) Although the Cys residue of the C-terminal domain of human Ctr1 is not required it has been shown that Cu(I) transfer between this domain of the transporter (*S. cerevisiae*) and Atx1 is possible *in vitro*.(*56*) The Ctr1 transporters are currently considered the entry point for copper uptake into the cell cytoplasm although it is unknown how the metallochaperones acquire Cu(I) from the these transporters.(*38*)

1.3   Copper Delivery to the Secretory Pathway

Copper delivery to the secretory pathway is by the Atx1 family of metallochaperones.(*15*) The first copper chaperone to be isolated was Atx1 from *S. cerevisiae*.(*40*) The protein so called due to the initial functioning of the protein thought to be involved in oxygen sensitivity responses in cells lacking superoxide dismutase through an antioxidant-like behaviour.(*40*) Around the same time a homologue was also discovered in the bacterium *E. hirae* and designated CopZ and subsequently also in humans (HAH1) and a range of other organisms.(*31,57,15*) The proteins are soluble, cytoplasmic, Cu(I)-binding species that deliver copper to the copper-transporting ATPases that transport copper into the Golgi compartment, for subsequent metallation of secreted proteins, and secretory vesicles.(*10,13,15,40*) The importance of the pathway is highlighted by the effects of disruption to this system. For example, yeast deficient in Atx1 display impaired iron uptake due to the inability to load Fet3 with copper in the Golgi vesicles.(*58*) Fet3 is a copper containing metalloreductase protein involved in iron uptake by the cell. Without Atx1 the supply of copper in the Golgi is restricted resulting in a failure to complement the secreted protein with the copper cofactor.(*58*) In humans disruptions to this pathway can be severe for health with mutations of the genes for ATP7A and ATP7B resulting in Menkes syndrome and Wilson's disease respectively.(*59,60,61*) Menkes syndrome results from a copper deficiency while Wilson's disease is associated with copper accumulation as described earlier.(*61*)

1.3.1 The Atx1 Metallochaperones

Most homologues of Atx1 metallochaperones are relatively small proteins with Atx1 and HAH1 being 73 and 68 amino acids in length, respectively.(*40,41*) The Atx1 metallochaperones contain a conserved CXXC motif which, in most cases, binds a single equivalent of Cu(I) with exceptionally high affinity (typically ~ 10^{17} M^{-1}).(*62-65*) A significant amount of research has been directed towards characterising the Atx1 proteins in order to determine the nature of Cu(I)-binding and transfer to the copper-transporting ATPases.

Details of the protein fold of Atx1 (*S. cerevisiae*) were first reported with the acquisition of the crystal structures for apo and Hg(II)-bound proteins.(*66*) The structures show the overall fold of Atx1 to consist of a βαββαβ fold with the CXXC Cu(I)-binding motif located on a surface exposed loop region between α1 and β1. The Cys residues (Cys15 and Cys18) of the CXXC motif are involved in coordination to Hg(II) in the Hg(II)-Atx1 structure through coordination in a near linear digonal coordination geometry. For the apo-Atx1 oxidised (Cys15-Cys18) structure the overall fold is almost identical but there are distortions to the metal binding loop region caused by the disulfide between the two Cys residues of the CXXC motif that result in displacement of the residues between and immediately adjacent Cys15. In both of the above structures it was found that residues in close proximity of the metal-binding site included Thr14 and Lys65 may be involved in interacting with the metal binding site. More revealing, however, are the NMR solution structures for apo reduced and Cu(I)-bound Atx1 (Figure 1.3).(*67*) Both structures reveal the same overall fold of the protein but demonstrate the digonal binding of Cu(I) to the Cys residues of the CXXC motif orders this region of the protein relative to the apo form with only minor changes to the remainder of the protein fold.(*67*) Subsequent studies of the Cu(I) coordination in Atx1 by extended x-ray absorption fine structure spectroscopy (EXAFS) indicate that the metal is coordinated trigonally by three S atoms, two of these being from the Cys residues of the CXXC motif, and a third from a yet unidentified source but which is most likely an exogenous thiol from a small thiol containing molecule or neighbouring protein.(*40*)

Overall the structures for Atx1 highlighted the conformational flexibility of the protein and the possible involvement of residues (specifically Thr14 and Lys65) in Cu(I)-binding through interactions that balance the negative charge generated by metal-binding.(*66,67*)

Figure 1.3

Solution structures for Apo (A) and Cu(I)-bound Atx1 (B) (PDB accession codes 1FES and 1FD8, respectively) drawn in Pymol. The Cys residues of the CXXC motifs and Lys65 of loop 5 are shown as stick representations and the copper ion in Cu(I)-Atx1 is shown as a gold sphere.
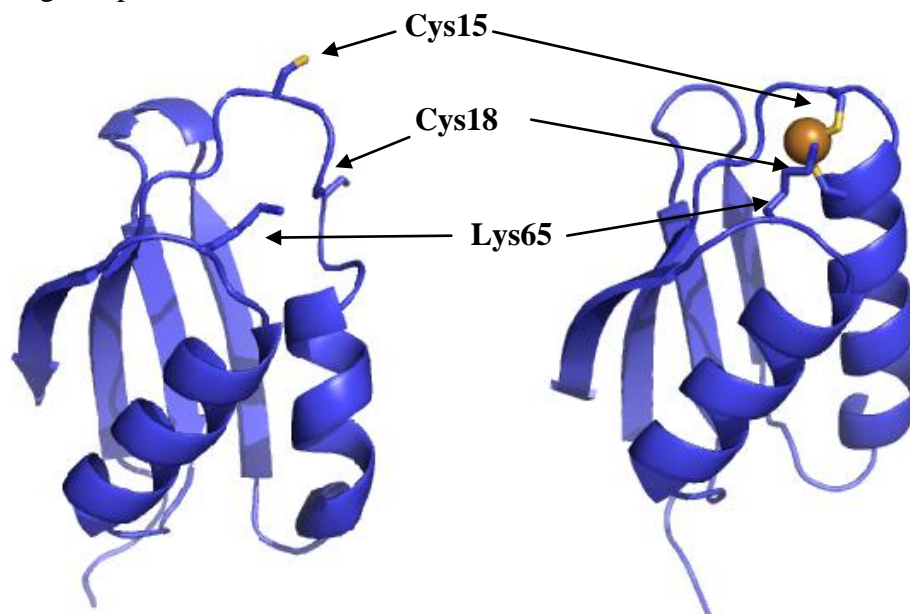
Structures for HAH1 include the Hg(II), Cd(II) and Cu(I)-bound crystal structures and apo and Cu(I)-bound NMR solution structures.(*68,69*) The crystal structures all crystallise as dimers with the metals bound between the CXXC motifs of two HAH1 monomers that have an overall protein fold similar to that for Atx1.While the Cd(II) structure shows co-ordination of the metal by all four Cys residues of two HAH1 monomers in a tetrahedral geometry, the structures for Hg(II) and Cu(I)-bound (Figure 1.4) forms display trigonal coordination by three Cys residues (Cys12 of one HAH1 monomer and Cys12 and Cys15 of the adjacent monomer).(*68*) Further analysis of Cu(I)-binding to HAH1 by EXAFS indicates digonal coordination of Cu(I) by the CXXC motif of one HAH1 monomer with trigonal coordination observed only in the presence of small thiol containing molecules GSH and dithiothreitol (DTT).*(70)* Intriguingly a hydrogen bonding network at the interface of the two monomers for all three structures is present.(*68*) A hydrogen bond interaction is present between the Thr11 side-chain of each monomer with the adjacent monomers Cys12 residues sulphur atom. In addition, a hydrogen bond between Lys60 and Cys15 of one monomer is mediated by an intervening water molecule. As seen for Atx1, the apo and Cu(I)-bound HAH1 NMR solution structures show conformational changes to the CXXC containing loop region upon Cu(I)-

11

binding, although, the changes are not as severe as only one Cys residue deviates from its positioning relative to that observed in the apo structure to bind Cu(I).(*69*) The Lys60 residue, in the NMR solution structure, is also orientated toward the metal binding site in the Cu(I)-loaded form indicating a role for the residue in modulating copper binding.

Crystal structures have also been obtained for Atx1 homologues CopZ (*B.subtilis*) and ScAtx1 (*Synechocystis*).(*71-74*) CopZ functions in Cu(I) delivery to CopA, a copper-transporting ATPase involved in export of copper from the cell whereas ScAtx1 functions in Cu(I) delivery to PacS, another copper-transporting ATPase, which is involved in copper import into the thylakoid for ultimate incorporation into Plastocyanin.(*71,73*) The structure for Cu(I)-bound CopZ shows a trimeric complex containing three copper ions coordinated by the Cys residues of the CXXC motifs within each monomer.(*72*) For ScAtx1 two $Cu_2ScAtx1_2$ forms were obtained in the absence and presence of NaCl and also a Cu_4ScAtx_2 structure.(*74*) The Cu(I)-bound trimer observed for CopZ was suggested to represent a form of the metallochaperone involved in Cu(I)-transfer to the target CopA while the Cu(I) clusters observed in ScAtx1 were proposed have roles in Cu(I) trafficking regulation and intracellular Cu(I) buffering.(*72,74*)

Overall the structures of the Atx1 metallochaperones verified a role for the CXXC motif in binding the Cu(I) ion and provided the insights regarding modulation of Cu(I)-binding through the interaction of the residues such as Lys65 in HAH1 with the CXXC Cu(I)-binding motif (discussed further in Chapter 3).(*10,12,13*) In addition, the crystal structure of Cu(I)-bound HAH1 provided insight into a possible mechanism of copper transfer from the Atx1 metallochaperones to the copper-transporting ATPases.(*68*) This has subsequently led to the determination of the nature of interaction between these metallochaperones and the ATPases discussed in section 1.3.3.

Figure 1.4

Crystal structure for Cu(I)-bound HAH1 dimer (PDB accession code 1FEE) The Cys residues of the CXXC motifs in each monomer and the Lys60 residue of loop5 are shown as stick representations and the copper ion is shown as a gold sphere.
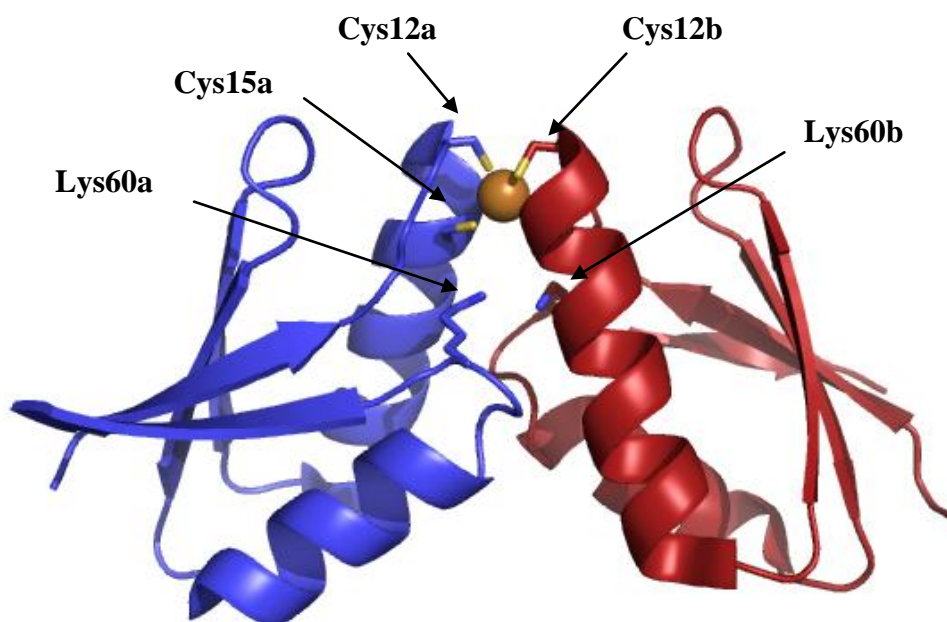
1.3.2 Copper-transporting ATPases

In prokaryotic and eukaryotic organisms the copper-transporting ATPases function to transfer copper through membranous compartments of the cell.(*75*) In eukaryotes the copper-transporting ATPases efflux copper from the cell via vesicles and import copper into the Golgi compartment for metallation of secreted proteins. The structure of a typical copper-transporting ATPase is shown in Figure 1.5.(*75*) The transporter consists of eight transmembrane domains (TMDs), metal binding domains (MBDs), a nucleotide binding domain (N domain), a phosphorylation domain (P domain) and an actuator domain (A domain) that couples nucleotide hydrolysis to copper ion transport.(*75-79*) A CPC motif in TMD6 is present and is suggested to represent a copper binding site within the transporter that is important for copper translocation. The number of MBDs varies between organisms, for example the transporter Ccc2 (*S. cerevisiae*) contains two while ATP7A and ATP7B (human) contain 6.(*76*) The MBDs are proposed to be the recipient of Cu(I) from the copper metallochaperones and also participate in regulation of the ATPases activity through copper responsive intracellular localisation.(*76,80-85*) A recent crystal structure for the copper-transporting ATPase CopA from *L. pneumophila* has been

determined which indicates a three stage copper transport mechanism. It is proposed the N-terminal transmembrane regions in concert with the MBDs aid in the capture of copper with subsequent transfer of this copper to the high affinity transmembrane region for eventual release through an exit site.*(86)* Structures for Ccc2, ATP7A and ATP7B MBDs show that the folds of the these components of the transporter consist of a βαββαβ fold, as for the Atx1 metallochaperones themselves, with the CXXC motif located on the analogous loop to that found in Atx1 and HAH1.(*78*)

Figure 1.5

Schematic showing the general domain structure of a mammalian copper-transporting ATPase. The eight trans-membrane domains (TMDs), the nucleotide-binding domain (N), the phosphorylation domain (P), the actuator domain (A) and the 6 metal-binding domains (MBDs) located in the cell cytosol at the N-terminus of the transporter are indicated.
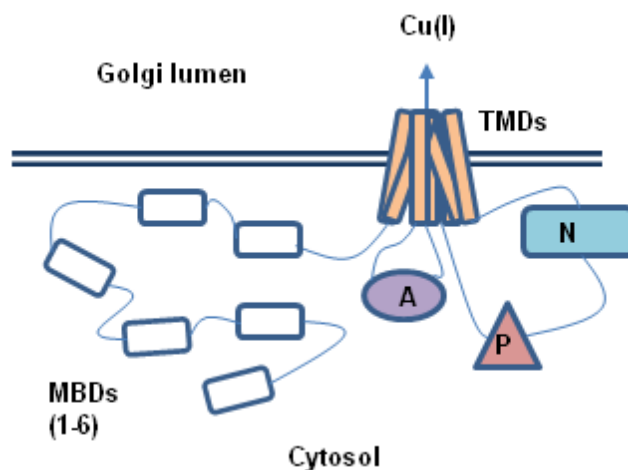
1.3.3 Atx1 Metallochaperones in Complex with their Cognate Copper-transporting ATPase MBDs

Solution structures of the Atx1 metallochaperones in complex with the copper-transporting ATPase MBDs in the presence of Cu(I) have been solved for Atx1 and Ccc2 and HAH1 and MNK1 (1st MBD of ATP7A). The NMR solution structure of the Atx1-Cu(I)-Ccc2 heterocomplex indicates coordination of two Cys residues from Ccc2 and one Cys from Atx1 (Cys13 and Cys16 of Ccc2 and Cys15 of Atx1) to the Cu(I) ion (Figure 1.6) with formation of the heterocomplex being dependent on bound Cu(I).(*87*) In addition, the interface region consists of both hydrophobic interactions and also complementary surface charges on either monomer unit. Atx1 contains a positively charged patch, consisting

14

mainly of Lys residues, on the surface of the protein that forms the dimer interface region that is complementary to a negatively charged patch on Ccc2.(*67,68,88*) These complementary surface interactions between Atx1 and Ccc2 were proposed to be important for mediating complex formation and indeed mutagenesis studies have shown that loss of the Lys residues that form the positively charged surface patch of Atx1 disrupt the function of this protein *in vivo,* resulting in reduced iron uptake and loss of Atx1:Ccc2 interaction studied by yeast two-hybrid interactions.(*88*)

The NMR solution structure for the analogous Cu(I)-bound heterocomplex between HAH1 and the first MBD of the ATB7B transporter (MNK1) also shows a similar coordination of the Cu(I) ion (Figure 1.6). Both Cys residues of the MNK1 (Cys15 and Cys18) coordinate Cu(I) but only Cys12 of HAH1 is involved in copper binding (*89*). As for the Atx1:Ccc2 heterocomplex the proteins exhibit complementary surface charges in the interface region with HAH1 having a positively charged patch and MNK1 a negatively charged patch.(*68,69,89*) Therefore the importance of protein-protein interactions is highlighted for copper transfer via this pathway and the structures suggest a mode of direct copper transfer between the partner proteins.(*68,89,90*) In support of this mechanism of copper transfer is the observation that *in vitro* copper transfer between Atx1 and Ccc2 can occur even in the presence of an excess of GSH.(*91*) Therefore Atx1 binds and retains Cu(I) but only releases it to the target protein. It has been shown that copper release by the HAH1 is slow to GSH but is fast to the bis-chelate Cu(I)-binding ligand bicinchoninic acid (BCA) indicating that the metal binding sites of the Atx1-like metallochaperones are optimised for rapid transfer of Cu(I) between partner proteins (BCA was used as a Cu(I)-binding protein mimic for studying Cu(I) transfer from HAH1).(*92*) Once copper is bound to the MBD of the copper-transporting ATPase it is thought that subsequent transfer of the metal by an ATP dependent process drives the uptake of copper into the Golgi compartment.(*76*)

Figure 1.6

Solution structure of the Cu(I)-bound Atx1:Ccc2 (A) and HAH1:MNK1 heterodimers (PDB accession codes 2GGP and 2K1R, respectively) drawn in Pymol. The Cys residues of the CXXC motifs in Atx1/HAH1 (blue) and Ccc2/MNK1 (red) are shown as stick representations and the copper ions are shown as gold spheres. The Lys60 and Phe67 of HAH1 and MNK1, respectively, are shown as stick representations.

16
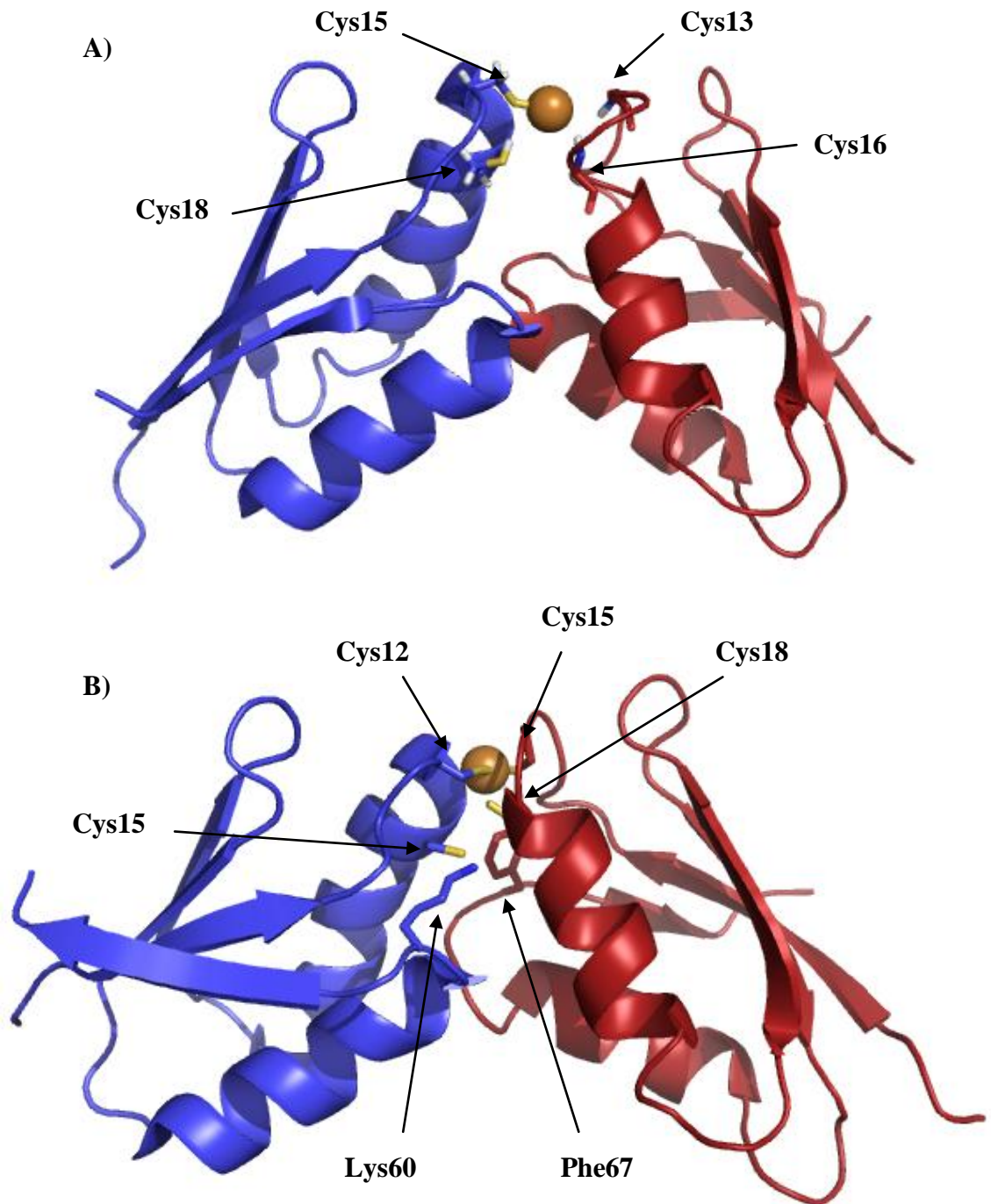
1.3.4 A Model for Copper Transfer between Atx1 Metallochaperones and Copper Transporting ATPase MBDs

Based on the available structures of the Cu(I)-bound Atx1 metallochaperones and heterocomplexes between these and their cognate copper-transporting ATPase MBDs the current model for Cu(I) transfer involves a sequence of ligand exchange reactions whereby Cu(I) transferred from the CXXC Cu(I)-binding motif of the Atx1 (Cu(I) donor) to the MBD (Cu(I) acceptor).(*68,87,89*) Computational studies have recently investigated the Cu(I) transfer process by considering the Cu(I)-bound heterocomplex structures as models for reaction intermediates.(*93*) The reaction pathway for copper transfer from Cu(I)-HAH1 to the fourth MBD of the ATP7A transporter (WD4) was investigated by quantum mechanical/molecular mechanics simulations.(*93*) A reaction pathway was considered between Cu(I)-bound HAH1 and apo-WD4 that included 2,3 and 4 coordinate intermediate species. It was found that the most favourable pathway for formation of Cu(I)-WD4 involved two 3-co-ordinate intermediate complexes. The first intermediate corresponds to Cu(I) co-ordinated by Cys12 and Cys15 of HAH1 and Cys14 of WD4. The second intermediate is more product like and involves Cu(I) co-ordination by Cys12 of HAH1 and Cys 15 and Cys17 of WD4. The second intermediate is then proposed to dissociate and leave apo-HAH1 and Cu(I)-bound WD4. It is notable that in both intermediates both Cys12 and Cys14 of HAH1 and WD4, respectively, are co-ordinated to the Cu(I) ion and correspond to the most solvent accessible Cys residue of each proteins CXXC motif. The intermediates proposed have been validated as being possible *in vitro* as mutagenesis studies show only three of the four Cys residues are required for HAH1-Cu(I)-MBD complex formation.(*87*) The homodimeric Cu(I)-bound form of HAH1 is also consistent for a role for Cys14 of WD4 in being the first Cys residue of the MBD that coordinates to the Cu(I) ion bound by HAH1.(*68*) Finally, the HAH1-Cu(I)-MNK1 structure shows a product like intermediate where both Cys residues of the target MBD are bound to the Cu(I) ion while only one Cys residue of HAH1 is coordinated.(*89*) The current model for transfer between Atx1-like metallochaperones and MBDs is as shown in Figure 1.7.(*68,87,89,93*)

Figure 1.7

Model for Cu(I)-transfer between an Atx1-like metallochaperone and the MBD of a copper-transporting ATPase. Cu(I)-bound Atx1 forms an intermediate 3 co-ordinate complex with a copper-transporting ATPase MBD which undergoes rearrangement so that both Cys residues of the target MBD coordinate Cu(I). Dissociation of the intermediate then occurs leaving apo-Atx1 and Cu(I)-bound MBD.
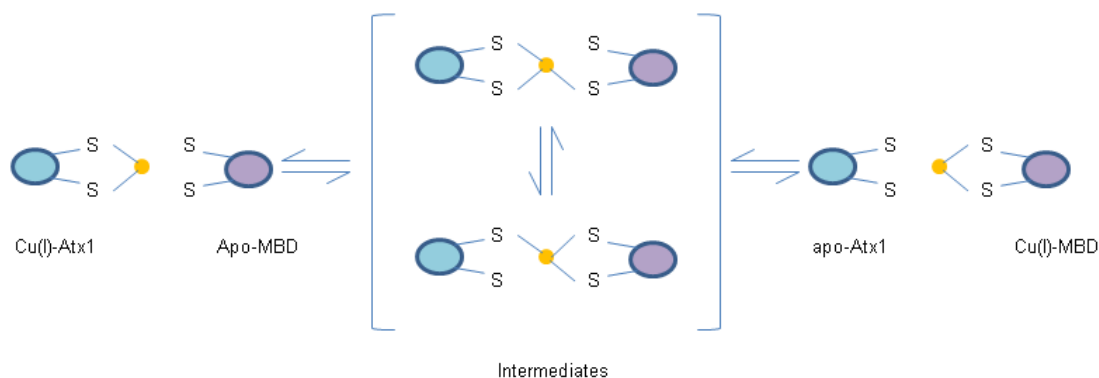
1.4   Copper Delivery to Cu,Zn-Superoxide Dismutase

The CCS metallochaperones deliver copper to the antioxidant enzyme SOD1.(*94*) SOD1 is a homodimeric copper and zinc requiring protein that is mainly localised in the cell cytosol although a small but significant fraction is also present in the mitochondrial inter membrane space (IMS).(*95,96*) The enzyme catalyses the disproportionation of damaging superoxide radicals by redox cycling of the copper bound in the active site of the protein, equations (1.5-1.6), resulting in the overall production of hydrogen peroxide and oxygen, equation (1.7), the hydrogen peroxide being subsequently converted to oxygen and water by catalase.(*94*)

$$Cu(II)\text{-}SOD1 + O_2^- \rightleftharpoons Cu(I)\text{-}SOD1 + O_2 \tag{1.5}$$

$$Cu(I)\text{-}SOD1 + O_2^- + 2H^+ \rightleftharpoons Cu(II)\text{-}SOD1 + H_2O_2 \tag{1.6}$$

$$2O_2^- + 2H^+ \rightleftharpoons O_2 + H_2O_2 \tag{1.7}$$
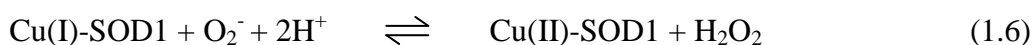
The main fold of SOD1 consists of a β-barrel composed of 8 anti-parallel sheets.(*97,98*) These are connected by intervening connecting loops that also form the copper and zinc metal binding sites and define the active site cavity through which the

superoxide substrate is guided to the copper ion.(*94,99*) Copper is bound by four His residues and a water molecule when in the +2 oxidation state and zinc is bound by three His residues, of which one is shared with that of the copper ion, and a fourth Asp ligand.(*98*) A conserved Cys disulfide is also present, between Cys57 and Cys146 in humans, and connects the metal binding loop region to that of the β-barrel.(*97*) Both the binding of copper and zinc and oxidation of the disulfide lead to increased stability of the protein resulting in an active homodimer.(*100-102*)

The CCS metallochaperones are implicated in both copper metallation of SOD1 and formation of the intramolecular disulfide.(*6,42,103*) Ccs1 was first discovered as a requirement for Sod1 activation in yeast through the identification of the *S. cerevisiae* LYS7 gene.(*42*) Without this gene encoding Ccs1 the Sod1 enzyme expressed at normal levels, is inactive as it lacks the necessary copper cofactor to carry out the required redox chemistry. The same gene, but in humans, encoding a similar protein was also discovered and activates human SOD1.(*42*) As in the case for yeast, mutations of this gene in mammals result in a drastic reduction of SOD1 activity. In mice containing a CCS deletion the incorporation of radiolabelled copper into SOD1 is severely attenuated and highlights the importance of the metallochaperone for activation of SOD1.(*104*)

1.4.1 The CCS Metallochaperones

The CCS metallochaperone is a ~30 kDa multidomain protein that located predominantly in the cell cytosol.(*42,105*) Initial characterisation of the protein led to the identification three distinct domains.(*6,42,105*) The N-terminal domain 1 (D1) is similar in sequence to the Atx1 metallochaperones and contains a conserved CXXC Cu(I)-binding motif which in Ccs1 is required for Ccs1 activation of Sod1 under copper limiting conditions while in humans is required under all conditions.(*104,106,107*) The central domain 2 (D2) is the largest domain and is similar in sequence to the SOD1 target protein itself and found to be essential for CCS activation of SOD1 *in vivo*.(*104,107*) The C-terminal domain (D3) is the shortest and contains an essential CXC Cu(I)-binding motif that was found to be absolutely essential for CCS activation of SOD1 *in vivo* both in yeast and humans.(*104,107*)

The determination of the crystal structure for Ccs1(*108*) (Figure 1.8) shows the N-terminal D1 to consist of an βαββαβ-fold with the CXXC Cu(I)-binding motif located on a loop analogous to that on which the same motif is located in Atx1.(*66*) Domain 2 consists

of an eight-stranded β-barrel fold which is analogous to that found in Sod1 however is missing all of the copper and zinc binding residues and so binds no metals within this region.(*97,108*) In addition this domain formed the dimerisation interface between the dimers of Ccs1 observed in this crystal structure through several hydrophobic residues and four main chain hydrogen bonding interactions.(*108*) The C-terminal D3 is not observed in this structure of Ccs1. A notable observation, however, is that the four Cys residues present in D1 are oxidised, forming disulfide bonds between Cys17 and Cys20 (CXXC Cys residues) and Cys27 and Cys64. Other Cys residues present in the structure being those residues of the CXC motif in D3 (Cys229 and Cys 231) and Cys159 (D2).(*108*) The subsequent determination of D2 of CCS showed the domain in the human homologue to be of a similar overall fold but to contain a zinc ion in a site analogous to that found in SOD1 but to lack, however, a His residue of the copper ligand set so that no copper was bound.(*109*) It is notable that a single Asp201 to His mutation in CCS results in a full ligand set for copper within this domain and the resulting species displays superoxide dismutase activity, albeit at a much lower level than for SOD1 itself. Intriguingly the CCS structure showed there to be four Cys residues located within this domain with two of these (Cys141 and Cys227) involved in a disulfide bond analogous to that found in SOD1.(*97,109*)

The crystal structure of Ccs1 in complex with a His48Phe Sod1 mutant led to the full structural characterisation of a CCS metallochaperone (Figure 1.8).(*110*) The proteins crystallised as a Ccs1:Sod1 heterodimer with the interface region consisting mainly of contacts between D2 of Ccs1 and that of the corresponding dimer interface in Sod1. The interface region is held together by hydrophobic regions and 4 main chain hydrogen bonds as is found between the monomers in the Ccs1 homodimer structure. D1 in the heterodimer structure is orientated differently to that of the same domain in the homodimer structure and highlights the flexibility of the linker region between D1 and D2.(*108,110*) Interestingly, the structure shows a disulfide bond between Cys229 of the CXC motif of D3 and Cys57 of the Sod1 monomer. Furthermore, there are a number of interactions between the D3 region and the active site channel of Sod1 indicating that these may help facilitate the delivery of copper to the sunken metal binding site in Sod1. The positioning of D1 and D3 within the heterodimeric structure and the interactions between D2 and Sod1 dimerisation interfaces have suggested that this complex may represent an important intermediate for activation of Sod1 by Ccs1.(*110*) In support of this a Ccs1:Sod1 heterocomplex has also been observed in solution.(*111,112*)

Although both CCS and Ccs1 are observed as dimers in their crystal structures the oligomeric behaviour of the proteins in solution differs with CCS existing as a dimer when apo but which forms tetrameric species when loaded with Cu(I).(*113*) In contrast, Ccs1 is a monomer when apo but is a dimer in the presence of Cu(I).(*111*) It has also been shown that at high Cu(I) loadings (~3 equivalents of Cu(I) per CCS) that CCS reverts to a dimer in which the D3 CXC motif forms the dimer interface through formation of a Cu(I) cluster between the motifs of two monomers of CCS.(*113*) This was proposed to open up the D2 dimerisation interface for interaction with the analogous dimer interface region of SOD1 however it is currently unknown whether this oligomeric form of CCS would form *in vivo*.(*113*)

The precise details of Cu(I) binding to CCS remains unclear due to the unavailability of structural characterisation of either D1 or D3 with the native metal. The apo structures, however, suggest D1 and D3, that contain the Cu(I)-binding CXXC and CXC motifs, respectively, are involved in binding copper and transferring it to SOD1, particularly D3, due to its close proximity to the copper binding site in Sod1 and the essential requirement of the CXC Cys residues *in vivo*.(*103,105,110*) In support of this, proteolytic trypsin digests of Cu(I)-bound Ccs1 have indicated that copper only binds to D1 and D3.(*107*) Furthermore, EXAFS analysis of Cu(I)-bound CCS and its CXXC and CXC Cys to Ser mutants has shown copper to be coordinated by these Cys residues.(*114*) The EXAFS data indicated a single Cu(I) resides in an environment indicative of that provided by the two Cys residues of the D1 CXXC motif with co-ordination by a third unidentified ligand whereas a copper cluster was attributed to binding of Cu(I) to the D3 CXC motif.(*113,114*) Analysis of x-ray absorption spectroscopy (XAS) data for Cys to Ala variants of CCS demonstrated that this cluster formation could be eliminated by mutation of either Cys residues of the CXC motif. A Cu_2S_6 adamantane-like structure has been proposed as the best fit to the XAS data for cluster formation between two D3 CXC motifs with two unidentified sulphur ligands. Subsequent studies of CCS variants in which the Cys residues of D2 are mutated have indicated a role for these residues in cluster formation, although the physiological significance of the D3 Cu(I) cluster is currently unknown.(*115*)

Figure 1.8

Crystal structures of apo-Ccs1 homodimer (A) and apo-Ccs1:H48FSOD1 heterodimer (B) (PDB accession codes 1QUP and 1JK9, respectively) drawn in Pymol. In (A) D2 of the two Ccs1 monomers are shown blue and red with associated D1 shown in green and magenta, respectively. In (B) Sod1 is shown in blue, Ccs1 D2 in red with D1 and D3 in magenta. The Cys residues of the CXXC and CXC motifs in each monomer of Ccs1 are shown as stick representations and the zinc ion of Sod1 is shown as a grey sphere.
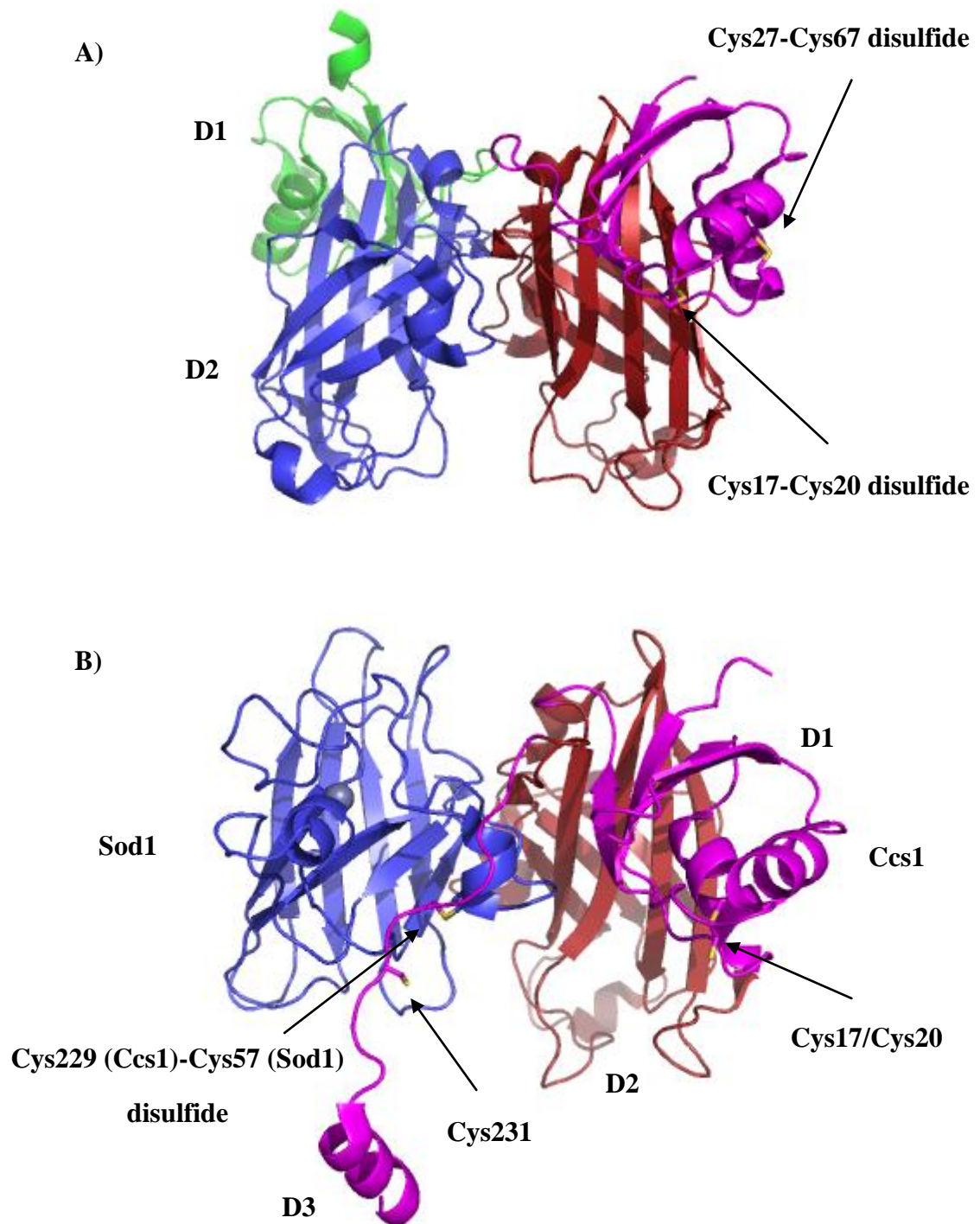
1.4.2 Oxygen Dependence of CCS Activation of SOD1

In addition to copper transfer CCS is also involved in facilitating the oxidation of the essential intramolecular disulfide in SOD1 between Cys57 and Cys146.(*103*) Oxidation of the disulfide has been found to require copper bound CCS and dioxygen. Furthermore, copper-bound CCS activation is dose dependant with respect to dioxygen and under anaerobic conditions SOD1 is unable to be activated by the CCS pathway.(*116*) The oxygen dependence of Sod1 activation by Ccs1 in particular has provided significant insights into the nature of this activity of the CCS metallochaperone in general and the intimate link between formation of the disulfide and metallation. Formation of the Sod1 disulfide by Ccs1 is rapidly accelerated for copper-bound reduced Ccs1 compared to either reduced or oxidised apo-Ccs1.(*103*) Therefore, the presence of copper is a requirement for the oxidation of the disulfide itself and copper binding to D3 is not only required for insertion into the Sod1 active site but also contributes to an disulfide forming function of the D3 CXC motif. This disulfide forming function of the CXC motif is highlighted by the presence of a disulfide between Cys229 of Ccs1 and Cys57 of Sod1 in the heterodimeric Ccs1:Sod1 crystal structure.(*110*) A disulfide linked heterodimer between Ccs1 and Sod1 is observed for a Cys146 to Ser mutation in Sod1 whereas no such form is found in the corresponding Cys57 mutant.(*103*) Therefore disulfide bond formation between Ccs1 and SOD1 appears to be regioselective for the two Sod1 Cys residues. This behaviour suggests a precise function for Ccs1 facilitated disulfide formation in Sod1 and that interaction between D3 and Sod1 during Ccs1:Sod1 heterocomplex formation may be important factors regarding this specificity. It has also been shown that Ccs1 distinguishes between reduced and oxidised apo-SOD1. Only the apo reduced form of Sod1 can be activated by copper-bound Ccs1 suggesting that the formation of the disulfide imposes structural changes to the protein fold of Sod1 that abrogates interaction with the Ccs1 metallochaperone.(*103*) The dose responsive nature of the oxygen dependent activation of CCS is proposed to be a major mechanism for posttranslational control of SOD1 activity with the activation of a pool of SOD1 within the cytoplasm providing for rapid response to changes in oxygen tension in the cell.(*116*) The available data so far indicates that copper transfer to SOD1 from CCS precedes or is concomitant with disulfide formation.(*104*)

1.4.3 CCS Activation of SOD1 in the Mitochondrial IMS

A small fraction of Ccs1 localises to the mitochondrial IMS and is has been shown to be important for the uptake of Sod1 and subsequent maturation and retention within this cellular compartment.(*105*) Ccs1 is transported into the IMS by the Mia40/Erv1 disulfide relay system and the presence of Sod1 within the mitochondria is dependent on this uptake of Ccs1 (*117,118*). Mia40 is a mitochondrial outer membrane import receptor and Erv1 is a thiol oxidase and both proteins play essential roles for uptake of Ccs1.(*44*) In the absence of Ccs1, Sod1 levels within the IMS are diminished. Furthermore, only the most immature form of Sod1 lacking the metal binding ions and the intramolecular disulfide can be transported into the IMS.(*105*) It has been shown that Ccs1 is a substrate for Mia40 and forms a mixed disulfide containing complex. Mia40 itself is oxidised by Erv1 and it has been proposed that the three proteins work in concert to transfer a disulfide bond to imported Ccs1.(*118*)

Until recently it was unknown which Cys residues of Ccs1 were required for import of the protein into the IMS. It has recently been discovered, however, that Cys27 and Cys64 of D1 play a role in mitochondrial uptake.(*119,120*) Cys to Ala mutations to either of the residues in D1 results in alterations to the localisation of the protein between the cytosol and the IMS but do not affect the activation of Sod1 itself *in vitro*.(*119*) It has been shown that Mia40 forms a disulfide bond with Cys67 of Ccs1 and that subsequently the majority of IMS localised Ccs1 is present as an oxidised form involving Cys27 and Cys64.(*120*) It has been proposed that this disulfide serves a structural role and stabilises this region of Ccs1 and prevents its removal from the IMS.(*120*) Transfer of this disulfide to Sod1 is then expected to then trap activated Sod1 within the IMS and then Ccs1 is oxidised by the Mia40/Erv1 system for subsequent turnover of newly imported immature Sod1. It is currently unknown how the human CCS is imported and retained in the IMS as this homologue does not contain the Cys pair present in Ccs1 that contribute to IMS import.

1.4.4 CCS Independent Activation of SOD1

In *S. cerevisiae* Ccs1 deletion results in undetectable Sod1 activity, whereas a CCS deletion in mice results in residual SOD1 activity.(*121*) Furthermore, there is lack of a CCS homologue in *C.elegans* which expresses a fully active SOD1 enzyme and a number of other organisms lacking a gene for CCS, yet which still express active SOD1 have also

been discovered and suggest an alternative route for SOD1 activation that is independent of CCS.(*122,123*) The cause of this difference in CCS dependence between organisms results from the absence of a Pro residue in the C-terminus of SOD1 in those species capable of CCS independent activation.(*124*) Sod1 (*S. cerevisiae*) contains a Pro144 residue in this C-terminal region which has been found to confer complete Ccs1 dependence for SOD1 activation in *S. cerevisiae.(124)* Interestingly, mutation of this single residue to the corresponding residue of the human homologue (Leu) results in the loss of this CCS dependence and a fully active Sod1 results in the absence of Ccs1. Mutating the corresponding residue in human SOD1 to a Pro results in complete CCS dependent activation. Due to the close proximity of the Pro residue of Sod1 to the essential intramolecular disulfide a role for the Pro in modulating the Sod1 Cys disulfide redox potential has been proposed.(*124*) In SOD1s lacking the C-terminal Pro residue the reduction potential for the disulfide was lowered and therefore resulting in a greater propensity for the disulfide to form. This CCS independence does not require the copper metallochaperones Atx1 or Cox17, and instead, roles for reduced glutathione and a low redox potential for the cell have been implicated.(*125*) It appears that most SOD1s, however, lack a total dependence on CCS and that Sod1 in *S. cerevisiae* is a rare exception. It is speculated that having two pathways for SOD1 activation allows organisms to maintain a basal level of SOD1 activity independently of CCS.(*124*)

1.4.5   Interaction of CCS with BACE1

CCS has recently been linked with Alzheimer's disease through interactions of the metallochaperone with β-secretase (BACE1).(*126*) BACE1 is one of many enzymes involved in the processing of the amyloid precursor protein (APP) which results in Aβ peptides, the main constituents of the plaques which are a pathological hallmark of the disease.(*127*) The Aβ peptides are small 40-42 amino acid chains that result from the cleavage of the membrane bound amyloid precursor protein (APP) through the consecutive action of the secretases which cut APP at specific sites.(*127*) The Aβ peptides are generally accepted to be neurotoxic and their release has been termed the amyloid cascade hypothesis.(*128*)

Recent evidence has suggested that altered uptake and metabolism of copper is strongly implicated in the processing of APP with binding of copper to various proteins involved in the biochemical pathway, including Aβ, APP.(*127*) BACE1 is a membrane spanning protein that has a cytosolic C-terminal domain containing a CXXC Cu(I)-

binding motif.(*127*) The BACE1-CCS interaction was found to occur through the C-terminal domain of the former and D1 of the latter.(*126*) It was found that the C-terminal cytoplasmic domain of BACE1 binds Cu(I) with high affinity. Metal binding investigated by UV/Vis spectroscopic titrations of a C-terminal peptide fragment of BACE1 with Cu(I) showed that the metal were coordinated by Cys residues, most likely from the CXXC motif and/or another nearby Cys residue as determined by titrations with a series of Cys to Ala mutants. The expression of BACE1 was found to reduce SOD1 activity in cells consistent with competition between SOD1 and BACE1 for CSS as overexpression of CCS enabled the restoration of SOD1 activity.(*126*) It was also found that both proteins co-immunoprecipitated from rat brain extracts and visualisation of the co-transport of BACE1 and CCS through nerve axons was observed.(*126*) Therefore, the binding of Cu(I) and CCS to BACE1 may be a mechanism for regulation of APP processing by BACE1 and hence Aβ production.

1.5   Copper Delivery to Cytochrome *c* Oxidase

Delivery of copper to the mitochondria is required for metallation of C*c*O, an essential membrane bound enzyme that is participates in the last stage of the mitochondrial electron transport chain.(*44*) The protein requires a total of three copper ions for formation of the Cu_A and Cu_B metal centres. It is proposed that Cox17 transfers and imparts specific Cu(I) metallation of the proteins Sco1 and Cox11 for subsequent transfer of the Cu(I) to Cox2 and Cox1, respectively, which form the initial building blocks of the C*c*O complex.(*129*)

1.5.1   Cox17

Cox17 is an 8 kDa protein with a helical hairpin fold that is stabilised by four Cys residues from two CX_9C motifs.(*44*) The protein contains a further two Cys residues in a CC Cu(I)-binding motif. Cox17 was found in the yeast cytoplasm, initially indicating that this protein may represent a copper metallochaperone that traffics copper from the cell surface transporters to the mitochondria.(*130*) Although Cox17 is localised to both the cytosol and inner membrane space of the mitochondria the tethering of the protein to the mitochondrial membrane does not disrupt metallation of C*c*O, hence it is uncertain whether this protein can be considered a true copper metallochaperone.(*131*)

1.5.2 Copper Ligand (CuL)

Due to the ability of Cox17 tethered to the mitochondrial membrane to maintain C*c*O biogenesis it became clear that another species in the cell must be responsible for copper transfer to this compartment. Copper has been found to be available within the mitochondria as a small soluble copper ligand complex (CuL).(*132,133*) CuL is present in the mitochondria of both yeast and humans and has been found in the apo state within the cytoplasm, indicating that this species may represent a route for copper entry into the mitochondria.(*133*) Little data is available for this potential copper metallochaperone and it is unknown if mechanisms for translocation of a copper-bound form into the mitochondria exist.

1.6   References

(1)   Kaim, W.; Schwederski, B. Bioinorganic Chemistry; Inorganic Elements in the Chemistry of Life, Wiley, **1995**.

(2)   Frausto da Silva, J. J. R.; Williams, R. J. P. The Biological Chemistry of the Elements, Oxford University Press, **2001**.

(3)   Burger, K. Biocoordination Chemistry, Ellis Horwood, **1990**.

(4)   Holm, R.H.; Kennepohl, P.; Solomon, E.I. *Chem. Rev.* **1996**, *7*, 2239-2314.

(5)   Halliwell, B.; Gutteridge, J. M. C. *Biochem. J.* **1984**, *219*, 1-14.

(6)   Rae, T.D.; Schmidt, P.J.; Pufahl, R.A.; Culotta, V.C.; O'Halloran, T.V. *Science* **1999** *284*, 805-808.

(7)   Puig. S.; Thiele. D. J. *Curr. Opin. Chem. Biol.* **2002**, *6*, 171-180.

(8)   Lutsenko. S.; Petris, M. J. *J. Membr. Biol.* **2003**, *191*, 1-12.

(9)   Maryon, E. B.; Molloy, S. A.; Zimnicka, A. M.; Kaplan, J. H. *Biometals* **2007**, *20*, 355-364.

(10) Rosenzweig, A. C. *Acc. Chem. Res.* **2001**, *34*, 119-128.

(11) Rosenzweig, A. C. *Chem. Biol.* **2002**, *9*, 673-677.

(12) Huffman, D.L.; O'Halloran, T.V. *Annu. Rev. Biochem.* **2001**, *70*, 677-701.

(13)   Robinson, N.J.; Winge, D.R. *Annu. Rev. Biochem.* **2010**, *79*, 537-562.

(14)   Tottey, S.; Harvie, D. R; Robinson, N. J. *Acc. Chem. Res.* **2005**, *38*, 775-783.

(15)   Singleton, C.; Le Brun, N.E. *Biometals* **2007**, *20*, 275-289.

(16)   Greenwood, N. N.; Earnshaw, A. Chemistry of the Elements, Elsevier, **2003**.

(17)   Gray, H. B.; Malmstrom, B. G.; Williams, R. J. P.; *J. Biol. Inorg. Chem.* **2000**, *5*, 551-559.

(18)   McCord, J. M.; Fridovich. I. *J. Biol. Chem.* **1969**, 6049-6055.

(19)   Sato, K,; Kohzuma, T.; Dennison, C. *J. Am. Chem. Soc.* **2003**, *125*, 2101-2112.

(20)   Strange, R. W.; Antonyuk, S. V.; Hough, M. A.; Doucette, P. A.; Valentine, J. S.; Hasnain, S. S.; *J. Mol. Biol*. **2006**, *356*, 1152-1162.

(21)   Lindley, P. F.; Card, G.; Zaitseva, I.; Zaitsev, V.; Reinhammar, B.; Selin-Lindgren, E.; Yoshida, K. *J. Biol. Inorg. Chem.* **1997**, *2*, 454-463.

(22)   Dennison, C. *Coord. Chem. Rev.* **2005**, 3025-3054.

(23)   Malmstrom, B.G,; Leckner, J. *Curr. Opin. Chem. Biol.* **1998**, *2*, 286–292.

(24)   St. Clair, C. S.; Gray, H. B.; Valentine, J. S. *Inorg. Chem.* **1992**, *31*, 925-927.

(25)   Azab, H. A.; Banci, L.; Borsari, M.; Luchinat, C.; Sola, M.; Viezzoli, M. S. *Inorg. Chem.* **1992**, *31*, 4649-4655.

(26)   Makino, N.; McMahill, P.; Mason, H. M. *J. Biol. Chem.* **1974**, *249*, 6062-6066.

(27)   Hutchens, T.W.; Allen, M.H.; Li, C.M.; Yip, T.T. *FEBS Lett.* **1992**, *309*, 170–174.

(28)   Predki, P.F.; Sarkar, B. *J. Biol. Chem.*, **1992**, *267*, 5842–5846.

(29)   Halliwell, B.; Gutteridge, J.M.C. *Meth. Enzymol.* **1990**, *186*, 1–85.

(30)   Jomova, K.; Valko, M. *Toxicology* **2011**, *283*, 65-87.

(31)   Kozlowski, H.; Janicka-Klos, A.; Brasun, J.; Gaggello, E.; Valensin, D.; Valensin, G. *Coord. Chem. Rev.* **2009**, *253*, 2665-2685.

(32) Ala, A; Walker, A.P.; Ashkan, K.; Dooley, J.S.; Schilsky, M.L. *Lancet* **2007**, *369*, 397–408.

(33) Dudev, T.; Lim, C. *Annu. Rev. Biophys.* **2008**, *37*, 97–116.

(34) Irving, H.; Williams, R. J. P.; *Nature* **1948**, *162*, 746-747.

(35) Irving, H.; Williams, R. J. P. *J. Chem. Soc.* **1953**, 3192–3210.

(36) Gorelsky, S.I.; Basumallick, L.; Vura-Weis, J.; Sarangi, R.; Hodgson, K.O.; Hedman, B.; Fujisawa, K.; Solomon, E.I. *Inorg Chem.* **2005**, *44*,4947-4960.

(37) Tottey, S.; Waldron, K.J.; Firbank, S.J.; Reale, B.; Bessant, C.; Sato, K.; Cheek, T.R.; Gray, J.; Banfield, M.J.; Dennison, C.; Robinson, N.J. *Nature* **2008**, *455*, 1138-1142.

(38) Kim, B.E.; Nevitt, T.; Thiele, D. J. *Nature Chem. Biol.* **2008**, *4*, 176-185.

(39) De Feo, C. J.; Aller, S. G.; Unger, V. M. *Biometals* **2007**, *20*, 705-716.

(40) Pufahl, R. A.; Singer, C. P.; Peariso, K. L.; Lin, S.J.; Schmidt, P.; Culotta, V. C.; Penner-Hahn, J. E.; O'Halloran, T. V. *Science* **1997**, *278*, 853-856.

(41) Hung, I. H.; Casareno, R. L. B.; Labesse, G.; Matthews, F. S; Gitlin, J. D. *J. Biol. Chem.* **1998**, *273*, 1749-1754.

(42) Culotta, V.C.; Klomp, L.W.; Strain, J.; Casareno, R.L.; Krems, B.; Gitlin, J.D. *J. Biol. Chem.* **1997**, *272*, 23469-23472.

(43) McCord, J.M.; Fridovich, I. *J. Biol. Chem.* **1969**, *244*, 6049-6055.

(44) Atkinson, A.; Winge, D.R. *Chem. Rev.* **2009,** *109,* 4708–4721.

(45) Dancis, A.; Haile, D.; Yuan, D. S.; Klausner, R. D. *J. Biol. Chem.* **1994**, *269*, 25660– 25667.

(46) Dancis, A.; Yuan, D. S.; Haile, D.; Askwith, C.; Eide, D.; Moehle, C.; Kaplan, J.; Klausner, R. D. *Cell* **1994**, *76*, 393– 402.

(47) Zhou, B.; Gitschier, J. *Proc. Natl. Acad. Sci. U.S.A.* **1997**, *94*, 7481-7486.

(48) Turski, M. L.; Thiele, D. J. *J. Biol. Chem.* **2009**, *284*, 717– 721.

(49) De Feo, C. J.; Aller, S. G.; Siluvai, G. S.; Blackburn, N. J.; Unger, V. M. *Proc. Natl. Acad. Sci. U.S.A.* **2009**, *106*, 4237– 4242.

(50) Aller, S. G.; Unger, V. M. *Proc. Natl. Acad. Sci. U.S.A.* **2006**, *103*, 3627– 3632.

(51) Klomp, A. E.; Juijn, J. A.; van der Gun, L. T.; van den Berg, I. E.; Berger, R.; Klomp, L. W. *Biochem. J.* **2003**, *370*, 881-889.

(52) Klomp, A. E.; Juijn, J. A.; van der Gun, L. T.; van den Berg, I. E.; Berger, R.; Klomp, L. W. *Biochem. J.* **2003**, *370*, 881-889.

(53) Eisses, J. F.; Kaplan, J. H.; *J. Biol. Chem.* **2005**, *280*, 37159-37168.

(54) Wu, X.; Sinani, D.; Kim, H.; Lee, J. *J. Biol. Chem.* **2009**, *284*, 4112-4122.

(55) Lee, J.; Pena, M. M. O.; Nose, Y.; Thiele, D. J. *J. Biol. Chem.* **2002**, *277*, 4380-4387.

(56) Xiao, Z.; Wedd, A. G. *Chem. Commun.* **2002**, 588-589.

(57) Odermatt, A.; Solioz, M. *J. Biol. Chem.* **1995**, *270*,4349–4354.

(58) Lin, S.; Pufahl, R.; Dancis, A.; O'Halloran, T. V.; Culotta, V. C. *J. Biol. Chem.* **1997**, *272*, 9215−9220.

(59) Yuan, D. S.; Stearman, R.; Dancis, A.; Dunn, T.; Beeler, T.; Klausner, R. D. *Proc. Natl. Acad. Sci. U.S.A.* **1995**, *92*, 2632-2636.

(60) Klomp, L. W. J.; Lin, S. J.; Yuan, D. S.; Klausner, R. D.; Culotta, V. C.; Gitlin, J. D. *J. Biol. Chem.* **1997**, *272*, 9221-9226.

(61) Mercer, J. F. B. *Trends Molec. Med.* **2001**, *7*, 64-69.

(62) Harris, Z. L.; Takahashi, Y.; Miyajima, H.; Serizawa, M.; MacGillivray, R. T.; Gitlin, J. D. *Proc. Natl. Acad. Sci. U.S.A.* **1995**, *92*, 2539−2543.

(63) Badarau, A.; Dennison, C. *J. Am. Chem. Soc*. 2011 133, 2983-2988.

(64) Xiao, Z.; Brose, J.; Schimo, S.; Ackland, S.M.; La Fontaine, S.; Wedd, A.G. *J Biol. Chem*. **2011**, *286*, 11047-11055.

(65) Zhou, L.; Singleton, C.; Le Brun, N.E.; *Biochem J.* **2008**, *413*, 459-465.

(66) Rosenzweig, A. C.; Huffman, D. L.; Hou, M. Y.; Wernimont, A. K.; Pufahl, R. A.; O'Halloran, T. V. *Structure* **1999**, *7*, 605-617.

(67) Arnesano, F.; Banci, L.; Bertini, I.; Huffman, D. L.; O'Halloran, T. V. *Biochemistry* **2001**, *40*, 1528-1539.

(68) Wernimont, A. K.; Huffman, D. L.; Lamb, A. L.; O'Halloran, T. V.; Rosenzweig, A. C. *Nat. Struct. Biol.* **2000**, *7*, 766-771.

(69) Anastassopoulou, I.; Banci, L.; Bertini, I.; Cantini, F.; Katsari, E.; Rosato, A. *Biochemistry* **2004**, *43*, 13046-13053.

(70) Ralle, M,; Lutsenko, S,; Blackburn, N. J. *J. Biol. Chem.* **2003**, *278*, 23163-23170.

(71) Radford, D. S.; Kihlken, M. A.; Borrelly, G. P.; Harwood, C. R.; Le Brun, N. E.; Cavet, J. S. *FEMS Microbiol. Lett.* **2003**, *220*, 105-112.

(72) Singleton, C.; Hearnshaw, S.; Zhou, L.; Le Brun, N.E.; Hemmings, A.M. *Biochem. J.* **2009**, *424*, 347-356.

(73) Tottey, S.; Rondet, S.A.; Borrelly, G.P.; Robinson, P.J.; Rich, P.R.; Robinson, N.J. *J. Biol. Chem.* **2002**, *277*, 5490-5497.

(74) Badarau, A.; Firbank, S.J.; McCarthy, A.A.; Banfield, M.J.; Dennison, C. *Biochemistry* **2010**, *49*, 7798-7810.

(75) Arguello, J. M.; Eren, E.; Gonzalez-Guerrero, M. *Biometals* **2007**, 20, 233-248.

(76) Lutsenko, S.; Kaplan, J. H. *Biochemistry* **1995**, *34*, 15607-15613.

(77) Arnesano, F.; Banci, L.; Bertini, I.; Ciofi-Baffoni, S.; Molteni, E.; Huffman, D. L.; O'Halloran, T. V. *Genome Res.* **2002**, *12*, 255-271.

(78) Barry, A.N.; Shinde, U.; Lutsenko, S. *J. Biol. Inorg. Chem.* **2010**, *1*, 47-59.

(79) Mandal, A. K.; Arguello, J. M. *Biochemistry* **2003**, *42*, 11040-11047.

(80) Strausak, D.; LaFontaine, S.; Hill, J.; Firth, S. D.; Lockhart, P. J.; Mercer, J. F. B. *J. Biol. Chem.* **1999**, *274*, 11170-11177.

(81) Achila, D.; Banci, L.; Bertini, I.; Bunce, J.; Ciofi-Baffoni, S.; Huffman, D. L. *Proc. Natl. Acad. Sci. U.S.A.* **2006**, *103*, 5729-5734.

(82) Hamza, I.; Schaefer, M.; Klomp, L. W. J.; Gitlin, J. D. *Proc. Natl. Acad. Sci. U.S.A.* **1999**, *96*, 13363-13368.

(83) Larin, D.; Mekios, C.; Das, K.; Ross, B.; Yang, A.-S.; Gilliam, T. C. *J. Biol. Chem.* **1999**, *274*, 28497-28504.

(84) Walker, J. M.; Tsivkovskii, R.; Lutsenko, S. *J. Biol. Chem.* **2002**, *277*, 27953-27959.

(85) Yatsunyk, L. A.; Rosenzweig, A. C. *J. Biol. Chem.* **2007**, *282*, 8622-8631.

(86) Gourdon, P.; Liu, X.Y.; Skjørringe, T.; Morth, J.P.; Møller, L.B.; Pedersen, B.P.; Nissen, P. *Nature* **2011**, *475*, 59-64.

(87) Banci, L.; Bertini, I.; Cantini, F.; Felli, I. C.; Gonnelli, L.; Hadjiliadis, N.; Pierattelli, R.; Rosato, A.; Voulgaris, P. *Nature Chem. Biol.* **2006**, *2*, 367-368.

(88) Portnoy, M.E.; Rosenzweig, A.C.; Rae, T.; Huffman, D.L.; O'Halloran, T.V.; Culotta, V.C. *J. Biol. Chem.* **1999**, *274*,15041–15045.

(89) Banci, L.; Bertini, I.; Calderone, V.; Della-Malva, N.; Felli, I. C.; Neri, S.; Pavelkova, A.; Rosato, A. *Biochem. J.* **2009**, *422*, 37– 42.

(90) Banci, L.; Bertini, I.; McGreevy, K.S.; Rosato, A. *Nat. Prod. Rep.* **2010**, *5*, 695-710.

(91) Huffman, D.L.; O'Halloran, T.V. *J. Biol. Chem.* **2000**, *275*, 18611–18614.

(92) Hussain, F.; Olson, J.S.; Wittung-Stafshede, P. *Proc. Natl. Acad. Sci. U.S.A.* **2008**, *105*, 11158-11163.

(93) Rodriguez-Granillo, A.; Crespo, A.; Estrin, D.A.; Wittung-Stafshede, P. *J. Phys. Chem. B*. **2010**, *114*, 3698-3706.

(94) Culotta, V.C.; Yang, M.; O'Halloran, T.V. *Biochim. Biophys. Acta.* **2006**, *1763*, 747-758.

(95) Field, L.S.; Furukawa, Y.; O'Halloran, T.V.; Culotta, V.C. *J. Biol. Chem.* **2003**, *278*, 28052–28059.

(96) Sturtz, L.A.; Diekert, K.; Jensen, L.T.; Lill, R.; Culotta, V.C. *J. Biol. Chem.* **2001**, *276*, 38084-38089.

(97) Strange, R. W.; Antonyuk, S. V.; Hough, M. A.; Doucette, P. A.; Valentine, J. S.; Hasnain, S. S. *J. Mol. Biol.* **2006**, *356*, 1152-1162.

(98) Djinovic, B. K.; Bolognesi, M. *J. Mol. Biol.* **1994**, *238*, 366–386.

(99) Perry, J.J.; Shin, D.S.; Getzoff, E.D.; Tainer, J.A. *Biochim. Biophys. Acta.* **2010**, *1804*, 245-262.

(100) Arnesano, F.; Banci, L.; Bertini, I.; Martinelli, M.; Furukawa, Y.; O'Halloran, T. V. *J. Biol. Chem.* **2004**, *279*, 47998-48003.

(101) Lindberg, M. J.; Normark, J.; Holmgren, A.; Oliveberg, M. *Proc. Natl. Acad. Sci. U.S.A.* **2004**, *45*, 15893-15898.

(102) Potter, S. Z.; Zhu, H.; Shaw, B. F.; Rodriguez, J. A.; Doucette, P. A.; Sohn, S. H.; Durazo, A.; Faull, K. F.; Gralla, E. B.; Nersissian, A. M.; Valentine, J. S. *J. Am. Chem. Soc.* **2007**, *129*, 4575-4583.

(103) Furukawa, Y.; Torres, A.S.; O'Halloran, T.V. *EMBO J.* **2004**, 23, 2872-2881.

(104) Wong, P.C.; Waggoner, D.; Subramaniam, J.R.; Tessarollo, L.; Bartnikas, T.B.; *Proc. Natl. Acad. Sci. U.S.A.* **2000**, *97*, 2886–2891.

(105) Schmidt, P.J.; Kunst, C.; Culotta, V.C. *J. Biol. Chem.* **2000**, *275*, 33771–33776

(106) Schmidt, P.J.; Rae, T.D.; Pufahl, R.A.; Hamma, T.; Strain, J. O'Halloran, T.V.; Culotta,V.C. *J. Biol. Chem.* **1999**, *274*, 23719-23725.

(107) Rae, T.D.; Torres, A.S.; Pufahl, R.A.; O'Halloran, T.V. *J. Biol. Chem.* **2001**, *276*, 5166-5176.

(108) Lamb, A.L.; Wernimont, A.K.; Pufahl, R.A.; Culotta, V.C.; O'Halloran, T.V. Rosenzweig, A.C. *Nat. Struct. Biol*. **1999**, *8*, 724-729.

(109) Lamb, A.L.; Wernimont, A.K.; Pufahl, R.A.; O'Halloran, T.V.; Rosenzweig, A.C. *Biochemistry* **2000**, *39*, 1589-1595.

(110) Lamb, A.L.; Torres, A.S.; O'Halloran, T.V.; Rosenzweig, A.C. *Nat. Struct. Biol.* **2001**, *8*, 751-755.

(111) Torres, A.S.; Petri, V.; Rae, T.D.; O'Halloran, T.V.; *J. Biol. Chem.* **2001**, *276*, 38410-38416.

(112) Lamb, A.L.; Torres, A.S.; O'Halloran, T.V.; Rosenzweig, A.C. *Biochemistry* **2000**, *39*, 14720-14727.

(113) Stasser, J.P.; Siluvai, G.S.; Barry, A.N.; Blackburn, N.J. *Biochemistry* **2007**, *46*, 11845-11856.

(114) Stasser, J.P.; Eisses, J.F.; Barry, A.N.; Kaplan, J.H.; Blackburn, N.J. *Biochemistry* **2005**, *44*, 3143-3152.

(115) Barry, A.N.; Clark, K.M.; Otoikhian, A.; van der Donk, W.A.; Blackburn, N.J. *Biochemistry* **2008**, *47*, 13074-13083.

(116) Brown, N.M.; Torres, A.S.; Doan, P.E. O'Halloran, T.V. *Proc. Natl. Acad. Sci. U. S. A.* **2004**, *101*, 5518-5523.

(117) Kawamata, H.; Manfredi, G.;.*Hum. Mol. Genet.* **2008**, *17*, 3303–3317.

(118) Reddehase, S.; Grumbt, B.; Neupert ,W.; Hell, K. *J. Mol. Biol.* **2009**, *385*, 331–338.

(119) Kloppel, C.; Suzuki, Y.; Kojer, K.; Petrungaro, C.; Longen, S.; Fiedler, S.; Keller, S.; Riemer, J. *Mol. Biol. Cell* **2011**, *20*, 3749-3757.

(120) Groß, D. P.; Burgard, C. A.; Reddehase, S.; Leitch, J. M.; Culotta, V. C.; Hell, K. *Mol. Biol. Cell* **2011**, *20,* 3758-3767.

(121) Subramaniam, J.R.; Lyons, W.E.; Liu, J.; Bartnikas, T.B.; Rothstein, J.; Price, D.L.; Cleveland, D.W.; Gitlin, J.D.; Wong, P.C. *Nat. Neurosci.* **2002**, *5*, 301-307.

(122) Kirby, K.; Jensen, L.T.; Binnington, J.; Hilliker, A.J.; Ulloa, J.; Culotta, V.C.; Phillips, J.P. *J. Biol. Chem.* **2008**, *283*, 35393-35401.

(123) Jensen, L.T.; Culotta, V.C. *J. Biol. Chem.* **2005**, *280*, 41373–41379.

(124) Leitch, J.M.; Jensen, L.T.; Bouldin, S.D.; Outten, C.E.; Hart, P.J.; Culotta, V.C. *J. Biol. Chem.* **2009**, *284*, 21863-21871.

(125) Carroll, M.C.; Girouard, J.B.; Ulloa, J.L.; Subramaniam, J.R.; Wong, P.C.; Valentine, J.S.; Culotta, V.C. *Proc. Natl. Acad. Sci. U.S.A.* **2004**, *101*, 5964-5969.

(126) Angeletti, B.; Waldron, K. J.; Freeman, K. B.; Bawagan, H.; Hussain, I.; Miller, C. C. J.; Lau, K.; Tennant, M. E.; Dennison, C.; Robinson, N. J.; Dingwall. C. *J. Biol. Chem.* **2005**, *280*, 17930-17937.

(127) Maynard, C. J.; Bush, A. I.; Masters, C. L.; Cappai, R.; Li, Q. *Int. J. Exp. Path.* **2005**, *86*, 147-159.

(128) Hardy, J. A.; Higgins, G. A. *Science* **1992**, *256*, 184-185.

(129) Horng, Y.C.; Cobine, P.A.; Maxfield, A.B.; Carr, H.S.; Winge, D.R. *J. Biol. Chem.* **2004**, *279*, 35334–35340.

(130) Beers, J.; Glerum, D.M.; Tzagoloff, A. *J. Biol. Chem.* **1997**, *272*, 33191–33196.

(131) Maxfield, A.B.; Heaton, D.N.; Winge, D.R. *J. Biol. Chem.* **2004**, *279*, 5072–5080

(132) Cobine, P.A.; Ojeda, L.D.; Rigby, K.M.; Winge, D.R. *J. Biol. Chem.* **2004**, *279*, 14447–14455.

(133) Cobine, P.A.; Pierrel, F.; Bestwick, M.L.; Winge, D.R. *J. Biol. Chem.* **2006**, *281*, 36552–36559.

Chapter 2

Binding Affinities of the CXXC and CXC Copper Binding Motifs of the Human Metallochaperone for Cu,Zn-Superoxide Dismutase[1]

The work presented in this Chapter has been published in the following article:

Allen, S.; Badarau, A.; Dennison, C. *Biochemistry* **2012**, 51, 1439-1448.

2.1   Introduction

The copper metallochaperone for Cu,Zn-superoxide dismutase; CCS in humans and Ccs1 in *S. cerevisiae,* is responsible for the activation of Cu,Zn-superoxide dismutase (designated SOD1 in humans and Sod1 in *S. cerevisiae*), the only currently known eukaryotic enzyme that acquires copper in the cytosol.(*1-11*) Activation of this enzyme not only involves the transfer of copper, but also the formation of an essential disulfide bond.(*9-11*) These are important reactions given that copper mis-handling is associated with a range of disorders,(*12-15*) including Alzheimer's disease (AD), and that mutations in SOD1, which can lead to misfolding, result in amyotrophic lateral sclerosis.(*14,15*) CCS and Ccs1 consist of a three domain structure (Figure 1.8B).(*3,6,7,16*) The N-terminal domain 1 (D1) has a βαββαβ-fold as found in the other cytosolic copper metallochaperone HAH1 (Atx1 in *S. cerevisiae*) that is involved in Cu(I) delivery to the secretory pathway.(*6,16-18*) HAH1 and D1 of CCS both bind Cu(I) via a CXXC motif. Domain 2 (D2) of the metallochaperone is structurally similar to the target enzyme (*16,19*) and is the main region of interaction between these partners.(*20*) CCS contains a Zn(II) site in D2 at the same location as that of SOD1 (*19*) which is absent in Ccs1.(*16*) The short C-terminal domain 3 (D3) contains a CXC Cu(I)-binding sequence. D3 of apo-Ccs1 is largely unstructured,(*16*) but some α-helical content is observed in the complex with Sod1, with the Cys residues of this domain ideally placed for copper insertion into the target enzyme.(*20*) Apo-CCS is a dimer whereas apo-Ccs1 is monomeric, with alterations in quaternary structure observed for both in the presence of Cu(I).(*3,21,22*) The transfer of metal to the target enzyme is thought to involve hetero-dimeric complexes (*20,21,23,24*) although a hetero-tetramer has also been suggested for CCS.(*22*)

The functional importance of the domains of CCS and Ccs1 has been studied *in vivo*. The CXXC motif of D1 of CCS is required for copper incorporation into SOD1.(*25*) In *S. cerevisiae* D1 is essential only under copper limiting conditions,(*3*) although it is required for optimal Ccs1 activity (Atx1 is also more important for copper transfer under limiting conditions(*26*)). Domain 3 is essential for Cu(I) transfer and disulfide formation in humans and *S. cerevisiae*.(*3,25*) Both of the Cu(I)-binding domains of CCS must play a role in Cu(I) transfer to SOD1, but the mechanism of this process is poorly understood. In particular, the details of the way in which the two domains containing the CXXC and CXC Cu(I)-binding motifs bind copper is lacking. As yet no detailed investigation into the metal binding stoichiometries and relative Cu(I)

affinities (K_b) of the of these two motifs has been performed. These are important biophysical parameters considering the events of copper binding and transfer between the D1 and D3 are crucial for the activity of the CCS. It has recently been reported that SOD1 has a 10-fold higher Cu(I) affinity than CCS loaded with 1 equivalent of Cu(I), providing a thermodynamic driving force for copper transfer.[27] However, no discrimination between Cu(I)-binding to the individual domains of CCS was made and therefore the roles of D1 and D3 in mediating what appears to be thermodynamically driven copper transfer from CCS to SOD1 have not been fully resolved.

A number of approaches for the determination of Cu(I) affinities for proteins involved in copper trafficking have led to insights into the mechanism of Cu(I) acquisition and transfer to target proteins (See chapter 3).[28,29] Direct approaches, such as the use of isothermal titration calorimetry, to determine K_b have been used, however, due to limitations in the techniques and the exceptionally high metal affinity of the copper metallochaperones ($K_b \sim 10^{17}$ M^{-1}) means that the values reported only represent lower limits of the metal affinity of the proteins.[29] Even at μM concentrations of protein the detection of the free metal is highly problematic. Therefore, the use of indirect equilibrium competition methods has become the technique of choice for accurate measurement of K_b values. In this approach, competition between a ligand (L) and the protein (P) for the metal (M) is used in order to determine K_b.

$$MP + 2L \quad \rightleftharpoons \quad ML_2 + P \qquad\qquad (2.1)$$

By varying only the concentration of either P or L and if ML_2 can be quantified by spectroscopic techniques the equilibrium concentrations of each species can be found. In addition, by considering the concentration of 'free' uncomplexed Cu(I) to be negligible, compared to that bound by the ligand and protein, the contribution of this species to the equilibrium can be ignored and therefore, in the absence of formation of protein-Cu(I)-ligand ternary complexes, a K_b value can be determined.[28,30] Bathocuproine disulfonate (BCS) and bicinchoninic acid (BCA) represent two chromophoric bi-dentate ligands that specifically bind Cu(I) in a tetrahedral CuL$_2$ complex and have been widely used to enable determination of Cu(I) K_b values by this and similar techniques.[31-35] BCA and BCS bind Cu(I) specifically with high affinity due to their preference for bis-chelate, tetrahedral coordination and their Cu(I)-bound complexes display characteristic

absorbance in the visible spectrum (λ_{max} of 562 and 483 nm respectively) and therefore represent ideal ligand probes for Cu(I).*(31)*

In this chapter a detailed investigation into Cu(I) binding by CCS is presented. Double Cys to Ser mutants of the CXXC and CXC motifs, in the full length protein, and D1 and D3 constructs have been prepared to allow the determination of Cu(I) binding stoichiometries and K_b values for D1 and D3 using the Cu(I) ligands BCS and BCA. In addition, the analysis of partitioning and transfer of Cu(I) between D1 and D3 has been performed to verify the determined K_b values. The K_b values of two related Cu(I) binding proteins HAH1 and the C-terminal domain of β-Secretase (BACE1), an enzyme involved in copper homeostasis and the development of AD (36), are also presented and highlight the interconnectivity of the copper trafficking pathways. Implications of the determined K_b values for D1 and D3 of CCS with regard to the mechanism of copper transfer from CCS to SOD1 are discussed.

Figure 2.1.1

Structures of the chromophoric Cu(I)-binding ligands BCS and BCA.

BCS   BCA
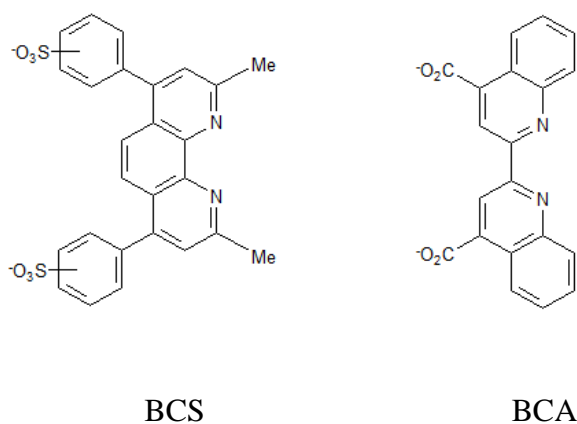
2.2   Experimental

2.2.1   Cloning and Mutagenesis

The gene for wild type (WT) CCS (pGEMT_WT-CCS) (see section 6.8) was cloned into pET29a via the Nde1/BamH1 sites giving pET29a_WT-CCS. The C22S/C25S-CCS and C244S/C246S-CCS mutations were prepared using Quikchange mutagenesis (Stratagene) and the primers listed in Table 2.2.1, giving pET29a_C22S/C25S-CCS and pET29a_C244S/C246S-CCS respectively. The DNA coding for residues 1-79 of CCS, corresponding to D1, was cloned (primers listed in Table 2.2.1), into the Nde1/BamH1 sites of pET29a to generate pET29a_D1-CCS. The gene for WT *S. cerevisiae* Ccs1 was cloned into pET29a using the Nde1/BamH1 sites of pET29a (pET29a_Ccs1) and the primers listed in Table 2.2.1.

2.2.2   Expression and Purification of Proteins

The proteins WT-CCS, C244S/C246S-CCS, C22S/C25S-CCS, D1-CCS and Ccs1 were expressed and purified as described in section 6.1. The protein HAH1 was provided by Dr Adriana Badarau.

2.2.3   The D3 and BACE1 C-Terminal Domain Peptides

The peptides GLFQNPKQICSCDGLTIWEERGRPIAGKGRKESAQPPAHL, which corresponds to D3 (Gly235 to Leu274) of CCS (D3-CCS), and CQWRCLRCLRQQHDDFADDISLLK, which corresponds to the cytoplasmic C-terminal domain (Cys478 to Lys501) of BACE1 (BACE1-CTD) (*36*) were purchased from GeneCust Europe (purity $\geq$ 95% and $\geq$ 90% respectively). The solid peptide, stored anaerobically, was dissolved directly in buffer immediately prior to use.

2.2.4   Protein Reduction and Quantification

Proteins (200-800 μM) were reduced by incubation with 10 mM DTT in 20 mM Tris pH 7.5 in an anaerobic chamber (Belle Technology, $O_2 \ll 2$ parts per million), typically for 2-3 h. These samples were desalted and exchanged into the required buffer using a PD10 column (GE Healthcare). Thiol quantification using 5,5'-dithiobis-(2-nitrobenzoic acid) (DTNB, Ellman's reagent) was routinely used for determining the concentration of D1-CCS (three thiols per monomer) which has little absorbance at 280 nm, and for the

assessment of the number of thiols in WT (WT-CCS), C244S/C246S (C244S/C246S-CCS) and C22S/C25S (C22S/C25S-CCS) CCS and Ccs1 as described in section 6.15. The concentrations of WT-CCS, C22S/C25S-CCS, C244S/C246S-CCS and Ccs1 were routinely determined using calculated ε values at 280 nm of 12,490 (CCS) and 30,940 (Ccs1) $M^{-1}cm^{-1}$.(*37*) Concentrations determined from Bradford assays (Coomassie Plus protein assay kit; Thermo Scientific) for WT-CCS, C22S/C25S-CCS and C244S/C246S-CCS using BSA standards required correction factors of 1.1-1.3 against values obtained using the absorbance at 280 nm. Bradford assays of D1-CCS using BSA standards required a correction factor of 1.5 compared to concentrations determined from Ellman's assays. A set of D1-CCS standards, whose concentrations were determined using DTNB, were also used for Bradford assays of mixtures of apo- and Cu(I)-D1-CCS.

The D3-CCS and BACE1-CTD peptides and HAH1 were quantified using DTNB assuming 2, 3 and 3 thiols, respectively. Bradford assays of D3-CCS using BSA standards required a correction factor of 1.7 compared to concentrations determined with DTNB (concentrations were approximately 20 % higher using a calculated (*37*) ε_{280} value of 5,500 M^{-1} cm^{-1} than those obtained from thiol quantifications). Reduction of the peptide with immobilized tris(2-carboxyethyl)phosphine gel (Thermo Scientific) overnight did not alter the thiol concentration. The concentration of the BACE1-CTD peptide determined using a calculated (*37*) ε_{280} of 5,500 M^{-1} cm^{-1} was within 10 % of that obtained from thiol quantification.

2.2.5   Cu(I) Binding Stoichiometries

High affinity Cu(I)-binding stoichiometries were performed as described in section 6.16.2. Titrations of Cu(I) into protein samples (10 μM) in the presence of 50-500 μM bicinchoninic acid (BCA) were performed in 20 mM Mes pH 6.5 or 20 mM Hepes pH 7.5, containing 200 mM NaCl.

2.2.6   Cu(I) Affinity Determinations

Cu(I) affinity (K_b) determinations were performed as described in section 6.16.3 except for those determined for WT-CCS, C22S/C25S-CCS, D3-CCS, Ccs1 and the BACE1-CTD. For WT-CCS, Ccs1 and BACE1-CTD competition experiments were performed only for titration of BCS and or BCA into the Cu(I)-protein. For D3-CCS, the apo-peptide was titrated into $[Cu(BCA)_2]^{3-}$ only. In all titrations equilibration for each point

was reached within 10 to 30 min, except for Cu(I) removal from C22S/C25S-CCS by BCA which required much longer. Therefore, mixtures containing different BCA concentrations and fixed amounts of Cu(I) and C22S/C25S-CCS were incubated for the required amount of time in the anaerobic chamber ($\leq$ 48 h). Titrations were performed in either 20 mM Mes pH 6.5 or 20 mM Hepes pH 7.5, in the presence of 200 mM NaCl (20 mM Hepes pH 7.5 plus 200 mM KCl for the BACE1-CTD peptide as precipitation was observed in the presence of NaCl).

2.2.7 Cu(I) Partitioning Assays

$[Cu(BCA)_2]^{3-}$ (1:2.5 Cu(I):BCA) was added to mixtures of D1-CCS plus either WT-CCS, C22S/C25S-CCS or C244S/C246S-CCS (100-200 μM of each) in 20 mM Mes pH 6.5 containing 150 mM NaCl (total volume 0.5 mL). The mixtures were incubated for up to 4 h, loaded onto a HiTrap Q HP anion exchange column (1 mL, GE Healthcare) pre-equilibrated in 20 mM Mes pH 6.5 containing 150 mM NaCl. D1-CCS did not bind to the column and WT-CCS, C22S/C25S-CCS and C244S/C246S-CCS were eluted with buffer plus 300 mM NaCl (2.0 mL fractions). The partitioning of Cu(I) (also supplied as $[Cu(BCA)_2]^{3-}$) between D1-CCS and D3-CCS (75 μM of each) was performed in 20 mM Mes pH 6.5 (total volume 0.5 mL). D3-CCS does not bind to the HiTrap Q column under these conditions whilst D1-CCS was eluted with buffer plus 150 mM NaCl (2.0 mL fractions). The protein concentrations in the fractions were determined using Bradford assays and checked, for D1-CCS only, by thiol quantification, and copper concentrations were measured with BCS and AAS. The partitioning of Cu(I) is expressed as an exchange equilibrium constant (K_{ex} value) for copper transfer from D1-CCS to CCS (either WT-CCS, C22S/C25S-CCS, C244S/C246S-CCS, or D3-CCS) according to equation (2.2);

$$K_{ex} = \frac{[apo-D1-CCS][Cu(I)-CCS]}{[Cu(I)-D1-CCS][apo-CCS]} \qquad (2.2)$$

in which [apo-D1-CCS] and [Cu(I)-D1-CCS] are the concentrations of apo- and Cu(I)-D1-CCS and [Cu(I)-CCS] and [apo-CCS] are the concentrations of the Cu(I)- and apo-forms of the partner protein (WT-CCS, C22S/C25S-CCS, C244SC246S-CCS or D3-CCS).

2.2.8 Cu(I) Transfer Assays

Cu(I) exchange between D1-CCS and C244S/C246S-CCS and C22S/C25S-CCS was performed by mixing Cu(I)–loaded protein with the partner apo-protein in 20 mM Mes pH 6.5 containing 150 mM NaCl (total volume 0.5 mL). The mixtures were incubated for up to 48 h, loaded onto a HiTrap Q HP anion column pre-equilibrated in the same buffer. Separation and quantification of protein and copper in fractions was performed as for the Cu(I) partitioning assays involving full length WT-CCS and Cys to Ser mutants. The equilibrium concentrations for each set of partner proteins K_{ex} was calculated using equation (2.3). Cu(I) exchange between D1-CCS and HAH1 was performed by mixing Cu(I)-loaded protein with the partner apo-protein in 20 mM Hepes pH 7.5 (total volume 1.0 mL). Mixtures were incubated for < 5 min prior to loading onto a HiTrap Q HP column pre-equilibrated in the same buffer. Buffer plus 100 and 200 mM NaCl were used to elute HAH1 and D1-CCS (apo- and Cu(I)-forms in both cases), respectively (2.0 mL fractions). The protein and copper content in fractions was determined by thiol quantification and AAS respectively, with K_{ex} calculated using eq (2.4):

$$K_{ex} = \frac{[Cu(I) - D1 - CCS][apo - HAH1]}{[apo - D1 - CCS][Cu(I) - HAH1]} \tag{2.3}$$

2.2.9 Cu(I) Removal from Cu(I)-Bound Proteins by BCA and BCS

Cu(I) removal from Cu(I)-C22S/C25S-CCS (20 μM) by BCA (500 μM) in 20 mM Mes pH 6.5 containing 200 mM NaCl was performed by measuring the increase in absorbance at 562 nm as a function of time to monitor the formation of the $[Cu(BCA)_2]^{3-}$ complex. Similar reactions were performed for Cu(I) removal from WT-CCS, C244S/C246S-CCS and C22S/C25S-CCS (20 μM) with 0.5 and 1.0 equivalents [and also 2.0 equivalents for WT-CCS] of bound Cu(I) by BCS (2.5 mM) in the same buffer, and the increase in absorbance at 483 nm measured to monitor formation of $[Cu(BCS)_2]^{3-}$. The reactions were initiated by injecting the appropriate amount of concentrated BCA or BCS, from a gas tight syringe (Hamilton), into a 1 ml septum sealed gas tight cuvette (Hellma) containing the Cu(I)-bound protein.

Table 2.2.1

Primers used for making the C244S/C246S-CCS and C22S/C25S-CCS mutants and cloning D1-CCS and Ccs1

Construct	Primer Sequence 5' to 3'
pET29a_C244S/C246S-CCS	CCAAGCAGATCTCCTCTTCCGATGGCCTCACC (Forward)
	GGTGAGGCC ATCGGAAGAGGAGATCTGCTTGG (Reverse)
pET29a_C22S/C25S-CCS	GCAGATGACCTCTCAGAGCTCTGTGGACGCG (Forward)
	CGCGTCCACAGAGCTCTGAGAGGTCATCTGC (Reverse)
pET29a_D1-CCS	GAACATAT*G*GCTTCGGATTCGGGGAAC (Forward)
	GAAGGATCCTCAGCCCATGCCCTTGAG (Reverse)
pET29a_Ccs1	GAAGGATCCCTATTTGATGTTGTTGGCCAAGGC (Forward)
	GAACATATGACCACGAACGATACATACGAGGC (Reverse)

2.3   Results

2.3.1   Purification and Initial Characterisation of Proteins

The purity of all final protein samples was determined by SDS-PAGE to be > 90 % and the molecular weights determined to be within 4 Da of expected values (Table 2.3.1). WT-CCS, C22S/C25S-CCS and C244S/C246S-CCS were isolated with 0.8 ± 0.2 zinc equivalents per monomer (protein concentrations determined using the ε_{280} value) and negligible copper. D1-CCS and Ccs1 were isolated with negligible zinc and copper. For reduced apo-samples the number of thiols, determined by Ellmans assay, ranged from 4.5-5.6, 2.4-3.3 and 3.5-4.6 for WT-CCS, C22S/C25S-CCS and C244S/C246S-CCS respectively (4.5-5.0 for Ccs1), based on protein concentrations determined from the absorbance at 280 nm. Using the Zn(II) concentrations, and assuming 1 Zn(II) per monomer for all proteins, gave 5.6-6.8, 3.3-4.6 and 4.4-5.8 thiols per Zn(II) ion, respectively. The number of thiols present in D1-CCS (used for protein concentration determination by Ellmans assay) was verified by a Cu(I)-binding stoichiometry of 1.0 Cu(I):D1-CCS (section 2.3.4).

2.3.2   CD Spectra

Far-UV CD spectra (Figure 2.3.1) show that the Cys to Ser mutations in the CXXC and CXC motifs of D1 and D3 respectively do not perturb the secondary structure of the proteins relative to WT-CCS. The far-UV CD spectrum of Ccs1 resembles that of CCS, as is expected due to the similar content of secondary structure elements, whilst that of D1-CCS is similar to those previously reported for HAH1 and related domains.(*38,39*)

2.3.3   Analytical Gel Filtration

Analytical gel filtration chromatography was used to determine the speciation of the proteins (see section 6.4) which demonstrates that, in the absence of Cu(I), WT-CCS and the Cys to Ser variants are all dimers, and D1-CCS is a monomer (Figure 2.3.2, Figure 2.3.3, Figure 2.3.4 and Table 2.3.2). D1-CCS and C244S/C246S-CCS remain monomeric and dimeric respectively upon the addition of 1 equivalent of Cu(I), while a mixture of dimeric and tetrameric forms are found for Cu(I)-WT-CCS and Cu(I)-C22S/C25S-CCS (Figure 2.3.3, Figure 2.3.5 and Table 2.3.2),(*22*) with tetramer formation favored by increasing the Cu(I):CCS ratio (Figures 2.3.3 and 2.3.5). Negligible amounts of tetrameric WT-CCS form below a Cu(I):CCS ratio of 0.5. The

tetrameric form of WT-CCS binds two Cu(I) ions per monomer, whilst only a single Cu(I) ion is bound per monomer in tetrameric C22S/C25S-CCS (Figure 2.3.6). Apo-Ccs1 is monomeric (Figure 2.3.2) as expected.(*3,21*)

2.3.4 Cu(I) Binding Stoichiometries

The high affinity Cu(I)-binding stoichiometry for WT-CCS, the Cys to Ser variants and D1-CCS was determined by titrating Cu(I) into the apo-proteins in the presence of BCA. WT-CCS binds two equivalents of Cu(I) tightly (Figure 2.3.7). C22S/C25S-CCS, C244S/C246S-CCS and D1-CCS all bind a single Cu(I) equivalent under the same conditions (Figure 2.3.7 B-D). For WT-CCS the first equivalent of Cu(I) is bound at a site with a much higher affinity than BCA (the affinity of the Cu(I) site in C244S/C246S-CCS and D1-CCS is also considerably tighter than that of BCA). The second Cu(I) equivalent binds to a lower affinity site in WT-CCS, similar to that seen for C22S/C25S-CCS. Similar results are obtained for pH 7.5 (Figure 2.3.8). Cu(I)-binding to WT-CCS, C244S/C246S-CCS and C22S/C25S-CCS was also monitored by measuring the increase in absorbance within the UV region and results showed that significant absorption occurred around 230-280 nm (Appendix A Figure 1). Increases in absorbance in the region of 265 nm are diagnostic of ligand to metal charge transfer involving thiol ligands bound to Cu(I) and in this case are attributed to Cu(I)-bound Cys residues in D1 and/or D3 of CCS. The Cu(I)-binding stoichiometry for Ccs1 (Figure 2.3.8) was almost identical to that obtained for WT-CCS, with one high affinity and one low affinity Cu(I)-binding sites. Cu(I)-binding stoichiometries for the D3-CCS and BACE1-CTD peptides were also determined (Figure 2.3.9) and show the binding of a single Cu(I) in each case. BACE1-CTD shows tight binding similar to that observed for D1-CCS and C244S/C246S-CCS whilst Cu(I)-binding to D3-CCS is weaker and compares favourably to that observed for C22S/C25S-CCS.

2.3.5 Cu(I) Binding Affinities

The K_b values for Cu(I)-binding to D1 and D3 were determined from competition titrations with BCS and BCA at pH 6.5 and 7.5. Experiments at pH 7.5 provide Cu(I) affinities that can be readily compared with literature values for related systems (typically measured at pH 7-8). Measuring affinities at pH 6.5 allows the same ligand (BCA) to be used for all proteins. The Cu(I) affinity for the first equivalent of Cu(I) bound to WT-CCS at pH 6.5 is $(4.4 \pm 1.0) \times 10^{16}$ M^{-1} (Figure 2.3.10) and almost identical values are found for C244S/C246S-CCS and D1-CCS (Figures 2.3.11 , 2.3.12

and Table 2.3.3). The Cu(I) affinities for these three proteins are also the same at pH 7.5, albeit the values are approximately 10-fold greater (Figures 2.3.10 to 2.3.12 and Table 2.3.3). The first equivalent of Cu(I) bound to Ccs1 from *S. cerevisiae* has a Cu(I) affinity of $(2.7 \pm 1.0) \times 10^{16}$ M^{-1} at pH 6.5, which increases $\sim$ 10-fold at pH 7.5 (Figure 2.3.13). Very similar K_b values were also obtained for the BACE1-CTD peptide at pH 7.5.

Fitting of the data for titrations of apo D1-CCS into $[Cu(BCA)_2]^{3-}$ and of BCA into Cu(I)-D1-CCS at pH 6.5 (Figure 2.2.14) allowed a mean β value for $[Cu(BCA)_2]^{3-}$ of $(5.4 \pm 2.7) \times 10^{16}$ M^{-2} to be determined from titrations in both directions using the K_b of D1-CCS determined using BCS. A β value of $(5.6 \pm 3.4) \times 10^{16}$ M^{-2} was obtained at pH 7.5 and therefore the Cu(I) affinity of BCA exhibits no dependence on pH in the range studied. These values are in good agreement with those determined previously at pH 7.0 and the value determined at pH 6.5 was therefore used for all subsequent K_b determinations using BCA (*28*). Cu(I) affinities of $(1.1 \pm 0.6) \times 10^{17}$ and $(0.9 \pm 0.5) \times 10^{17}$ M^{-1} were determined at pH 6.5 for WT-CCS and C244S/C246S-CCS, respectively, and the K_b value for the latter was 10-fold greater at pH 7.5 (Figures 2.3.15 and 2.3.16 and Table 2.3.3). The minor differences (2-3 fold) between the Cu(I) affinities for WT-CCS and C244S/C246S-CCS measured at both pH values with BCA and BCS (Table 2.3.3) are within the error of the determination of the β value for $[Cu(BCA)_2]^{3-}$ [$(5.4 \pm 2.7) \times 10^{16}$ M^{-2}. The Cu(I) affinity of C22S/C25S-CCS was determined to be $(2.9 \pm 1.7) \times 10^{16}$ M^{-1} at pH 6.5 and the K_b value, as in the case for C244S/C246S-CCS, also 10-fold greater at pH 7.5 (Figure 2.3.16 and Table 2.3.3). Similar K_b values are obtained for the D3-CCS peptide at both pH values (Figure 2.3.17 and Table 2.3.3).

2.3.6   Cu(I) Partitioning between CCS domains 1 and 3

Copper was added as $[Cu(BCA)_2]^{3-}$ to D1-CCS and either WT-CCS, C22S/C25S-CCS, C244S/C246S-CCS or D3-CCS. These mixtures were separated and copper partitioning, expressed as an equilibrium constant for Cu(I) exchange (K_{ex}), determined (Tables 2.3.4-2.3.7). In all cases these reactions are largely complete within minutes, indicating that Cu(I) equilibration from $[Cu(BCA)_2]^{3-}$ between domains is relatively fast (occurs within the dead time of the experiment which is approximately 2 min). The Cu(I) partitioning between D1-CCS and either WT-CCS or C244S/C246S-CCS gave average K_{ex} values 1.9 and 1.7 respectively. Partitioning between D1-CCS and either C22S/C25S-CCS or D3-CCS gave average K_{ex} values of 0.05 and 0.08 respectively that are consistent with the K_b values for the same partner proteins in section 2.3.5.

2.3.7 Cu(I) Transfer between CCS domains 1 and 3

Copper transfer between D1-CCS and either C244S/C246S-CCS or C22S/C25S-CCS at pH 6.5 was performed in both directions and K_{ex} values determined (Tables 2.3.8 and 2.3.9). The transfer of Cu(I) between D1-CCS and C244S/C246S-CCS in both directions, that is from D1-CCS to C244S/C246S-CCS and vice versa, was found to be almost complete within the dead time of the experiment (approximately 2 minutes), and gives K_{ex} values of similar to those obtained from the Cu(I) partitioning experiments. The Cu(I) transfer between D1-CCS and C22S/C25S-CCS was much slower and required significantly longer incubation periods. The transfer of Cu(I) from D1-CCS to apo-C22S/C25S-CCS was faster than that observed in the opposite direction, with transfer of Cu(I) from C22S/C25S-CCS to D1-CCS requiring incubation periods of ~48 hours (Table 2.3.9).

2.3.8 Cu(I) Transfer between D1-CCS and HAH1

Copper transfer was performed between D1-CCS and HAH1 at pH 7.5 and found to be complete within the dead time of the experiment (approximately 2 minutes). Copper transfer performed in both directions, from Cu(I)-D1-CCS to apo-HAH1 and Cu(I)-HAH1 to apo-D1-CCS, and gave a K_{ex} of 1.1 (Table 2.3.10), consistent with their independently determined K_b values of $(5.4 \pm 0.2) \times 10^{17}$ and $(9.3 \pm 0.1) \times 10^{17}$ M^{-1} respectively at pH 7.5 (experiments performed by by Dr Adriana Badarau). The K_{ex} values for Cu(I) transfer between D1-CCS and HAH1 are also similar to those obtained for the Cu(I) partitioning experiments between WT-CCS and C244S/C246S (Figure 2.3.11)

2.3.9 Cu(I) Removal from Cu(I)-Bound Proteins by BCA and BCS

Cu(I) transfer from Cu(I)-C22S/C25S-CCS to BCA is slow and for 20 μM Cu(I)-C22S/C25S-CCS in the presence of 500 mM BCA at pH 6.5 (Figure 2.2.18) equilibrium takes ~ 48 hours to be established. Cu(I) transfer to BCS from WT-CCS, C244S/C246S-CCS and C22S/C25S-CCS with various metal stoichiometries (Figure 2.2.18) was more convenient due to the higher β value of the $[Cu(BCS)_2]^{3-}$, compared to $[Cu(BCA)_2]^{3-}$, allowing for almost complete Cu(I) transfer to BCS. Cu(I) transfer from Cu(I)-WT-CCS was fast (~5 mins for ~95% transfer) for Cu(I):CCS ratios of ≤ 0.5 but significantly slower at ratios ≥ 1.0 (~15 mins for 90 % transfer). Cu(I) transfer from Cu(I)-

C244S/C246S-CCS to BCS up to Cu(I):CCS ratios of 1.0 were comparable to that observed for Cu(I)-WT-CCS $\leq$ 0.5. The Cu(I) transfer from 0.5 and 1.0 Cu(I)-bound C22S/C25S-CCS to BCS was slower than that observed for Cu(I)-WT-CCS at Cu(I):CCS ratios $\geq$ 1.0, taking up to ~60 minutes for ~90% transfer.

Table 2.3.1

Fourier transform ion cyclotron resonance (FT-ICR) and matrix assisted laser desorption ionization time of flight (MALDI-TOF) mass spectrometry (MS) data for purified proteins

protein	technique	experimental mass (kDa)	theoretical mass (kDa)
WT-CCS[a]	FT-ICR MS	28903.3	28907.4 (-Met)
244S/C246S-CCS[a]	FT-ICR MS	28873.3	28875.2 (-Met)
C22S/C25S-CCS[a]	FT-ICR MS	28871.3	28875.2 (-Met)
D1-CCS	FT-ICR MS	8215.1	8215.3 (-Met)
Ccs1[b,c]	MALDI-TOF MS	27195.5 (-Met) and 27328.7	27196.7 (-Met) and 27327.9

[a] Theoretical mass considers the presence of a disulfide in D2 of WT-CCS, C244S/C246S-CCS and C22S/C25S-CCS. [b] Ccs1 was purified as a mixture of full length and a truncated form missing the N-terminal Met residue. [c] Theoretical mass considers the presence of a disulfide in domain 1 of Ccs1.

Table 2.3.2

Elution volumes and apparent molecular weights for apo and Cu(I)-bound WT-CCS, C244S/C246S-CCS, C22S/C25S-CCS, D1-CCS and Ccs1 determined on a Superdex 75 10/300 GL column in 20 mM Mes pH 6.5 containing 200 mM NaCl.

protein	Cu(I):protein ratio	elution volume(s) ($\pm$ 0.1 ml)	apparent mass [a] (kDa)
WT-CCS	0	9.7	64 ($\pm$ 2)
WT-CCS	0.5	9.6, 8.6 (shoulder)	67 ($\pm$ 2), 100 ($\pm$ 4)
WT-CCS	1.0	9.7, 8.6	64 ($\pm$ 2), 100 ($\pm$ 4)
C244S/C246S-CCS	0	9.6	67 ($\pm$ 2)
C244S/C246S-CCS	1.0	9.7	64 ($\pm$ 2)
C22S/C25S-CCS	0	9.7	64 ($\pm$ 2)
C22S/C25S-CCS	0.5	9.7, 8.6	64 ($\pm$ 2), 100 ($\pm$ 4)
C22S/C25S-CCS	1.0	9.6, 8.6	67 ($\pm$ 2), 100 ($\pm$ 4)
D1-CCS[b]	0	13.5	14 ($\pm$ 0.5)
D1-CCS[b]	1.0	13.5	14 ($\pm$ 0.5)
Ccs1	0	11.7	29 ($\pm$ 1)

[a] The errors indicated for the apparent masses of proteins are deduced from the error in the measurement of the elution volumes and therefore will be significantly lower than the real error observed (see section 6.4). [b] The high apparent molecular weight of D1-CCS is expected to be caused by the asymmetrical dimensions of this protein.

Table 2.3.3

Summary of mean Cu(I) affinities (K_b Values) at pH 6.5 and 7.5

protein	pH	K_b (BCA)(M^{-1})	K_b (BCS)(M^{-1})
D1-CCS[a]	6.5	-	$(5.6 \pm 2.6) \times 10^{16}$
	7.5	-	$(5.5 \pm 3.5) \times 10^{17}$
WT-CCS[b]	6.5	$(1.1 \pm 0.6) \times 10^{17}$	$(4.4 \pm 1.0) \times 10^{16}$
	7.5	-	$(5.5 \pm 0.6) \times 10^{17}$
C244S/C246S-CCS[c]	6.5	$(0.9 \pm 0.5) \times 10^{17}$	$(4.6 \pm 2.5) \times 10^{16}$
	7.5	$(1.1 \pm 0.6) \times 10^{18}$	$(4.6 \pm 1.0) \times 10^{17}$
C22S/C25S-CCS[d]	6.5	$(2.9 \pm 1.7) \times 10^{15}$	-
	7.5	$(2.7 \pm 1.4) \times 10^{16}$	-
D3-CCS[e]	6.5	$(4.2 \pm 1.0) \times 10^{15}$	
	7.5	$(6.4 \pm 0.3) \times 10^{16}$	
Ccs1[b]	6.5	-	$(2.7 \pm 1.0) \times 10^{16}$
	7.5	-	$(2.4 \pm 0.5) \times 10^{17}$

[a] D1-CCS was used for the calculation of an overall formation constant (β) for [Cu(BCA)$_2$]$^{3-}$ (see section 2.3.5) and therefore K_b values using this ligand are not included. [b] Data only acquired from titrations of BCA and/or BCS into Cu(I)-protein. Titrations in this direction at pH 7.5 were only determined with BCS due to Cu(I) affinities being too high to be measured with BCA. [c] The K_b value at pH 7.5 using BCA was obtained only by titrating [Cu(BCA)$_2$]$^{3-}$ with apo-C244S/C246S-CCS. [d] Data from competition experiments with BCS are not included due to the possible formation of a BCS-Cu(I)-C22S/C25S-CCS complex. [e] From titrations of the apo-peptide into [Cu(BCA)$_2$]$^{3-}$ only.

Table 2.3.4

Exchange equilibrium constant determinations for Cu(I) partitioning from $[Cu(BCA)_2]^{3-}$ between a mixture of D1-CCS and WT-CCS

initial concentrations (µM)			equilibrium concentrations (µM)[b]				incubation	K_{ex}
Cu(I)[a]	D1-CCS	WT-CCS	Cu(I)-D1-CCS	D1-CCS	Cu(I)-WT-CCS	WT-CCS	time	
100	100	100	50	42	59	30	min[c]	1.7
100	100	100	55	62	50	33	min[c]	1.7
75	150	150	32	101	45	77	1 h	1.8
100	100	100	52	69	49	43	1 h	1.5
75	150	150	32	98	45	76	4 h	1.8

[a] Cu(I) is present as the $[Cu(BCA)_2]^{3-}$ complex prior to addition to the protein mixture [2.5 molar excess of BCA over Cu(I)]. [b] Concentrations corrected for dilutions. [c] Proteins were separated in approximately 2 min.

Table 2.3.5

Exchange equilibrium constant determinations for Cu(I) partitioning from $[Cu(BCA)_2]^{3-}$ between a mixture of D1-CCS and C244S/C246S-CCS

initial concentrations (µM)			equilibrium concentrations (µM)[b]				incubation time	K_{ex}
Cu(I)[a]	D1-CCS	C244S/C246S-CCS	Cu(I)-D1-CCS	D1-CCS	Cu(I)-C244S/C246S-CCS	C244S/C246S-CCS		
100	100	100	48	61	58	35	min[c]	2.1
100	100	100	42	46	51	31	1 h	1.8

[a] Cu(I) is present as the $[Cu(BCA)_2]^{3-}$ complex prior to addition to the protein mixture [2.5 molar excess of BCA over Cu(I)]. [b] Concentrations corrected for dilutions. [c] Proteins were separated in approximately 2 min.

Table 2.3.6

Exchange equilibrium constant determinations for Cu(I) partitioning from $[Cu(BCA)_2]^{3-}$ to a mixture of D1-CCS and C22S/C25S-CCS

initial concentrations (μM)			equilibrium concentrations (μM)[b]				incubation time	K_{ex}
Cu(I)[a]	D1-CCS	C22S/C25S-CCS	Cu(I)-D1-CCS	D1-CCS	Cu(I)-CCSC22/25S-CCS	C22S/C25S-CCS		
180	200	200	152	68	28	156	min[c]	0.08
75	100	200	58	44	16	140	min[c]	0.09
112	100	200	60	44	24	153	1 h	0.12
75	150	150	67	77	12	116	1 h	0.12
100	100	100	77	26	26	57	1 h	0.15
75	150	150	65	77	11	116	4 h	0.11

[a] Cu(I) is present as the $[Cu(BCA)_2]^{3-}$ complex prior to addition to the protein mixture [2.5 molar excess of BCA over Cu(I)]. [b] Concentrations corrected for dilutions. [c] Proteins were separated in approximately 2 min.

Table 2.3.7

Exchange equilibrium constant determination for Cu(I) partitioning from $[Cu(BCA)_2]^{3-}$ to a mixture D1-CCS and D3-CCS

initial concentrations (μM)			equilibrium concentrations (μM)[b]				incubation time	K_{ex}
Cu(I)[a]	D1-CCS	D3-CCS	Cu(I)-D1-CCS	D1-CCS	Cu(I)-D3-CCS	D3-CCS		
75	75	75	50	16	14	52	min[c]	0.09

[a] Cu(I) is present as the $[Cu(BCA)_2]^{3-}$ complex prior to addition to the protein mixture [2.5 molar excess of BCA over Cu(I)]. [b] Concentrations corrected for dilutions. [c] Proteins were separated in approximately 2 min.

Table 2.3.8

Exchange equilibrium constant determinations for Cu(I) exchange between D1-CCS and C244S/C246S-CCS

proteins	initial concentrations (μM)				equilibrium concentrations (μM)[a]				K_{ex}
	Cu(I)-D1-CCS	D1-CCS	Cu(I)-C244S/C246S CCS	C244S/C246S CCS	Cu(I)-D1-CCS	D1-CCS	Cu(I)-C244S/C246S CCS	C244S/C246S CCS	
Cu(I)-D1-CCS + C244S/C246S CCS (min[b])	75	25	0	100	36	62	48	56	1.5
Cu(I)-D1-CCS + C244S/C246S CCS (1 h)	75	25	0	100	28	57	42	48	1.8
Cu(I)-C244S/C246S-CCS + D1 CCS (min[b])	0	100	75	25	26	82	32	72	1.4
Cu(I)-C244S/C246S-CCS + D1 CCS (1 h)	0	100	75	25	23	78	27	66	1.4

[a] Concentrations corrected for dilutions. [b] Proteins were separated in approximately 2 min.

Table 2.3.9

Exchange equilibrium constant determinations for Cu(I) exchange between D1-CCS and C22S/C25S-CCS

proteins	initial concentrations (μM)				equilibrium concentrations (μM)[a]				K_{ex}
	Cu(I)-D1-CCS	D1-CCS	Cu(I)-C22S/C25S-CCS	C22S/C25S CCS	Cu(I)-D1-CCS	D1-CCS	Cu(I)-C22/C25S-CCS	C22S/C25S CCS	
Cu(I)-D1-CCS + C22S/C25S-CCS (min[b])	75	25	0	150	67	30	9	117	0.03
Cu(I)-D1-CCS + C22S/C25S -CCS (1 h)	75	25	0	150	53	32	10	109	0.06
Cu(I)-D1-CCS + C22S/C25S -CCS (4 h)	75	25	0	150	58	28	17	97	0.08
Cu(I)-C22S/C25S-CCS + D1-CCS (min[b])	0	100	75	75	23	67	65	56	3.4
Cu(I)-C22S/C25S-CCS + D1-CCS (1 h)	0	100	75	75	29	53	46	60	1.4
Cu(I)-C22S/C25S-CCS + D1-CCS (48 h)	0	100	75	75	59	41	24	103	0.16

[a] Concentrations corrected for dilutions. [b] Proteins were separated in approximately 2 min.

Table 2.3.10

Exchange equilibrium constant determinations for Cu(I) exchange between D1-CCS and HAH1

proteins	initial concentrations (μM)				equilibrium concentrations (μM)[a]				K_{ex}
	Cu(I)-HAH1	HAH1	Cu(I)-D1-CCS	D1-CCS	Cu(I)-HAH1	HAH1	Cu(I)-D1-CCS	D1-CCS	
Cu(I)-HAH1 + D1-CCS (min[b])	50	50	0	100	24	56	26	56	1.1
Cu(I)-D1-CCS + HAH1 (min[b])	0	100	50	50	24	58	26	66	0.95

[a] Concentrations corrected for dilutions. [b] Proteins were separated in approximately 2 min.

Table 2.3.11

Summary of K_{ex} values for Cu(I) partitioning between proteins at pH 6.5 and exchange between HAH1 and D1-CCS at pH 7.5

protein mixture	incubation time	K_{ex}	$K_{ex}^{calc\ a}$
apo-D1-CCS + apo-WT-CCS[b]	min[c]	1.7	1.9
	1 h	1.7	
	4 h	1.8	
apo-D1-CCS + apo-C244S/C246S-CCS[b]	min[c]	2.1	1.7
	1 h	1.8	
apo-D1-CCS + apo-C22S/C25S-CCS[b]	min[c]	0.09	0.05
	1 h	0.13	
	4 h	0.11	
apo-D1-CCS + apo-D3-CCS[b]	min[c]	0.09	0.08
Cu(I)-HAH1 + apo-D1-CCS	min[c]	1.1	0.58
Cu(I)- D1-CCS + apo- HAH1	min[c]	0.95	

[a] Calculated from the K_b values of the partner proteins using $K_{ex}^{calc} = K_b$ (WT-CCS,C244S/C246S, C22S/C25S-CCS or D3-CCS)$/K_b$ (D1-CCS) or $K_{ex}^{calc} = K_b$ (D1-CCS)$/K_b$ (HAH1). [b] Cu(I) was added as $[Cu(BCA)_2]^{3-}$ to a mixture of apo-proteins. [c] Proteins were separated in approximately 2 min.

Figure 2.3.1

CD spectra of apo-WT-CCS (blue line), apo-C22S/C25S-CCS (green), apo-C244SC246S-CCS (red), apo-D1-CCS (black) and apo-Ccs1 (magenta) (all 0.5 mg/ml) in 100 mM potassium phosphate pH 6.5.
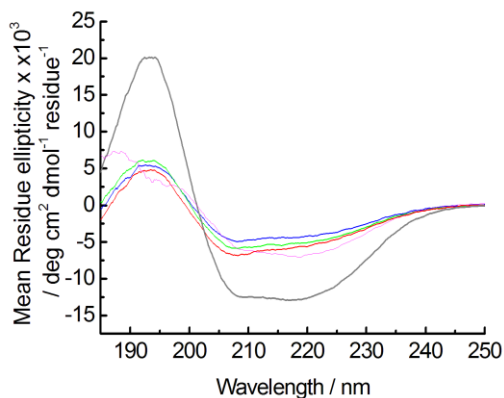
Figure 2.3.2

Gel filtration chromatograms for apo-WT-CCS (blue), apo-C22S/C25S-CCS (green), apo-C244SC246S-CCS (red), apo-D1-CCS (black) and apo-Ccs1 (magenta) (100 μM) in 20 mM Mes pH 6.5 containing 200 mM NaCl. Absorbance measured at 280 nm except for D1-CCS (240 nm) and the absorbance values for Ccs1 have been divided by 3. Elution volumes and apparent molecular weights listed in Table 2.3.2.

61

Figure 2.3.3

Gel filtration chromatograms for apo- (A) and Cu(I)-bound (0.5 (B) and 1.0 (C) equivalents) WT-CCS (100 μM) in 20 mM Mes pH 6.5 containing 200 mM NaCl, with absorbance measured at 280 nm. Protein eluting at ~ 9.7 ml (~ 64 kDa) correspond to dimer and those eluting at ~ 8.6 ml (~ 100 kDa) to tetramer.
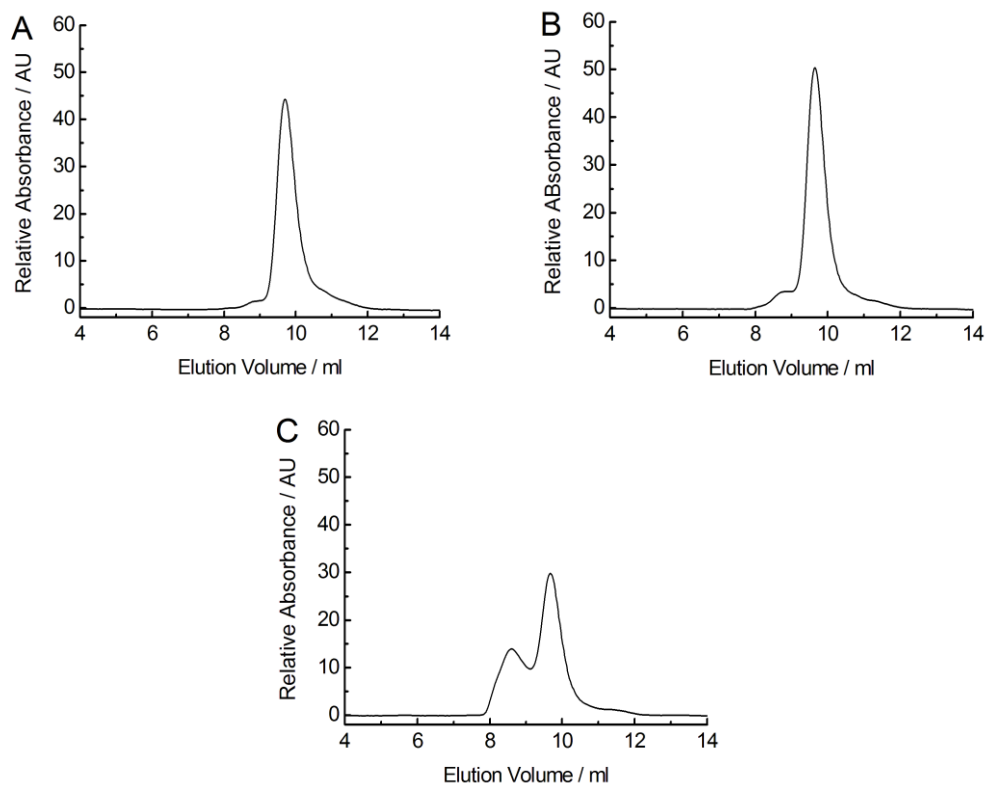
Figure 2.3.4

Gel filtration chromatograms for apo-C244S/C246S-CCS (A), apo-C22S/C25S-CCS (B) and Cu(I)-bound (1 equivalent) C244S/C246S-CCS (C) and (0.5 equivalent) C22S/C25S-CCS (D) (100 µM) in 20 mM Mes pH 6.5 containing 200 mM NaCl, with absorbance measured at 280 nm. Protein eluting at ~ 9.7 ml (~ 64 kDa) correspond to dimer and those eluting at ~ 8.6 ml (~ 100 kDa) to tetramer.
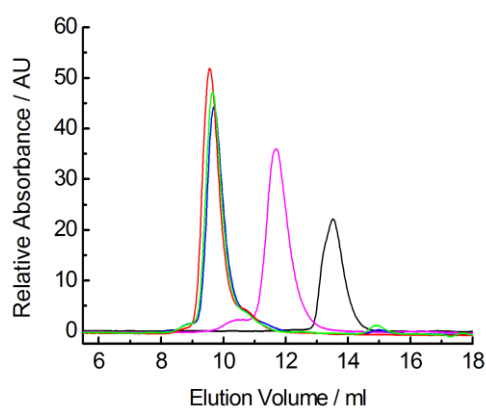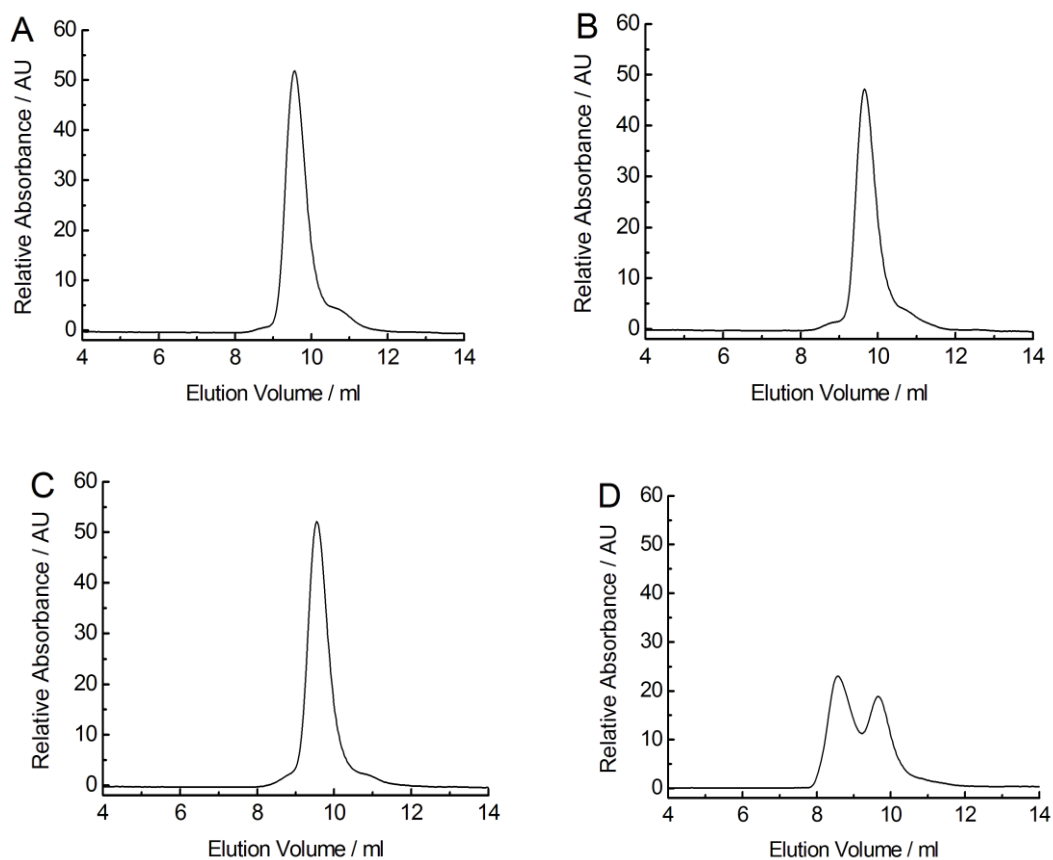
Figure 2.3.5

Gel filtration chromatograms for apo- (A) and Cu(I)-bound (0.5 (B) and 1.0 (C) equivalents) C22S/C25S-CCS (10 µM) in 20 mM Mes pH 6.5 containing 200 mM NaCl, with absorbance measured at 280 nm. Protein eluting at ~ 9.7 ml (~ 64 kDa) corresponds to dimer and that at ~ 8.6 ml (~ 100 kDa) to tetramer.
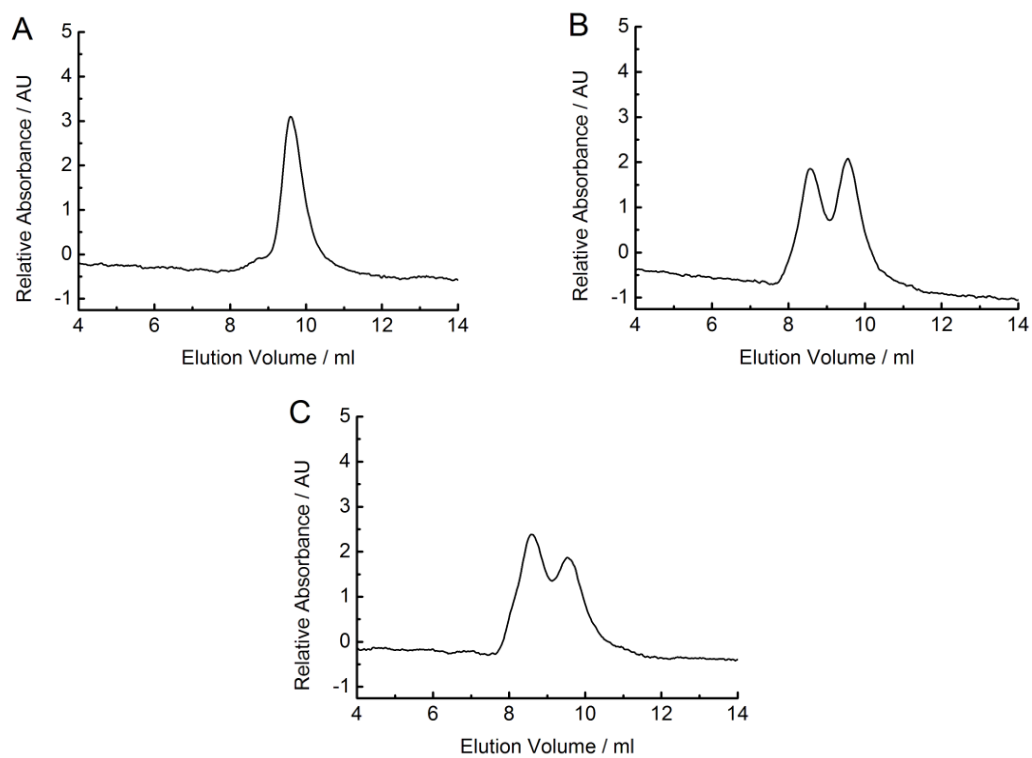
Figure 2.3.6

Gel filtration chromatograms of WT-CCS (200 μM Cu(I)-protein) (A) and C22SC25S-CCS (200 μM protein plus 100 μM Cu(I)) (B) in 20 mM Mes pH 6.5 containing 200 mM NaCl. Copper (□) and protein (○) content of tetrameric and dimeric, fractions 29-35 and 36-45 respectively, is shown in each case. The addition of 1.0 and 0.5 equivalents of Cu(I) to WT-CCS and C22SC25S-CCS respectively ensures partial Cu(I)-occupancy of the domain 3 site in both cases.
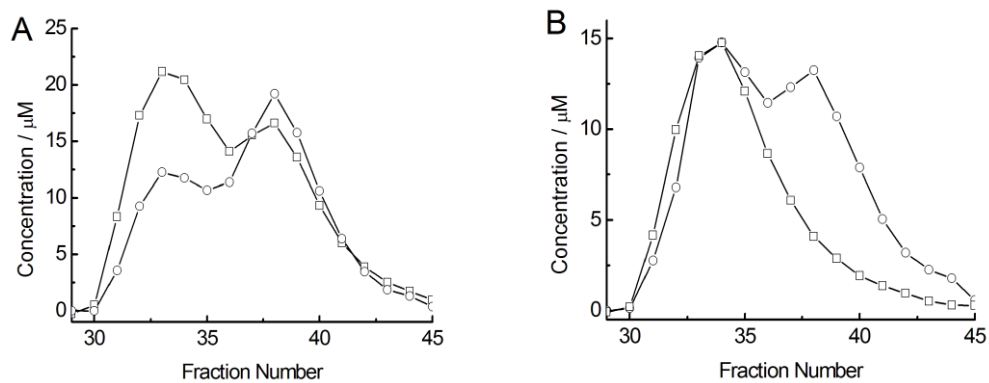
Figure 2.3.7

Titrations of Cu(I) into apo-WT-CCS (A), apo-C22S/C25S-CCS (B), apo-C244S/C246S-CCS (C) and apo-D1-CCS (D) (10 μM) in 20 mM Mes pH 6.5 containing 200 mM NaCl and 50 μM BCA.
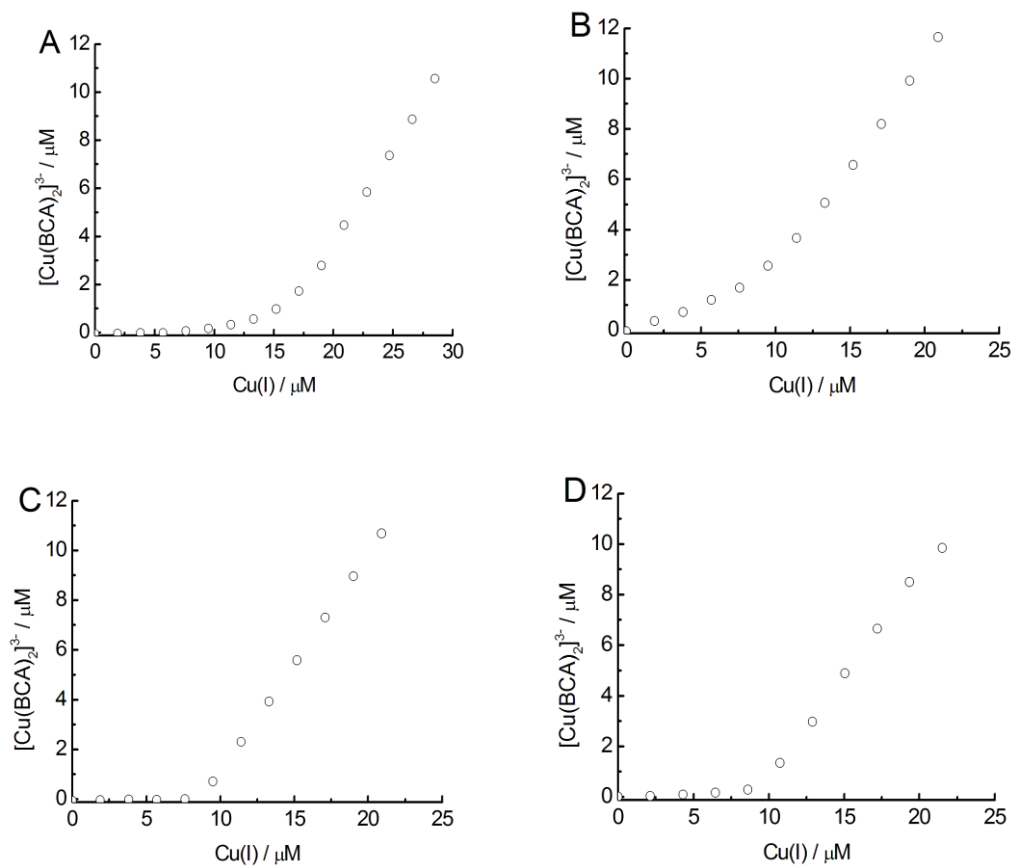
Figure 2.3.8

Titrations of Cu(I) into apo-WT-CCS (A), apo-C22S/C25S-CCS (B), apo-C244S/C246S-CCS (C) and apo-D1-CCS (D) (10 μM) in 20 mM Hepes pH 7.5 containing 200 mM NaCl and 500 μM BCA.
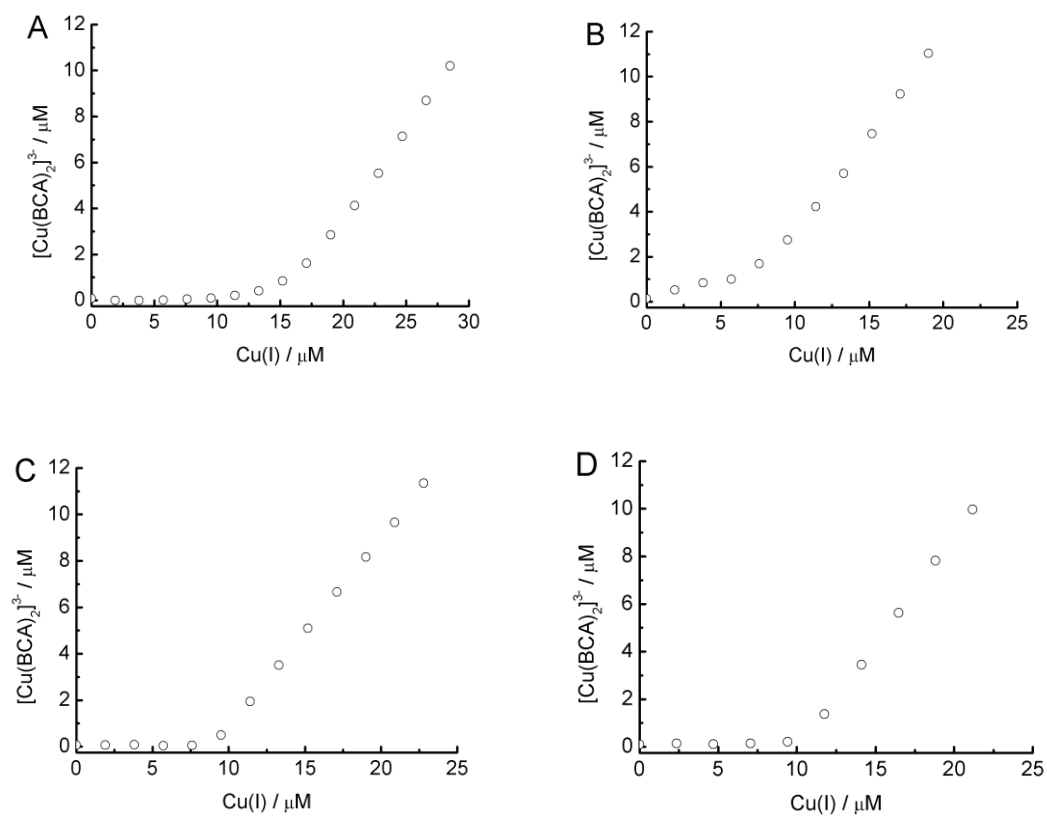
Figure 2.3.9

Titration of Cu(I) into apo-Ccs1 (10 μM) (A) in 20 mM Hepes pH 7.5 containing 200 mM NaCl and 500 μM BCA. Titration of Cu(I) into apo-D3-CCS (10 μM) (B) in 20 mM Mes pH 6.5 containing 200 mM NaCl and 30 μM BCA and apo-BACE1-CTD (10 μM) (C) in 20 mM Hepes pH 7.5 containing 200 mM NaCl and 500 μM BCA.

Figure 2.3.10

Titration of BCS into Cu(I)-WT-CCS (10 μM) plus excess apo-WT-CCS (10 μM) in 20 mM Mes pH 6.5 containing 200 mM NaCl is shown in (A). Titrations of BCS into Cu(I)-WT-CCS (5 μM) plus excess apo-WT-CCS (15 μM) (B) and Cu(I)-WT-CCS (10 μM) plus excess apo-WT-CCS (10 μM) (C) in 20 mM Hepes pH 7.5 containing 200 mM NaCl. Lines show fits of data, to equation (6.1), giving K_b values of $(5.4 \pm 0.2) \times 10^{16}$ (A), $(5.5 \pm 0.3) \times 10^{17}$ (B) and $(5.2 \pm 0.1) \times 10^{17}$ (C) M^{-1}.
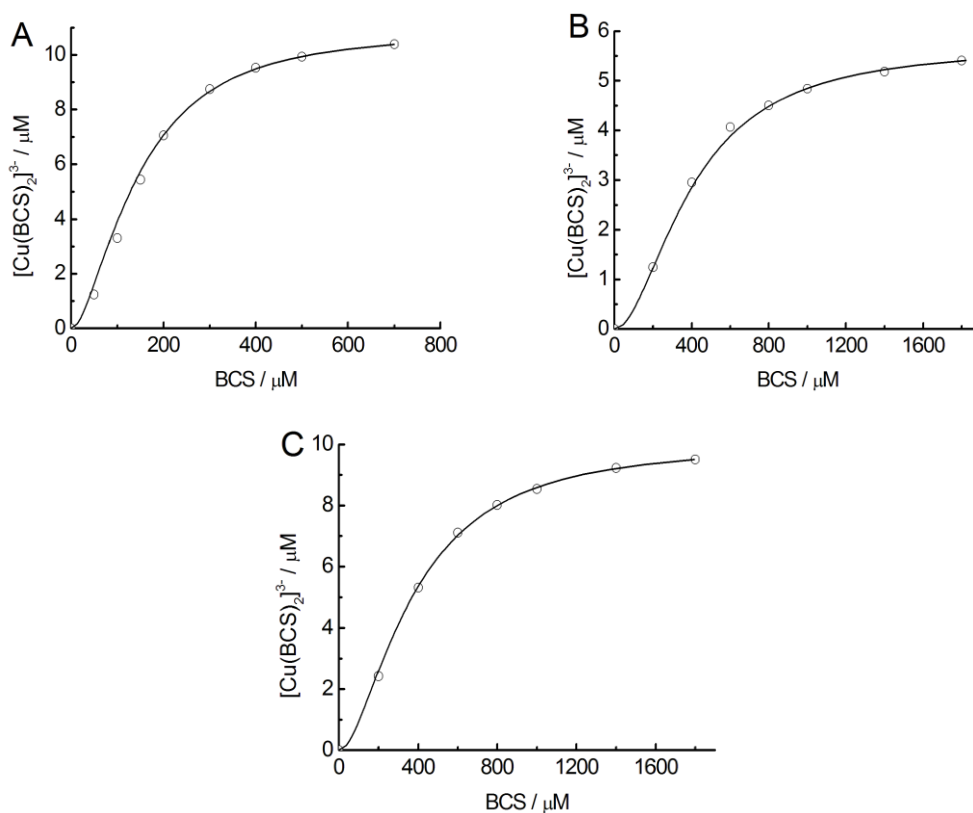
Figure 2.3.11

Titrations of apo-C244S/C246S-CCS into $[Cu(BCS)_2]^{3-}$ (10 µM) plus 20 µM at pH 6.5 (A) and plus 140 µM BCS at pH 7.5 (B), respectively. Titrations of BCS into Cu(I)-C244S/C246S-CCS (10 µM) plus apo-C244S/C246S-CCS (10 µM) at pH 6.5 (C) and pH 7.5 (D), respectively. Lines show fits of data, to equations (6.2) (A and B) and (6.1) (C and D), giving K_b values of $(5.0 \pm 0.4) \times 10^{16}$ (A), $(5.6 \pm 0.1) \times 10^{17}$ (B), $(5.5 \pm 0.1) \times 10^{16}$ (C) and $(4.4 \pm 0.2) \times 10^{17}$ M^{-1} (D).

Figure 2.3.12

Titrations of apo-D1-CCS into $[Cu(BCS)_2]^{3-}$ (10 μM) plus 5 μM at pH 6.5 (A) and plus 100 μM BCS at pH 7.5 (B), respectively. Titrations of BCS into Cu(I)-D1-CCS (10 μM) plus apo-D1-CCS (10 μM) at pH 6.5 (C) and pH 7.5 (D), respectively. Lines show fits of data, to equations (6.2) (A and B) and (6.1) (C and D), giving K_b values of $(4.1\pm 0.1) \times 10^{16}$ (A), $(6.3\pm 0.3) \times 10^{17}$ (B), $(6.0 \pm 0.1) \times 10^{16}$ (C) and $(4.8 \pm 0.2) \times 10^{17}$ (D) M^{-1}.
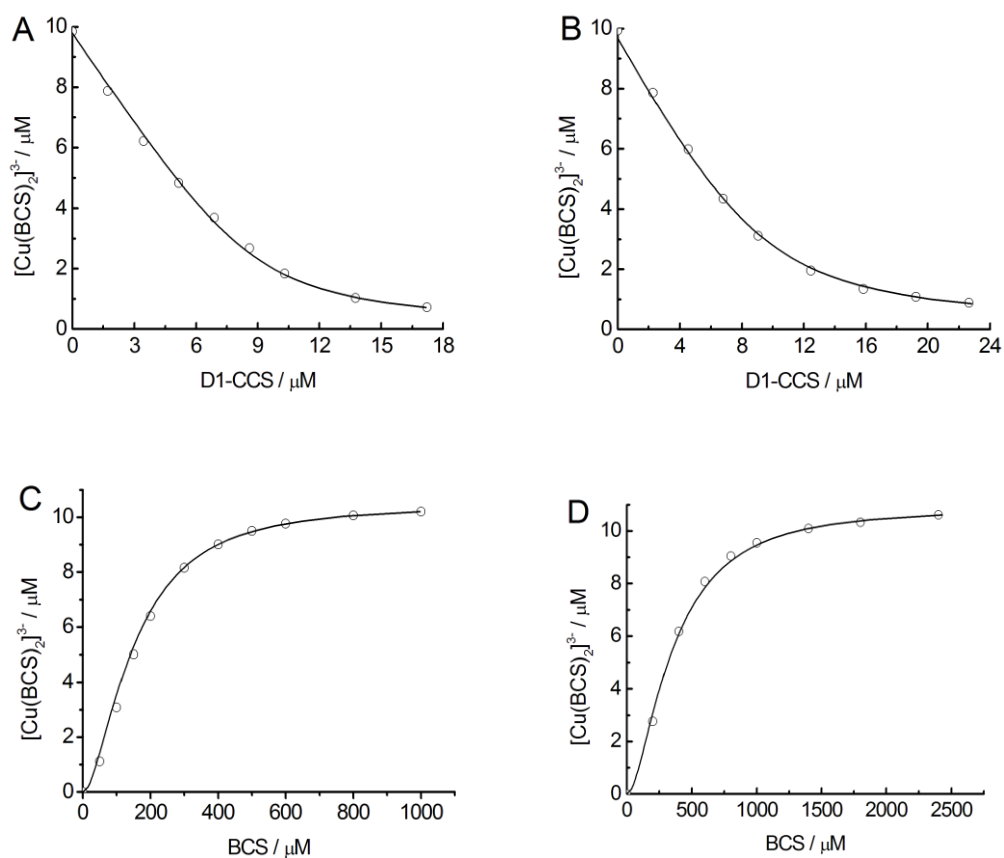
Figure 2.3.13

Titrations of BCS into Cu(I)-Ccs1 (10 μM) plus apo-Ccs1 (10 μM) at pH 6.5 (A) and pH 7.5 (B). Titration of BCS into Cu(I)-BACE1-CTD (10 μM) plus apo-BACE1-CTD (10 μM) at pH 7.5 is shown in (C). The lines show fits of the data to equation (6.1) giving K_b values of $(1.6 \pm 0.1) \times 10^{16}$ (A), $(2.8 \pm 0.1) \times 10^{17}$ (B) and $(1.8 \pm 0.1) \times 10^{17}$ M^{-1} (C).
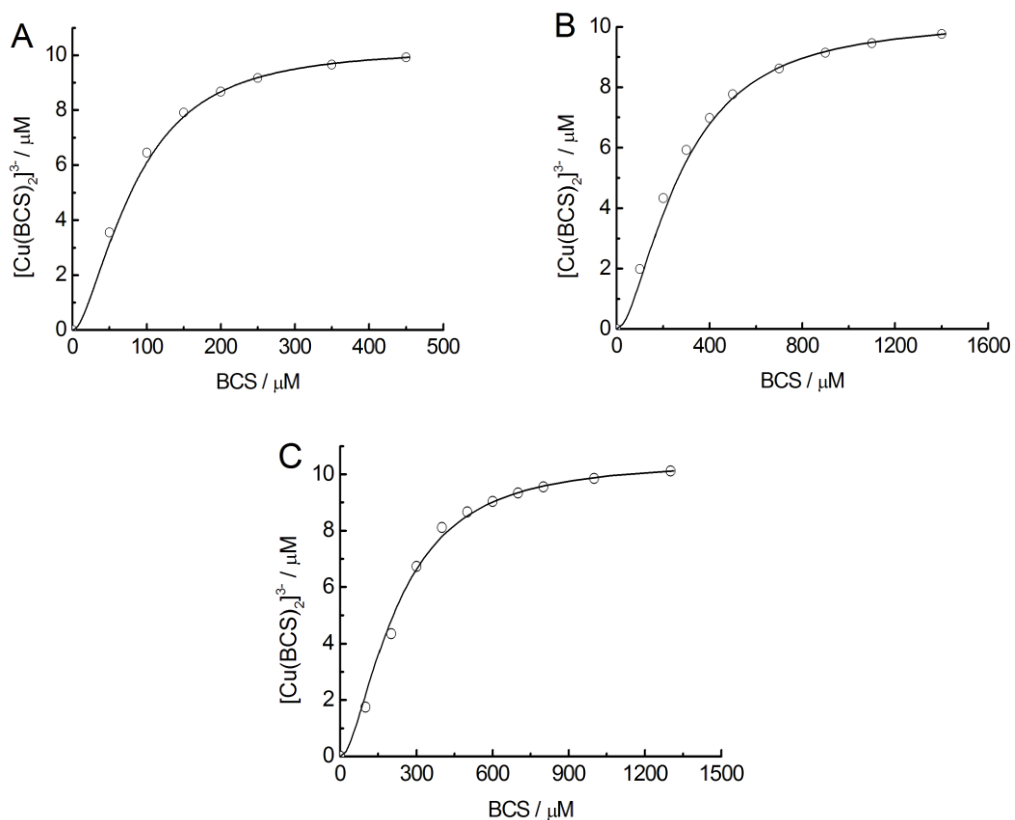
Figure 2.3.14

Titrations of apo-D1-CCS into $[Cu(BCA)_2]^{3-}$ (10 μM) plus 1580 μM at pH 6.5 (A) and plus 7480 μM BCA at pH 7.5 (B), respectively. The titration of BCA into Cu(I)-D1-CCS (5 μM) plus excess apo-D1-CCS (5 μM) at pH 6.5 is shown in (C). The lines show fits of the data, to equations (6.2) (A and B) and (6.1) (C), with K_b kept constant (5.6×10^{16} and 5.5×10^{17} M^{-1} at pH 6.5 and 7.5, respectively) giving β values for $[Cu(BCA)_2]^{3-}$ of $(5.3 \pm 0.2) \times 10^{16}$ (A) and $(5.7 \pm 0.1) \times 10^{16}$ (C) M^{-2} at pH 6.5 and $(5.9 \pm 0.2) \times 10^{16}$ M^{-2} at pH 7.5 (B).
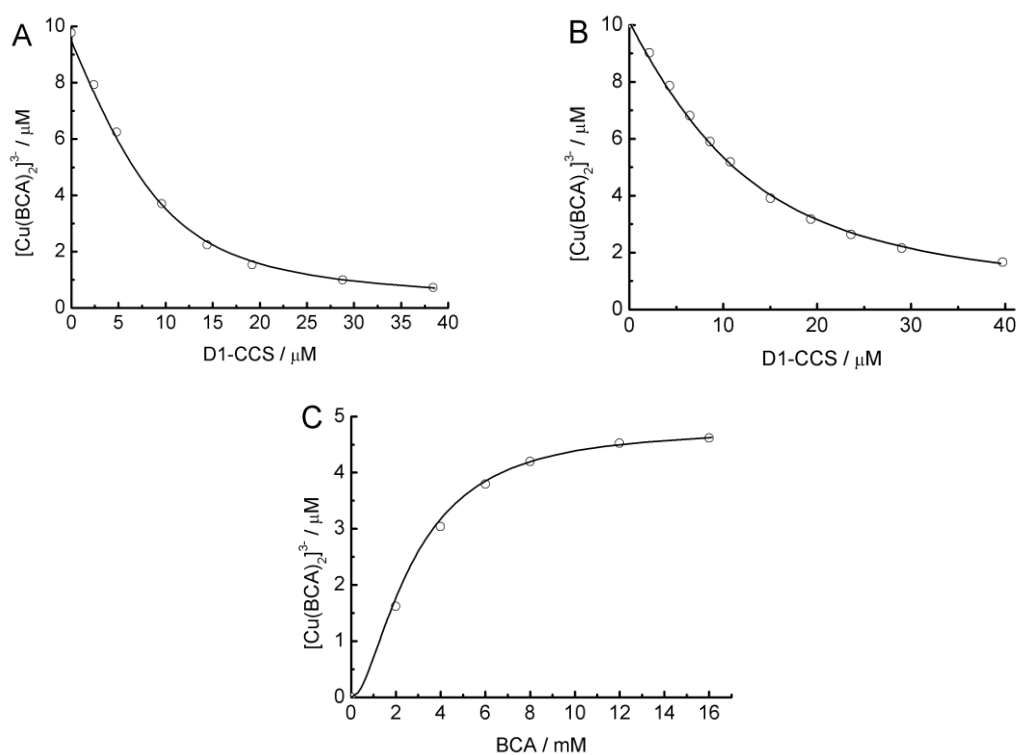
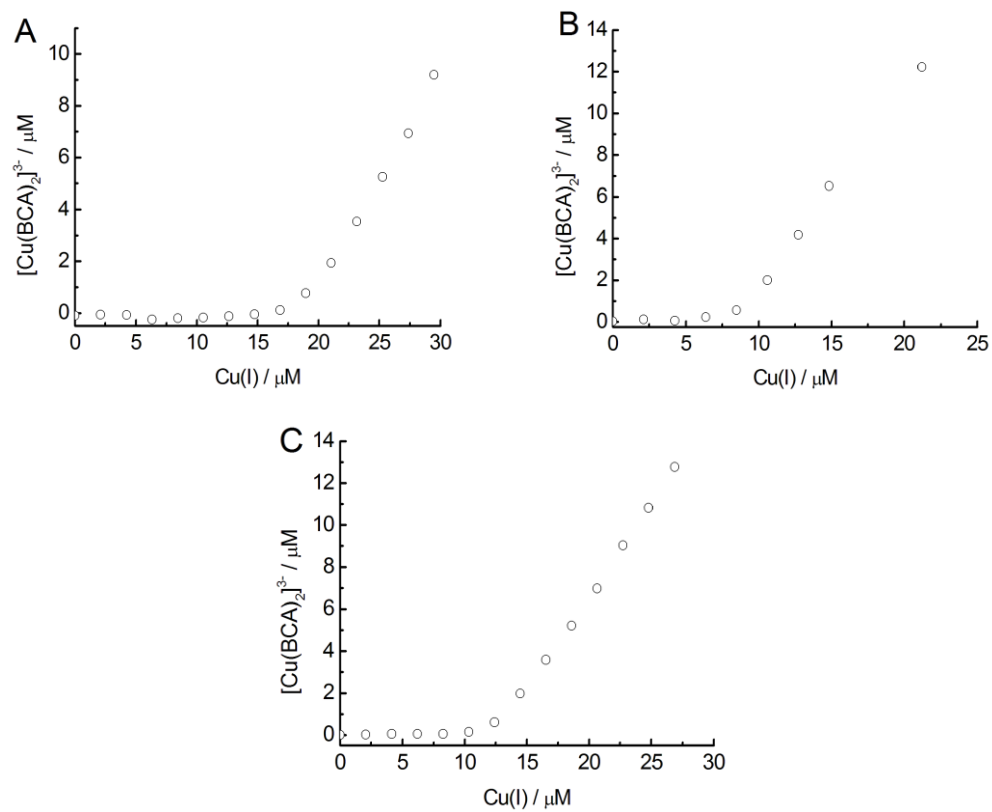**Figure 2.3.15**

Titration of BCA into Cu(I)-WT-CCS (5 µM) plus apo-WT-CCS (15 µM) 20 mM Mes pH 6.5 containing 200 mM NaCl. Line shows fit of data, to equation (6.1) giving a K_b value of $(8.9\pm 0.9) \times 10^{16}$ M^{-1}.
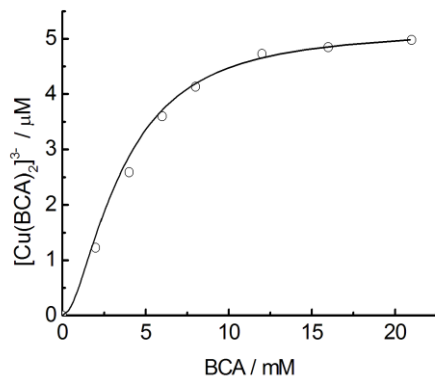
Figure 2.3.16

Titrations of apo-C244S/C246S-CCS (A) and apo-C22S/C25S-CCS (B) into $[Cu(BCA)_2]^{3-}$ (10 μM) in the presence of 1180 and 140 μM BCA respectively. Titrations of BCA into Cu(I)-C244S/C246S-CCS (5 μM) plus apo-C244S/C246S-CCS (5 μM) (C) and Cu(I)-C22S/C25S-CCS (10 μM) plus apo-C22S/C25S-CCS (10 μM) (D). All titrations were performed in 20 mM Mes pH 6.5 plus 200 mM NaCl. The lines show fits of the data to equations (6.2) (A and B) and (6.1) (C and D), giving K_b values of $(8.8 \pm 0.6) \times 10^{16}$ (A), $(2.2 \pm 0.6) \times 10^{15}$ (B), $(1.0 \pm 0.1) \times 10^{17}$ (C) and $(3.0 \pm 0.4) \times 10^{15}$ M^{-1} (D).
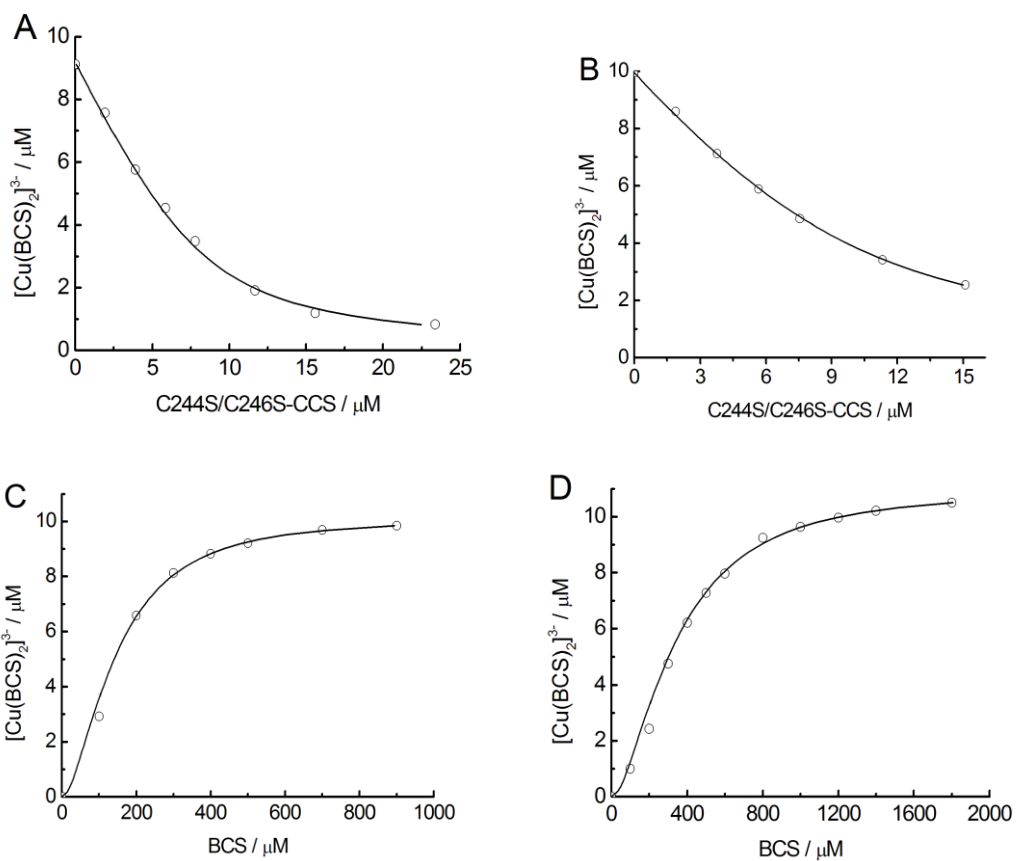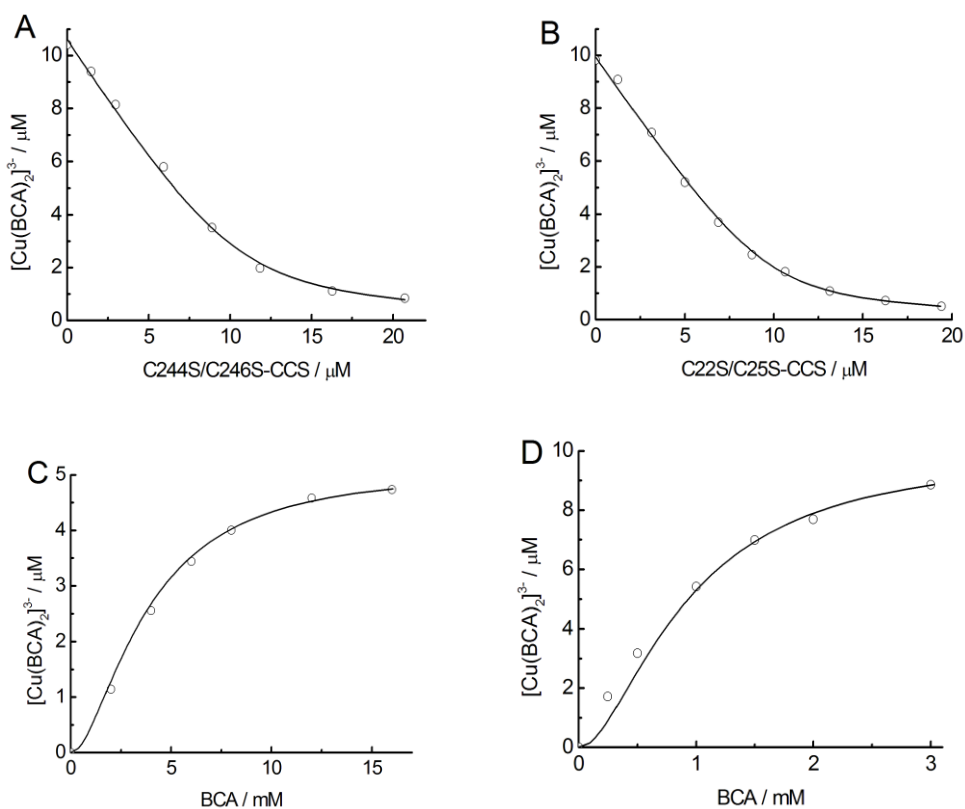
Figure 2.3.17

Titrations of apo-D3-CCS into $[Cu(BCA)_2]^{3-}$ (10 μM) plus 340 μM (A) and plus 1980 μM BCA (B) in 20 mM Mes pH 6.5 and 20 mM Hepes pH 7.5 containing 200 mM NaCl, respectively. Lines show fits of data, to equations (6.2) giving K_b values of (5.0± 0.4) × 10^{15} (A) and (4.4 ± 0.3) × 10^{16} M^{-1} (B).
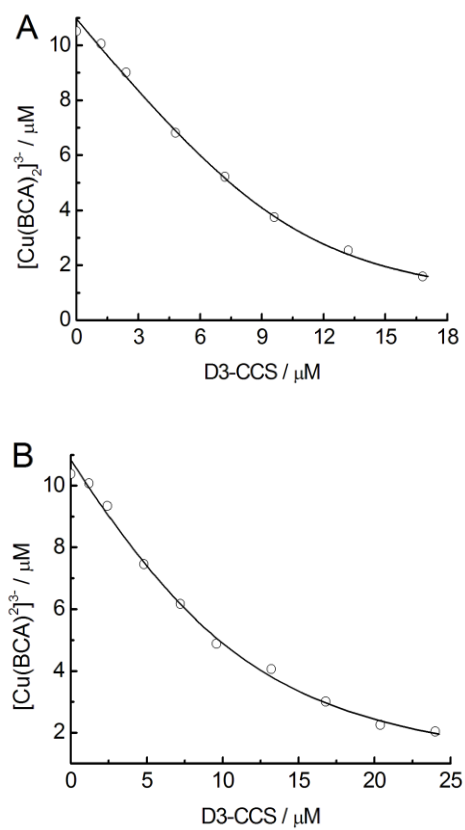
Figure 2.3.18

Cu(I) removal from Cu(I)-C22S/C25S-CCS (20 μM) by BCA (500 μM) in 20 mM Mes pH 6.5 containing 200 mM NaCl (A). Cu(I) removal from Cu(I)-bound (0.5 (solid), 1.0 (dot) and 2.0 (dash) equivalents) WT-CCS (B), C244S/C246S-CCS (C) and C22S/C25S-CCS (D) (10 μM) in 20 mM Mes pH 6.5 containing 200 mM NaCl and 2.5 mM BCS. The final point in (A) gives a K_b value of 3.9×10^{15} M^{-1}.
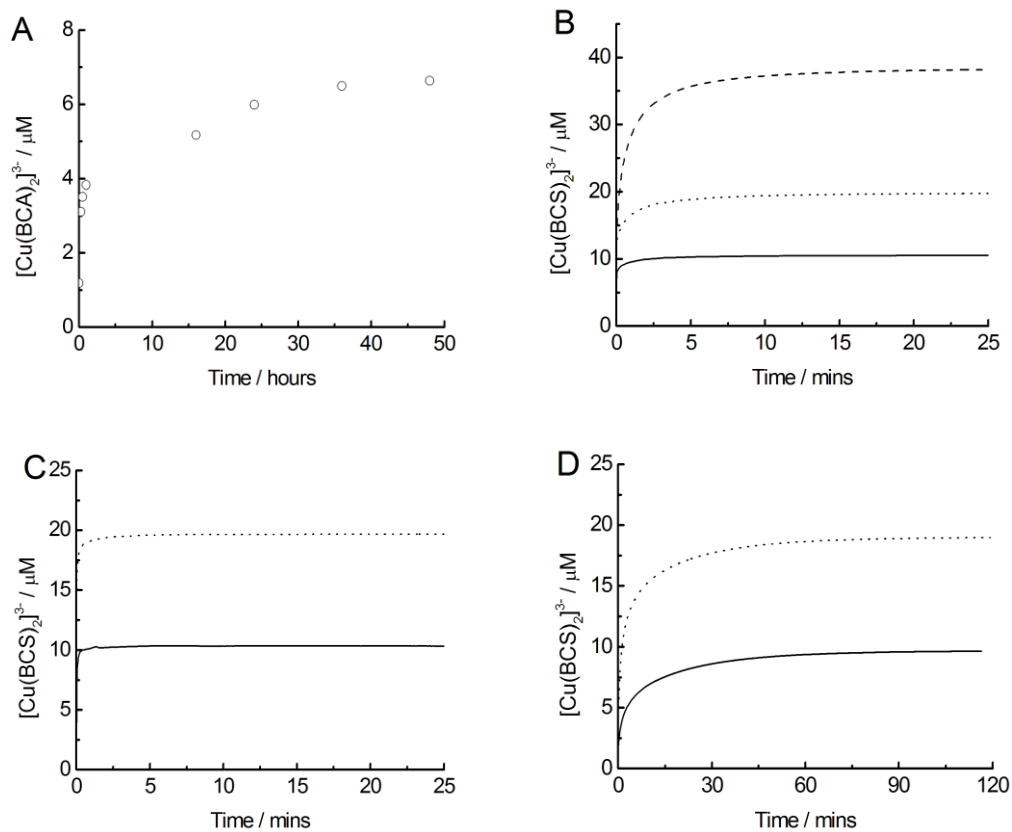
2.4   Discussion

The affinities measured for WT-CCS (first copper equivalent), C244S/C246S-CCS and D1-CCS must be for Cu(I) bound to the CXXC motif of D1, with the pH dependence due to protonation of the Cys ligands (see chapter 3).(*28)* The data for C244S/C246S-CCS highlight that the loss of the Cys residues in D3 does not affect the binding of Cu(I) to D1 of CCS, therefore D1 binds Cu(I) independently of D3. The first equivalent of Cu(I) bound to Ccs1 from *S. cerevisiae* has a similar affinity to D1 of CCS at pH 6.5, and the Cu(I) affinity has a similar dependence on pH as that for D1 for CCS and therefore, presumably, involves the CXXC site of D1. These Cu(I) affinities are in the same range as values reported for the CXXC-containing copper metallochaperones elsewhere for HAH1 (*28,32*) Atx1 (*S. cerevisiae* and *Synechocystis* PCC 6803),(*30,33*) CopZ (*B. subtilis*),(*34*) and also to that for the BACE1-CTD peptide which also contains a CXXC motif. The Cu(I) affinities determined for C22S/C25S-CCS and D3-CCS are very similar and must be for Cu(I) bound to the CXC motif of D3. The Cu(I) affinities for C22S/C25S-CCS and D3-CCS are both an order of magnitude lower than those for the CXXC of D1 both at pH 6.5 and 7.5 and therefore, the CXC motif in D3 is a significantly lower affinity copper site compared to D1.

The K_{ex} values for Cu(I) partitioning and transfer between the proteins are in good agreement with those calculated based on Cu(I) affinities. The K_{ex} for Cu(I) partitioning between D1-CCS and C244S/C246S-CCS, and also between D1-CCS and WT-CCS, is consistent with the CXXC site having similar Cu(I) affinities in these proteins. The K_{ex} for Cu(I) partitioning between D1-CCS and C22S/C25S-CCS, and also between D1-CCS and D3-CCS, confirms that the CXC motif of D3 has a Cu(I) affinity at least 10-fold lower than that of the D1 CXXC site.

The high Cu(I) affinity of D1, compared to D3, suggests that the Atx1-like domain of CCS must be involved in the acquisition and protection of Cu(I). A pool of copper exists in the eukaryotic cytosol,(*2,27,41*) and the matched Cu(I) affinities of CCS (D1) and HAH1, and of Ccs1 (D1) and Atx1 (although the K_b of Ccs1 determined here at pH 7.5 indicates a slightly weaker affinity for Cu(I) compared to reported values for Atx1 of 5.0×10^{17} M^{-1} and 1.6×10^{18} M^{-1} at pH 7.0 and 8.0 respectively (*32,33*)), along with similar protein levels (quantified in *S. cerevisiae* (*2,42*)) demonstrates that thermodynamically these metallochaperones can compete for available copper. It has been suggested that CCS and HAH1 may obtain Cu(I) from the same location in the

78

cytosol, possibly the high affinity copper importer Ctr1.(*43*) However, *in vivo* studies in *S. cerevisiae* have indicated that Ccs1 and Atx1 do not acquire copper directly from metal transporters,(*44*) although Ctr1-bound copper can be transferred to Atx1 *in vitro*.(*33*) The surface properties, particularly in the vicinity of the CXXC motifs, differ between these two copper metallochaperones, and *in vivo* complementation assays in *S. cerevisiae* demonstrate that D1 of Ccs1 and Atx1 are not interchangeable,(*3*) highlighting the importance of protein interactions for copper trafficking pathways.(*45*) The altered surface features of these two copper metallochaperones reflect very different targets; Atx1 interacts with the copper-transporting ATPase Ccc2 whereas Ccs1 delivers directly to a copper-requiring enzyme. A similar situation may exist for HAH1 and CCS as comparison of the surface features of HAH1 with D1-CCS (Figure 2.4.1) shows that D1 of CCS lacks the positively charged surface patch near the CXXC motif. It remains to be discovered from where these metallochaperones acquire copper.

The transfer of copper observed between D1-CCS and HAH1 suggests these copper trafficking pathways can equilibrate via the metallochaperones, with the availability of, and copper uptake by, SOD1 and the copper-transporting ATPases being factors that will favor passage of the metal down either route. In support of this idea, it has recently been shown that macrophage cells exposed to hypoxia respond by increasing copper flow to the secretory pathway via enhanced expression of ATP7A, with a resulting decrease in SOD1 activity.(*46*) This is accompanied by a lowering of the expression levels of CCS, signifying that a link between the secretory and cytosolic copper trafficking pathways does exist. Furthermore recent studies have shown that mouse fibroblasts with a CCS deletion result in increased expression of metallothionein and ATP7A with a concomitant reduced expression of the Ctr1 copper importer.(46) Copper allocation in a cell is particularly important considering that copper metabolism has been associated with neurodegenerative disorders, including AD.(*12-15*) BACE1 catalyses the first step in the processing of the amyloid precursor protein to yield Aβ, a major constituent of senile plaques in the brains of AD patients. It has been shown, by two-hybrid assays, that the BACE1-CTD can interact with D1 of CCS (*28*) and also HAH1 (*47*), and Cu(I) binding to BACE1 may modulate the production of Aβ.(*28*) The Cu(I) affinity of the BACE1-CTD is weaker than those of D1-CCS and HAH1, which will decrease competition with the metallochaperones for cytosolic copper under equilibrium conditions.

The CXXC motif of D1 of Ccs1 is ~ 35 Å from the copper site of Sod1 in the crystal structure of the complex (Figure 1.8B), whereas the D3 Cys residues are ideally placed for shuttling Cu(I) to the buried active site.(*20*) The D3 CXC motif is also involved in disulfide bond formation during the CCS activation of SOD1.(*9-11*) The mechanism of activation of this enzyme appears to differ in humans and *S. cerevisiae*, and a CCS-independent pathway of SOD1 activation exists in humans.(*49-51*) In certain organisms the D1 CXXC motif is missing, and CCS can still activate SOD1 under copper replete conditions.(*51,52*) In *S. cerevisiae* D1 is only essential under copper deplete conditions,(*3*) but it has clearly been shown for human CCS that D1 and the CXXC motif are essential for SOD1 activity *in vivo* under both copper replete and limiting conditions.(*25*) The Cu(I) affinities that have been determined demonstrate that when CCS docks with SOD1, particularly under copper-limiting conditions, copper is much more likely to be bound to D1 (Figure 2.4.2), which is probably also the case for Ccs1. Copper loading of SOD1 by CCS will require metal bound at D1 to be transferred to D3, which is thermodynamically unfavorable. However, the relative Cu(I) affinity of SOD1(*27*) is ~ 10-fold tighter than that of D1 of CCS, and therefore > 100-fold tighter than the Cu(I) affinity of D3. Two-coordinate Cu(I) bound to the D1 CXXC site will be co-ordinatively unsaturated and susceptible to attack from another ligand,(*6,7,17,39,45,53,54*) such as a Cys residue from D3, facilitating Cu(I) transfer via ligand exchange reactions. Cu(I) transfer does occur *in vitro* between D1 and D3, and the Cu(I) affinity and buried nature of the SOD1 copper site may drive the reaction. The ability of the largely unstructured D3 to access the active site of the target enzyme and insert copper seems to be more important than its affinity for Cu(I). Currently known copper metallochaperones usually either traffic copper or insert the metal into the target enzyme.(*7,27,55*) CCS has evolved to possess both of these functionalities providing an entropic advantage for copper uptake by SOD1, due to the vital role of this enzyme in maintaining a healthy cell.

Figure 2.4.1

Qualitative representation of the electrostatic surface properties surrounding the CXXC Cu(I)-binding motifs for D1-CCS (A) (from section 3.3.4) and HAH1 (B) (PDB accession code 1TL5 (HAH1)) drawn in Pymol. The surfaces of the proteins are color coded according to the electrostatic potential (red is negative, white is zero and blue is positive) with the positions of the Cys residues of the CXXC motifs and Arg71 and Lys60 residues of D1-CCS and HAH1 respectively, indicated. Surface generated in Pymol using protein contact potential.
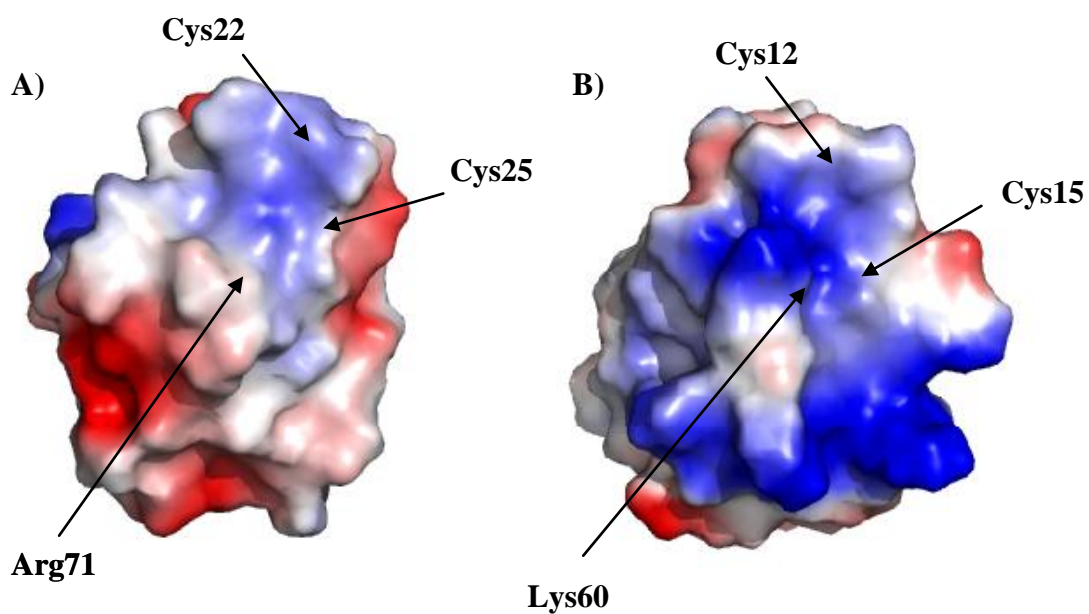
Figure 2.4.2

The proposed roles of D1 and D3 of CCS in Cu(I) loading of SOD1 during the activation of the reduced copper-free protein (E,Zn-SOD1), with both CCS and SOD1 shown as monomers.
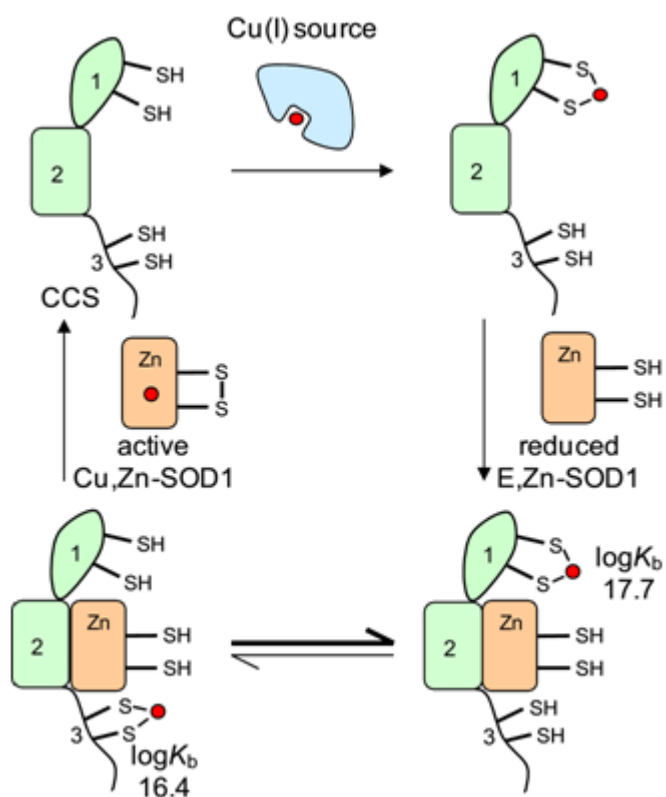
2.5   References

(1)   Culotta, V. C.; Klomp, L. W. J.; Strain, J.; Casareno, R. L. B.; Krems, B.; Gitlin, J. D. *J. Biol. Chem.***1997**, *272*, 23469-23472.

(2)   Rae, T. D.; Schmidt, P. J.; Pufahl, R. A.; Culotta, V. C.; O'Halloran, T. V. *Science* **1999**, *284*, 805-808.

(3)   Schmidt, P. J.; Rae, T. D.; Pufahl, R. A.; Hamma, T.; Strain, J.; O'Halloran, T. V.; Culotta, V. C. *J. Biol. Chem.* **1999**, *274*, 23719-23725.

(4)   Wong, P. C.; Waggoner, D.; Subramaniam, J. R.; Tessarollo, L.; Bartnikas, T. B.; Culotta, V. C.; Price, D. L.; Rothstein, J.; Gitlin, J. D. *Proc. Natl. Acad. Sci. U.S.A.* **2000**, *97*, 2886-2891.

(5)   Rae, T. D.; Torres, A. S.; Pufahl, R. A.; O'Halloran, T. V. *J. Biol. Chem.* **2001**, *276*, 5166-50176.

(6)   Rosenzweig, A. C. *Acc. Chem. Res.* **2001**, *34*, 119-128.

(7)   Huffman, D. L.; O'Halloran, T. V. *Annu. Rev. Biochem.* **2001**, *70*, 677-701.

(8)   Culotta, V. C.; Yang, M.; O'Halloran, T. V. *Biochim. Biophys. Acta.* **2006**, *1763*, 747-758.

(9)   Brown, N. M.; Torres, A. S.; Doan P. E.; O'Halloran T. V. *Proc. Natl. Acad. Sci. U.S.A.* **2004**, *101*, 5518-5523.

(10)   Furukawa, Y.; Torres, S. A.; O'Halloran, T. V. *EMBO J.* **2004**, 23, 2872-2881.

(11)   Furukawa, Y.; O'Halloran, T. V. *Antioxid. Redox Signal.* **2006**, 8, 847-867.

(12)   Bush, A. I. *Curr. Opin. Chem. Biol.* **2000**, *4*, 184-191.

(13)   Gaggelli, E.; Kozlowski, H.; Valensin, D.; Valensin, G. *Chem. Rev.* **2006**, *106*, 1995-2044.

(14)   Madsen, E.; Gitlin, J. D. *Annu. Rev. Neurosci.* **2007**, *30*, 317-337.

(15)   Cleveland, D. W.; Rothstein, J. D. *Nat. Rev. Neurosci.* **2001**, *2*, 806-819.

(16)   Lamb, A. L.; Wernimont, A. K.; Pufahl, R. A.; Culotta, V. C.; O'Halloran, T. V.; Rosenzweig, A. C. *Nat. Struc. Biol.* **1999**, *6*, 724-729.

(17)   Wernimont, A. K.; Huffman, D. L.; Lamb, A.L.; O'Halloran, T. V.; Rosenzweig, A. C. *Nat. Struc. Biol.* **2000**, *7*, 766-771.

(18)   Arnesano, F.; Banci, L.; Bertini. I. *Biochemistry* **2001**, *40*, 1528-1539.

(19)   Lamb, A. L.; Wernimont A. K.; Pufahl, R. A.; O'Halloran, T. V.; Rosenzweig, A. C. *Biochemistry* **2000**, *39*, 1589-1595.

(20)   Lamb, A. L.; Torres, A. S.; O'Halloran, T. V.; Rosenzweig, A. C. *Nat. Struc. Biol.* **2001**, 8, 751-755.

(21)   Torres, A. S.; Petri, V.; Rae, T. D.; O'Halloran, T. V. *J. Biol. Chem.* **2001**, 276, 38410-38416.

(22)   Stasser, J. P.; Silivai, G. S.; Barry, A. N.; Blackburn, N. *Biochemistry* **2007**, *46*, 11845-11856.

(23)   Lamb, A. L.; Torres, A. S.; O'Halloran, T. V.; Rosenzweig, A. C. *Biochemistry* **2000**, *39*, 14720-14727.

(24)   Hall, L. T.; Sanchez, R. J.; Holloway, S. P.; Zhu, H.; Stine, J. E.; Lyons, T. J.; Demeler, B.; Schirf, V.; Hansen, J. C.; Nersissian, A. M.; Valentine, J. S.; Hart, P. J, *Biochemistry* **2000**, 39, 3611-3623.

(25)   Caruano-Yzermans, A. L.; Bartnikas, T. B.; Gitlin, J. D. *J. Biol. Chem.* **2006**, *281*, 13581-13587.

(26)   Lin, S. J.; Pufahl, R. A.; Dancis, A.; O'Halloran, T. V.; Culotta, V. C. *J. Biol. Chem.* **1997**, *272*, 9215-9220.

(27)   Banci, L.; Bertini, I.; Ciofi-Baffoni, S.; Kozyreva, T.; Zovo, K.; Palumaa, P. *Nature* **2010**, *465*, 645-648.

(28)   Badarau, A.; Dennison, C. *J. Am. Chem. Soc.* **2011**, *133*, 2983-2988.

(29)   Xiao, Z.; Wedd, A. G. *Nat. Prod. Rep.* **2010**, *27*, 768-789.

(30)   Badarau, A.; Dennison, C. *Proc. Natl. Acad. Sci. U.S.A.* **2011**, 108, 13007-13012.

(31)   Xiao, Z.; Donelly, P. S.; Zimmerman, M.; Wedd, A. G. *Inorg. Chem.* **2008**, 47, 4338-4347.

(32)   Xiao, Z.; Brose, J.; Schimo, S.; Ackland, S. M.; La Fontaine S.; Wedd, A. G. *J. Biol. Chem.* **2011**, *286*, 11047-11055.

(33)   Xiao, Z.; Loughlin, F.; George, G. N.; Howlett, G. J.; Wedd, A. G. *J. Am. Chem. Soc*. **2004**, *126*, 3081-3090.

(34)   Zhou, L.; Singleton, C.; Le Brun, N.; *Biochem. J.* **2008**, *413*, 459-465.

(35)   Singleton, C.; Le Brun, N.E. *Dalton Trans.* **2009**, 4, 688-96.

(36)   B. Angeletti, B.; Waldron, K. J.; Freeman, K. B.; Bawagan, H.; Hussain, I.; Miller, C. C. J.; Lau, K. F.; Tennant, M. E.; Dennison, C.; Robinson N. J.; Dingwall, C. *J. Biol. Chem.* **2005**, *280*, 17930-17937.

(37)   Pace, C. N.; Vajdos, F.; Fee, L.; Grimsley, G.; Gray, T. *Protein Sci.* **1995**, 11, 2411-2423.

(38)   Badarau, A.; Firbank, S. J.; McCarthy, A. A.; Banfield, M. J.; Dennison, C. *Biochemistry,* **2010**, *49,* 7798-7810.

(39)   Hussain, F.; Olson, J. S.; Wittung-Stafshede, P. *Proc. Natl. Acad. Sci. U.S.A.* **2008**, *105,* 11158-11163.

(40)   Stasser, J. P.; Eisses, J. F.; Barry, A. N.; Kaplan, J. H.; Blackburn, N. J. *Biochemistry* **2005**, *44*, 3143-3152.

(41)   Finney, L. A.; O'Halloran, T. V. *Science* **2003**, *300*, 931-936.

(42)   Portnoy, M. E.; Rosenzweig, A. C.; Rae, T.; Huffman, D. L.; O'Halloran, T. V.; Culotta, V. C. *J. Biol. Chem.* **1999**, *274*, 15041-15045.

(43)   Lutsenko, S.; *Curr. Opin. Chem. Biol.* **2010**, *14*, 211-217.

(44)   Portnoy, M. E.; Schmidt, P. J.; Rogers, R. S.; Culotta, V. C. *Mol. Genet. Genomics* **2001**, *265*, 873-882.

(45)   Banci, L.; Bertini, I.; McGreevy, K. S.; Rosato, A. *Nat. Prod. Rep.* **2010**, *27*, 695-710.

(46)   White, C.; Kambe, T.; Fulcher, Y. G.; Sachdev, S. W.; Bush. A. I.; Fritsche, K.; Lee. J.; Quinn, T. P.; Petris, M. J. *J. Cell. Sci.* **2009**, *122*, 1315-1321.

(47)   Aggarwal, S. PhD Thesis, Newcastle University, **2011**

(48)   Hiraoka, D.; Ogra, T. *Metallomics* **2001**, 3, 693-701.

(49)   Carroll, M. C.; Girouard, J. B.; Ulloa, J. L.; Subramaniam, J. R.; Wong, P. C.; Valentine, J. S.; Culotta, V. C. *Proc. Natl. Acad. Sci. U.S.A.* **2004**, *101*, 5964-5969.

(50)   Leitch, J. M.; Jensen, L. T.; Bouldin, S. D.; Outten, C. E.; Hart, P. J.; Culotta, V. C. *J. Biol. Chem.* **2009**, *284*, 21863-21871.

(51)   Leitch, J. M.; Yick, P. J.; Culotta, V. C. *J. Biol. Chem.* **2009**, *284*, 24679-24683.

(52)   Kirby, K.; Jensen, L. T.; Binnington, J.; Hilliker, A. J.; Ulloa, J.; Culotta, V. C.; Phillips, J. P. *J. Biol. Chem.* **2008**, *283*, 35393-35401.

(53)   Hearnshaw, S.; West, C.; Singleton, C.; Zhou, L.; Kihlken, M. A.; Strange, R. W.; Le Brun, N. E.; Hemmings, A. M. *Biochemistry* **2009**, 48, 9324-9326.

(54)   Ralle, M.; Lutsenko, S.; Blackburn, N. J. *J. Biol. Chem.* **2003**, *278*, 23163-23170.

(55)   Horng, Y. C.; Cobine, P. A.; Maxfield, A. B.; Carr, H. S.; Winge, D. R. *J. Biol. Chem.* **2004**, *279*, 35334-35340.

(56)   Strange, R. W.; Antonyuk, S. V.; Hough, M. A.; Doucette, P. A.; Valentine, J. S.; Hasnain, S. S. *J. Mol. Biol.* **2006**, 356, 1152-1162.

Chapter 3

Modulation of the Cys pK_a's and Copper Affinities of the CXXC and

CXC Motifs of Human CCS

3.1   Introduction

Most known copper metallochaperones, especially Atx1's and the metal binding domains (MBDs) of the copper-transporting ATPases, contain the CXXC motif that provides the two Cys residues responsible for binding Cu(I) with high affinity.(*1,2*) The CXXC motif is also employed by enzymes that participate in disulfide reduction, isomerisation and formation and has been extensively studied within these proteins, providing insights into the way in which the reactivity of the two Cys residues be modulated by the surrounding protein structure.(*3,4*) Thioredoxin (Trx) (*E. coli*) (*5,6*) is involved in disulfide reduction, protein disulfide isomerase (PDI) (*S. cerevisiae*) (*7,8*) catalyses the isomersation of disulfides and the oxidoreductase DsbA (*E. coli*) (*9*) catalyses their formation. The striking feature of these three proteins is the variation in reactivity of the same CXXC motif within a similar tertiary structure.(*10-12*) It has been found that the reduction potential of the CXXC motif is affected by the nature of the intervening residues and is correlated with the acidity (pK_a) of the N-terminal Cys (Cys_N).(*4*) In DsbA an unusually low pK_a of 3 for the Cys_N of the CXXC motif has been determined and results from a stabilising interaction of the Cys_N thiolate with an adjacent His residue.(*13*) The stabilisation of the reduced form of the protein leads to a thermodynamic driving force for oxidation of the thiols of the enzymes substrate. This family of proteins demonstrates that the properties of the Cys residues within a CXXC motif can therefore be modulated by the surrounding protein scaffold and so optimise the Cys residues reactivity for a particular function.

It is now emerging that the two Cys residues of the CXXC motif in the copper metallochaperone proteins can also be fine tuned for their role in binding copper and transferring the metal to partner proteins. The presence of a residue located on loop 5 of various Atx1 metallochaperones and copper-transporting ATPase MBDs that is in close proximity to and interacts with the metal binding loop region containing the CXXC motif has been reported (Figure 3.1.1).(*14*) In Atx1 from prokaryotic and eukaryotic organisms the residue is typically a Tyr and Lys, respectively. In the MBDs of ATP7A and ATP7B (human copper-transporting ATPases), and also the yeast homologue Ccc2, the residue is a Phe. In human HAH1 the Lys60 residue is within hydrogen bonding distance of the C-terminal Cys (Cys_C) of the CXXC motif in and has been implicated in affecting Cu(I) transfer from Cu(I)-HAH1 to the ATP7A and ATP7B MBDs.(*15-18*) The pH dependence of the Cu(I) affinities of wild-type (WT) HAH1 and a Lys60Ala mutant differ and at pH 7.0 a threefold difference in Cu(I) affinity is observed.(*18*) In a Lys60Ala HAH1 mutant an increase of the pK_a of the Cys_C residue is observed relative to that for WT HAH1. The

88

difference in Cu(I) affinities for WT and Lys60Ala HAH1 occurs as a result of the lowering of the pK_a of the Cys$_C$ residue of the CXXC motif in WT HAH1. This is brought about due to the stabilization of the Cys$_C$ thiolate through a hydrogen bonding interaction with the Lys60 side chain. The Cu(I) affinity of the ATP7A MBD1 also has a pH dependence and the thermodynamic gradient for Cu(I) transfer between HAH1 and MBD1 is therefore dependant on pH. The importance of the pH dependence of the Cu(I) affinities is highlighted by the presence of a shallow but favourable thermodynamic gradient for Cu(I) transfer between HAH1 and ATP7A MBD1 at physiological pH (pH 7.0-7.4) which becomes unfavourable at lower pH's (pH < 7).([18, 19]) It is notable that other Cu(I) trafficking pathways also have shallow gradients for copper transfer at physiological pH([20]) and therefore, in instances where the cell cytosol becomes acidic, for example during apoptosis or disease, the copper trafficking pathways could potentially be compromised and metal dishomeostasis result.([21-23])

The pK_a's of the Cys residues also allow the relative nucleophilicities, and leaving group abilities, of the Cu(I)-binding Cys residues of the copper metallochaperones to be assessed. In general the lower the pK_a of a Cys residue the better a leaving group it becomes and therefore a lower pK_a Cys residue in the donor is favoured for Cu(I) transfer to the acceptor. This was found in the case of Cu(I) transfer from HAH1 to ATP7A MBD1 where the relative nucleophilicities of the Cu(I)-binding Cys residues would lower the activation barrier for transfer from HAH1 to ATP7A MBD1.([18]) Therefore, the kinetics of copper transfer are affected by the pK_a's of the Cys residues of the Cu(I)-binding motifs and can be tuned to provide a low activation energy barrier for copper transfer between partner proteins.

It is also interesting to note that the majority of the Atx1 metallochaperones and MBDs also have a conserved Met residue located 1 amino acid upstream of the CXXC motif (Figure 3.1.2).([14]) This residue has been found to stabilise the metal binding loop region and although it does not appear to affect the affinity of the site for Cu(I) it has been implicated in modulating the kinetics of Cu(I) transfer.([24,25]) It was found that Cu(I) abstraction from HAH1 was slower in a Met11Ala mutant. Therefore, amino acid residues other than those of loop 5, can also modulate the Cu(I)-binding characteristics of the Atx1s.

The presence of residues that modulate the Cu(I) affinity and transfer characteristics of CXXC motif of the Atx1 metallochaperones, poses the question of

whether analogous residues are present in the Atx1-like domains of the CCS metallochaperones, particularly for Ccs1 (*S. cerevisiae*) and CCS (human). D1 of Ccs1 contains the conserved CXXC motif and is similar in overall fold to that observed for the Atx1 metallochaperones and contains a loop analogous to loop 5 for HAH1.(*26*) In the crystal structure of Ccs1 the Lys66 residue is analogous to Lys65 and Lys60 found in HAH1 and Atx1, respectively, and is also located on loop 5 and orientates towards the CXXC motif (Figure 3.1.1). In human CCS, however, the corresponding residue determined by sequence alignment with HAH1, Atx1 and Ccs1 is Arg71 (Figure 3.1.2). The CXC motif of domain 3 (D3) of CCS is retained in all known homologues and it is interesting whether any residues in this domain other than the Cys residues affect Cu(I)-binding characteristics. However, the lack of structural data for D3 makes it difficult to identify any residues that are likely to interact with the Cys residues of this domain.(27) Sequence alignment of D3 from various organisms indicates multiple conserved residues (Figure 3.1.3) but it is currently unknown what purpose these residues serve.

In this Chapter, work that shows the pH dependence of the Cu(I) affinities of the D1 CXXC and D3 CXC motifs is presented. The crystal structure of D1 confirms the anticipated binding of Cu(I) by the CXXC motif of this domain of CCS and the involvement of the Arg71 residue in an interaction with the Cys residues of the Cu(I)-binding CXXC motif. The Arg71Ala D1-CCS mutant has been characterized and the effect of the loss of the Arg71 residue on the pK_a of the Cys residues of the CXXC motif and the pH dependence of the Cu(I) affinity is investigated. The pK_a's of the Cys residues of the metal binding motifs in full length CCS Cys to Ser mutants of the CXXC and CXC motifs are also determined from the pH dependence of their Cu(I) affinity. Implications for Cu(I) transfer between CCS and its target Cu,Zn-Superoxide Dismutase (SOD1), with respect to the pK_a's of the metal binding Cys residues are discussed.

Figure 3.1.1

Structures of HAH1 (A) and D1 of Ccs1 (B) (PDB accession codes 1TL5 and 1JK9 respectively) drawn in Pymol. The co-ordinating Cys residues of the CXXC Cu(I)-binding motifs of both HAH1 and Ccs1, and the Lys residues of loop 5, are shown as stick representations.
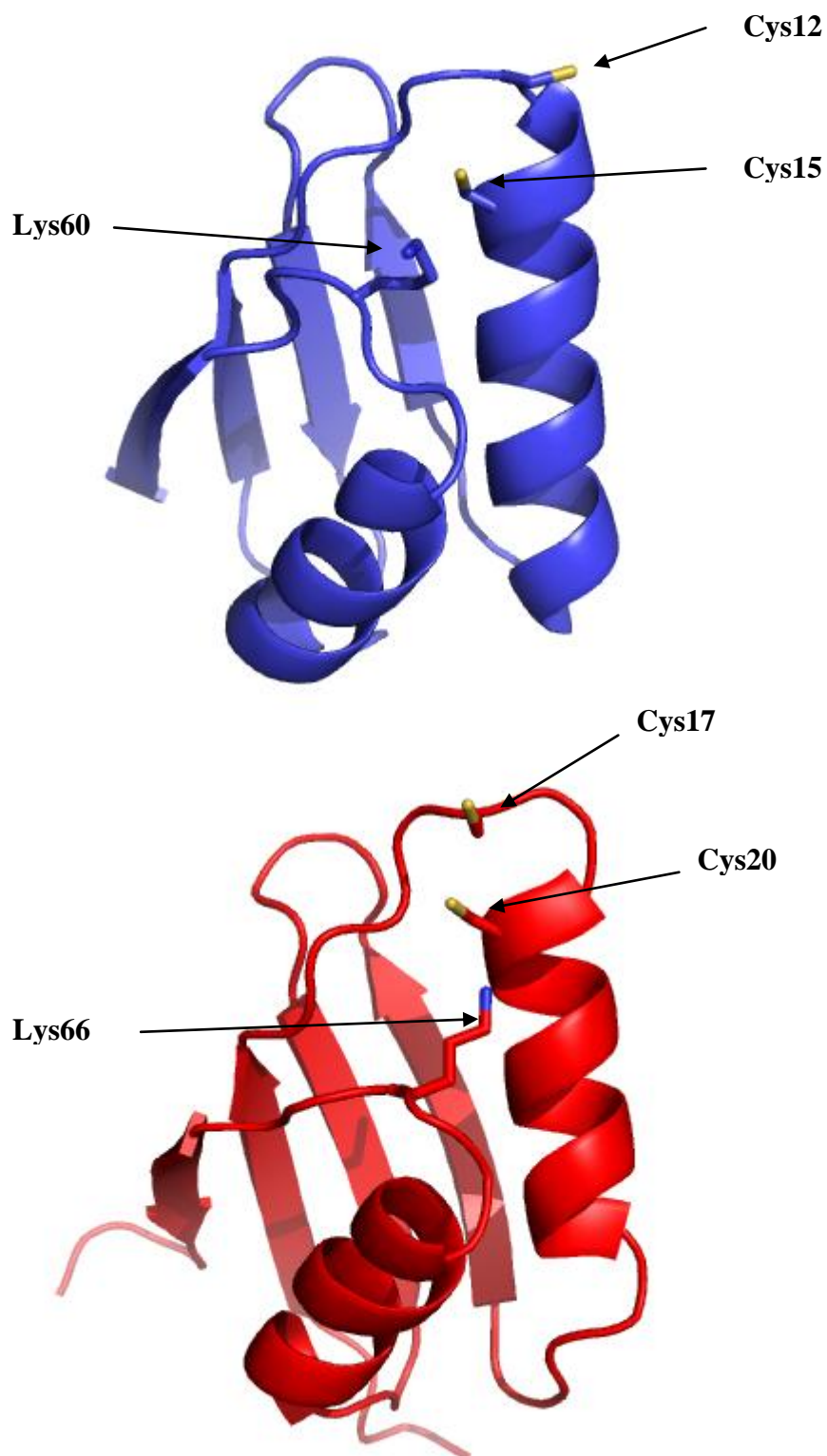
Figure 3.1.2

Sequence alignment of D1 CCS, with HAH1, Atx1 and D1-Ccs1 generated by ClustalW using protein sequences obtained from the NCBI Protein Database. The residues 1-79 and 1-77 of CCS and Ccs1, respectively, corresponding to the Atx1-like D1, were considered. Conserved residues are highlighted red while the Cys residues of the CXXC Cu(I)-binding motif are highlighted orange. The residues located in loop 5 of the protein fold are highlighted blue and the conserved residues within this loop region are highlighted red.

```
                                                                    Loop 5
CCS      MASDSGNQGTLCTLEFAVQMTCQSCVDAVRKSLQGVAG-VQDVEVHLEDQMVLVHTTLPSQEVQALLEGTGRQAVLKGMG---
HAH1     ----------MPKHEFSVDMTCGGCAEAVSRVLNKLG--GVKYDIDLPNKKVCIESEHSMDTLLATLKKTGKTVSYLGLE---
Atx1     -------MAEIKHYQFNVVMTCSGCSGAVNKVLTKLEPDVSKIDISLEKQLVDVYTTLPYDFILEKIKKTGKEVRSGKQL---
Ccs1     -----MTTNDTYEATYAIPMHCENCVNDIKACLKNVPG-INSLNFDIEQQIMSVESSVAPSTIINTLRNCGKDAIIRGAGKPN
```

Figure 3.1.3

Sequence alignment of D3-CCS from various organisms obtained using ClustalW using protein sequences obtained from the NCBI Protein Database. Conserved residues are highlighted red while the conserved Cys residues of the CXC Cu(I)-binding motif are highlighted orange.

```
Human        GLFQNPKQICSCDGLTIWEERGRPIAGKGRKESAQPPAHL
Yeast        GVWENNKQVCACTGKTVWEERKDALANNIK----------
Mouse        GLFQNPKQICSCDGLTIWEERGRPIAGQGRKDSAQPPAHL
Rat          GLFQNPKQICSCDGLTIWEERGRPIAGQGRKDSAQPPAHL
Drosophila   GILENFKRICACDGVTLWDERNKPLAGKERSQKL------
Arabidopsis  GVGENYKKLCSCDGTVIWEATNSDFVASKV----------
Tomato       GVGENYKKLCTCDGTTIWEATSKI----------------
Soybean      GVGENYKKLCTCDGTTIWEATDTDFVTSKV----------
```

3.2   Experimental

3.2.1   Mutagenesis and Cloning

The Arg71Ala D1-CCS mutation was prepared by Quikchange mutagenesis (Stratagene). The plasmid pGEMT_D1-CCS (section 2.2.1) was used as template for the mutagenesis reaction using the forward and reverse primers 5'-ggcacgggggcgcaggcggtactcaagggc-3' and 5'-gcccttgagtaccgcctgcgcccccgtgcc-3', respectively, giving the construct pGEMT_R71A-D1-CCS. DNA sequencing was used to verify the Arg71Ala mutation and the gene was then cloned using the BamH1/Nde1 restriction sites into pET29a giving pET29a_R71A-D1-CCS.

3.2.2   Expression and Purification of Proteins

The proteins D1-CCS, Arg71Ala D1-CCS, C244S/C246S-CCS and C22S/C25S-CCS were expressed and purified as described in section 6.1.

3.2.3   Protein Reduction and Quantification

The proteins D1-CCS, Arg71Ala D1-CCS, C244S/C246S-CCS and C22S/C25S-CCS (200-800 μM) were reduced by incubation with 10 mM dithiothreitol (DTT) in 20 mM tris(hydroxymethyl)aminomethane (Tris) pH 7.5 in an anaerobic chamber (Belle Technology, $O_2 \ll 2$ parts per million), typically for 2-3 hours. These samples were then desalted and exchanged into the required buffer using a PD10 column (GE Healthcare). Thiol quantification using Ellman's assay, as described in section 6.15, was used for determining the concentration of Arg71Ala-D1-CCS assuming three free thiols per monomer, according to the amino acid sequence. Bradford assays of Arg71Ala D1-CCS using BSA standards required a correction factor of 2.3 compared to concentrations determined from Ellman's assays. The concentrations of D1-CCS, C244S/C246S-CCS and C22S/C25S-CCS were determined as described in section 2.2.4.

3.2.4   Cu(I) Binding Stoichiometry of Arg71Ala D1-CCS

Cu(I) stock solutions and Cu(I)-proteins were prepared as described in section 6.16. Titrations of Cu(I) into protein samples (10 μM) in the presence of 500 μM bicinchoninic acid (BCA) were performed in 20 mM 4-(2-hydroxyethyl)piperazine-1-ethanesulfonic acid (Hepes) pH 7.5 containing 200 mM NaCl, in a septum sealed gas

tight cuvette (Hellma). Copper concentrations were determined using either bathocuproine disulfonic acid (BCS) or BCA, and occasionally by AAS as described in section 6.16.1

3.2.5 Crystallization, Data Collection, Structure Determination and Refinement for D1-CCS

Cu(I)-D1-CCS was prepared by addition of 1 equivalent of Cu(I) to apo D1-CCS in 5 mM Tris pH 7.5. The protein was then concentrated to ~5 mg/ml in the same buffer using a Vivaspin 500 concentrator (Millipore). Crystals were prepared (aerobically) using the sitting drop method of vapour diffusion using 200 nL of the Cu(I)-bound protein solution and 100 nL of well solution (50 mM Mes pH 6.5 containing 5 mM ZnCl and 10 % w/v PEG 6000). The crystal trial tray, containing the crystallisation mixture drop and well solution, was incubated for 5 mins in an anaerobic chamber prior to sealing and diffraction quality crystals (~ 3) typically appeared after 1-2 weeks of incubation at room temperature. Crystals were harvested and frozen, aerobically, using paratone-N as the cryoprotectant by Dr Susan Firbank. All diffraction data were collected at 100 K using synchrotron radiation (DLS, Oxford, U.K.). The collection of data and processing, the structure solution, model building and refinement were performed by Dr Arnaud Basle. The data were scaled using Scala.([28]) The phase problem was solved by copper-SAD (single anomalous diffraction) using shelxC/D/E pipeline ([29]) and the model was built using coot and refined with the phenix suite.([30,31]) The data collection and processing statistics are shown in Table 3.3.1.

3.2.6 pH Dependence of Cu(I) Affinities

Cu(I) affinities (K_b values) were determined by competition assays with BCS and BCA using the approach described in section 6.16.3 and refs (*18,32-3*). The buffers 2-(*N*-morpholino)ethanesulfonic acid (Mes) (pH 5.5-6.8), Hepes (pH 7.0-8.0), N-tris(hydroxymethyl)methyl-3-aminopropanesulfonic acid (Taps) (pH 8.0-9.0), 2-(N-cyclohexylamino)ethanesulfonic acid (Ches) (pH 9.0-10.0) and 3-(cyclohexylamini)-1-propanesulfonic acid (Caps) (pH 10.0-11.0) were used to obtain K_b values in the pH range 5.9-10.6. Experiments were performed in 20 mM buffer containing 200 mM NaCl. The overall stability constant (β value) for $[Cu(BCS)_2]^{3-}$ at various pH values was calculated assuming a pK_a of 5.7 and using the maximal β value of 6.3×10^{19} M^{-2} (pH $\geq$ 8.0).(*20*) The β value for $[Cu(BCA)_2]^{3-}$ of $(5.4 \pm 2.7) \times 10^{16}$ M^{-2} (section 2.3.5) was used

in the pH range 6.5 to 10.3 for all K_b determinations involving BCA. The pH dependence of K_b was fit to equations for single, equation (3.1), or double, equation (3.2), ionization models as appropriate.(*18*)

$$K_b = \frac{K_{bmax}}{1 + \frac{[H^+]}{K_a}} \tag{3.1}$$

$$K_b = \frac{K_{bmax}}{1 + \frac{[H^+]}{K_{a1}} + \frac{[H^+]^2}{K_{a1}K_{a2}}} \tag{3.2}$$

In which K_b is the affinity constant for the protein at a specified pH, K_b^{max} is the maximal Cu(I) affinity of the protein, K_{a1} and K_{a2} are the acid dissociation constants of the Cys residues whose ionization influences the K_b and $[H^+]$ is the proton concentration.

3.2.7 Cys pK_a Determination by UV Spectroscopy

pK_a values of the Cys residues present in apo-D1-CCS and Arg71Ala apo-D1-CCS were determined by measurement of the extinction coefficient at 240 nm as a function of pH by Dr Adriana Badarau.(*35,36*) Reduced apo-proteins (25 μM) were prepared in 50 mM buffer (*vide supra*) containing 200 mM NaCl within the pH range 4 to 10.5 with the corresponding absorbance at 240 nm measured. Spectra for the apo-proteins were measured against a solution of the buffer minus the protein at each pH value. The data were fitted using equation (3.3) to determine the pK_a values of the Cys residues.

$$\varepsilon_{app} = \frac{\frac{\varepsilon_3[H^+]^3}{K_{a1}K_{a2}K_{a3}} + \frac{\varepsilon_2[H^+]^2}{K_{a1}K_{a2}} + \frac{\varepsilon_1[H^+]}{K_{a1}} + \varepsilon_0}{1 + \frac{[H^+]}{K_{a1}} + \frac{[H^+]^2}{K_{a1}K_{a2}} + \frac{[H^+]^3}{K_{a1}K_{a2}K_{a3}}} \tag{3.3}$$

In which ε_{app} is the apparent extinction coefficient at a particular pH, ε_1, ε_2 and ε_3 are the extinction coefficient of the PH PH$_2$ and PH$_3$ species, K_{a1}, K_{a2} and K_{a3} are the acid dissociation constants of the Cys residues, respectively, and $[H^+]$ is the proton concentration. The pH dependence of the ε_{240} for Cu(I)-bound D1-CCS and Arg71Ala D1-CCS were also measured to enable the pK_a of the third non-Cu(I) ligating Cys

residue to be estimated and demonstrate the involvement of the two lower pK_a cysteine residues of the CXXC motif in Cu(I)-binding.

3.3   Results

3.3.1   Purification and the Initial Characterization of Arg71Ala D1-CCS

The purity of Arg71Ala D1-CCS variant was determined by SDS-PAGE to be > 90 % and the molecular weight determined by matrix assisted laser desorption Ionisation time-of-flight (MALDI) mass spectrometry (MS) to be 8131 Da which corresponds to the protein minus its N-terminal Met residue (the calculated value based on the amino acid sequence is 8130). Arg71Ala D1-CCS was isolated with negligible copper and zinc as determined by AAS.

3.3.2   Analytical Gel Filtration of Arg71Ala D1-CCS

The analytical gel filtration chromatograms for Apo and Cu(I)-bound Arg71Ala D1-CCS (Figure 3.3.1) are very similar to those obtained for D1-CCS (Table 2.3.2) and the elution volumes correspond to an apparent molecular mass of ~14-15 kD. The high apparent mass of the protein, as found for D1-CCS, is likely due to the asymmetrical dimensions of this domain.(*26*)

3.3.3   Cu(I) Binding Stoichiometry of Arg71Ala D1-CCS

The high affinity Cu(I)-binding stoichiometry of Arg71Ala D1-CCS was determined by titrating Cu(I) into apo-protein in the presence of BCA. Arg71Ala D1-CCS binds a single equivalent of Cu(I) with high affinity under these conditions (Figure 3.3.2). The data is very similar to that obtained for D1-CCS and C244SC/C246S-CCS (section 2.3.4) and is indicative of the Cu(I) ion binding to the CXXC motif.

3.3.4   Crystal Structure of Cu(I)-bound D1-CCS

The crystal structure of Cu(I)-bound D1-CCS has been determined and represents the first structure of an Atx1-like domain of CCS to be obtained in the presence of copper. Cu(I)-bound D1-CCS crystallizes as a head-to-head dimer with an interface composed of two copper ions coordinated by the Cys residues of the CXXC motif of each monomer (Figure 3.3.3). As expected the overall-fold of the domain is that of a βαββαβ fold with

the CXXC motif located between β1 and α1 (Figure 3.3.3).(*1*) Each copper ion is ligated by Cys22 and Cys25 of one monomer and Cys25 from the adjacent monomer with Cys to copper distances of 2.3-2.4 Å. The copper to copper distance is 2.9 Å. As indicated by the sequence alignment data (*vide supra*) Arg71 is located in close proximity to the metal binding motif of each monomer and is within hydrogen bonding distance of Cys25 (3.0-3.1 Å) of the same monomer and Cys22 (3.6-3.8 Å) of the adjacent monomer. The third Cys of the protein (Cys12) is located ~30 Å away from the CXXC motif on β1 of the protein and does not participate in Cu(I) binding.

3.3.5   CD Spectra of Proteins

Far-UV CD spectra of the apo-proteins were obtained within the pH range 6.5-10.5 to determine the stability and suitability of the proteins for Cu(I) affinity measurements within extremes of pH and to determine if the Arg71Ala D1-CCS mutant is folded. The similarity of the far-UV CD spectra of Arg71Ala D1-CCS and D1-CCS (Figure 3.3.5) indicates the Arg71Ala mutation does not perturb the secondary structure of the protein and the spectra of both proteins change little in the pH range 6.5 to 10.5 (Figure 3.3.6). The Far-UV CD spectra of C244S/C246S-CCS and C22S/C25S-CCS remain similar between pH 6.5 and 8.5 but change significantly, more so for C22S/C25S-CCS, above pH 8.5 indicating the secondary structure is perturbed at high pH (Figure 3.3.6). The stability of the D1 constructs relative to the two full length CCS variants suggests the secondary structure of D2/D3 is compromised at high pH.

3.3.6   The pH dependence of the Cu(I) Affinity of the D1 CXXC Motif

The Cu(I) affinity of Arg71Ala D1-CCS determined by titration of apo-protein into $[Cu(BCS)_2]^{3-}$ plus excess BCS and of BCS into Cu(I)-protein plus excess apo-protein at pH 6.5 and 7.5 (Figure 3.3.7) show that the K_b values from the titrations in either direction agree within 30 %. The Cu(I) affinity of $(5.8 \pm 1.8) \times 10^{17}$ M^{-1} determined at pH 7.5 from several titrations is very similar to those determined for D1-CCS and C244S/C246S-CCS at the same pH (section 2.3.5). The Cu(I) affinities of the three proteins are dependent on pH (Tables 3.3.2 to 3.3.4 and Figures 3.3.8 to 3.3.11). The pH dependence of the Cu(I) affinity for D1-CCS and C244S/C246S-CCS is similar between pH 5.9 and 10.6. The pH dependence of the Cu(I) affinity for D1-CCS and C244S/C246S-CCS is first order with respect to $[H^+]$ within the pH range 6 to ~8 after which the Cu(I) affinity plateaus in both cases to similar values (Figure 3.3.8). The Cu(I)

affinity of CXXC motif is primarily influenced by the pK_a of the Cys ligands. The first order dependence of Cu(I) affinity on $[H^+]$ for D1-CCS and C244S/C246S-CCS is indicative of the deprotonation of a single Cys residue of the Cu(I)-binding CXXC motif. Fitting the data for both proteins to a single ionisation model gives determinations of the maximal Cu(I) affinities of (30 ± 2) and $(32 \pm 4) \times 10^{17}$ M^{-1} and Cys pK_a's of 8.1 and 8.3 for D1-CCS and C244S/C246S-CCS, respectively (Figure 3.3.10 and Table 3.3.6). The second Cys residue of the CXXC motif cannot be determined from this data as the pK_a of this residue is lower than pH 6 (*vide infra*). The Cu(I) affinity for Arg71Ala D1-CCS is also first order with respect to $[H^+]$ within the pH range 7.0 to 8.5 and plateaus at high pH but at a higher overall affinity than D1-CCS and C244S/C246S-CCS (Figure 3.3.11). The Cu(I) affinity of this protein, however, has a second order dependence on $[H^+]$ below pH 7.0 which is not observed for either of the other proteins. Fitting of the data for this variant to a double ionisation model gives a maximal Cu(I) affinity of $(75 \pm 8) \times 10^{17}$ M^{-1} and pK_a's for the two Cys residues of 6.8 and 8.5 (Figure 3.3.11 and Table 3.3.6). The pK_a of 8.5 is similar to those obtained for D1-CCS and C244S/C246S-CCS but the maximal Cu(I) affinity is higher.

3.3.7   The pH dependence of the Cu(I) Affinity of the D3 CXC Motif

The Cu(I) affinity of C22S/C25S-CCS also depends on pH (Table 3.3.5 and Figure 3.3.12) The Cu(I) affinity of C22S/C25S-CCS was determined over the pH range 6.0 to 10.3 using BCA (Table 3.3.5), the use of the ligand BCA, as opposed to BCS used in section 3.3.6, is explained in section 2.3.5. The Cu(I) affinity has a second order dependence on $[H^+]$ below pH 7.0 with a first order dependence between pH 7 to 9 and then plateaus at higher pH (Figure 3.3.13). The data was fitted to a double Cys protonation model which gives a maximal Cu(I) affinity of $(20 \pm 5) \times 10^{17}$ M^{-1} and pK_a's for the two Cys residues of 6.3 and 9.4 (Figure 3.3.13 and Table 3.3.6). The maximal Cu(I) affinity is lower and one Cys pK_a is higher and the second is similar to those determined for the CXXC containing D1-CCS and C244S/C246S-CCS. There is an order of magnitude difference between the Cu(I) affinities of C22S/C25S-CCS and D1-CCS (and also C244S/C246S-CCS) in the pH range ~6 to ~8 after which the Cu(I) affinities become more similar at pH 10.3 (Figure 3.3.14).

3.3.8 Determination of pK_a Values for the CXXC Motif Cys Residues

An independent determination of the pK_a's of the CXXC motif Cys residues in D1-CCS and Arg71Ala D1-CCS was made to verify those obtained from the Cu(I) affinity measurements in 3.3.6. The pK_a's were determined by measuring the extinction coefficient at 240 nm (ε_{240}) of the apo-proteins as a function of pH for each protein as thiolates absorb strongly in this region of the UV spectrum (*36*). Both D1-CCS and Arg71Ala D1-CCS have three Cys residues of which two form the CXXC motif with the third located ~30 Å away on β1 (*vide supra*). The data obtained for D1-CCS and Arg71Ala D1-CCS shows the presence of three Cys residues (Figure 3.3.15). A fit of the data to a model that considers the three ionisations enables the pK_a of each Cys residue to be determined. The fit of the data for D1-CCS yields Cys pK_a's of 5.7, 8.4 and 10.3 (Figure 3.3.15 and Table 3.3.7). The pK_a of 8.4 corresponds to that of the pK_a determined for one of the Cys residues from the pH dependence of the Cu(I) affinity data. The data for Arg71Ala D1-CCS fits to the same model, however, an initial fit allowing all parameters to vary gave pK_a values which were different to those obtained with D1-CCS (Appendix Figure 2). Since the highest pK_a determination is prone to greater uncertainty due to the absence of data and a clear end point at this extreme of pH, some of the parameters were constrained and refitted. A fit of the data with the two higher pK_a's constrained to the values obtained for D1-CCS yielded a pK_a of 6.8 which is identical to that of the lower Cys pK_a determined from the pH dependence of Cu(I) affinity data (Figure 3.3.15 and Table 3.3.7). Similar experiments performed on the Cu(I)-bound forms of the two proteins show that binding of a single equivalent of Cu(I) in each case shields the Cys of the CXXC motif from protonation but the third higher pK_a Cys is still observed indicating that this residue does not participate in metal binding (Figure 3.3.16). Therefore the higher pK_a Cys in the above determinations corresponds to the Cys residue not involved in the CXXC motifs of D1-CCS and Arg71Ala D1-CCS.

Table 3.3.1

Data collection and processing statistics for Cu(I)-D1-CCS crystal structure

	Cu(I)-D1-CCS high resolution	Cu edge
Beamline	DLS I24	DLS IO2
Date	22.2.2010	14.2.2010
Wavelength (Å)	0.9780	1.3790
Resolution (Å)	32.78-1.60 (1.69-1.60)	44.72-2.19 (2.31-2.19)
Space group	$P2_12_12_1$	$P2_12_12_1$
Unit-cell parameters		
a (Å)	44.35	44.23
b (Å)	44.80	44.72
c (Å)	65.56	65.54
α, β, γ (°)	90.0	90.0
Unit-cell volume (Å^3)	130260	130260
Solvent content (%)	40	40
No. of measured reflections	62656	91254
No. of independent reflections	17690	7119
Completeness (%)	99.2 (99.3)	99.8 (100.0)
Redundancy	3.5 (3.5)	12.8 (13)
Rmerge (%)	6.2 (38.4)	7.8 (15)
$<I>/<\sigma(I)>$	11.6 (3.4)	22.9 (13.6)
Anomalous Completeness (%)	N/A	99.9 (100.0)
Anomalous Redundancy	N/A	7.0 (6.9)

	Refinement statistics	
Rwork (%)	14.54	N/A
Rfree[#] (%)	22.67	N/A
No. of non-H atoms		
No. of protein, atoms	1097	N/A
No. of water molecules	122	N/A
No. of ions atoms	7	N/A
R.m.s. deviation from ideal values		
Bond length (Å)	0.008	N/A
Angle distance (Å)	1.129	N/A
Average B factor (Å^2)		
Protein	27.15	N/A
Ions	22.86	N/A
Solvent water	37.14	N/A
Ramachandran plot[+], residues in allowed and most favoured regions (%)	100	N/A

*(Values in parenthesis are for the highest resolution shell).
[#]5% of the randomly selected reflections excluded from refinement.
[+]Calculated using MOLPROBITY.

Table 3.3.2

The pH dependence of the Cu(I) affinity (K_b) for D1-CCS measured by competition titrations with BCS in 20 mM buffer containing 200 mM NaCl.

pH	K_b (M^{-1})	$\log_{10} K_b$
5.89	1.60×10^{16}	16.20
6.32	5.30×10^{16}	16.72
6.53	8.20×10^{16}	16.91
7.02	2.70×10^{17}	17.43
7.51	5.20×10^{17}	17.72
7.91	1.04×10^{18}	18.02
8.40	1.91×10^{18}	18.28
9.02	2.53×10^{18}	18.40
9.40	3.11×10^{18}	18.49
10.3	3.17×10^{18}	18.50

Table 3.3.3

The pH dependence of the Cu(I) affinity (K_b) for C244S/C246S-CCS measured by competition titrations with BCS in 20 mM buffer containing 200 mM NaCl

pH	K_b (M^{-1})	$\log_{10} K_b$
5.92	1.10×10^{16}	16.04
6.62	6.70×10^{16}	16.83
7.51	4.30×10^{17}	17.63
8.54	1.90×10^{18}	18.28
9.47	2.40×10^{18}	18.38
10.59	4.10×10^{18}	18.61

Table 3.3.4

The pH dependence of the Cu(I) affinity (K_b) for Arg71Ala D1-CCS measured by competition titrations with BCS in 20 mM buffer containing 200 mM NaCl

pH	K_b (M^{-1})	$\log_{10} K_b$
5.92	2.30×10^{15}	15.36
6.26	1.30×10^{16}	16.11
6.49	3.50×10^{16}	16.54
7.03	1.70×10^{17}	17.23
7.45	6.20×10^{16}	17.79
7.87	1.31×10^{18}	18.12
8.25	3.12×10^{18}	18.49
9.04	5.13×10^{18}	16.71
9.40	5.92×10^{18}	18.77
10.3	9.31×10^{18}	18.97

Table 3.3.5

The pH dependence of the Cu(I) affinity (K_b) for C22S/C25S-CCS measured by competition titrations with BCA in 20 mM buffer containing 200 mM NaCl

pH	K_b (M^{-1})	$\log_{10} K_b$
5.9	1.90×10^{14}	14.28
6.5	1.20×10^{15}	15.08
7.0	6.40×10^{15}	15.81
7.5	1.90×10^{16}	16.28
8.0	5.60×10^{16}	16.75
8.5	2.90×10^{17}	17.46
9.5	9.80×10^{17}	17.99
10.3	1.80×10^{18}	18.26

Table 3.3.6

Maximal Cu(I) affinity ($K_b{}^{max}$) and pK_a values determined from the pH dependence of K_b profile data for D1-CCS, Arg71Ala D1-CCS, C244S/C246S-CCS and C22S/C25S-CCS

Protein	$K_b{}^{max}$ ($\times\ 10^{17}\,M^{-1}$)	pK_a (1,2)
D1-CCS	30 ± 2	8.1 ± 0.1 (1)
Arg71Ala D1-CCS	75 ± 9	8.5 ± 0.1 (1), 6.8 ± 0.1 (2)
C244S/C246S-CCS	32 ± 4	8.3± 0.1 (1)
C22S/C25S-CCS	20 ± 5	9.4± 0.2 (1), 6.3± 0.2 (2)

Table 3.3.7

pK_a values determined from abs 240 nm data for D1-CCS and Arg71Ala D1-CCS

	D1-CCS	**Arg71Ala D1-CCS**
pK_{a1}	5.7 ± 0.1	6.8 ± 0.2
pK_{a2}	8.4 ± 0.1	8.4 [a]
pK_{a3}	10.3 ± 0.1	10.3 [a]
ε_1 (mM cm^{-1})	3.5 ± 0.1	3.8 ± 0.2
ε_2 (mM cm^{-1})	6.6 ± 0.1	6.5 ± 0.4
ε_3 (mM cm^{-1})	10.2 ± 0.2	11.4 ± 0.2

[a] pK_{a1} and pK_{a2} for the fit of the data for Arg71Ala (Figure 3.3.15) were constrained to values obtained for D1-CCS.

Figure 3.3.1

Chromatograms for apo (A) and Cu(I)-bound (B) (1.0 equivalent) Arg71Ala D1-CCS (100 μM) in 20 mM Mes pH 6.5 containing 200 mM NaCl. Absorbance was measured at 240 nm and protein eluting at 13.4 (± 0.1) ml, corresponds to an apparent mass of 15 (± 0.5) kDa.
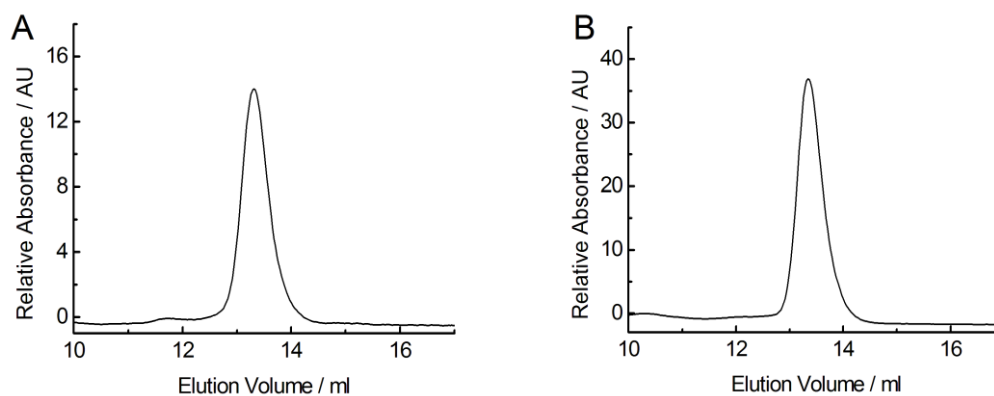
Figure 3.3.2

Titration of Cu(I) into Arg71Ala apo-D1-CCS (10 μM) in 20 mM Hepes pH 7.5 containing 200 mM NaCl and 500 μM BCA.

Figure 3.3.3

Crystal structure of Cu(I)-bound D1-CCS showing key residues at the metal binding site drawn in Pymol. The two monomers are shown in blue and red with the copper ions represented as gold spheres at the dimer interface. The copper coordinating Cys residues of the CXXC motifs of both monomers, the third non-copper ligating Cys residue (Cys12), and the conserved Arg residue of loop 5 are shown as stick representations.
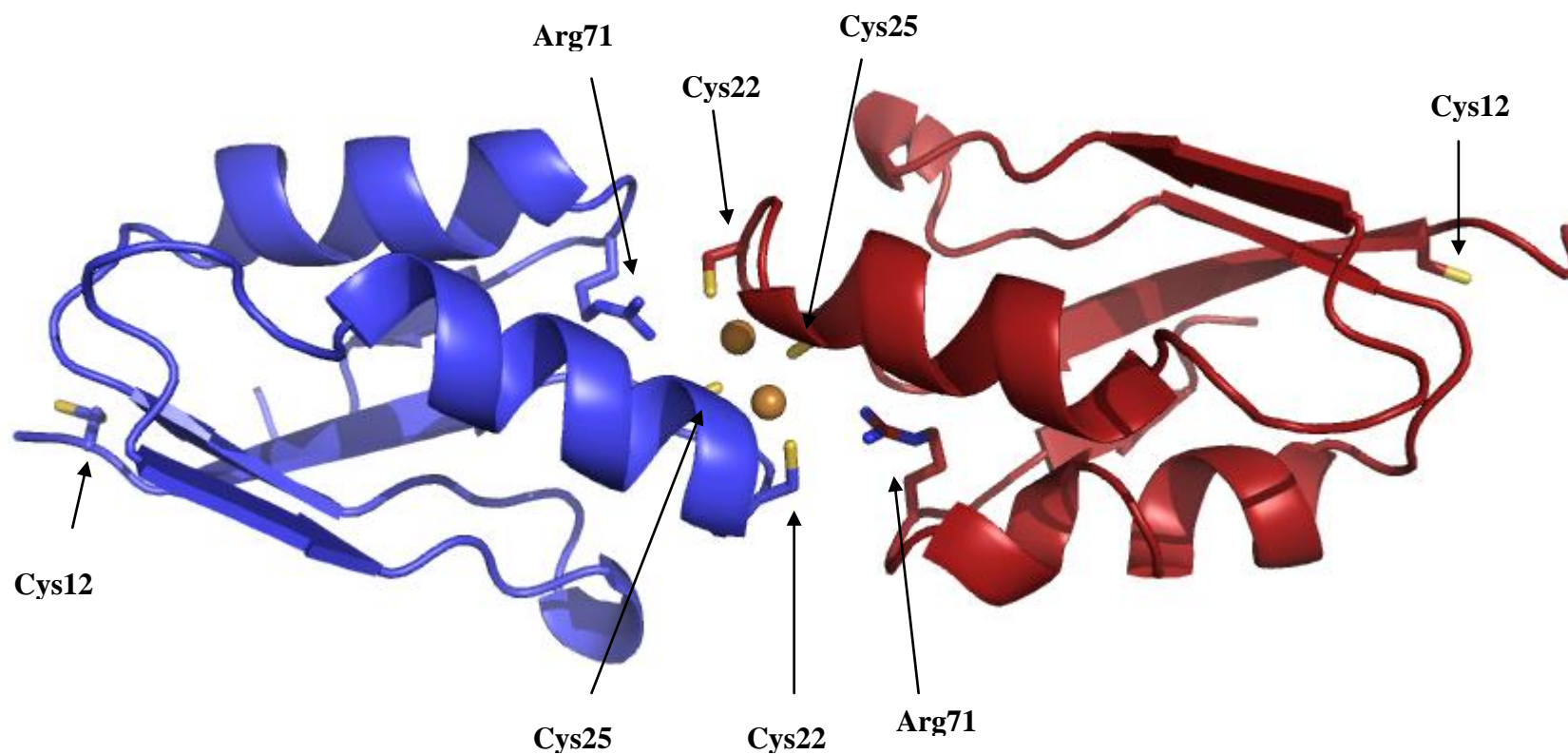
Figure 3.3.4

Stick representation of the copper site structure of Cu(I)-D1-CCS with Cys residues coordinating the copper ions (orange spheres) and A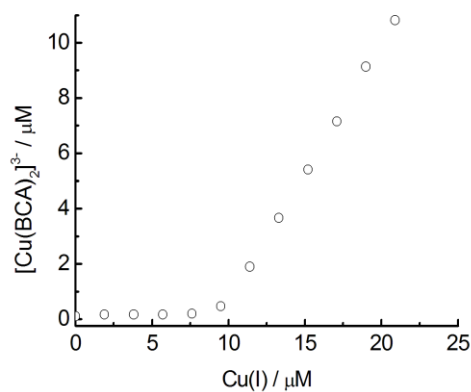rg residues indicated and colour coded according to their association with each monomer (blue and red; see Figure 3.3.3) of the dimeric crystal structure drawn using PyMol. The interactions between the conserved Arg and Cys residues (A) and between the copper and Cys residues (B) are indicated in Å units.
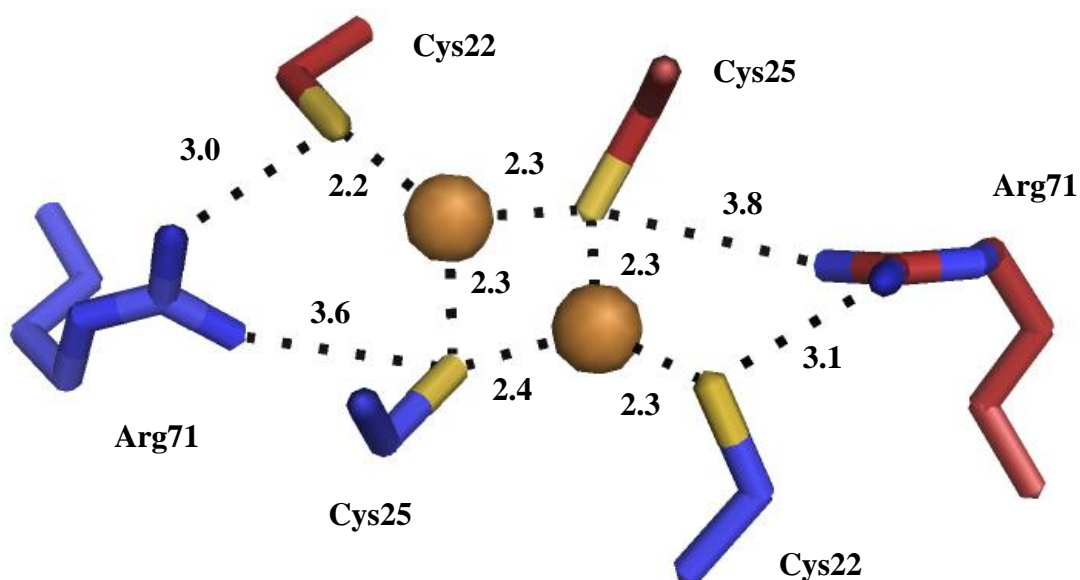
Figure 3.3.5

Far-UV CD spectra of Arg71Ala apo-D1-CCS (solid) and D1-CCS (dotted) (0.5 mg/ml) in 20 mM Mes pH 6.5 containing 200 mM NaCl.
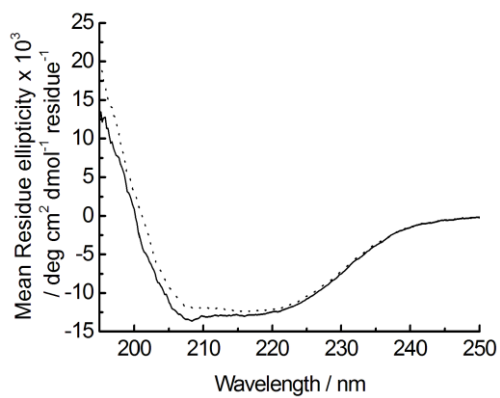
Figure 3.3.6

Far-UV CD spectra of apo D1-CCS (A), Arg71Ala D1-CCS (B) , C244S/C246S-CCS (C) and C22S/C25S-CCS (D) (0.5 mg/ml at different pH values). The lines colored black, red, green, blue and cyan indicate spectra measured at pH 6.5, 7.5, 8.5, 9.5 and 10.5 respectively.
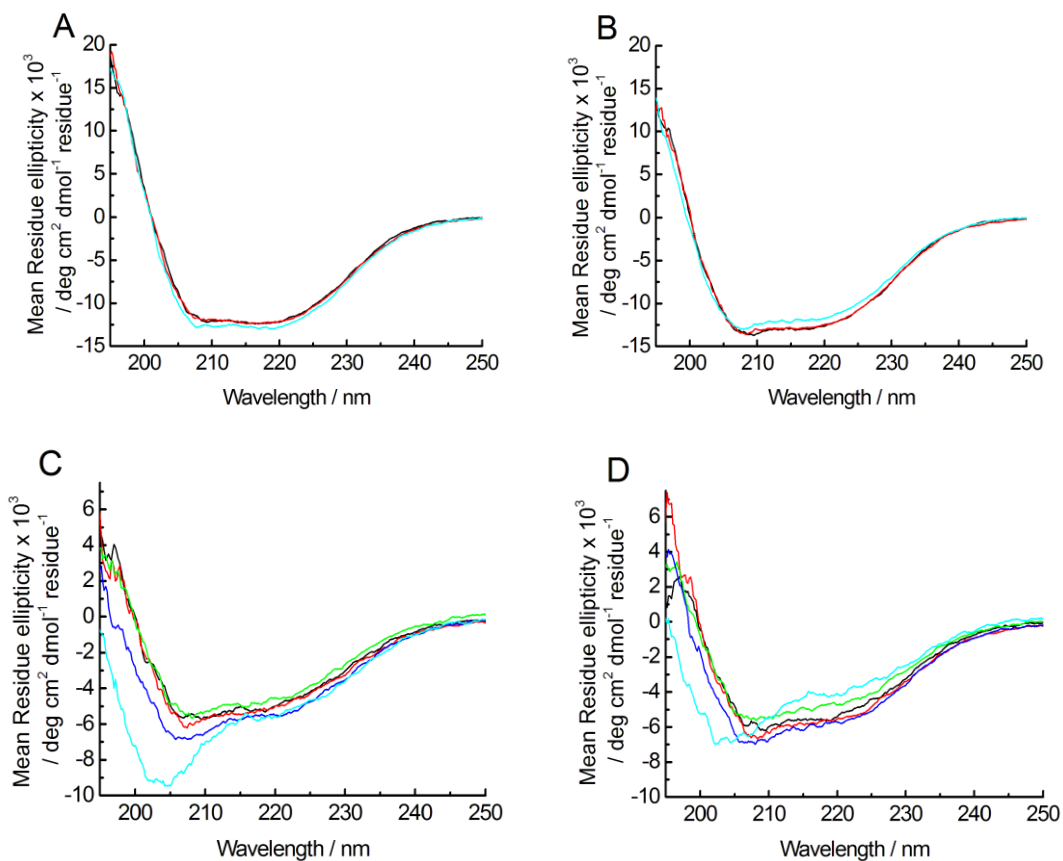
Figure 3.3.7

Titrations of Arg71Ala apo-D1-CCS into $[Cu(BCS)_2]^{3-}$ (10 μM) plus 40 μM BCS at pH 6.5 (A) and plus 140 μM BCS at pH 7.5 (B). Titrations of BCS into Arg71Ala Cu(I)-D1-CCS (10 μM) plus Arg71Ala apo-D1-CCS (10 μM) at pH 6.5 (C) and pH 7.5 (D). Lines show fits of data, to equations (6.2) (A and B) and (6.1) (C and D), giving K_b values of $(3.5 \pm 0.1) \times 10^{16}$ (A), $(6.1 \pm 0.2) \times 10^{17}$ (B), $(2.5 \pm 0.1) \times 10^{16}$ (C) and $(5.3 \pm 0.1) \times 10^{17}$ M^{-1} (D).
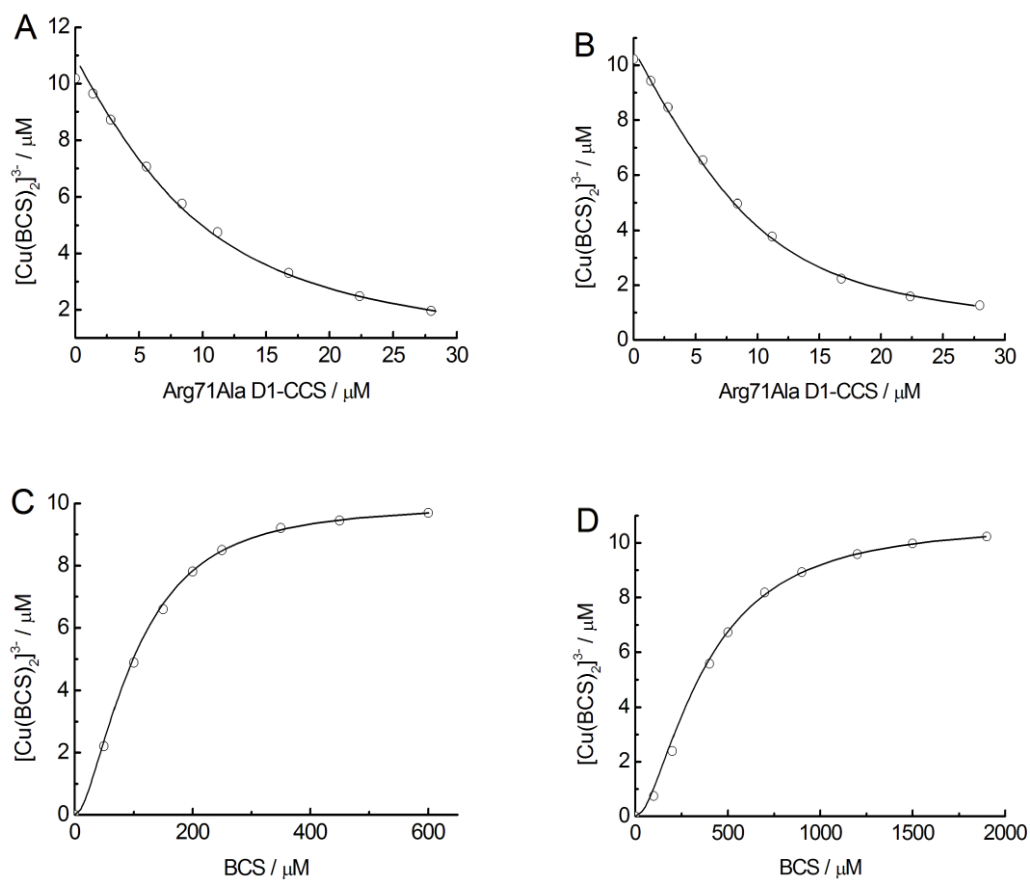
Figure 3.3.8

Titrations of apo-D1-CCS into $[Cu(BCS)_2]^{3-}$ (10 μM) plus 140 μM BCS at pH 7.5 (A) and plus 480 μM BCS at pH 10.3 (C). Titrations of BCS into Cu(I)-bound C244S/C246S-CCS (5 μM) plus apo C244S/C246S-CCS (5 μM) at pH 6.5 (C) and pH 10.6 (D). Lines show fits of data, to equations (6.2) (A and C) and (6.1) (B and D), giving K_b values of $(5.4 \pm 0.1) \times 10^{17}$ (A), $(4.4 \pm 0.4) \times 10^{17}$ (B), $(31.6 \pm 0.9) \times 10^{17}$ (C) and $(40.6 \pm 1.4) \times 10^{17}$ M^{-1} (D).
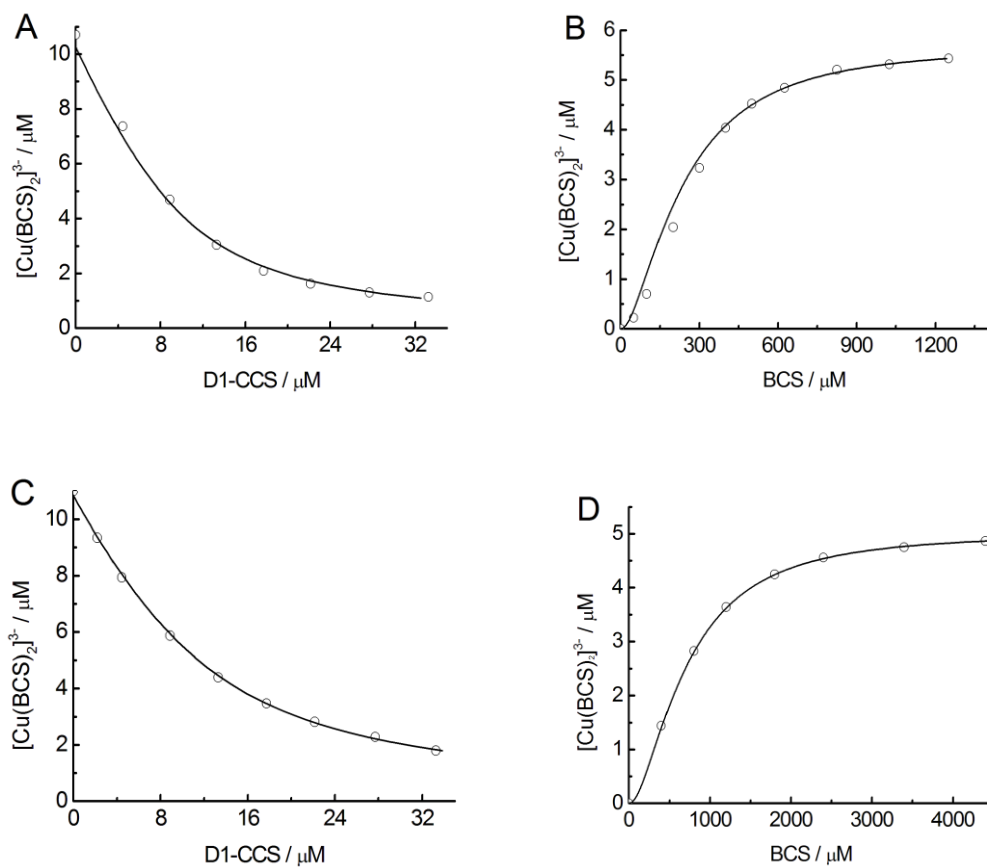
Figure 3.3.9

Titrations of Arg71Ala apo-D1-CCS into $[Cu(BCS)_2]^{3-}$ (10 μM) plus 140 μM BCS at pH 7.5 (A) and plus 480 μM BCS at pH 10.3 (C). Lines show fits of data to equation (6.2) giving K_b values of $(6.1 \pm 0.2) \times 10^{17}$ (A), $(93.1 \pm 2.4) \times 10^{17}$ M^{-1} (B).
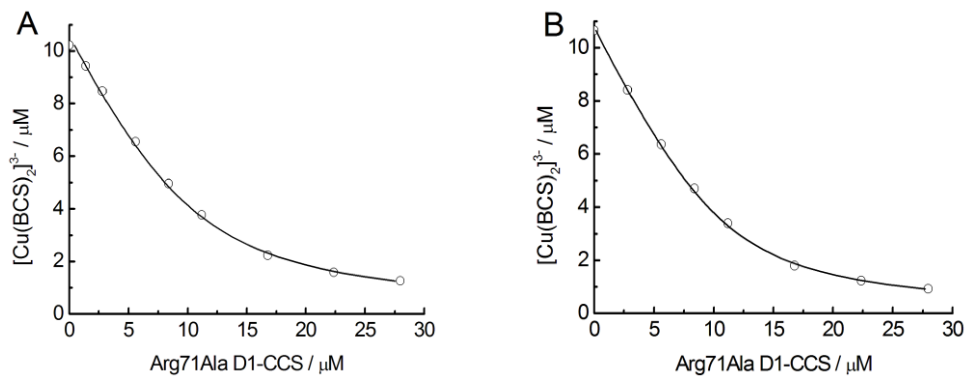
Figure 3.3.10

Plots of $\log_{10} K_b$ against pH for D1-CCS (open circles) and C244S/C246S-CCS (closed circles). The lines show fits of the data to equation (3.1) giving K_b^{max} and pK_a values listed in Table 3.3.6.
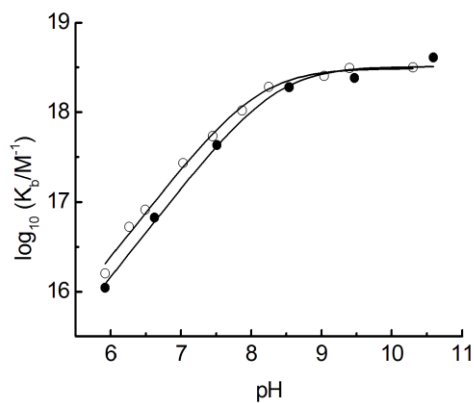
Plots of $\log_{10} K_b$ against pH for D1-CCS (open circles) and Arg71Ala D1-CCS (closed circles). The lines show fits of the data to equation (3.1) for D1-CCS and (3.2) for Arg71Ala D1-CCS, giving the K_b^{max} and pK_a values listed in Table 3.3.6.
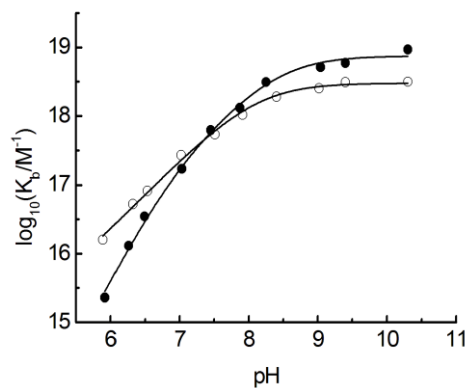
Figure 3.3.12

Titrations of apo-C22S/C25S-CCS into $[Cu(BCA)_2]^{3-}$ (10 μM) plus 880 μM BCA at pH 7.5 (A) and plus 480 μM BCS at pH 10.6 (C). Lines show fits of data to equation (6.2) giving K_b values of $(1.9 \pm 0.1) \times 10^{16}$ (A) and $(17.9 \pm 0.8) \times 10^{17}$ M^{-1} (B).
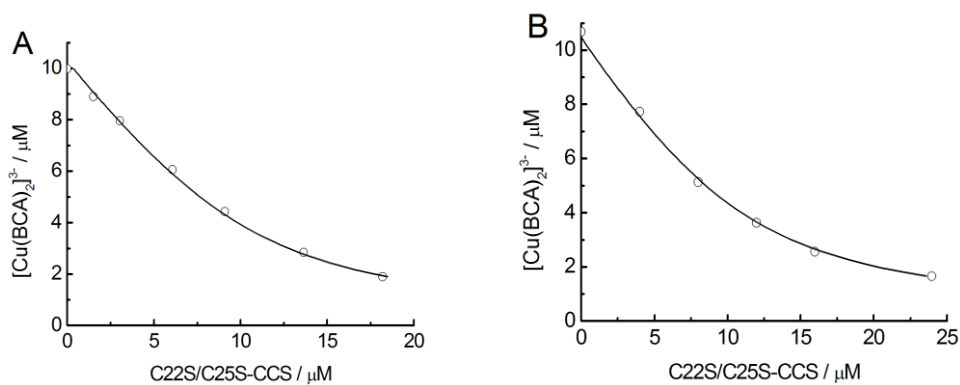
Figure 3.3.13

Plot of $\log_{10} K_b$ against pH for C22S/C25S-CCS. The line shows a fit of the data to equation (3.2) giving the K_b^{max} and pK_a values listed in Table 3.3.6.
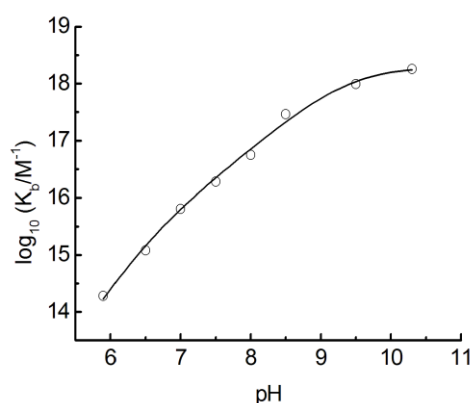
Figure 3.3.14

Comparison of $\log_{10} K_b$ against pH data for D1-CCS (black open circles), C244S/C246S-CCS (black open squares), Arg71Ala D1-CCS (black closed circles) and C22S/C25S-CCS (black closed squares). The lines show fits of the data to equation (3.1) for D1-CCS and C244S/C246S-CCS and (3.2) for Arg71Ala D1-CCS and C22S/C25S-CCS.
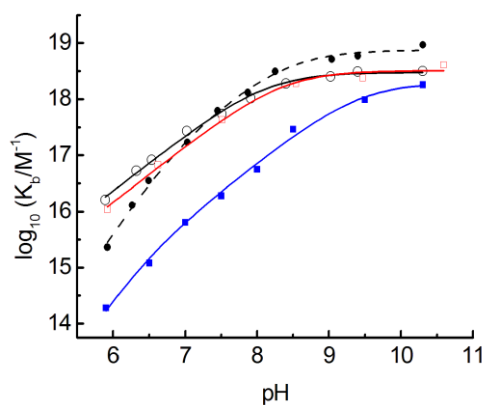
Figure 3.3.15

Plots of ε_{240nm} as a function of pH for apo-D1-CCS (A) and Arg71Ala apo-D1-CCS (B). The lines show fits of the data to equation (3.3) giving the pK_a and $\Delta\varepsilon$ values listed in Table 3.3.7.*
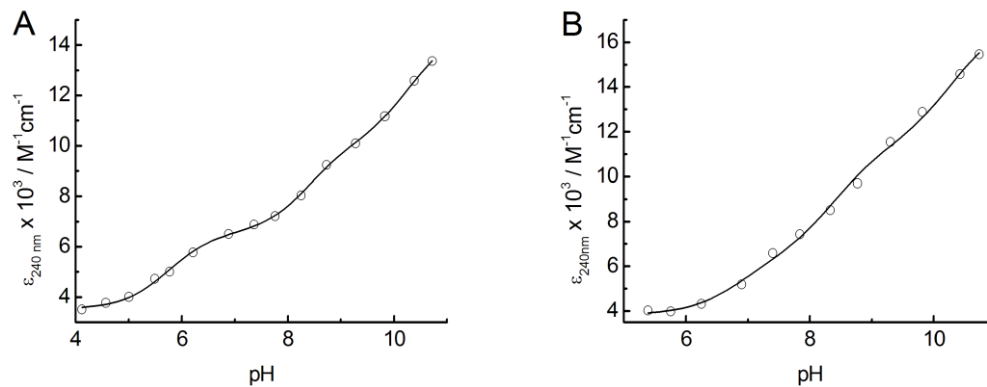
*Data in above figure was acquired by Dr Adriana Badarau

Figure 3.3.16

Plots of ε_{240nm} as a function of pH for Cu(I)-D1-CCS (A) and Arg71Ala Cu(I)-D1-CCS (B).
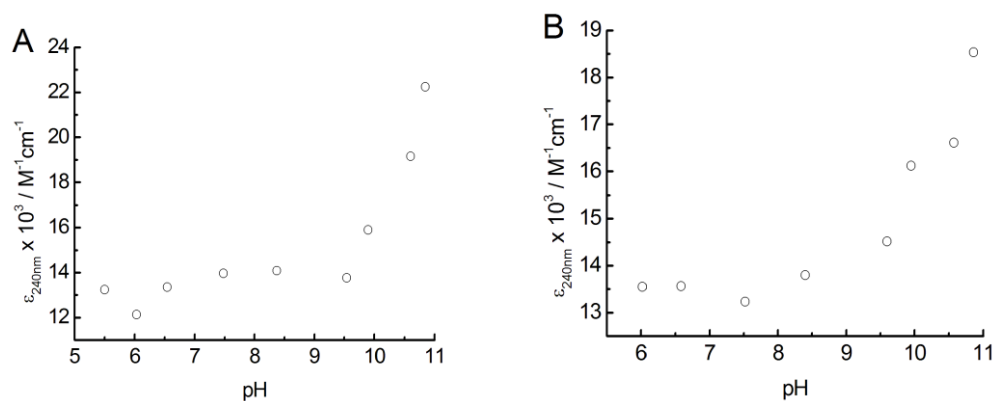
3.4   Discussion

The crystal structure of Cu(I)-bound D1-CCS represents the first Cu(I)-bound structural determination of D1 of CCS. The overall fold is similar to that of D1 of the analogous domain in Ccs1 and also to that of the Atx1-like metallochaperones HAH1 and Atx1.(*26,37-39*) The structure reveals that, as expected, the Cys residues of the CXXC motif are involved in ligation to the bound metal and also that Arg71 of loop 5 is within hydrogen bonding distance of Cys22 (Cys$_C$) of the motif. Unexpectedly, however, the protein has crystallised as a dimer with the two D1-CCS monomers (each binding a single Cu(I) ion) interacting head-to-head through the bound Cu(I) ions. This is unexpected as gel filtration shows Cu(I)-bound D1-CCS to elute as for apo-D1-CCS which is monomeric. The structure, however, is not unprecedented as crystal structures of the Cu(I)-bound Atx1-like metallochaperones ScAtx1 (*Synechocystis*) and CopZ (*B. Subtilis*) demonstrate formation of dimeric and trimeric proteins, respectively, with Cu(I)-Cys cluster formation.(*40-42*) Such species have been proposed to be involved in the transfer of Cu(I) between proteins, in the cases of ScAtx1 and CopZ specifically transfer of Cu(I) to their cognate Cu(I)-transporting ATPases. It is unclear whether the Cu(I)-bound D1-CCS dimer observed in the crystal structure is of any relevance for CCS *in vivo* due to full length CCS being present as a dimer and the absence of any Cu(I)-dependent oligomerisation for C244S/C246S-CCS (section 2.3.3).

The Cu(I) affinities for D1-CCS and C244S/C246S-CCS have a similar dependence on pH and indicate that the Cu(I) affinity of the CXXC motif of D1 of CCS is modulated by residues residing in this domain of CCS alone. The Cu(I) affinities of D1-CCS and the Arg71Ala variant are similar at physiological pH (pH 7.0-7.4) but differ markedly above and below this range. At pH ~ 6 the Cu(I) affinity of the Arg71Ala variant is almost an order of magnitude lower while at pH 10.3 it is over 2-fold greater demonstrating the significant role of the Arg71 residue in affecting the Cu(I)-binding characteristics of the CXXC motif. The Cu(I) affinities of C22S/C25S-CCS are almost an order of magnitude lower than that of D1-CCS between pH ~6 to 8 but become similar at pH 10.3. The CXC motif therefore has a significantly lower affinity for Cu(I) than the CXXC motif under the ranges of pH that is experienced in the cell cytosol.(*19,23*)

The pH dependence of the Cu(I) affinities are the result of competition between protons and Cu(I) for the Cys residues of the CXXC and CXC motifs.(*18,43*) In the pH range studied the Cu(I) affinities are dependent on the protonation of a single residue for

D1-CCS and C244S/C246S-CCS and on two residues for Arg71Ala D1-CCS and C22S/C25S-CCS. The pK_a's for the two CXXC Cys residues have been measured as 5.7 and 8.4 and 6.8 and 8.4 for D1-CCS and the Arg71Ala variant respectively. The lowering of one of the Cys pK_a's by ~1 pH unit is likely due to a thiolate stabilizing hydrogen bond interaction between Arg71 and Cys25 (Cys$_C$) side-chains that is observed in the crystal structure of Cu(I)-D1-CCS. The structure therefore allows for the assignment of the pK_a's to the Cys residues of the CXXC motif for D1-CCS and Arg71Ala D1-CCS with the lower pK_a in each case corresponding to Cys$_C$. Similar assignments of the Cys pK_a's for the CXXC motif in HAH1, MNK1, MerP and MerA have been reported.([18,44,45]) In HAH1 the pK_a of Cys$_C$ is lowered by ~1.5 pH units by an interaction with Lys60 located on the loop analogous to that on which Arg71 is situated in D1 of CCS.([18]) The pK_a's obtained for C22S/C25S-CCS cannot be assigned to specific Cys residues of the CXC motif due to a lack of structural data for this domain of CCS. It is unusual that one Cys pK_a of the CXC motif is very high while the second is low. There are multiple residues within the D3 sequence, including Arg and Lys residues, which could participate in stabilising interactions with one the Cys thiolates of the CXC motif that could lower one of the Cys residues pK_a (Figure 3.1.3). Alternatively interactions with either D1 or D2 or both could be present due to the flexibility of this domain and interactions have been proposed between Cu(I)-bound D3 and D2.([26,37,46]) Another possibility is that deprotonation of one of the Cys could result in a thiolate that interacts with the adjacent thiol to effect a stabilizing hydrogen bond. This would favour the formation of the thiolate but oppose the removal of a subsequent proton from the neighbouring thiol giving low and high pK_a's for the two Cys residues. A stabilising interaction between the two Cys residues is the most likely cause of high and a low pK_a's of for the CXC motif of D3.

It has been shown that the nucleophilicity series of the coordinating Cys residues of the HAH1 and MNK1 CXXC motifs is Cys$_N$ (HAH1) ~ Cys$_N$ (MNK1) > Cys$_C$ (MNK) > Cys$_C$ (HAH1) based on their pK_a values.([18]) This nucleophilicity series is supported by the structure of the Cu(I)-bound HAH1/MNK1 heterocomplex where the lower pK_a Cys$_C$ of HAH1 does not participate in coordination to the Cu(I) ion.([15]) In addition, the structure of the Cu(I)-bound Atx1/Ccc2 heterocomplex shows the Cys$_C$ of Atx1, analogous to Cys$_C$ of HAH1, is also non-coordinating.([47]) It has been shown that the rate determining step for transfer of Cu(I) between two CXXC motifs is likely to be the conversion of a three coordinate heterocomplex from a more reactant like form, where Cys$_C$ of the donor is coordinating, to a more product like form, where Cys$_C$ of the acceptor

is coordinating.(*48*) It has been proposed that the more nucleophillic Cys_C in the Cu(I) acceptor and less nucleophillic Cys_C in the donor will favour the transfer of the Cu(I).(*18*) This would ensure that the activation energy for Cu(I) transfer from source to target is lowered and promote vectorial Cu(I) transfer to the target protein. The lowering of the pK_a for Cys_C in D1 of CCS caused by an interaction with Arg71 located within the same domain enhances the leaving group ability of this Cys residue. The pK_a of one of the Cys residues of the D3 CXC motif, however, appears to be optimised for enhanced nucleophilicity. The lower pKa of one of the D3 CXC Cys may also be important for the disulfide isomerase function of CCS which is involved in facilitating the formation of the intramolecular disulfide in SOD1.(*49*) The nucleophilicities of the CXXC and CXC residues based on their pK_a values is Cys_1 (D3) ~ Cys_N (D1) > Cys_2 (D3) > Cys_C (D1). This would suggest that in the case of CCS, Cys_C of the D1 CXXC motif will be the best leaving group in an intermediate/transient complex of CCS:SOD1, proposed in section 2.4, where Cu(I) is co-ordinated by Cys residues in both D1 and D3 for transfer of Cu(I) from D1 to D3 for subsequent insertion into the SOD1 copper site. Therefore the Cys pK_a's of the two metal binding motifs of CCS appear to be such as to lower the activation barrier for vectorial copper transfer from D1 to D3 for ultimate copper incorporation into SOD1.

The Cu(I) affinity pH profiles for the CXXC and CXC motif-containing proteins indicate that within the physiological pH range of the cytosol a thermodynamic gradient is for copper transfer exists between D1 and D3 which is in favour of Cu(I)-binding to the D1 CXXC motif. Therefore, according to the model proposed in section 2.4, during heterocomplex formation between Cu(I)-bound CCS and apo-SOD1 the Cu(I) bound to D1 is attacked by a Cys residue from D3. The subsequent concerted attack of the second Cys of D3 and dissociation of Cys_C of D1 would then occur before final dissociation of Cys_N of D1 to enable the insertion of Cu(I) bound by D3 into the apo-SOD1 active site. The high affinity of D1 ensures Cu(I) is bound to CCS that complexes with apo-SOD1 but the pK_a of the Cys of the CXXC and CXC motifs, however, ensure that Cu(I) transfer is kinetically favoured in the direction of the CXC motif of D3. The Cu(I)-binding domains of CCS therefore appear optimised for facilitating vectorial Cu(I) transfer from CCS to SOD1 by providing a low activation energy pathway. The results presented within this chapter highlight the potential importance of the kinetics of Cu(I) transfer in the mechanism of action of the CCS metallochaperone.

3.5   References

(1)   Boal, A. C.; Rosenzweig, A. C. *Chem. Rev.* **2009**, 109, 4760-4779.

(2)   Singleton, C.; Le Brun, N. E. *Biometals* **2007**, 20, 275-289.

(3)   Hiniker, A.: Bardwell, J. C. A. *Biochemistry* **2003**, 42, 1179-1185.

(4)   Chivers, P. T.; Prehoda, K. E.; Raines, R. T. *Biochenistry* **1997**, 36, 4061-4066.

(5)   Holmgren, A. *Eur. J. Biochem.* **1968**, 6, 475-484.

(6)   Moore, E.C; Reichard, P.; Thelander, L. *J. Biol. Chem.* **1964**, 239, 3445-3452.

(7)   Lundstrom, J.; Holmgrem, A. *Biochemnistry* **1993**, 32, 6649-6655.

(8)   Laboissiere, M. C. A.; Sturley, S. L.; Raines, R. T. *J. Biol. Chem.* **1995**, 270, 28006-28009.

(9)   Huber-Wunderlich, M.; Glockshuber, R. *Fold. Des.* **1998**, 3, 161-171.

(10)   Kemmink, J.; Darby, N. J.; Dijkstra, K.; Nilges, M.; Creighton, T. E. *Biochemistry* **1996**, 35, 7684-7691.

(11)   Ferrari, D. M.; Soling, H.D. *Biochem. J.* **1999**, 339, 1-10.

(12)   Martin, J. L; Bardwell, J. C..; Kuriyan, J. *Nature* **1993**, 365, 464-468.

(13)   Zapun, A.; Bardwell, J. C.; Creighton, T. E. *Biochemistry* **1993**, 32, 5083-5092.

(14)   Arnesano, F.; Banci, L.; Bertini, I.; Ciofi-Baffoni, S.; Molteni, E.; Huffman, D.L.; O'Halloran, T.V. *Genome Res.* **2002**, 12, 255-271.

(15)   Anatassopoulou, I.; Banci, L.; Bertini, I.; Cantini, F.; Katsari, E.; Rosato, A. *Biochemistry* **2004**, 43, 13046-13053.

(16)   Banci, L.; Bertini, I.; Calderone, V.; Della-Malva, N.; Felli, I. C.; Neri, S.; Pavelkova, A.; Rosato, A. *Biochem. J.* **2009**, 422, 37-42.

(17)   Hussain, F.; Rodriguez-Granillo, A.; Wittung-Stafshede, P. *J. Am. Chem. Soc.* **2009**, 131, 16371-16373.

(18)   Badarau, A.; Dennison, C. *J. Am. Chem. Soc.* **2011**, 133, 2983–2988.

(19)   Bright, G. R.; Fisher, G. W.; Rogowska, U.; Taylor, D. L. *J. Cell. Biol*. **1987**, 104, 1919-1033.

(20)   Xiao, Z.; Loughlin, F.; George, G. N.; Howlett, G. J.; Wedd, A. G. *J. Am. Chem. Soc*. **2004**, *126*, 3081-3090.

(21)   Madsen, E.; Gitlin, J. D. *Annu. Rev. Neurosci.* **2007**, *30*, 317-337.

(22)   Gaggelli, E.; Kozlowski, H.; Valensin, D.; Valensin, G. *Chem. Rev*. **2006**, *106*, 1995-2044.

(23)   Nilsson, C.; Kagedal, K.; Johansson, U.; Ollinger, K. *Methods Cell Sci.* **2003**, 25, 185-194.

(24)   Rodriguex-Granillo, A.; Wittung-Stafshede, P. *J. Phys. Chem. B.* **2009**, 113, 1919-1932.

(25)   Hussain, F.; Olson, J. S.; Wittung-Stafshede, P. *Proc. Natl. Acad. Sci. U.S.A.* **2008**, 105, 11158-11163.

(26)   Lamb, A. L.; Wernimont, A. K.; Pufahl, R. A.; Culotta, V. C.; O'Halloran, T. V.; Rosenzweig, A. C. *Nat. Struc. Biol.* **1999**, *6*, 724-729.

(27)   Kirby, K.; Jensen, L. T.; Binnington, J.; Hilliker, A. J.; Ulloa, J.; Culotta, V. C.; Phillips, J. P. *J. Biol. Chem.* **2008**, *283*, 35393-35401.

(28)   Evans, P. *Acta Crystallogr. Biol. Crystallogr.* **2006**, *62*, 72-82.

(29)   Schneider, T. R.; Sheldrick, G. M. *Acta Crystallogr. Biol. Crystallogr.* **2002**, *58* 1772-1779.

(30)   Emsley, P.; Lohkamp, B.; Scott, W.G.; Cowtan, K. *Acta Crystallogr. D. Biol. Crystallogr.* **2010**, *66*, 486-501.

(31)   Adams, P.D.; Afonine, P.V.; Bunkoczi, G.; Chen, V.B.; Davis, I.W.; Echols, N.; Headd, J.J.; Hung, L.W.; Kapral, G.J.; Grosse-Kunstleve, R.W.; McCoy, A.J.; Moriarty, N.W.; Oeffner, R.; Read, R.J.; Richardson, D.C.; Richardson, J.S.; Terwilliger, T.C.; Zwart, P.H. *Acta Crystallogr. D. Biol. Crystallogr.* **2010**, *66*, 213-221.

(32)   Xiao, Z.; Wedd, A. G. *Nat. Prod. Rep.* **2010**, *27*, 768-789.

(33)   Badarau, A.; Dennison, C. *Proc. Natl. Acad. Sci. U.S.A.* **2011**, *108*, 13007-13012.

(34)   Xiao, Z.; Brose, J.; Schimo, S.; Ackland, S. M.; La Fontaine S.; Wedd, A. G. *J. Biol. Chem.* **2011**, *286*, 11047-11055.

(35)   Polgar, L. *FEBS Lett.* **1974**, 38, 187– 190.

(36)   Witt, A. C.; Lakshminarasimhan, M.; Remington, B. C.; Hasim, S.; Pozharski, E.; Wilson, M. A. *Biochemistry* **2008**, 47, 7430– 7440.

(37)   Lamb, A. L.; Torres, A. S.; O'Halloran, T. V.; Rosenzweig, A. C. *Nat. Struc. Biol.* **2001**, 8, 751-755.

(38)   Wernimont, A,K.; Huffman, D. L.; Lamb, A.L, O'Halloran TV, Rosenzweig AC. *Nat. Struct. Biol.* **2000**, 9, 766-771.

(39)   Rosenzweig, A,C.; Huffman, D. L.; Hou, M. Y.; Wernimont, A. K.; Pufahl, R. A.; O'Halloran, T. V. *Structure.* **1999**, 6, 605-617.

(40)   Badarau, A.; Firbank, S. J.; McCarthy, A.A.; Banfield, M. J.; Dennison, C. *Biochemistry* **2010***, 36*, 7798-7810.

(41)   Singleton, C.; Hearnshaw, S.; Zhou, L.; Le Brun, N.E.; Hemmings, A.M. *Biochem. J.* **2009**, 3, 347-356.

(42)   Hearnshaw, S.; West, C.; Singleton, C.; Zhou, L.; Kihlken, M.A.; Strange, R.W.; Le Brun, N.E.; Hemmings, A.M. *Biochemistry* **2009**, 40, 9324-9326.

(43)   Zhou, L.; Singleton, C.; Le Brun, N. E. *Biochem. J.* **2008**, 413, 459-465.

(44)   Powlowski, J.; Sahlman, L. *J. Biol. Chem.* **1999**, 274, 33320– 33326.

(45)   Ledwidge, R.; Hong, B.; Dotsch, V.; Miller, S. M. *Biochemistry* **2010**, 49, 8988-8998.

(46)   Schmidt, P. J.; Rae, T. D.; Pufahl, R. A.; Hamma, T.; Strain, J.; O'Halloran, T. V.; Culotta, V. C. *J. Biol. Chem.* **1999**, *274*, 23719-23725.

(47)   Banci, L.; Bertini, I.; Cantini, F.; Felli, I. C.; Gonnelli, L.; Hadjiliadis, N.; Pierattelli, R.; Rosato, A.; Voulgaris, P. *Nat. Chem. Biol.* **2006**, 2, 367– 368.

(48)   Rodriguez-Granillo, A.; Crespo, A.; Estrin, D. A.; Wittung-Stafshede, P. *J. Phys. Chem. B* **2010**, 114, 3698– 3706.

(49)   Furukawa, Y.; Torres, S. A.; O'Halloran, T. V. *EMBO J.* **2004**, 23, 2872-2881.

(50)   B. Angeletti, B.; Waldron, K. J.; Freeman, K. B.; Bawagan, H.; Hussain, I.; Miller, C. C. J.; Lau, K. F.; Tennant, M. E.; Dennison, C.; Robinson N. J.; Dingwall, C. *J. Biol. Chem.* **2005**, *280*, 17930-17937.

Chapter 4

The Quaternary Structure of Human CCS and its Interaction with Cu,Zn-Superoxide Dismutase is Affected by Zinc Binding to Domain 2

4.1   Introduction

A key feature of CCS is the presence of the Cu,Zn-superoxide dismutase (SOD1) like domain 2 (D2).(*1-3*) This domain is the largest of CCS and connects the Cu(I)-binding domains 1 (D1) and 3 (D3) and serves as a region for dimerization of the protein and the interaction with SOD1.(*3-7*) The structure of the D2 in human CCS consists of an 8 stranded antiparallel β-barrel and is similar in overall fold and shares many features with SOD1 (*1,8*) (Figure 4.1.1). In particular key features of the loop regions of SOD1 are conserved in CCS. In loop 4 a region corresponding to the intramolecular disulfide and zinc binding site of SOD1 is present. The residues Cys141 and Cys227 are involved in a disulfide bond analogous to that between Cys57 and Cys146 of SOD1, which is essential for function of the enzyme. The zinc-binding residues His147, His155, His164 and Asp167 are also conserved and bind a single zinc ion in a distorted tetrahedral geometry. Although three of the four His residues (His130, His132 and His147), which correspond to copper ligands of SOD1 are present, the fourth His is replaced by Asp201, and CCS is not thought to bind copper at this potential metal binding site. Loop 7 of D2 in CCS corresponds to the electrostatic channel loop of SOD1, which guides superoxide to the copper for dismutation, and is of similar length and position in both proteins, but in CCS is missing several of the catalytically important residues.

The dimer interface of CCS is located on the opposite side to the loop regions (Figure 4.1.1) containing the zinc-binding site and is very similar in both structure and amino acid content to that for SOD1.(*1-3,8*) Residues involved in dimerization include Gly135, Gly195 and Arg232 that form hydrogen bonds to the opposite monomer at the interface and there are also a number of residues that contribute to hydrophobic contact regions. In the yeast Ccs1 structure D2 has a fold similar to SOD1, and also yeast Sod1, but lacks the Cys residues of the disulfide, the entire zinc loop and the copper binding residues. Ccs1, in contrast to CCS, binds no metals within D2.(*2, 3*) The loop of Ccs1 corresponding to the electrostatic channel loop of SOD1 is also much shorter and positioned differently to that for CCS, SOD1 and Sod1. Despite these differences Ccs1 does retain a dimer interface that is analogous to that observed in Sod1 and CCS and contains the residues that participate in hydrogen bonding and hydrophobic contacts.

Although D2 of CCS and Ccs1 are observed as dimers in their crystal structures their behaviour in solution is distinct. CCS exists as a dimer when apo for copper, whereas apo Ccs1 is monomeric.(*5,6,7,10*) In both cases the binding of copper leads to

oligomerisation; CCS existing as a mixture of dimer and tetramer whereas Ccs1 is present as a mixture of monomer and dimer. Ccs1 and Sod1 form a heterodimer in solution, both in the absence and presence of copper.(*6,7*) The crystal structure of the Ccs1:H48F-Sod1 heterodimer shows how the interface of Ccs1, used for homodimerisation, associates with the corresponding interface of Sod1 to form what is widely regarded as the complex that promotes copper transfer to and disulfide oxidation of Sod1.(*3,11,12*) Because of these observations, and the fact that D2 of CCS is required for SOD1 activation, it is assumed that the role of D2 is for target recognition and orientation of the copper binding domains D1 and D3 for efficient transfer of the metal into the copper binding site of SOD1.(*4,5,9,10,12*)

Zinc-binding and the intramolecular disulfide in human SOD1 have been shown to stabilise of the dimeric enzyme.(*13-15*) Loop 4 that contains the copper and zinc metal binding residues and Cys57 of the disulfide contributes to the dimer interface region. The Cys57-Cys146 disulfide also links this loop to the β-barrel fold and ordering of this loop region by both metal binding and the disulfide stabilise a conformation of the protein that favours dimerization.(*16-18*) Mutations to the zinc binding residues, that prevent zinc binding, affect the structuring of this region of SOD1 and lead to a loss of SOD1 activity *in vivo* (*19*). It has been shown that mutation of the zinc-binding residues His147 and Asp167 in CCS have an effect *in vivo* resulting in a growth-retarding phenotype for yeast (ΔCcs1) expressing the mutant CCS.(*20*) In addition the effects are more pronounced under copper limiting conditions and are attributed to a reduced activity of SOD1 due to a loss of CCS dependent activation. It appears, therefore, that zinc binding to CCS plays an important role in the maturation of CCS itself and is required for proper functioning of the protein. Due to the similarities between D2 of CCS and SOD1, the role of zinc binding might be expected to be similar; namely stabilising a particular conformation of the protein fold that results in an active enzyme.

Understanding the role of metal binding to D2 for the functioning of human CCS has not been studied *in vitro*. The significance of the differences observed for the structures and oligomerisation behaviour of CCS and Ccs1 when activating what appear to be very similar target proteins has also received little attention. SOD1 and Sod1 require the same post-translational processing that includes acquisition of both copper and zinc and formation of the essential disulfide between Cys57 and Cys146.(*3, 8*) Therefore it is unusual that CCS contains a zinc binding site, but Ccs1 does not, and it is currently unknown what propose this metal serves in the functioning of CCS. The work presented in

this chapter details an investigation of the nature of zinc binding to D2 of CCS and the effect on both the quaternary structure of CCS and its interaction with, and activation of, SOD1.

Figure 4.1.1

Crystal structures of D2 of human CCS (A) and human Cu,Zn-SOD1 (B) (one monomer of dimer shown) (PDB accession codes 1DO5 and 1SPD, respectively) drawn in Pymol. The zinc and copper ions are shown as grey and gold spheres, respectively, and the co-ordinating residues and the Cys residues of the disulfide are shown in stick representations. Regions corresponding to the SOD1 zinc loop (CCS loop 4) and the SOD1 electrostatic channel loop (CCS loop 7) are highlighted in green and blue, respectively.
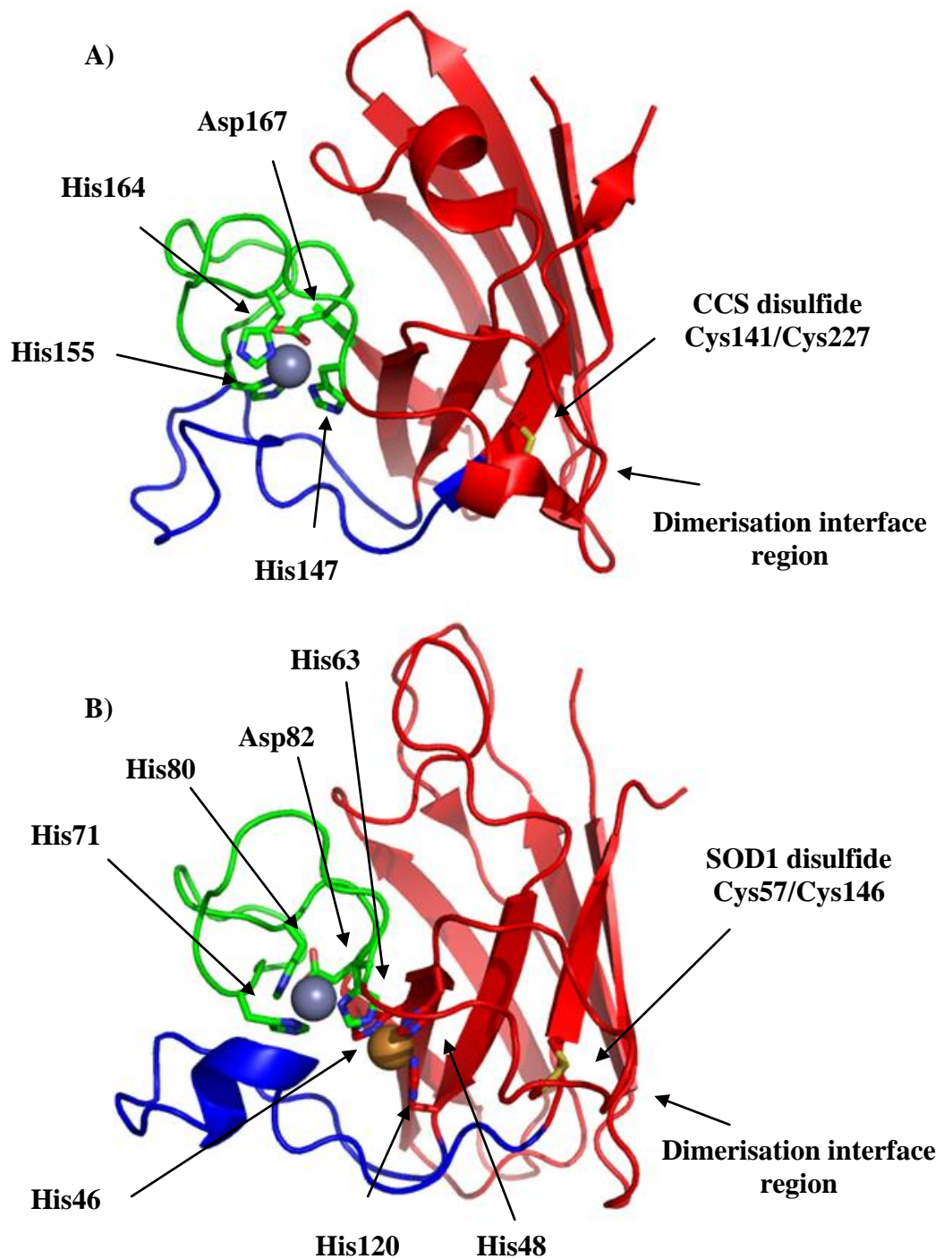
4.2   Experimental

4.2.1   PCR and Cloning of SOD1

The gene for SOD1 was cloned from pCLneo_SOD1 (see section 6.8) by PCR using the forward and reverse primers 5'- GAACATATGGCGACGAAGGCCGTGTGCG -3' and 5'-GAAGAATTCTTATTGGGCGATCCCAATTACACC-3', respectively, giving the construct pGEMT_SOD1 with the gene insert present as an Nde1/EcoR1 fragment. DNA sequencing was used to verify the product by sequencing both strands of the plasmid. The gene was then cloned using the Nde1/EcoR1 restriction sites into pET29a giving pET29a_SOD1.

4.2.2   Expression and Purification of Proteins

WT-CCS, C244S/C246S-CCS, C22S/C25S-CCS, D1-CCS and SOD1 were expressed and purified as described in section 6.10.

4.2.3   Preparation of Zn-depleted WT-CCS

The removal of zinc from as-isolated WT-CCS was achieved through use of a modified protocol reported for demetallation of Sod1.(*5*) As-isolated WT-CCS (10-20 mg) in 5 ml of 20 mM tris(hydroxymethyl)aminomethane (Tris) pH 7.5 containing 1 mM dithiothreitol (DTT) was dialysed against 500 ml of 50 mM acetate at pH 4.5 containing 50 mM ethylenediaminetetraacetic acid (EDTA) to remove bound zinc at 4 ^{o}C. Dialyses required two buffer exchanges of ~3 hours and one left overnight. The protein was then exchanged, by further dialysis, into 20 mM 4-(2-hydroxyethyl)piperazine-1-ethanesulfonic acid (Hepes) pH 7.5 containing 200 mM NaCl and 1 mM DTT using 3 buffer exchanges (~3 hours each). The protein was then concentrated (Amicon Ultra 4, 10 kDa MWCO, Millipore) and injected onto a Superdex 75 column (10/300 GL, GE Healthcare) pre-equilibrated in 20 mM Hepes pH 7.5 containing 200 mM NaCl and 1 mM DTT. Fractions corresponding to monomeric WT-CCS (*vide infra*) were collected and combined and the final sample of Zn-depleted WT-CCS assayed for copper and zinc by AAS.

4.2.4   Protein Reduction and Quantification

As-isolated SOD1 (E,Zn-SOD1) (200-800 μM) was reduced by incubation with 10 mM DTT in 20 mM Tris pH 7.5 in an anaerobic chamber (Belle Technology, O_2 << 2 parts

per million) typically for 12 hours. DTT treated SOD1 was then desalted and exchanged into the required buffer using a PD10 column (GE Healthcare). The concentration of E,Zn-SOD1 was determined by using an epsilon value at 280 nm (ε_{280}) of 5,500 M^{-1} cm^{-1} .[21] Free thiols were assessed by Ellman's assay as described in section 6.15. A correction factor of ~1.2 was required for Bradford assays of E,Zn-SOD1 relative to concentrations determined by the epsilon value at 280 nm. The concentration of as-isolated WT-CCS and its variants (including Zn-depleted WT-CCS) were determined as described in section 2.2.4.

4.2.5 Cu(I) Binding Stoichiometry of Zn-depleted WT-CCS

Preparation of Cu(I) stock solutions, Cu(I)-proteins and the determination of the high affinity Cu(I)-binding stoichiometry of Zn-depleted WT-CCS was performed as described in sections 6.16.1 and 6.16.2. Copper concentrations were determined using bathocuproine disulfonic acid (BCS) and occasionally by AAS also described in section 6.16.1.

4.2.6 Cu(I) Affinity of Zn-depleted WT-CCS

The Cu(I) affinity (K_b value) of Zn-depleted WT-CCS was determined by competition assays with BCS using the approach described in section 6.16.3. Titrations were performed by adding BCS into Cu(I)-protein (5 μM) containing an excess of apo-protein (5 μM) in 20 mM Hepes pH 7.5 containing 200 mM NaCl.

4.2.7 Zn(II) Reconstitution of Zn-depleted WT-CCS

Zn(II) from a 1 mM aqueous stock of ZnSO$_4$, was added slowly to Zn-depleted WT-CCS (10-20 μM) in 20 mM Tris pH 7.5 containing 200 mM NaCl in an anaerobic chamber. Samples were incubated for 5 minutes to ~12 hours and assayed for dimerisation using gel filtration chromatography. Samples (150 μL) were injected onto a Superdex 75 column (10/300 GL, GE Healthcare) pre-equilibrated in 20 mM Hepes pH 7.5 containing 200 mM NaCl (with and without 1 mM DTT). Buffers were purged with N$_2$ and protein elution was monitored by measuring the absorbance at 280 nm.

4.2.8 Cu(II) Loading of E,Zn-SOD1

Copper loaded SOD1 (Cu,Zn-SOD1) was prepared from E,Zn-SOD1 (50-100 μM) by the addition ~1.4 molar equivalents of Cu(II) from a 1 mM aqueous stock of $Cu(NO_3)_2$ in 20 mM Tris pH 7.5 containing 200 mM NaCl. The copper-bound protein was then exchanged into fresh buffer, to remove adventitiously bound copper, by performing three buffer exchanges of 10-fold dilution and subsequent concentration (Vivaspin 500, 5 kDa MWCO, Sartorius). The concentration of the protein in the final sample was determined by Bradford assays using E,Zn-SOD1 as described in 4.2.4. Metal content of the final Cu,Zn-SOD1 sample was determined by AAS.

4.2.9 Interaction between as-isolated and Zn-depleted WT-CCS and SOD1

The interactions between the as-isolated and Zn-depleted WT-CCS (with and without bound Cu(I)) and E,Zn-SOD1 were investigated by gel filtration chromatography. Typically Zn-depleted WT-CCS, as-isolated WT-CCS (both with and without 1 molar equivalent of Cu(I) at 10 or 50 μM protein concentration) was mixed with an equimolar amount of E,Zn or Cu,Zn-SOD1 under anaerobic conditions. Mixtures were then incubated for ~5 minutes prior to injection (~150 μL) on a Superdex 75 column (10/300 GL, GE Healthcare) pre-equilibrated in 20 mM Hepes pH 7.5 containing 200 mM NaCl. 1 mM DTT was added to the column buffer for analysis of samples under reducing conditions. All column buffers were purged with N_2 and protein elution was monitored by measuring the absorbance at 280 nm.

4.2.10 Activation of E,Zn-SOD1 by as-isolated and Zn-depleted WT-CCS

The ability of Zn-depleted WT-CCS and as-isolated WT-CCS to activate SOD1 was assayed using a SOD1 activity determination kit (Fluka). The assay utilizes 2-(4-Iodophenyl)-3-(4-nitophenyl)-5-(2,4-disulfophenyl)-2H-tetrazolium, monosodium salt (WST-1), that produces a formazan dye, with a λ_{max} at 440 nm, upon reduction with superoxide. The assay measures the ability of SOD1 to inhibit the reduction of the WST-1 dye by superoxide generated by xanthine oxidase. By measuring the absorbance at 450 nm the ability of CCS to activate E,Zn-SOD1 was measured. Reaction mixtures consisted of Cu(I)-protein (Zn-depleted WT-CCS or as-isolated WT-CCS, C244S,C246S-CCS, C22SC25S-CCS and D1-CCS) (5 μM) with an excess of the protein apo for copper (5 μM) mixed with E,Zn-SOD1 (10 μM) in 20 mM Hepes pH 7.5

containing 200 mM NaCl plus 50 μM BCS. Mixtures were incubated for 10 minutes in an anaerobic chamber and diluted 50-fold in the same buffer prior to the activity assay. Controls included measuring the activity of E,Zn-SOD1 and also Cu,Zn-SOD1 prepared in 4.2.8.

4.3   Results

4.3.1   Purification and the Initial Characterisation of E,Zn-SOD1

The purity of E,Zn-SOD1 was determined by SDS-PAGE to be > 90 % and matrix assisted laser desorption ionization mass spectrometry (MALDI-MS) analysis showed peaks of 15,995 and 15,797 kDa corresponding to the protein with and without the N-terminal Met (calculated values of 15,996 and 15,806 kDa for the full length and N-terminal Met cleaved proteins). The protein was isolated with negligible copper but contained 1.0 ± 0.2 zinc ions per monomer as determined by AAS. Gel filtration on a Superdex 75 column shows the protein to elute predominantly as a dimer (Figure 4.3.1 and Table 4.3.1). There is a shoulder present, however, at lower protein concentrations that corresponds to a monomeric form. Since zinc binding or Cys oxidation results in the stabilization of dimeric SOD1 this proportion of SOD1, which migrates as the monomeric form, may be either disulfide reduced or not contain bound zinc.(*13*) Free thiol determinations of E,Zn-SOD1 indicated the presence of ~1 thiol per monomer whereas overnight incubation with an excess of DTT results in the presence of ~2 thiols. There are a total of 4 Cys residues in SOD1 of which two, Cys57 and 147, form the conserved disulfide. In Cu,Zn-SOD1, Cys6 and Cys111 are not solvent accessible.(*22,23*) Therefore, the Cys thiols observed for DTT reduced E,Zn-SOD1 may correspond to Cys57 and Cys147. This assignment seems the most likely as no significant peaks were observed for gel filtration of E,Zn-SOD1 that ran heavier than dimer. The Far-UV CD spectrum of E,Zn-SOD1 (Figure 4.3.2) is similar to that reported elsewhere for E,Zn-SOD1 and indicates substantial β-sheet content as expected based on solution and crystal structures of this form of SOD1.(*13,15,18*)

4.3.2   Preparation of Zn-depleted WT-CCS

Zn-depleted WT-CCS was prepared by dialysis of as-isolated WT-CCS against an excess of EDTA at pH 4.5 to remove the zinc ion bound in D2 and then separated from the presence of minor higher order oligomers and impurities by gel filtration chromatography.

The final purified sample of Zn-depleted WT-CCS was found to contain negligible copper and zinc by AAS with the concentration of the protein determined using an ε_{280} value for as-isolated WT-CCS. Analytical gel filtration chromatography of Zn-depleted WT-CCS showed the protein eluting as a single peak at a volume corresponding to an apparent molecular mass of ~41 kDa indicating the zinc-depleted WT-CCS protein is monomeric (Figure 4.3.3). Neither increased concentration nor reducing conditions alters the elution volume of the protein (Figure 4.3.3). The Far-UV CD spectrum for Zn-depleted WT-CCS is almost identical to that for as-isolated WT-CCS (Figure 4.3.4), indicating that the removal of the zinc ion from D2 does not alter the secondary structure of the protein. Free thiol determination for Zn-depleted WT-CCS indicated 7.0 ± 1.0 thiols per monomer and the sample was stable, with regards to thiol oxidation and oligomerisation, under anaerobic conditions for at least several days. Therefore, the removal of zinc destabilises the dimer and also results in an increase in the number of detectable thiols compared to that for as-isolated WT-CCS (section 2.3.1). WT-CCS contains a total of 9 Cys residues with 4 of these contained within D2, of which two of these are involved a disulfide (Cys141 and Cys227).(*1*) It was found previously (section 2.3.1) that only the Cys residues of D1 and D3 appear to be solvent accessible in as-isolated WT-CCS; 3 in D1 and 2 in D3. This means that the 4 Cys residues present in D2 are either involved in a stable disulfide or buried. That zinc removal causes an increase in the number of detectable thiols by two suggests that the disulfide of this domain may become exposed and reduced by DTT or that the previously buried Cys residues become solvent accessible.

4.3.3   Cu(I) Binding Stoichiometry of Zn-depleted WT-CCS

The high affinity Cu(I)-binding stoichiometry of Zn-depleted WT-CCS was determined by titrating Cu(I) into the protein in the presence of BCA (Figure 4.2.5). Zn-depleted WT-CCS binds up to 3 equivalents of Cu(I) tightly under these conditions. The first two equivalents of Cu(I) are bound in a site, or sites, with a much higher affinity than BCA. The third equivalent of Cu(I) is bound less tightly and is similar to that observed for the second equivalent of Cu(I) bound to as-isolated WT-CCS and for the first bound to C22S/C25S-CCS (section 2.3.4). Zinc removal from D2 has resulted in the formation of a second high affinity Cu(I)-binding site within zinc-depleted WT-CCS. This second high affinity Cu(I)-binding site is coincident with the appearance of two additional thiols in Zn-depleted WT-CCS. Both D1 and D3 recruit copper through two Cys residues and it may be possible that the two additional thiols recruit the additional copper ion in zinc-

depleted WT-CCS. UV/Spectra of Cu(I) titration of Zn-depleted CCS gives rise to charge transfer bands characteristic of Cu(I)-thiolate binding for up to at least three equivalents of added Cu(I) (Appendix A Figure 3), indicating all three Cu(I) ions are bound to metal sites involving Cys ligation of the metal.

4.3.4   Cu(I) Affinity of Zn-depleted CCS

In order to quantify the Cu(I) affinity (K_b) for Zn-depleted WT-CCS competition experiments with BCS were performed at pH 7.5 (Figure 4.3.6). An average K_b value of $(5.6 \pm 0.9) \times 10^{17}$ M^{-1} was determined from multiple titrations for the first equivalent of Cu(I) bound to the protein. The affinity of Cu(I) for the Zn-depleted WT-CCS is identical to those determined for as-isolated WT-CCS, C244S/C246S-CCS and D1-CCS (section 2.3.5) where Cu(I) binds to the CXXC motif in D1. The K_b value for Zn-depleted WT-CCS suggests that the CXXC motif of D1 remains the higher affinity copper site.

4.3.5   Zn(II) Reconstitution of Zn-depleted CCS

In order to determine whether zinc-binding by D2 of CCS is reversible, Zn-depleted WT-CCS was incubated with zinc and samples assayed for dimer formation by gel filtration chromatography (Figure 4.3.7). After 5 minutes of incubation with 0.5 and 1.0 equivalents of zinc the chromatograms show the appearance of a significant peak at the same elution volume to that obtained for dimeric as-isolated WT-CCS. In addition, the peak intensity correlates with the amount of added zinc. Increasing the incubation period up to 6 hours results in chromatograms where the majority of the protein, especially for the sample treated with an equimolar amount of zinc, runs as the dimeric form. Interestingly, the sample with 0.5 equivalents of added zinc displays a monomer-dimer equilibrium that strongly favours the dimeric state. Leaving samples for longer periods does not alter the monomer-dimer equilibrium further and the equilibrium is unaffected by the presence of reductant indicating the dimer is unlikely to be the result of a disulfide linked form of CCS. Therefore the addition of Zn(II) to Zn-depleted WT-CCS appears to reform the as-isolated WT-CCS dimer.

4.3.6   Interaction between Zn-depleted and as-isolated WT-CCS and E,Zn-SOD1

The interaction of Zn-depleted and as-isolated WT-CCS with E,Zn-SOD1 was assessed by gel filtration chromatography. The proteins can be assayed by this technique due to the

significant difference between the elution volumes for as-isolated and Cu(I)-bound SOD1 (Figure 4.3.8) and CCS (with or without Cu(I) and Zn(II)). The incubation of as-isolated WT-CCS with E,Zn-SOD results in a chromatogram with peaks corresponding to both homodimeric proteins but also shows the appearance of a new peak at an elution volume corresponding to that for a CCS:SOD1 heterocomplex (Figure 4.3.9 and Table 4.3.2). The chromatogram for Cu(I)-bound as-isolated WT-CCS also shows the heterodimeric CCS:SOD1 complex peak but also a peak corresponding to a CCS tetramer formed by copper binding to the D3 CXC as observed in section 2.3.3. The chromatograms for Zn-depleted WT-CCS or Cu(I)-bound Zn-depleted WT-CCS with E,Zn-SOD1 is missing the peak for heterodimeric CCS:SOD1, and the Cu(I)-bound Zn-depleted form shows a peak at an elution volume corresponding to dimeric CCS (Figure 4.3.9 and Table 4.3.2). Similar results for all of the above mixtures are obtained under reducing conditions, however the peaks corresponding to tetrameric Cu(I)-bound as-isolated WT-CCS and Cu(I)-bound dimeric Zn-depleted WT-CCS are absent indicating that DTT prevents copper dependent oligomerisation of both proteins (Figure 4.3.10 and Table 4.3.3). As the heterodimeric CCS:SOD1 complex is unaffected by reducing conditions the complex likely results from non-covalent interactions between dimerisation interfaces of CCS and SOD1. Identical results are also obtained at 5-fold higher protein concentrations (Figure 4.3.11 and Table 4.3.4). Zinc binding to D2 of CCS, therefore, appears to stabilise the CCS:SOD1 complex. A mixture of as-isolated WT-CCS and Cu,Zn–SOD shows that the fully metallated form of SOD1 does not form a heterocomplex with CCS (Figure 4.3.12).

4.3.7 Activation of E,Zn-SOD1 by as-isolated and Zn-depleted CCS

In order to determine if Zn-depleted WT-CCS is an active metallochaperone an assay for SOD1 activation by CCS was performed (Figure 4.3.13). The activation of E,Zn-SOD1 was similar for both Cu(I)-bound as-isolated and Zn-depleted WT-CCS and resulted in the activation of SOD1 within similar levels observed for Cu,Zn-SOD1 prepared in 4.2.8. The activation of E,Zn-SOD1 by Cu(I)-bound C22S/C25S-CCS, missing the CXXC Cys residues of D1, was also similar to that observed for Cu(I)-bound as-isolated WT-CCS. The activation of E,Zn-SOD1 by both Cu(I)-bound D1-CCS and C244S/C246S-CCS however, was significantly lower indicating that, as expected, the loss of the D3 CXC motif Cys residues results in loss of CCS activation of SOD1. *In vitro* Zn-depleted WT-CCS can therefore still activate E,Zn-SOD1. Time course measurements for the activation of E,Zn-SOD1 (Appendix A, Figure 4) show that the kinetics for activation were similar

for as-isolated and Zn-depleted WT-CCS, and also C22S/C25S-CCS,indicating that Zn-depletion of CCS, under the conditions of the assay, does not affect kinetics of activation of E,Zn-SOD1. The time course measurements for D1-CCS and C244S/C246S-CCS showed kinetics for activation that are significantly slower than for WT-CCS, as expected, due to the absence of the essential CXC motif of D3.(*4,10*)

Table 4.3.1

Elution volumes and apparent molecular weights for E,Zn-SOD1 and Zn-depleted WT-CCS determined on a Superdex 75 10/300 GL column in 20 mM Mes pH 6.5 containing 200 mM NaCl.

protein	elution volume(s) ($\pm$ 0.1 ml)	apparent mass [a] (kDa)
E,Zn-SOD1 (50 μM)	11.4, 12.4	33 ($\pm$ 1), 22 ($\pm$ 1)
E,Zn-SOD1 (100 μM)	11.4	33 ($\pm$ 1)
Zn-depleted WT-CCS (10 μM)	10.8	41 ($\pm$ 1)
Zn-depleted WT-CCS (50 μM)	10.8	41 ($\pm$ 1)

[a] The errors indicated for the apparent masses of proteins are deduced from the error in the measurement of the elution volumes and therefore will be significantly lower than the real error observed (See section 6.4).

Table 4.3.2

Elution volumes and apparent molecular weights for mixtures of as-isolated and Zn-depleted WT-CCS (with and without 1 equivalent of bound Cu(I)) with E,Zn-SOD1 (both 10 μM) on a Superdex 75 10/300 GL Column in 20 mM Hepes pH 7.5 Containing 200 mM NaCl.

protein / protein mixture	elution volume (± 0.3 ml)	apparent mass [a] (kDa)
As-isolated WT-CCS + E,Zn-SOD1	9.7	64 (± 7)
	10.4	48 (± 5)
	11.0 [b]	38 (± 4)
Cu(I)-bound as-isolated WT-CCS	8.8 [b]	92 (± 10)
+ E,Zn-SOD1	9.7	64 (± 7)
	10.4	48 (± 5)
	11.0 [b]	38 (± 4)
Zn-depleted WT-CCS + E,Zn-SOD1	11.0	38 (± 4)
Cu(I)-bound Zn-depleted WT-CCS	9.6 [b]	67 (± 7)
+ E,Zn-SOD1	11.0	38 (± 4)

[a] The errors indicated for the apparent masses of proteins are deduced from the error in the measurement of the elution volumes and therefore will be significantly lower than the real error observed (See section 6.4). [b] Minor peaks.

Table 4.3.3

Elution volumes and apparent molecular weights for mixtures of as-isolated and Zn-depleted WT-CCS (with and without 1 equivalent of bound Cu(I)) with E,Zn-SOD1 (both 10 μM) on a Superdex 75 10/300 GL Column in 20 mM Hepes pH 7.5 Containing 200 mM NaCl plus 1 mM DTT.

protein / protein mixture	elution volume (± 0.3 ml)	apparent mass [a] (kDa)
As-isolated WT-CCS + E,Zn-SOD1	9.7	64 (± 7)
	10.4	48 (± 5)
	11.0 [b]	38 (± 4)
Cu(I)-bound as-isolated WT-CCS	9.7	64 (± 7)
+ E,Zn-SOD1	10.4	48 (± 5)
	11.0 [b]	38 (± 4)
Zn-depleted WT-CCS + E,Zn-SOD1	11.0	38 (± 4)
Cu(I)-bound Zn-depleted WT-CCS	11.0 (Broad)	38 (± 4)
+ E,Zn-SOD1		

[a] The errors indicated for the apparent masses of proteins are deduced from the error in the measurement of the elution volumes and therefore will be significantly lower than the real error observed (See section 6.4). [b] Minor peaks.

Table 4.3.4

Elution volumes and apparent molecular weights for mixtures of as-isolated and Zn-depleted WT-CCS (with and without 1 equivalent of bound Cu(I)) with E,Zn-SOD1 (both 50 μM) on a Superdex 75 10/300 GL Column in 20 mM Hepes pH 7.5 Containing 200 mM NaCl.

protein / protein mixture	elution volume (± 0.2 ml)	apparent mass [a] (kDa)
Zn-depleted WT-CCS	11.0	38 (± 4)
As-isolated WT-CCS	9.7	64 (± 7)
as-isolated WT-CCS + E,Zn-SOD1	9.7 [b]	64 (± 7)
	10.4	48 (± 5)
	11.0 [b]	38 (± 4)
Cu(I)-bound as-isolated WT-CCS + E,Zn-SOD1	9.0 [b]	85 (± 9)
	9.7	64 (± 7)
	10.4	48 (± 5)
	11.0 [b]	38 (± 4)
Zn-depleted WT-CCS + E,Zn SOD1	11.0	38 (± 4)
Cu(I)-bound Zn-depleted WT-CCS + E,Zn-SOD1	11.0	38 (± 4)

[a] The errors indicated for the apparent masses of proteins are deduced from the error in the measurement of the elution volumes and therefore will be significantly lower than the real error observed (See section 6.4). [b] Minor peaks.

Figure 4.3.1

Gel filtration chromatograms for E,Zn-SOD1 [50 μM (A) and 100 μM (B)] in 20 mM Hepes pH 7.5 containing 200 mM NaCl. Absorbance measured at 280 nm. Protein eluting at 11.4 ml (~ 33 kDa) corresponds to dimeric SOD1 and the shoulder present in (A) at 12.4 ml (~ 22 kDa) corresponds to monomeric SOD1.
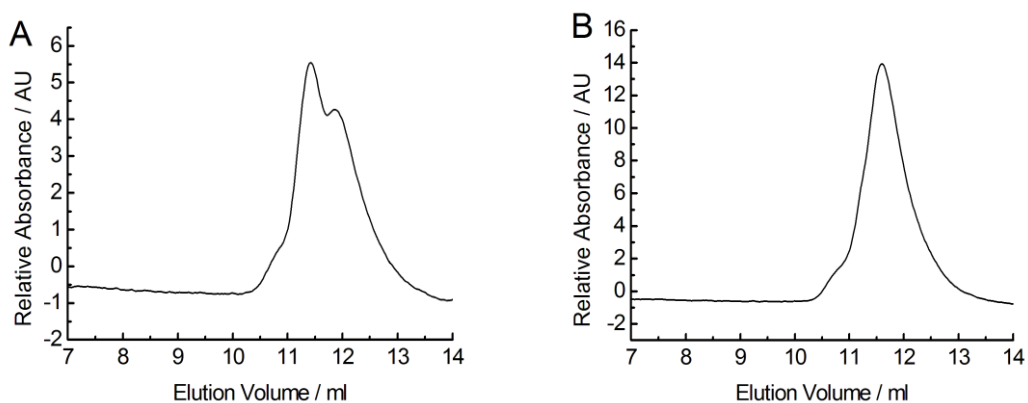
Figure 4.3.2

Far-UV CD spectra for as-isolated E,Zn-SOD1 in 20 mM Hepes pH 7.5 containing 200 mM NaCl.
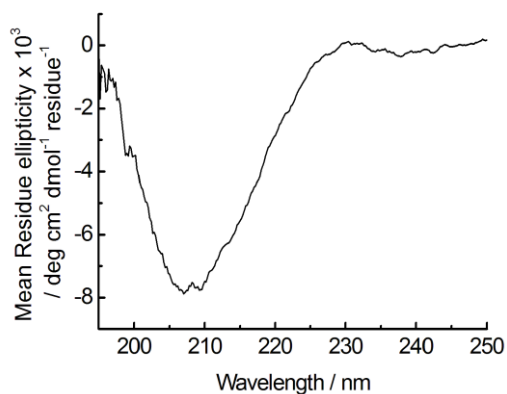
Figure 4.3.3

Gel filtration chromatograms for Zn-depleted WT-CCS [10 μM (A) and 50 μM (B)] and under reducing conditions (10 μM) (C). Gel filtration chromatogram for Cu(I)-bound Zn-depleted WT-CCS [1 molar equivalent Cu(I)] is shown in (D). All chromatograms obtained in 20 mM Hepes pH 7.5 containing 200 mM NaCl, except for (C) which contained 1 mM DTT. Absorbance measured at 280 nm. Elution volumes of ~10.8 and ~9.7 ml correspond to apparent molecular masses of ~41 and ~64 kDa for the monomeric and dimeric forms of CCS, respectively.
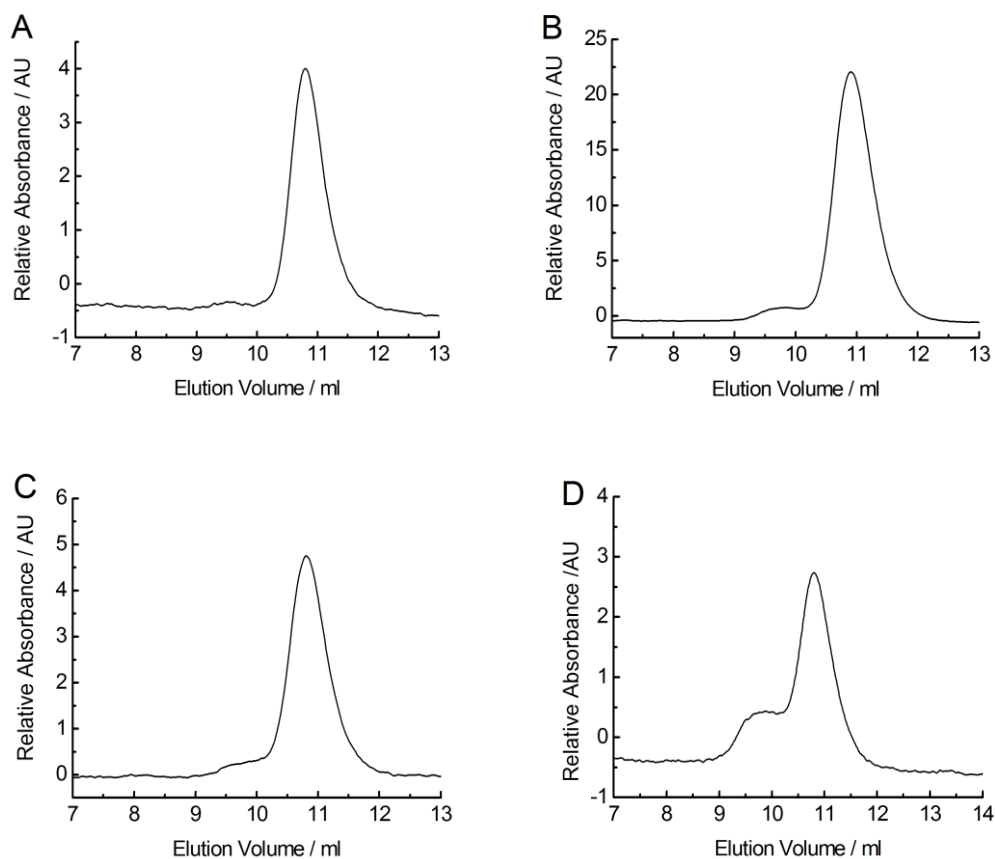
Figure 4.3.4

Far-UV CD spectra for Zn-depleted WT-CCS (solid) and as-isolated WT-CCS (dotted) (both 0.5 mg/ml) in 20 mM Hepes pH 7.5 containing 200 mM NaCl.
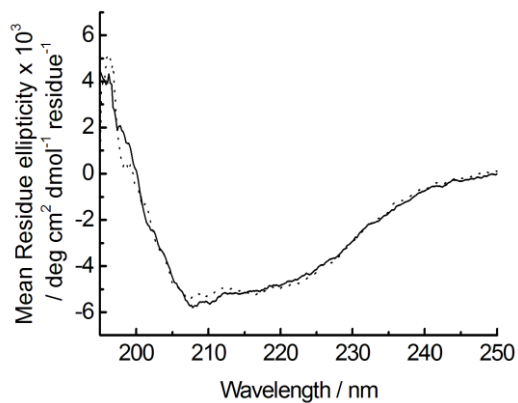
Figure 4.3.5

Titration of Cu(I) into Zn-depleted WT-CCS (10 μM) in 20 mM Hepes pH 7.5 containing 200 mM NaCl and 500 μM BCA.
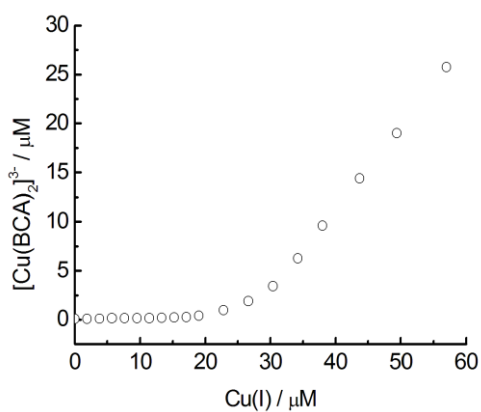
Figure 4.3.6

Titration of BCS into Cu(I)-bound Zn-depleted WT-CCS (10 μM) plus excess Zn-depleted WT-CCS (10 μM) in 20 mM Hepes pH 7.5 containing 200 mM NaCl. The line shows a fit of the data to equation 5.1, giving a K_b value of $(5.2 \pm 0.4) \times 10^{17}$ M^{-1}.
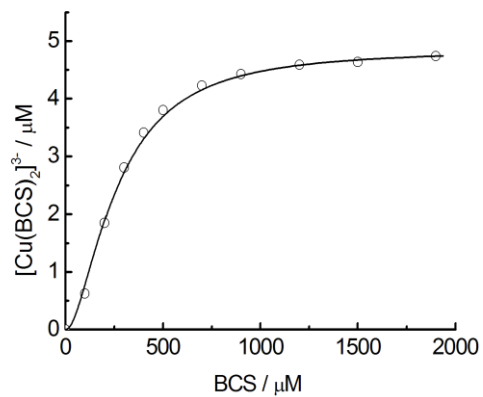
Figure 4.3.7

Gel filtration chromatograms for Zn-depleted WT-CCS (10 μM) reconstituted with 0.5 (solid line) and 1 (dashed line) equivalents of Zn(II) after 5 minutes (A) and 6 hours (B) of incubation. Gel filtration chromatogram for Zn-depleted WT-CCS (10 μM) reconstituted with 1 equivalent of Zn(II) after overnight incubation (C). All chromatograms obtained in 20 mM Hepes pH 7.5 containing 200 mM NaCl except for (C) which also contained 1 mM DTT. Absorbance measured at 280 nm. Elution volumes of ~10.8 and ~9.7 ml correspond to apparent molecular masses of ~41 and ~64 kDa for the monomeric and dimeric forms of CCS, respectively.
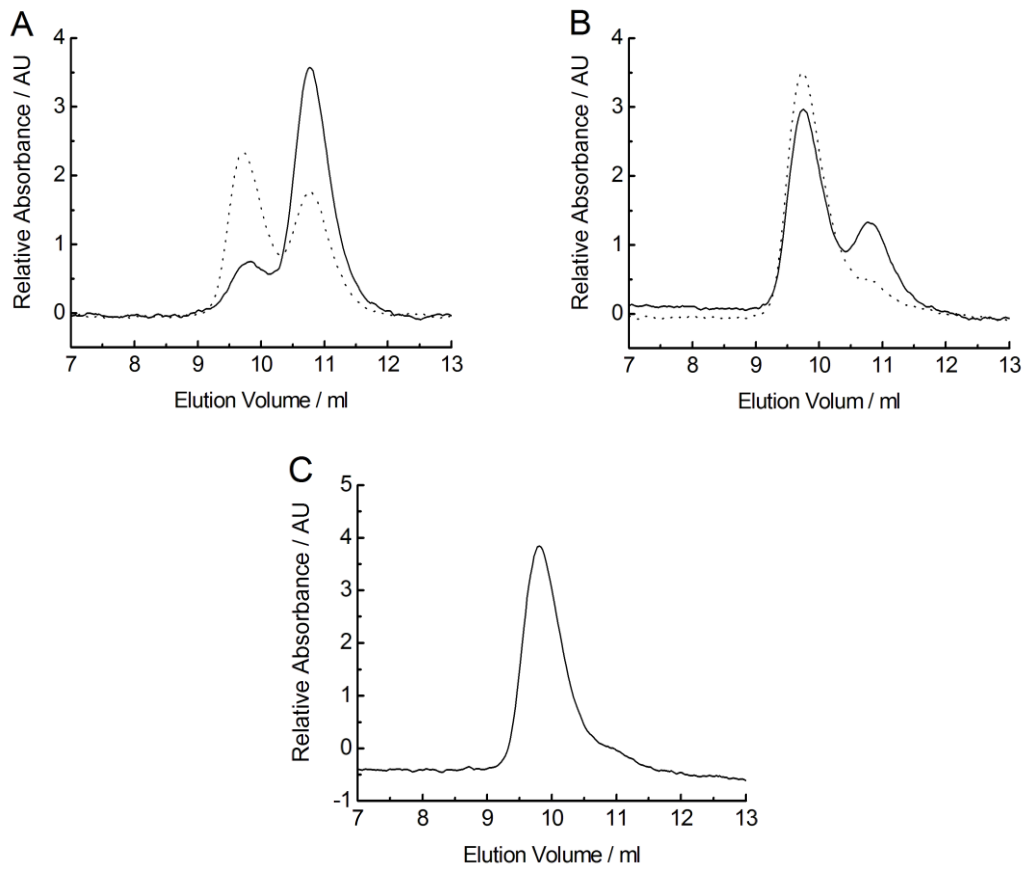
Figure 4.3.8

Gel filtration chromatograms for E,Zn-SOD1 (10 μM) (A) and Cu,Zn-SOD1 (10 μM) (B) in 20 mM Hepes pH 7.5 containing 200 mM NaCl. Absorbance measured at 280 nm. Elution volume of ~11.4 ml corresponds to an apparent molecular mass of ~33 kDa for dimeric SOD1.
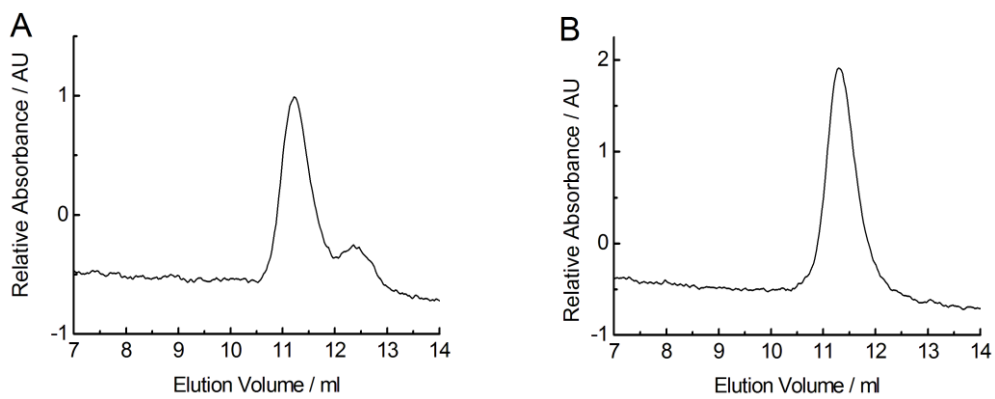
Figure 4.3.9

Gel filtration chromatograms for as-isolated WT-CCS and E,Zn-SOD1 (A), Cu(I)-bound as-isolated WT-CCS and E,Zn-SOD1 (B), Zn-depleted WT-CCS and E,Zn-SOD1 (C) and Cu(I)-bound Zn-depleted WT-CCS and E,Zn-SOD1 (D) (all 10 μM) in 20 mM Hepes pH 7.5 containing 200 mM NaCl. Absorbance measured at 280 nm. Elution volumes and apparent molecular weights are listed in Table 4.3.2.
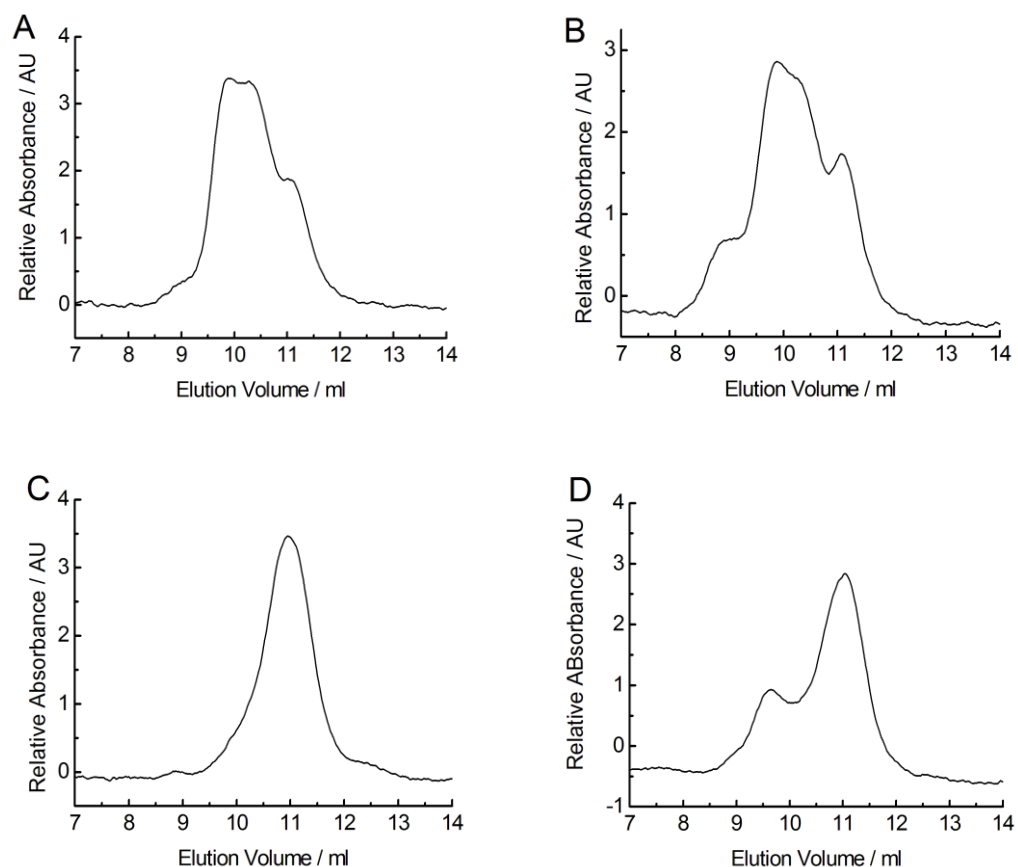
Figure 4.3.10

Gel filtration chromatograms for as-isolated WT-CCS and E,Zn-SOD1 (A), Cu(I)-bound as-isolated WT-CCS and E,Zn-SOD1 (B), Zn-depleted WT-CCS and E,Zn-SOD1 (C) and Cu(I)-bound Zn-depleted WT-CCS and E,Zn-SOD1 (D) (all 10 μM) in 20 mM Hepes pH 7.5 containing 200 mM NaCl plus 1 mM DTT. Absorbance measured at 280 nm. Elution volumes and apparent molecular weights are listed in Table 4.3.3.
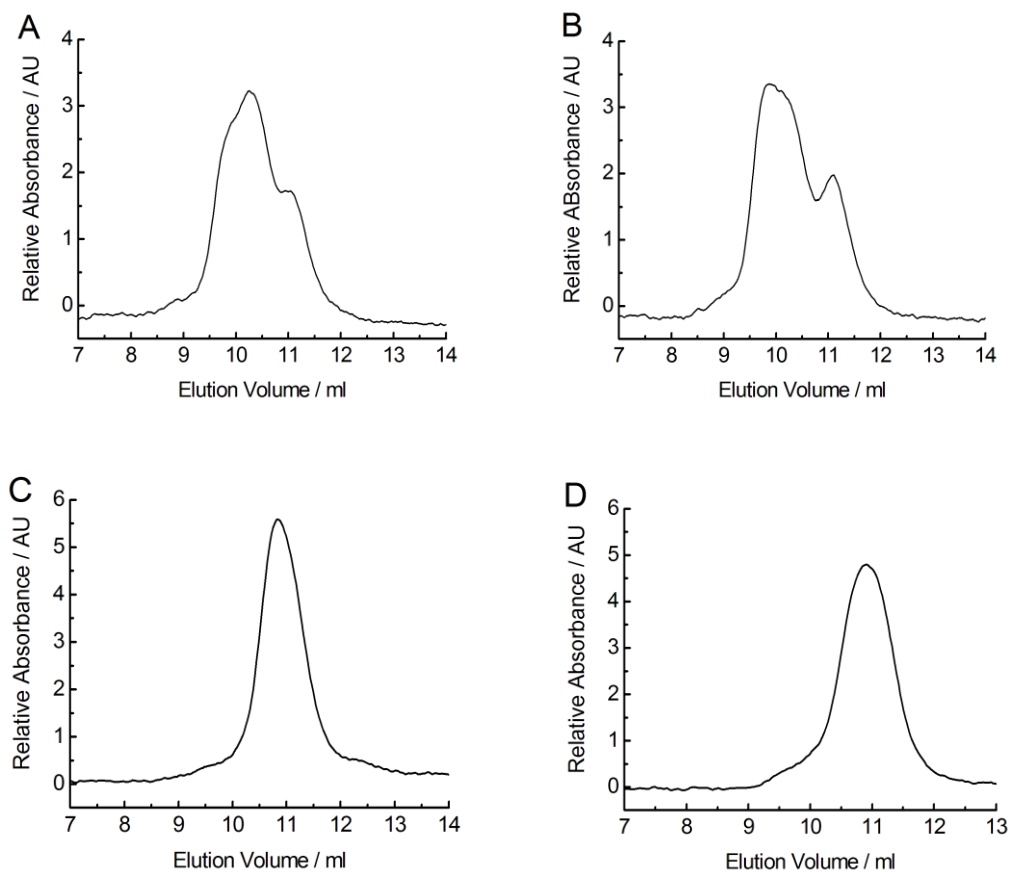
Figure 4.3.11

Gel filtration chromatograms for Zn-depleted WT-CCS (A) as-isolated WT-CCS (B) as-isolated WT-CCS and E,Zn-SOD1 (C), Cu(I)-bound as-isolated WT-CCS and E,Zn-SOD1 (D), Zn-depleted WT-CCS and E,Zn-SOD1 (E) and Cu(I)-bound Zn-depleted WT-CCS and E,Zn-SOD1 (F) (all 50 μM) in 20 mM Hepes pH 7.5 containing 200 mM NaCl. Absorbance measured at 280 nm. Elution volumes and apparent molecular weights are listed in Table 4.3.4.
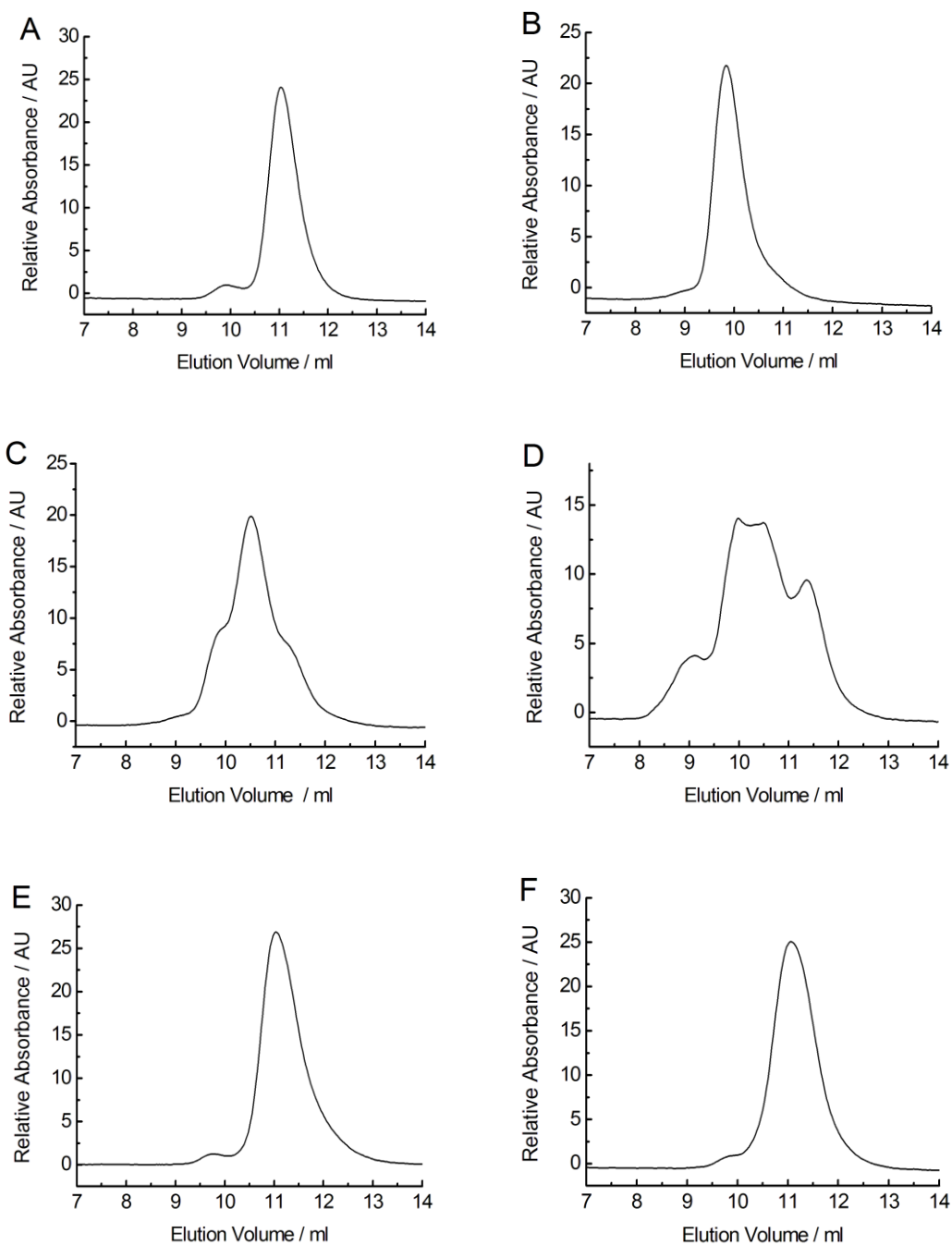
Figure 4.3.12

Gel filtration chromatogram for as-isolated WT-CCS and Cu,Zn-WT-SOD1 (both 10 μM) in 20 mM Hepes pH 7.5 containing 200 mM NaCl. Absorbance measured at 280 nm. Elution volumes of ~11.4 and ~9.7 ml correspond to apparent molecular masses of ~33 and ~64 kDa for the dimeric forms of SOD1 and CCS, respectively.
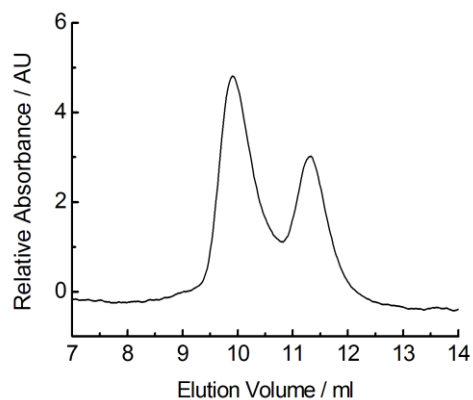
Figure 4.3.13

CCS activation of SOD1 assayed by xanthine oxidase WST-1 reduction inhibition. Assay of SOD1 activity for reaction mixtures containing Cu(I)-bound CCS (5 μM) and excess apo-CCS (5 μM) with E,Zn-SOD1 (10 μM) in 20 mM Hepes pH 7.5 containing 200 mM NaCl and 50 μM BCS for Zn-depleted WT-CCS, as-isolated WT-CCS, C22S/C25S-CCS, C244S/C246S-CCS and D1-CCS.
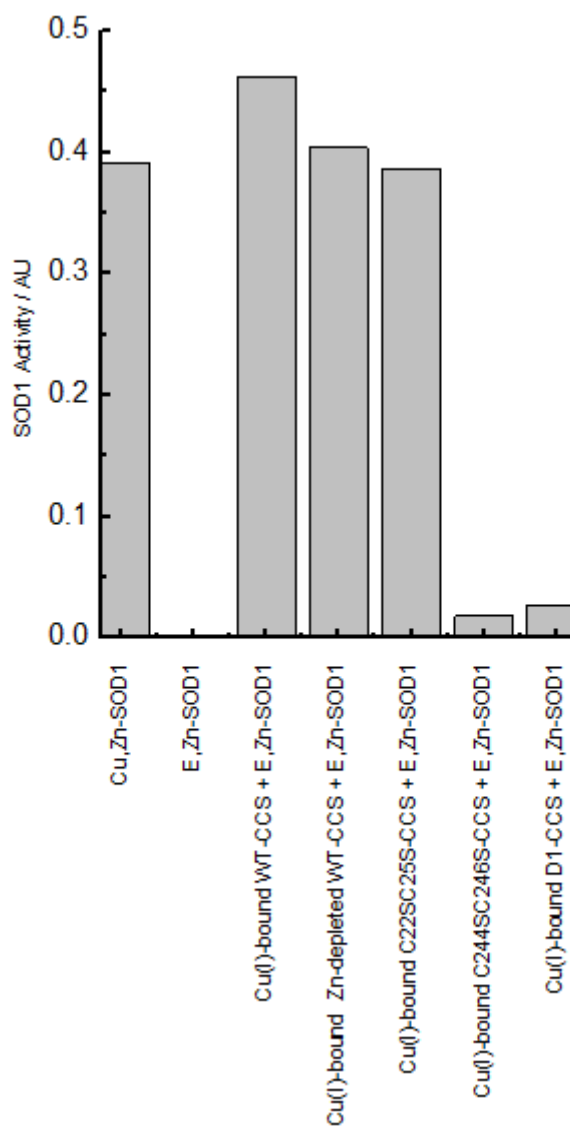
4.4   Discussion

Demetallation of as-isolated WT-CCS at low pH in the presence of excess metal chelators yields Zn-depleted WT-CCS. In contrast to the zinc-bound dimeric form, Zn-depleted WT-CCS is a monomer. Despite the change in oligomeric state, from dimer to monomer, the Zn-depleted form of WT-CCS retains the same secondary structure as the zinc-bound as-isolated (copper free) WT-CCS as determined by CD spectroscopy. Therefore changes to the proteins tertiary structure, due to the binding of zinc in D2, affect monomer-dimer stability of CCS. Zn-depleted copper free WT-CCS binds up to three equivalents of Cu(I) with high affinity with the first two equivalents binding tightly but the third more weakly. This compares with the binding of two equivalents of Cu(I) for the as-isolated zinc-bound WT-CCS which has one high and one low affinity sites. The affinity of the first bound Cu(I) to zinc-depleted WT-CCS is similar to that determined for the D1 CXXC motif (section 2.3.5) and indicates that the CXXC-containing D1 likely represents one of the high affinity Cu(I) sites in zinc-depleted WT-CCS. The additional 2 thiols in the zinc-depleted WT-CCS indicate that changes to the D2 structure includes exposure of previously buried Cys residues. D2 of CCS contains 4 Cys residues of which 3 are located in close proximity to each other with two of these involved in a disulfide (Cys141 and Cys227).(*1*) It is possible that the Cys residues of the disulfide may become exposed and reduced upon demetallation resulting in the formation of an additional high affinity Cu(I) site in zinc-depleted WT-CCS. The Cu(I)-binding characteristics of the third copper are similar to those observed for Cu(I)-binding to C22S/C25S-CCS (section 2.3.4) and suggest that this third copper binds to the CXC motif of D3.

D2 of CCS shares many features with SOD1 including a similar protein fold, zinc binding site and a conserved intramolecular disulfide and so it is possible to propose a hypothesis for the effects of zinc binding to CCS by considering the available SOD1 structures.(*1,8,17,18*) Structures for SOD1 that are apo for both copper and zinc typically display disorder in the metal binding regions. The binding of zinc re-orients the loop regions of SOD1, specifically loop 4 on which the majority of the metal binding residues are located, and contributes to the positioning of the anti-parallel β-strands that are involved in the formation of a stable homodimer.(*18*) Zinc binding to monomeric apo reduced SOD1 shifts the equilibrium towards the formation of the dimer.(*13*) The conserved Cys residues (Cys57 and Cys146) also have a significant effect on the quaternary structure with apo oxidized SOD1 existing as a dimer in both crystal structures and solution.(*13,14,17,18*) The disulfide connects loop 4 to β-sheet 8 of the β-barrel fold

and contributes to the overall arrangement of the β-sheets. Both zinc binding and Cys oxidation in SOD1 stabilise the homodimer. Zinc-binding to Zn-depleted WT-CCS results in a homodimer suggesting that similar changes to the loop regions upon metallation of the protein contribute to dimer stabilisation. In SOD1, apo for copper and zinc, the zinc binding residues are solvent exposed and ready to bind the zinc ion.[17] A similar conformation of the metal binding site for Zn-depleted WT-CCS seems likely given the reversibility of zinc binding.

The interaction between CCS and the E,Zn-SOD1 is either abolished or severely disrupted upon removal of zinc from CCS, which indicates that zinc-binding is a prerequisite for formation of a stable CCS:SOD1 heterocomplex. This heterocomplex is proposed to be an intermediate in the pathway for CCS activation of SOD1.[3] Therefore the binding of zinc to D2 of CCS not only stabilises homodimer formation but also optimises the tertiary structure of CCS for interaction with E,Zn-SOD1. The structure of E,Zn-SOD1 shows that the vacant copper binding site region remains disordered and exposed.[18] Therefore the binding of zinc to CCS and SOD1 would both promote heterodimer formation and subsequent transfer of copper through the opening up of the copper binding site in SOD1. It is noteworthy that we also show that WT-CCS, with Zn bound in D2, does not form a heterocomplex with Cu,Zn-SOD1. The dimerisation interface of CCS appears to distinguish between E,Zn-SOD1 and Cu,Zn-SOD1. The structure of E,Zn-SOD1 is more similar to that of the Cu,Zn-SOD1 than to E,E-SOD1 with only minor changes to the structure upon the binding of copper.[8,17,18] The structural changes, however, may be sufficient to abolish the interaction with CCS once the fully metallated Cu,Zn-SOD1 enzyme is formed. This specificity of the CCS:SOD1 interaction would prevent unnecessary interactions between the fully matured SOD1 protein and CCS. It seems likely that the effects of metallation on both CCS and SOD1 affect the tertiary structures in a way that optimises the proteins for each stage of the SOD1 maturation process.

Although activation of SOD1 by Zn-depleted CCS *in vitro* is possible it is not known whether Zn-depleted CCS is functional *in vivo*. Mutations to the zinc co-ordinating His147 and Asp167 residues of CCS, however, result in a reduced level of SOD1 activation *in vivo*.[20] It was proposed that the reduced level of SOD1 activity was due to these residues playing a role in transferring copper to SOD1, or because of a change in conformation in CCS that resulted in a loss of interaction between the two proteins. The levels of CCS in the cell, however, were reduced for proteins carrying these two

deleterious mutations and so this would result in less available CCS for activation of SOD1. Although the Zn-depleted WT-CCS is found to be stable *in vitro* under anaerobic conditions, it may be unstable *in vivo* and lead to protein aggregation or it may be processed by the cell. That we see activation of SOD1 *in vitro* with Zn-depleted WT-CCS may mean that although the heterodimeric CCS: SOD1 complex is destabilised it may still form, albeit weakly, allowing for CCS activation of SOD1.

In *S. cerevisiae* Sod1 localisation to the mitochondrial IMS is dependent upon the presence of Ccs1 which is recruited by the Mia40/Erv1 disulfide relay system through a disulfide dependent mechanism.(*25,26*) It has been shown that the disulfide reduced apo-Sod1 represents a physiologically important form as the metallated and oxidized forms are not transported into the mitochondria.(*25*) Therefore, only the most immature form of Sod1 is taken up into the IMS. A similar immature form of CCS may also be required by the Mia40/Erv1 system for mitochondrial uptake, for subsequent activation of SOD1 in the mitochondria. It is known that the Cys residues of D1 (Cys27 and Cys64) in Ccs1, that form an intramolecular disulfide, are involved in uptake to the mitochondria.(*3,27,28*) CCS does not contain the corresponding Cys residues in D1, however it does have a disulfide present in D2, which is absent in Ccs1, and this disulfide may play a role in mitochondrial uptake.(*1,5*) This would indicate that Zn-depleted WT-CCS may represent a physiologically relevant form of CCS that is taken up into the mitochondria as the disulfide in D2 of this form is likely to be reduced (two extra thiols present in Zn-depleted WT-CCS compared to as-isolated (Zn-bound) WT-CCS) in the cell cytosol.

A model whereby Zn-binding to CCS modulates the interaction of the metallochaperone with the SOD1 target could be envisioned. Zn-binding to CCS would initially encourage the formation of the CCS: SOD1 heterodimeric complex, a complex generally regarded as an important intermediate for copper transfer to and oxidation of SOD1.(*3*) After metallation and disulfide reduction of SOD1 the tertiary structure of SOD1 is altered in such a way as to promote dissociation of the heterocomplex and formation the active and stabilised SOD1 homodimer and leaving CCS free to turnover more SOD1. The results in this chapter provide the first *in vitro* details for a role of the zinc binding site of D2 in human CCS.

4.5 References

(1)   Lamb, A. L.; Wernimont A. K.; Pufahl, R. A.; O'Halloran, T. V.; Rosenzweig, A. C. *Biochemistry* **2000**, *39*, 1589-1595.

(2)   Lamb, A. L.; Wernimont, A. K.; Pufahl, R. A.; Culotta, V. C.; O'Halloran, T. V.; Rosenzweig, A. C. *Nat. Struc. Biol.* **1999**, *6*, 724-729.

(3)   Lamb, A. L.; Torres, A. S.; O'Halloran, T. V.; Rosenzweig, A. C. *Nat. Struc. Biol.* **2001**, 8, 751-755.

(4)   Schmidt, P. J.; Rae, T. D.; Pufahl, R. A.; Hamma, T.; Strain, J.; O'Halloran, T. V.; Culotta, V. C. *J. Biol. Chem.* **1999**, *274*, 23719-23725.

(5)   Rae, T. D.; Torres, A. S.; Pufahl, R. A.; O'Halloran, T. V. *J. Biol. Chem.* **2001**, *276*, 5166-50176.

(6)   Torres, A. S.; Petri, V.; Rae, T. D.; O'Halloran, T. V. *J. Biol. Chem.* **2001**, 276, 38410-38416.

(7)   Lamb, A. L.; Torres, A. S.; O'Halloran, T. V.; Rosenzweig, A. C. *Biochemistry* **2000**, *39*, 14720-14727.

(8)   Strange, R. W.; Antonyuk, S. V.; Hough, M. A.; Doucette, P. A.; Valentine, J. S.; Hasnain, S. S. *J. Mol. Biol.* **2006**, 356, 1152-1162.

(9)   Rosenzweig, A. C. *Acc. Chem. Res.* **2001**, *34*, 119-128.

(10)   Furukawa, Y.; Torres, S. A.; O'Halloran, T. V. *EMBO J.* **2004**, 23, 2872-2881.

(11)   Culotta, V. C.; Yang, M.; O'Halloran, T. V. *Biochim. Biophys. Acta* **2006**, *1763*, 747-758.

(12)   Stasser, J. P.; Silivai, G. S.; Barry, A. N.; Blackburn, N. *Biochemistry* **2007**, *46*, 11845-11856.

(13)   Arnesano, F.; Banci, L.; Bertini, I.; Martinelli, M.; Furukawa, Y.; O'Halloran, T. V. *J. Biol. Chem.* **2004**, 279, 47998-48003.

(14)   Lindberg, M. J.; Normark, J.; Holmgren, A.; Oliveberg, M. *Proc. Natl. Acad. Sci. U.S.A.* **2004**, 45, 15893-15898.

(15)   Potter, S. Z.; Zhu, H.; Shaw, B. F.; Rodriguez, J. A.; Doucette, P. A.; Sohn, S. H.; Durazo, A.; Faull, K. F.; Gralla, E. B.; Nersissian, A. M.; Valentine, J. S. *J. Am. Chem. Soc.* **2007**, 129, 4575-4583.

(16)   Banci, L.; Bertini, I.; Cramaro, F.; Conte, R. D.; Viezzoli, M. S. *Biochemistry*, **2003**, 42, 9543-9553.

(17)   Banci, L.; Bertini, I.; Cantini, F.; D'Amelio, N.; Gaggelli, E. *J. Biol. Chem.* **2006**, 281, 2333-2337.

(18)   Strange, E. W.; Antonyuk, S.; Hough. M. A.; Doucette, P. A.; Rodriguez, J. A.; Hart, P. J.; Hayward, L. J.; Valentine, J. S.; Hasnain, S. S. *J. Mol. Biol.* **2003**, 328, 877-891.

(19)   Son, M.; Srikanth, U.; Puttaparthi, K.; Luther, C.; Elliot, J. L. *J. Neurochem.* **2011**, 118, 891-901.

(20)   Endo, T.; Fujii, T.; Sato, K. Taniguchi, N.; Fujii, J. *Biochim. Biophys. Acta* **2000**, *276*, 999-1004.

(21)   Pace, C. N.; Vajdos, F.; Fee, L.; Grimsley, G.; Gray, T. *Protein Sci.* **1995**, 11, 2411-2423.

(22)   Banci, L.; Bertini, I.; Boca, M.; Calderone, V.; Cantini, F.; Girotto, S.; Vieru, M. *Proc. Natl. Acad. Sci. U.S.A.* **2009**, 106, 6980-6985.

(23)   Banci, L.; Bertini, I.; Durazo, A.; Girotto, S.; Gralla, E. B.; Martinell, M.; Valentine, J. S.; Vieru, M.; Whitelegge, J. P. *Proc. Natl. Acad. Sci. U.S.A.* **2007**, 104, 11263-11267.

(24)   Hallewell, R. A.; Imlay, K. C.; Lee, P.; Fong, N. M; Gellegos, C.; Getzoff, E. D.; Tainer, J. A.; Cabelli, D. E.; Tekamp-Olson, P. *Biochem. Biophys. Res. Comm.* **1991**, 181, 474-480.

(25)   Field, L. S.; Furukawa, Y. O'Halloran, T. V.; Culotta, V. C. *J. Biol. Chem.* **2003**, 278, 28052-29059.

(26)   Reddehase, S.; Grumbt, B.; Neupert, W.; Hell, K. *J. Mol. Biol.* **2009**, 385, 331-338.

(27)   Kloppel, C.; Suzuki, Y.; Kojer, K.; Petrungaro, C.; Longen, S.; Fiedler, S.; Keller, S.; Riemer, J. *Mol. Biol. Cell* **2011**, 20, 3749-3757.

(28)   Groß, D. P.; Burgard, C. A.; Reddehase, S.; Leitch, J. M.; Culotta, V. C.; Hell, K. *Mol. Biol. Cell* **2011**, 20, 3758-3767.

Chapter 5

Discussion and Future Work

5.1 Discussion

Intracellular copper availability in eukaryotes is severely restricted due to the potential toxicity of the metal(*1,2*) and copper trafficking pathways have evolved to populate copper-requiring proteins.(*3,4*) These pathways contain soluble copper metallochaperones that bind and deliver copper to appropriate cellular targets.(*3-8*) Atx1 delivers copper to the copper-transporting ATPases of the Golgi for incorporation into secreted proteins, CCS delivers copper to the antioxidant enzyme Cu,Zn-superoxide dismutase (SOD1) while Cox17 is involved in the metallation of cytochrome *c* oxidase.(*1,9-12*) The binding of Cu(I) by Cys-based sites with exceptionally high affinity allow the metallochaperones to bind and retain the metal.(*13-16*) The predominantly digonal coordination of Cu(I) in these sites along with their surface exposed nature and specific protein-protein interactions ensure copper transfer by ligand exchange to target proteins.(*13-23*) Extensive study of the Atx1 metallochaperones has contributed significantly to our current understanding of copper trafficking.(*7,8,24-28)* In contrast, despite its biological importance, CCS has undergone relatively little study, especially concerning copper-binding and delivery.(*7,11,29*) Furthermore, CCS is unique among the metallochaperones in that it is involved in both the chaperoning and insertion of copper into the final target protein.(*6,7,11*) Knowledge of the molecular details of copper-binding by CCS are fundamental to an understanding of the mechanism of action of this metallochaperone and copper trafficking in eukaryotes.

The Cu(I) affinities determined for CCS (human CCS) in Chapter 2 demonstrate that the CXXC motif of domain 1 (D1) and the CXC motif of domain 3 (D3) have high Cu(I) affinities. D1 binds Cu(I) ~10-fold tighter than D3 with an affinity similar to that for the structurally homologous metallochaperone HAH1 (human Atx1).(*13,30*) D1 of CCS must play a role similar to that of HAH1, participating in copper acquisition and transfer. Communication between copper-trafficking pathways has previously been suggested.(*31*) The observation of *in vitro* Cu(I) transfer between CCS D1 and HAH1 (Chapter 2) demonstrates that the two cytosolic copper-trafficking pathways could interact via the metallochaperones.(*31*) Although D3 is responsible for copper insertion into SOD1 its affinity for Cu(I) is lower than that of D1 and the copper site of SOD1(*32*) highlighting that Cu(I) affinities alone are insufficient to describe the mechanism of copper transfer. The structural flexibility of D3 and its ability to insert copper into the buried active site of SOD1 appear to be more important than its affinity for copper.

The Cu(I) affinities of numerous copper metallochaperones and their partner proteins are similar and the resulting thermodynamic gradients for copper transfer are not always favourable.[13,14,32,33] Other factors, such as the kinetics of copper transfer between partners, must be important for copper trafficking.[13,34] The results presented in Chapter 3 demonstrate that the pK_a's of the Cys residues of the CXXC and CXC motifs of CCS affect Cu(I)-binding. In particular, the pK_a of the N-terminal Cys residue of the D1 CXXC motif is lowered by ~ 1 unit by a thiolate-stabilising hydrogen-bonding interaction with Arg71 on loop 5 of the same domain. A similar interaction is present between the corresponding Cys residue of HAH1 and Lys60, which also results in a lowering of the pK_a.[13] Such tuning of the pK_a indicates altered nucleophilicity of the Cys ligands and in the case of HAH1 has been suggested to lower the activation energy for copper transfer from the metallochaperone to the metal-binding domains of the copper-transporting ATPases.[13] In CCS, the relative nucleophilicities of the Cu(I)-binding Cys residues of the CXXC and CXC motifs, inferred from their pK_a's, also suggests a lowering of the activation energy for copper-transfer from D1 to D3. Therefore D1, despite having the higher Cu(I) affinity, is kinetically optimised to transfer copper to D3, which ultimately inserts copper into SOD1. The ability to tune the reactivity of the copper-binding ligands would appear crucial for the function of CCS and further explains the selection of Cys rather than Met ligation in copper metallochaperones.

Protein-protein interactions play a crucial role in ensuring the metallochaperones deliver copper to appropriate partner proteins.[20,21,22] Domain 2 (D2) of CCS is structurally similar to SOD1.[35] The formation of a heterodimer between CCS and SOD1, mediated via D2, is thought to optimally position the copper-binding domains of CCS for SOD1 activation.[36] D2 of CCS is unusual in that it maintains the zinc-binding site of SOD1.[35] In Chapter 4 the importance of zinc-binding to D2 and its effects on CCS oligomerisation and target binding has been investigated. The results demonstrate that CCS exists as a monomer in the absence of Zn(II) and that the binding of Zn(II) to D2 stabilises the dimeric form of the protein. Furthermore, the binding of Zn(II) to CCS is required for the formation of a heterodimer with SOD1. It has been shown previously that mutations to the zinc-binding residues of D2 of CCS result in significantly attenuated activation of SOD1 *in vivo*.[37] Interestingly, these mutations result in a decrease in the amount of soluble CCS [37] indicating a role for Zn(II) in stabilising the protein within the cell. The binding of Zn(II) to the structurally similar SOD1 is known to drive the dimerization of SOD1 monomers and substantially increases the stability of the protein

fold.(*38-40*) The binding of Zn(II) to D2 of CCS would therefore appear crucial to the stability and function of the metallochaperone and likely maintains a tertiary structure that favours formation of a CCS homodimer and the CCS:SOD1 heterodimer. The biological significance of the CCS monomer is currently unresolved.

5.2 Future Work

There remain aspects of the CCS copper trafficking pathway that require further study, in particular, the mechanism of metal insertion into SOD1 is still poorly understood. It would be advantageous to determine the Cu(I) affinity of SOD1, using methods similar to those employed for Cu(I) affinity determinations of CCS D1 and D3, to enable reliable comparisons of the relative Cu(I) affinities of the two proteins. In addition, since SOD1 contains four Cys residues, of which two are involved in a intramolecular disulfide in close proximity to the copper-binding site, it would be useful to compare the Cu(I) affinities for WT SOD1 and Cys to Ser variants in which the four Cys residues are systematically mutated to Ser.(*41*) This would allow for the assessment of the involvement of Cys residues within SOD1 that may play a role in the copper insertion mechanism facilitated by CCS. Furthermore, the determination of a crystal structure for CCS in complex with SOD1, analogous to the complex observed for the homologous proteins from *S. cerevisiae*, but in the presence of Cu(I) would provide significant structural details of the mechanism of SOD1 activation.(*36*) The preliminary data within this work shows CCS from *S.cerevisiae* (Ccs1) to bind comparable amounts of Cu(I) to CCS, however, the relative affinities of D1 and D3, for Ccs1, are yet to be determined. This is particularly important due to the differences between CCS and Ccs1, which include D1 of CCS being absolutely required for CCS function whereas for Ccs1 the same domain is only required under copper limiting conditions.(*35,42*) A comparison of the relative Cu(I) affinities of D1 and D3 of Ccs1 would provide important details required to explain the different dependencies of D1 for the CCS and Ccs1 metallochaperones.

In order to verify the Cys residue pK_a determinations for the D3 CXC in chapter 3, obtained from the pH dependence of the Cu(I) affinity, it is essential that an independent determination of the pK_a's is performed as obtained for the D1 CXXC motif. Since the protein construct for study of D3 also incorporates D1 and D2 (D1 CXXC Cys residues mutated to Ser) the protein contains other Cys residues (1 in D1 and 4 in D2) that may interfere with such a determination. Therefore, Cys to Ser mutants of the remaining Cys residues contained within D1 and D2 would be required. This would allow for the accurate

measurement of the pK_a's of the two D3 Cys residues for verification of those determined from the Cu(I) affinity data to ensure the determined pK_a's are those of the CXC motif. In addition, it would be revealing to determine the pH dependence of the Cu(I) affinities of other copper-binding proteins present within the cell cytosol. For example, the pH dependence of the Cu(I) affinity of BACE1 (section 2.3.5), a membrane bound protein involved in copper homeostasis and implicated in Alzheimer's disease, is unknown.(*43*) An assessment of the pH dependence of the Cu(I) affinity of BACE1 would provide insight into both the directionality of copper transfer, under different conditions of pH within the cell, and also whether Cu(I)-binding Cys pK_a tuning exists for CXXC motif containing species other than the Atx1 and CCS metallochaperones.

The role of zinc-binding to CCS has received little attention despite the consequences its binding has for CCS oligomerisation and target protein complex formation. Further study is required to reveal the nature and significance of the binding of this particular metal for CCS metallochaperone function. This is especially important with regard to the role of Zn(II) in CCS: SOD1 heterodimer formation, formation of which is considered a crucial step for SOD1 activation by CCS.(*36*) Zinc-binding to SOD1 and CCS itself could represent an important regulatory element for the CCS trafficking pathway.(*44*) Study of this aspect of CCS metal-binding could therefore help identify species involved in the activation of CCS itself prior to its participation in the copper trafficking pathways of the cell.

5.3 References

(1)   Rae, T.D.; Schmidt, P.J.; Pufahl, R.A.; Culotta, V.C.; O'Halloran, T.V. *Science* **1999** *284*, 805-808.

(2)   Jomova, K.; Valko, M. *Toxicology* **2011**, *283*, 65-87.

(3)   Puig, S.; Thiele. D. J. *Curr. Opin. Chem. Biol.* **2002**, *6*, 171-180.

(4)   Maryon, E. B.; Molloy, S. A.; Zimnicka, A. M.; Kaplan, J. H. *Biometals* **2007**, *20*, 355-364.

(5)   Rosenzweig, A. C. *Acc. Chem. Res.* **2001**, *34*, 119-128.

(6)   Huffman, D.L.; O'Halloran, T.V. *Annu. Rev. Biochem.* **2001**, *70*, 677-701.

(7)   Robinson, N.J.; Winge, D.R. *Annu. Rev. Biochem.* **2010**, *79*, 537-562.

(8)   Singleton, C.; Le Brun, N.E. *Biometals* **2007**, *20*, 275-289.

(9)   Pufahl, R. A.; Singer, C. P.; Peariso, K. L.; Lin, S.J.; Schmidt, P.; Culotta, V. C.; Penner-Hahn, J. E.; O'Halloran, T. V. *Science* **1997**, *278*, 853-856.

(10)   Hung, I. H.; Casareno, R. L. B.; Labesse, G.; Matthews, F. S; Gitlin, J. D. *J. Biol. Chem.* **1998**, *273*, 1749-1754.

(11)   Culotta, V.C.; Klomp, L.W.; Strain, J.; Casareno, R.L.; Krems, B.; Gitlin, J.D. *J. Biol. Chem.* **1997**, *272*, 23469-23472.

(12)   Atkinson, A.; Winge, D.R. *Chem. Rev.* **2009,** *109,* 4708–4721.

(13)   Badarau, A.; Dennison, C. *J. Am. Chem. Soc*. **2011**, *133*, 2983-2988.

(14)   Badarau, A.; Dennison, C. *Proc. Natl. Acad. Sci. U.S.A.* **2011**, 108, 13007-12.

(15)   Xiao, Z.; Brose, J.; Schimo, S.; Ackland, S.M.; La Fontaine, S.; Wedd, A.G. *J. Biol. Chem*. **2011**, *286*, 11047-11055.

(16)   Zhou, L.; Singleton, C.; Le Brun, N.E. *Biochem. J.* **2008**, *413*, 459-465.

(17)   Rosenzweig, A. C.; Huffman, D. L.; Hou, M. Y.; Wernimont, A. K.; Pufahl, R. A.; O'Halloran, T. V. *Structure* **1999**, *7*, 605-617.

(18)   Arnesano, F.; Banci, L.; Bertini, I.; Huffman, D. L.; O'Halloran, T. V. *Biochemistry* **2001**, *40*, 1528-1539.

(19)   Yatsunyk, L. A.; Rosenzweig, A. C. *J. Biol. Chem.* **2007**, *282*, 8622-8631

(20)   Banci, L.; Bertini, I.; Cantini, F.; Felli, I. C.; Gonnelli, L.; Hadjiliadis, N.; Pierattelli, R.; Rosato, A.; Voulgaris, P. *Nature Chem. Biol.* **2006**, *2*, 367-368.

(21)   Banci, L.; Bertini, I.; Calderone, V.; Della-Malva, N.; Felli, I. C.; Neri, S.; Pavelkova, A.; Rosato, A. *Biochem. J.* **2009**, *422*, 37– 42.

(22)   Portnoy, M.E.; Rosenzweig, A.C.; Rae, T.; Huffman, D.L.; O'Halloran, T.V.; Culotta, V.C. *J. Biol. Chem.* **1999**, *274*,15041–15045.

(23)   Huffman, D.L.; O'Halloran, T.V. *J. Biol. Chem.* **2000**, *275*, 18611–18614.

(24)   Odermatt, A.; Solioz, M. *J. Biol. Chem.* **1995**, *270*,4349–4354.

(25)   Lin, S.; Pufahl, R.; Dancis, A.; O'Halloran, T. V.; Culotta, V. C. *J. Biol. Chem.* **1997**, *272*, 9215−9220.

(26)   Yuan, D. S.; Stearman, R.; Dancis, A.; Dunn, T.; Beeler, T.; Klausner, R. D. *Proc. Natl. Acad. Sci. U.S.A.* **1995**, *92*, 2632-2636.

(27)   Klomp, L. W. J.; Lin, S. J.; Yuan, D. S.; Klausner, R. D.; Culotta, V. C.; Gitlin, J. D. *J. Biol. Chem.* **1997**, *272*, 9221-9226.

(28)   Mercer, J. F. B. *Trends Molec. Med.* **2001**, *7*, 64-69.

(29)   Boal, A. K.; Rosenzweig, A.C.; *Chem. Rev.* **2009**, *109*, 4760-4779.

(30)   Wernimont, A. K.; Huffman, D. L.; Lamb, A. L.; O'Halloran, T. V.; Rosenzweig, A. C. *Nat. Struct. Biol.* **2000**, *7*, 766-771.

(31)   Lutsenko, S.; *Curr. Opin. Chem. Biol.* **2010**, *14*, 211-217.

(32)   Banci, L.; Bertini, I.; Ciofi-Baffoni, S.; Kozyreva, T.; Zovo, K.; Palumaa, P. *Nature* **2010**, *465*, 645-648.

(33)   Xiao, Z.; Loughlin, F.; George, G. N.; Howlett, G. J.; Wedd, A. G. *J. Am. Chem. Soc*. **2004**, *126*, 3081-3090.

(34)   Rodriguez-Granillo, A.; Crespo, A.; Estrin, D.A.; Wittung-Stafshede, P. *J. Phys. Chem. B*. **2010**, *114*, 3698-3706.

(35)   Lamb, A.L.; Wernimont, A.K.; Pufahl, R.A.; O'Halloran, T.V.; Rosenzweig, A.C. *Biochemistry* **2000**, *39*, 1589-1595.

(36)   Lamb, A.L.; Torres, A.S.; O'Halloran, T.V.; Rosenzweig, A.C. *Nat. Struct. Biol.* **2001**, *8*, 751-755.

(37)   Endo, T.; Fujii, T.; Sato, K. Taniguchi, N.; Fujii, J. *Biochim. Biophys. Acta* **2000**, *276*, 999-1004.

(38)   Arnesano, F.; Banci, L.; Bertini, I.; Martinelli, M.; Furukawa, Y.; O'Halloran, T.V. *J. Biol. Chem.* **2004**, 279, 47998-48003.

(39)   Potter, S.Z.; Zhu, H.; Shaw, B.F.; Rodriguez, J.A.; Doucette, P.A.; Sohn, S.H.; Durazo, A.; Faull, K.F.; Gralla, E.B.; Nersissian, A.M.; Valentine, J.S. *J. Am. Chem. Soc.* **2007**, 129, 4575-4583.

(40)   Miller, A-F. *Curr. Opin. Chem. Biol.* **2004**, 8, 162-168.

(41)   Strange, R. W.; Antonyuk, S. V.; Hough, M. A.; Doucette, P. A.; Valentine, J. S.; Hasnain, S. S. *J. Mol. Biol.* **2006**, *356*, 1152-1162.

(42)   Wong, P.C.; Waggoner, D.; Subramaniam, J.R.; Tessarollo, L.; Bartnikas, T.B.; *Proc. Natl. Acad. Sci. U.S.A.* **2000**, *97*, 2886–2891.

(43)   Angeletti, B.; Waldron, K. J.; Freeman, K. B.; Bawagan, H.; Hussain, I.; Miller, C. C. J.; Lau, K. F.; Tennant, M. E.; Dennison, C.; Robinson N. J.; Dingwall, C. *J. Biol. Chem.* **2005**, *280*, 17930-17937.

(44)   Lamb, A.L.; Torres, A.S.; O'Halloran, T.V.; Rosenzweig, A.C. *Biochemistry* **2000**, *39*, 14720-14727.

Chapter 6

Experimental Methods

6.1   Buffer Solutions

All buffer solutions were prepared using Milli-Q grade water (Millipore "Simplicity" water purification system) with a rated resistivity of $\geq 18M\ \Omega cm$.

6.1.1   Tris(hydroxymethyl)aminomethane Buffer

Tris(hydroxymethyl)aminoethane (Tris) (Sigma) buffer was used primarily in the pH range of 7.2-8.0. The pH was adjusted by addition of either HCl (BDH, AnalR) or NaOH (Sigma). This buffer was mainly used for the isolation, purification and storage of proteins.

6.1.2   Sodium Acetate Buffer

Sodium acetate (NaOAc) (BDH) buffer was used to buffer protein solutions in the pH range 4.0-5.5. The pH was adjusted by addition of either HCl or NaOH. This buffer was primarily used for protein K_b measurements at low pH and preparation of Zn-depleted WT-CCS.

6.1.3   2-(N-morpholino)ethanesulphonic Acid Buffer

2-(N-morpholino)ethanesulphonic (Mes) (Sigma) buffer was used to buffer solutions in the pH range 5.5-6.5. The pH was adjusted by addition of either HCl or NaOH. This buffer was used primarily for protein K_b measurements, Cu(I) partitioning/transfer experiments, and protein purification.

6.1.4   4-(2-Hydroxyethyl)piperazine-1-ethanesulfonic Acid Buffer

4-(2-Hydroxyethyl)piperazine-1-ethanesulfonic acid (Hepes) (VWR) was used to buffer solutions in the pH range 7.0-8.0. The pH was adjusted by addition of either HCl or NaOH. This buffer was used primarily for protein K_b measurements and Cu(I) transfer experiments.

6.1.5   N-Tris(hydroxymethyl)methyl-3-aminopropanesulfonic Acid Buffer

N-Tris(hydroxymethyl)methyl-3-aminopropanesulfonic acid (Taps) (Sigma) was used to buffer solutions in the pH range 8.0-9.0. The pH was adjusted by addition of either HCl or NaOH. This buffer was used for primarily for protein K_b measurements.

6.1.6 2-(Cyclohexylamino)ethanesulfonic Acid Buffer

2-(Cyclohexylamino)ethanesulfonic acid (Ches) (Sigma) was used to buffer solutions in the pH range 9.0-10.0. The pH was adjusted by addition of either HCl or NaOH. This buffer was used for primarily for protein K_b measurements.

6.1.7 3-(cyclohexylamino)-1-propanesulfonic Acid Buffer

3-(cyclohexylamino)-1-propanesulfonic acid (Caps) (Sigma) was used to buffer solutions in the pH range 10.0-11.0. The pH was adjusted by addition of either HCl or NaOH. This buffer was used for primarily for protein K_b measurements.

6.1.8 Phosphate Buffer

Phosphate buffer was used to buffer solutions in the pH range 6.0 to 8.0. Buffers were prepared by mixing stock solutions of 1 M dibasic and monobasic potassium phosphate, K_2HPO_4 and KH_2PO_4, respectively (Fluka). Dibasic and monobasic phosphates were combined in the proportions shown in Table 6.1.1 for a particular pH. Fine tuning of pH was achieved by addition of either HCl or NaOH as required.

Table 6.1.1

Volumes of 1 M stocks of K_2HPO_4 and KH_2PO_4 required to prepare 1 L of 0.1 M potassium phosphate buffer solutions in the pH range 6.0-8.0.([1])

K_2HPO_4 (ml)	KH_2PO_4 (ml)	pH
13.2	86.8	6.0
19.2	80.8	6.2
27.8	72.2	6.4
38.1	61.9	6.6
49.7	50.3	6.8
61.5	38.5	7.0
71.7	28.3	7.2
80.2	19.8	7.4
86.6	13.4	7.6
90.8	9.2	7.8
94.0	6.0	8.0

6.2   Measurement of pH Values

Measurement of pH values for buffer solutions were made using an Orion 420A pH meter connected to a Russell glass pH electrode (Thermo, type KCMAW11). The pH meter was calibrated prior to use with two standard buffer solutions of either pH 4.0 and 7.0 or 7.0 and 10.0 (Sigma) depending on pH range measured.

6.3   Ion-Exchange Chromatography

Ion-exchange chromatography was used for purification of proteins and separation of proteins for Cu(I) partitioning/transfer experiments. Diethylaminoethyl (DEAE) sepharose (GE Healthcare) fast flow (FF) column material was used to prepare anion exchange columns for the purification of WT-CCS, C244S/C246S-CCS, C22S/C25S-CCS, D1-CCS, Arg71Ala D1-CCS and SOD1 proteins. Sulfopropyl (SP) sepharose (GE Healthcare) FF column material was used to prepare cation exchange columns for the purification of Ccs1. Resource Q (6 ml) columns (GE Healthcare) were used for purification of WT-CCS, C244S/C246S-CCS and C22S/C25S-CCS proteins. HiTrap Q (HP, 1 ml) columns (GE Healthcare) were used for separation of proteins for Cu(I) partitioning/transfer experiments.

6.3.1   Equilibration of Ion-Exchange Column Material

Ion-exchange column material (DEAE and SP sepharose FF) was washed with 2 L of buffer solution prior to use of column for protein purification. The pH of the eluate was checked to ensure equilibration of column. All columns were ran and stored at 4 ^{o}C.

6.3.2   Loading and Elution of Protein on Ion-Exchange Column Material

Proteins were loaded onto DEAE and SP sepharose FF columns in the same buffer as that of the column material. Elution of proteins was achieved by increasing the ionic strength of the buffer by providing a NaCl gradient between 0-500 mM NaCl by mixing two buffers with and without the salt.

6.3.3   Regeneration of Ion-Exchange Column Material

DEAE and SP sepharose FF column material was regenerated by washing with 500 ml of 2 M NaCl (contact time ~ 30 mins) to remove bound proteins. The column material was

then washed with 1 L of distilled water followed by 500 ml of 1 M NaOH (contact time ~30 mins). The material was then washed with distilled water until the pH was neutral. Column materials were stored in 20 % ethanol at 4°C.

6.3.4   Ion-Exchange Chromatography using Resource Q Column

Resource Q columns, attached to an AKTA Prime or Purifier (GE Healthcare), were equilibrated with 5 column volumes of buffer solution. Proteins were loaded in the same buffer as that of the column and eluted with a linear 0-300 mM NaCl gradient. The column was regenerated by passing 5 column volumes of 1 M NaCl through the column to remove any bound proteins. The column was then washed with 5 column volumes of milli-Q water followed by 5 column volumes of 0.5 M NaOH. The column was then washed with milli-Q water until the eluate was neutral. Resource Q columns were stored in 20 % ethanol at 4°C.

6.3.5   Ion-Exchange Chromatography using HiTrap Q Column

Equilibration and column regeneration were performed as for the Resource Q column in section 5.3.4. Protein elution was achieved by applying buffer solutions (by syringe) containing increasingly higher concentrations of NaCl within the range 0-400 mM for separation of proteins in an anaerobic chamber for Cu(I) partitioning and transfer experiments.

6.4   Gel Filtration Chromatography

Preparative gel filtration chromatography was used for the purification of proteins whilst analytical gel filtration chromatography was used to determine the oligomeric state of proteins. Masses of proteins, determined on preparative and analytical gel filtration chromatography columns, were deduced by comparison of elution volumes against a set of protein standards of known molecular weight (see section 6.4.1 and 6.4.2). Due to deviations of protein structures from perfect spheres the determined molecular weights are apparent molecular weights and as such errors due to the non-spherical nature of the proteins, in addition to those from measuring protein elution volumes, are present for all determinations shown in chapters 2, 3 and 4. Consequently, the method employed is suitable for determining protein oligomerisation state but unreliable for determining the absolute molecular mass.

6.4.1   Preparative Gel Filtration Chromatography

A Supderdex 75 (16/60 HiLoad, GE Healthcare, 120 ml) column attached to an AKTA prime or purifier (GE Healthcare) was used for purification of proteins by gel filtration chromatography. A buffer of 20 mM Tris pH 7.5 containing 200 mM NaCl and 1 mM DTT was used as the column buffer. Injection volumes were typically ≤ 2 % of the column volume and eluted at a flow rate of 1 ml/min. Elution of proteins was typically monitored at 280 nm and 240 nm (AKTA purifier) or 280 nm (AKTA prime). The column was calibrated using a low molecular weight calibration kit (GE Healthcare) containing: blue dextran (2000 kDa), conalbumin (75 kDa), ovalbumin (43 kDa), carbonic anhydrase (29 kDa), ribonuclease A (13.7 kDa) and aprotinin (6.5 kDa).

6.4.2   Analytical Gel Filtration Chromatography

Analytical gel filtration chromatography of apo and metal-bound protein samples was performed using a Superdex 75 column (10/300 GL GE Healthcare, 24 ml). A buffer of 20 mM Mes pH 6.5 or 20 mM Hepes pH 7.5 containing 200 mM NaCl (with or without 1 mM DTT) was used as column buffer. Buffers were purged prior to and during experiments with N_2 from an oxygen-free cylinder. Injection volumes were typically ≤ 2 % of the column volume and proteins eluted at a flow rate of 0.8 ml/min. Elution of proteins was typically monitored at 240 or 280 nm. The column was calibrated using a LMW calibration kit (GE Healthcare) as described in section 6.4.1.

6.5   Ultrafiltration

6.5.1   Centrifugal Ultrafiltration

Amicon ultra 4 (10 kDa MWCO (molecular weight cut-off), Millipore) and Vivaspin 500 (5 kDa MWCO, Sartorius) centrifugal concentrators were used to concentrate protein solutions and remove adventitiously bound metals through buffer exchange. Exchanging buffer involved concentrating the protein solution and then diluting the sample 10-fold in the concentrator and repeating this process 3 times. A fixed angle rotor operating at ~ 16 k x g was used to centrifuge samples.

6.5.2 Amicon Stirred Cell Ultrafiltration

An Amicon stirred cell (10 or 200 ml cell, Amicon) fitted with an appropriate regenerated cellulose membrane (3-30 kDa MWCO, Millipore) was used to perform buffer exchanges during the purification of proteins. A pressure of approximately 3-4 bar supplied from an N_2 oxygen-free cylinder was applied during operation of the stirred cell.

6.6   Dialysis

6.6.1 Preparation of Dialysis Tubing

Dialysis tubing (14 kDa MWCO, Sigma) was prepared by soaking the tubing for 1 hour in an aqueous solution of 1 % acetic acid followed by exchange into distilled water and stirring for several minutes. The tubing was then placed into a solution of 1mM ethylenediaminetetraacetic acid (EDTA) and 1 % sodium carbonate and stirred for a further ~3 minutes. The solution was then refreshed and the dialysis tubing heated to ~60 ^{o}C and then allowed to cool to room temperature over a period of 30 minutes. The above heating process was repeated once more and dialysis tubing exchanged into Milli-Q water and heated again to 60 ^{o}C and allowed to cool before storing in fresh Milli-Q water (at 4°C).(*2*)

6.6.2 Dialysis of Protein Solutions

Dialysis was used for buffer exchange during the preparation of Zn-depleted WT-CCS. Dialysis tubing was washed thoroughly prior to use in buffer to be used during dialysis. Protein solutions were sealed in tubing and dialysed against buffer solution at 4°C for 3-4 hours, and also o/n, with stirring. The buffer solution (50-100 $\times$ sample volume) was typically changed 3 times.

6.7   Electrophoresis

6.7.1 Sodium Dodecyl Sulfate-Polyacrylamide Gel Electrophoresis (SDS-PAGE)

A 12.5 % or 15 % acrylamide/bis-acrylamide (BioRAD) running gel containing 375 mM Tris pH 8.8, 0.1 % SDS, 0.1 % ammonium persulfate (APS, Aldrich) and 0.05 % N,N,N',N'-tetramethylene diamine (TEMED, Aldrich) was prepared in deionised water and allowed to set for 30 mins. The stacking gel, 5 % acrylamide/bis-acrylamide

containing 100 mM Tris pH 6.8, 0.1 % SDS, and 0.1 % APS and 0.1 % TEMED in deionised water, was poured directly on top of the running gel. A comb containing 10 ridges was inserted into the stacking gel to produce wells for sample loading. The stacking gel was allowed to set for 45 mins. Protein samples for electrophoresis were prepared in cracking buffer [50 mM Tris pH 6.8, 1 % SDS (Aldrich), 15 % glycerol (Sigma), 2 % β-mercaptoethanol (Aldrich) and 0.025 % bromophenol blue (BDH) in water. Protein samples in cracking buffer were heated at 95°C for 5 mins. Typically 10 μL of this protein in cracking buffer was loaded into the wells of the gel. Broad range molecular weight marker (BioRAD) was loaded onto most gels as a reference. The SDS-PAGE buffer was 5 mM Tris pH 8.8 containing 200 mM glycine (Sigma) and 0.1 % SDS. All electrophoresis experiments were performed using a Mini-Protean II Cell from BioRAD with a constant voltage of 150-200 V and current of ~60 mA per gel applied from a powerpack. Gel staining was achieved by incubating the running gel in a solution of Instant Blue (Expedian) and the gel was subsequently destained in distilled water.

6.7.2   Agarose Gel Electrophoresis

Agarose (0.8-1.5 %) (Melford) in electrophoresis buffer, Tris-acetate-EDTA (TAE; 40 mM Tris, 40 mM acetate and 1mM EDTA pH 8.0) was heated in a microwave oven until all of the agarose dissolved. This molten agarose solution was then cooled (~ 50-55 °C) and poured into a tray with a comb with 8 or 15 fingers. After ~ 60 min the set agarose was transferred to an electrophoresis tank and covered with TAE buffer. DNA samples were was mixed with 5× loading buffer (20 % Ficoll 400, 0.1 M EDTA, 1 % SDS and 0.25 % bromophenol blue) and applied to a well in the agarose gel. A voltage of 100 V was applied and electrophoresis was carried out until the bromophenol blue approached the edge of the agarose gel. The Agarose gel was then stained by incubation in a solution of ethidium bromide (10 μg/mL in TAE buffer) for ~ 20 mins. Excess ethidium bromide in the gel was removed by incubating the gel in the same buffer minus ethidium bromide for ~ 10 min. DNA in agarose gels was detected using an ultraviolet trans-illuminator (UV Tec). When DNA fragments in the agarose gel were required they were excised using a scalpel and purified from the agarose gel using the GeneElute Miniprep Kit (Sigma).

6.8   DNA Cloning and Mutagenesis

The pGEMT_WT-CCS and pGEMT-WT-CCS construct was received from Prof. Colin Dingwall, Kings College London, UK. The pCLneo_SOD1 construct was received from

Prof. Christopher Miller, Kings College London, UK. pJG4.5_Ccs1 was received from Dr Katie Freeman, Comparative Genomics, GlaxoSmithKline, Pennsylvania 19426, USA. All of the constructs used and prepared in this project are listed in Table 6.8.1.

<u>**Table 6.8.1**</u>

Plasmid constructs used in this project

plasmid	containing protein	source
pGEMT_WT-CCS	WT-CCS	Colin Dingwall
pGEMT_C22S/C25S-CCS	C22S/C25S-CCS	this project
pGEMT_C244S/C246S-CCS	C244S/C245S-CCS	this project
pGEMT_D1-CCS	D1-CCS	this project
pCLneo_SOD1	SOD1	Christopher Miller
pJG4.5_Ccs1	Ccs1	Katie Freeman
pGEMT_SOD1	SOD1	this project
pGEMT_Ccs1	Ccs1	this project
pET29a_WT-CCS	WT-CCS	this project
pET29a_C22S/C25S-CCS	C22S/C25S-CCS	this project
pET29a_C244S/C246S-CCS	C244S/C245S-CCS	this project
pET29a_D1-CCS	D1-CCS	this project
pET29a_Ccs1	Ccs1	this project
pET29a_SOD1	SOD1	this project

6.8.1   Isolation of Plasmid DNA from *E. coli*

Plasmid DNA was isolated and purified from *E. coli* using the GenElute Plasmid Miniprep Kit (Sigma). *E. coli* containing the plasmid were grown in 10 mL fresh Luria broth (LB; 10 g/L tryptone, 5 g/L yeast extract and 10 g/L NaCl) with 100 µg/mL ampicillin or 100 µg/mL kanamycin, o/n at 37 °C and 250 rpm after 100-fold dilution of pre-culture (a 10 mL culture of LB containing 100 µg/mL ampicillin or 100 µg/mL kanamycin, inoculated with a single colony of the fresh transformant and grown for ~ 8 h at 37 °C and 250 rpm). A 5 mL volume of the o/n culture was used to purify plasmid DNA. The purity of plasmid DNA was judged by measuring the UV spectrum and using the relative absorbance's at 260 and 280 nm, where an A_{260}/A_{280} ratio of 1.5-1.8 usually indicated a suitably pure DNA sample with little RNA contamination.

6.8.2 Determination of Plasmid DNA Concentration

The concentration of plasmid DNA was determined by measuring the absorbance of a sample at 260 nm and using the relationship that 1 OD_{260} unit is equal to 50 μg/mL of double stranded DNA. The concentration of primers purchased from MWG/Sigma was based on the DNA synthesis report provided by the companies.

6.8.3 Plasmid DNA Digestion

The digestion of plasmid DNA (from Section 6.8.1) was carried out using restriction enzymes (*EcoR1*, *BamH1* and *Nde1*, New England Biolabs) according to the manufacturer's instructions to provide restriction sites for ligation reactions. Typically ~1000-3000 ng of plasmid DNA to be digested in a 40 μL solution containing the required restriction enzymes was incubated at 37 ^{o}C for 2 hours followed by heating at 80 ^{o}C to inactivate the restriction enzymes. Smaller amounts of DNA (~ 100s of ng plasmid DNA) were used when only confirmation of fragment sizes was required. Digested plasmid was then used directly in ligation reactions or loaded onto an agarose gel for DNA size determination and excision where required.

6.8.4 Ligation Reactions of Plasmid and Insert DNA

Ligation of digested plasmid DNA (pGEMT, Promega or pET29a, Novogen (lab stocks)) and insert DNA was achieved using the T4 DNA ligase kit (Promega) according to the manufacturer's instructions. Required amounts of plasmid and insert DNA in 10-60 μL of T4 DNA ligase buffer with the appropriate amount of T4 DNA ligase were typically incubated at 4 °C o/n for ligation reaction. The ligation reaction sample was then transformed into fresh *E. coli* (JM101) TSS competent cells.

6.8.5 Gene Amplification

Polymerase chain reaction (PCR) was used to amplify the gene sequence for SOD1 and Ccs1 from pClneo_SOD1 and pJG4.5_Ccs1 to incorporate Nde1/EcorR1 and Nde1/BamH1 restriction sites, respectively, for ligation into pET29a vector. The PCR reaction contained 2 ng of template plasmid DNA, 0.4 mM deoxyribonucleotide triphosphates (dNTPs) mix (Promega), 125 ng of each primer (forward and reverse), 1 unit of *Pfu* polymerase (Stratagene, UK) and 1 μL of 10x *Pfu* buffer made up to 10 μL volume

by addition of H_2O. The PCR conditions were as for manufacturer's instructions for *Pfu* polymerase.

6.8.6   Site-directed Mutagenesis

Mutations in plasmid DNA for were carried out using the Quickchange site-directed mutagenesis kit (Stratagene). Typically, reactions (10-60 μL) contained 5-20 ng of template plasmid DNA, 125 ng of each primer (forward and reverse), 0.5 mM dNTPs mix, 1-5 units of *Pfu* polymerase (as appropriate for reaction volume) and *Pfu* buffer made up to volume with H_2O. The reaction conditions were as for the specified Quikchange manufacturers protocol and performed in a PCR machine. Te restriction enzyme *Dpn1* was added to reaction mixtures after PCR to digest template plasmid DNA. The reaction mixture was then transformed into *E. coli* (XL1 Blue) for growing and subsequent extraction of plasmid for sequencing to confirm mutation of the template DNA sequence.

6.8.7   DNA Sequencing

DNA sequencing was used to verify mutated and amplified genes in plasmid DNA. Size and purity of DNA was typically assessed by agarose gel electrophoresis and measurement of absorbance of samples at 260 and 280 nm. DNA sequence analysis was then commissioned to Lark Technology.

6.9   Growing of *E. coli*

6.9.1   Preparation of Competent *E. coli* Cells

LB (10 ml of 10 g/L of NaCl and Tryptone (Melford) and 5g/L Yeast extract (Melford)) was inoculated with a single colony of *E. coli* and incubated overnight at 37°C with shaking (250rpm). The o/n culture was then diluted 100-fold into fresh LB (10ml) and grown for a further 2 hours under the same conditions. Cells were then spun down at ~1500 × g for 10 mins and the cell pellet resuspended in ice cold TSS (1ml of a solution of 85% LB, 10% PEG, 5% DMSO and 50mM MgCl).(*3*)

6.9.2   Transformation of *E.coli*

To 100 μL of competent cells 1-3 μL of plasmid DNA was added and incubated on ice for 20 minutes before heat shocking at 42°C for ~1 min. The solution was incubated on

ice for a further 2 mins before adding 900 μL of LB and incubating at 37°C with shaking (250rpm) for 1 hour. After incubation dilutions were made and plated onto freshly prepared LB/Agar plates (LB with 1.8 % w/w agar and appropriate antibiotics (100μg/mL ampicillin or 50μg/mL kanamycin as required)). Plates were incubated o/n at 37 °C. (3)

6.9.3 Expression Studies; Total Cell Protein

In order to determine the growing period for optimal protein expression (as judged by SDS-PAGE) small-scale trials were carried out with the pET29a expression plasmid, containing the required protein gene insert, transformed into *E.coli* strain BL21 (DE3).

LB (10 ml containing 100 μg/mL kanamycin plus 100 mM Zn(II) for WT-CCS C244S/C246S-CCS, C22S/C25S-CCS and SOD1) was inoculated with a single colony containing the expression plasmid and grown o/n at 37 °C with shaking (250 rpm). The next day a 100-fold dilution of each culture into LB (50 ml containing 100 μg/mL kanamycin plus 100 mM Zn(II) for WT-CCS C244S/C246S-CCS. C22S/C25S-CCS and SOD1) was made and incubated for 2 hours at 37 °C with shaking (i.e. until the OD_{600} had reached ~0.6-0.8). Isopropyl β-D-1-thiogalactopyranoside (IPTG) was then added to an effective concentration of 1 mM. Samples (5 ml) of the cultures were taken at times of 0, 2, 4, 6 hours and over night after induction with IPTG. The samples were spun down at 13.2 k rpm in a desktop centrifuge for ~ 5 mins, the supernatant removed and the cell pellet resuspended in SDS-PAGE loading buffer volumes of 100, 150, 300, 500 and 500 μl, respectively, and frozen at –20°C. Samples were loaded onto SDS-PAGE gels for analysis of total protein expression.

6.9.4 Expression Studies; Detection of Soluble Cell Protein

To determine the growing period that resulted in the largest yield of soluble protein when using pET29a as an expression vector the amount of soluble expressed protein was also assessed in *E.coli* strain BL21 (DE3). LB (10 ml containing 100 μg/mL kanamycin plus 100 mM Zn(II) for WT-CCS C244S/C246S-CCS. C22S/C25S-CCS and SOD1) were inoculated with a single colony of BL21 (DE3) containing the expression vector and grown o/n at 37 °C with shaking (250 rpm). The next day a 100-fold dilution of o/n culture into LB (50 ml containing 100 μg/mL kanamycin plus 100 mM Zn(II) for WT-CCS C244S/C246S-CCS. C22S/C25S-CCS and SOD1) was made and incubated for 2 hours at 37 °C with shaking (i.e. until OD_{600} had reached ~0.6-0.8). IPTG was then added to an

effective concentration of 1 mM. Samples (5 ml) of the cultures were taken at times of 0, 2, 4, 6 hours and o/n after induction with IPTG. Samples from cultures were sonicated and 100μl was removed for total protein content. The remaining solution was pelleted at ~ 16 k x g in a desktop centrifuge for ~ 5 minutes and 100μl of the supernatant removed for soluble protein content. 20μl of 5x SDS-PAGE loading buffer was added to both the total and soluble protein samples which were frozen at -20 ^{o}C. Samples were then analysed by SDS-PAGE to judge an optimal cell harvesting time after protein induction.

6.10   Expression and Purification of Proteins from *E. coli* BL21

6.10.1 Expression and Purification of WT-CCS and the Cys to Ser Mutants

A modified protocol was used for the purification of WT-CCS and the Cys to Ser variants was used.(*4*) *E. coli* BL21 (DE3) transformed with either pET29a_WT-CCS, pET29a_C22S/C25S-CCS or pET29a_C244S/C246S-CCS was grown in LB containing antibiotics and 100 μM Zn(II) at 37 ^{o}C until an OD$_{600}$ of 0.6-0.8 was reached (~ 2 hours). Protein expression was induced by the addition of 1 mM IPTG and cells were incubated for a further 6 hours before harvesting, with pellets stored at -20 ^{o}C. Cells were resuspended in 20 mM Tris pH 7.5 containing 4 mM EDTA and 4 mM dithiothreitol (DTT), sonicated and centrifuged at 35000 g for 20 min. The supernatant was diluted 4-fold with Milli-Q water prior to loading onto a DEAE Sepharose FF column (~40 mL, GE Healthcare) and eluted with a linear NaCl gradient (0-300 mM) in 5 mM Tris pH 7.5 containing 1 mM EDTA and 1 mM DTT. Fractions containing CCS [identified by SDS-PAGE] were combined and exchanged via ultrafiltration [Amicon stirred cell with a 30 kDa MWCO membrane] into 5 mM Tris pH 7.5 containing 1 mM DTT. The final purification step used a Resource Q column (6 mL, GE Healthcare) with a 0-300 mM NaCl gradient, and fractions containing pure protein (≥ 90% pure as judged by SDS-PAGE) were combined.

6.10.2 Expression and Purification of D1-CCS

D1-CCS was expressed and purified as for the full length protein except that the final purification step involved a Superdex 75 column (16/60 GE Healthcare) in 20 mM Tris pH 7.5 containing 200 mM NaCl and 1 mM DTT. D1-CCS eluted from this column as a single peak and the fractions containing pure protein (≥ 90% pure as judged by SDS-PAGE) were combined.

6.10.3 Expression and Purification of Ccs1

Expression of Ccs1 was achieved as for CCS, and purification used a modified version of a reported procedure.(*5*) Thawed cell pellets were re-suspended in 80 mM Mes pH 6.0 containing 4 mM EDTA and 4 mM DTT, sonicated and centrifuged at 35000 g for 20 min, and the supernatant diluted 4-fold prior to loading onto a SP Sepharose FF column (~40 mL, GE Healthcare). The protein was eluted with a linear NaCl gradient (0-500 mM) in 20 mM Mes pH 6.0 containing 1 mM EDTA and 1 mM DTT. Fractions containing Ccs1 (identified by SDS-PAGE) were combined and exchanged using ultrafiltration (Amicon stirred cell with a 10 kDa MWCO membrane) into 20 mM Tris pH 7.5 plus 200 mM NaCl and 1 mM DTT. The final purification step involved a Superdex 200 column (16/60 GE Healthcare) in 20 mM Tris pH 7.5 plus 200 mM NaCl and 1 mM DTT. Ccs1 eluted from this column as a single peak and the fractions containing pure protein ($\geq$ 90% pure as judged by SDS-PAGE) were combined.

6.10.4 Expression and Purification of SOD1

SOD1 was expressed and purified as for WT-CCS with modifications to the final stage of the purification procedure. *E. coli* BL21 (DE3) transformed with either pET29a_SOD1 was grown in LB containing antibiotics and 100 μM Zn(II) at 37 ^{o}C until an OD_{600} of 0.6-0.8 was reached (~ 2 hours). Protein expression was induced by the addition of 1 mM IPTG and cells were incubated for a further 6 hours before harvesting, with pellets stored at -20 ^{o}C. Cells were resuspended in 20 mM Tris pH 7.5 containing 4 mM EDTA and 4 mM DTT, sonicated and centrifuged at 35000 g for 20 min. The supernatant was diluted 4-fold with Milli-Q water prior to loading onto a DEAE Sepharose FF column (~40 mL, GE Healthcare) and eluted with a linear NaCl gradient (0-300 mM) in 5 mM Tris pH 7.5 containing 1 mM EDTA and 1 mM DTT. Fractions containing CCS [identified by SDS-PAGE] were combined and exchanged via ultrafiltration [Amicon stirred cell with a 10 kDa MWCO membrane] into 5 mM Tris pH 7.5 containing 1 mM DTT. The final purification step involved a Superdex 75 column (16/60 GE Healthcare) in 20 mM Tris pH 7.5 plus 200 mM NaCl and 1 mM DTT. SOD1 eluted from this column as a single peak and the fractions containing pure protein ($\geq$ 90% pure as judged by SDS-PAGE) were combined.

6.11   Determination of the Molecular Weight of Proteins

The molecular weight (MW) of proteins was determined with either an Applied Biosystems Voyager-DE STR matrix assisted laser desorption ionisation time-of-flight (MALDI-TOF) or a Thermo LTQ fourier transform ion cyclotron resonance (FT-ICR) mass spectrometer (MS) system by Dr J. Gray (Pinnacle, Newcastle University, UK).

6.12   UV/Vis Spectroscopy

All UV/Vis spectra were acquired on a Perkin-Elmer λ35 spectrophotometer. Measurements were mainly made using 10 mm path length quartz cuvette (anaerobic cuvettes were used when anaerobic conditions required).

6.13   CD Spectroscopy

Far-UV circular dichroism (CD) spectra (185-250 nm) of proteins were obtained on a Jasco J-810 spectrometer using a 0.2 mm path length quartz cuvette. The cuvette compartment was maintained at a temperature of 20 $^{\circ}$C during all measurements and 5 scans were accumulated per for both blank and protein sample spectra.

6.14   Atomic Absorption Spectroscopy

Atomic absorption spectroscopy (AAS) was performed on a Thermo Electran M Series AA Spectrometer to determine the copper and zinc content of purified proteins and to verify copper and zinc concentrations in solutions of the metals. All samples were measured against a set of calibration standards of 0.2-1.0 ppm copper and zinc (Fluka)

6.15   Protein Thiol Quantification

Thiol quantification using 5,5'-dithiobis-(2-nitrobenzoic acid) (DTNB, Ellman's reagent) was routinely used for the assessment of the number of thiols in all proteins. The extinction coefficient (ε value) of the thio(2-nitrobenzoate) (TNB^{2-}) product of the reaction of DTNB with thiols (14150 $M^{-1}cm^{-1}$ at 412 nm (*6*)) was verified using a solution of cysteamine of known concentration. Thiol quantification was typically carried out anaerobically in 100 mM potassium phosphate plus 1 mM EDTA at pH 8.0 containing 500 μM DTNB.

6.16 Spectrophotometric Determination of Cu(I) Binding to Proteins

All experiments were performed under anaerobic conditions in an anaerobic chamber (Belle Technology, $O_2 \ll 2$ parts per million). Septum sealed gas-tight quartz cuvettes (Hellma) were used to allow for measurements of samples outside the chamber and all titrations were performed using a gas tight syringe (Hamilton).

6.16.1 Preparation of Cu(I) Stock Solutions and Cu(I)-Proteins.

Cu(I)-proteins were made by the addition of the desired amount of Cu(I) from a 1 mM Cu(I) stock prepared from a 50-fold dilution of 50 mM $[Cu(CH_3CN)_4]PF_6$ (Sigma) in 100% acetonitrile into the appropriate buffer. Copper concentrations were determined using either bathocuproine disulfonic acid (BCS) or bicinchoninic acid (BCA) (Both supplied by Sigma), and occasionally by AAS. For measurements using BCS and BCA, ε_{483} and ε_{562} values of 12500 and 7700 $M^{-1}cm^{-1}$, respectively, for $[Cu(BCS)_2]^{3-}$ and $[Cu(BCA)_2]^{3-}$ were used. These were determined by titrating a $[Cu(CH_3CN)_4]PF_6$ solution (standardized with AAS) into BCS or BCA (40 μM) in 20 mM Mes pH 6.5 containing 200 mM NaCl and measuring the increase in absorbance at 483 and 562 nm to determine the molar extinction coefficients for BCS and BCA, respectively.(7-9)

6.16.2 Cu(I) Binding Stoichiometries

High affinity Cu(I) binding stoichiometries were determined by measuring the competition between proteins and BCA for Cu(I). Titrations of Cu(I) into protein samples (10 μM) in the presence of 30-500 μM BCA were performed with measurement of the increase in absorbance at 562 nm due to the formation of $[Cu(BCA)_2]^{3-}$. Titrations were performed in 20 mM Mes pH 6.5 or 20 mM Hepes pH 7.5 containing 200 mM NaCl.

6.16.3 Cu(I) Affinity Determinations

Cu(I) affinities (K_b values) were determined by competition assays with BCS and BCA using an approach described previously.(7,8,10,11) Titrations were performed by adding either BCS or BCA (25 to 100 mM) into a solution of Cu(I)-protein (5-20 μM) containing an excess of apo-protein [5-20 μM, with $\leq$ 0.5 equivalents of Cu(I) in all cases]. Apo-protein (300-800 μM) was also titrated into a solution of $[Cu(BCS)_2]^{3-}$ or

$[Cu(BCA)_2]^{3-}$ (10-15 μM) with an excess of BCS or BCA (10 μM to ~10 mM). After each addition of BCS/BCA or protein the absorbance at 483 or 562 nm was measured, for determination of the concentrations of $[Cu(BCS)_2]^{3-}$ or $[Cu(BCA)_2]^{3-}$ respectively, after equilibration (typically 10-30 mins).

All titration data were fit using Origin 7 to a 1:1 Cu(I):protein binding model using equations (5.1) and (5.2) below.(7)

$$[L] = 2[CuL_2] + \sqrt{\frac{K_b([P]-[Cu]+[CuL_2])[CuL_2]}{([Cu]-[CuL_2])\beta}}$$ (5.1)

$$[P] = \frac{([Cu]-[CuL_2])([L]-2[CuL_2])^2\beta}{K_b[CuL_2]} + [Cu] - [CuL_2]$$ (5.2)

In equations (5.1) and (5.2), [L] is the total concentration of BCS or BCA, $[CuL_2]$ is concentration of $[Cu(BCS)_2]^{3-}$ or $[Cu(BCS)_2]^{3-}$, [P] is the total protein concentration, [Cu] is total Cu(I) concentration, K_b is the proteins Cu(I) affinity constant and β is the overall affinity constant for formation of $[Cu(BCS)_2]^{3-}$ or $[Cu(BCA)_2]^{3-}$. $[Cu(BCS)_2]^{3-}$ has an overall stability constant (β value) of 6.3×10^{19} M^{-2} (at pH $\geq$ 8.0),(12) and alterations in the β value with pH were calculated assuming a pK_a of 5.7(12) according to equation (5.3).(7)

$$\beta = \frac{\beta_{max}}{\left(1 + \frac{[H^+]}{K_a}\right)^2}$$ (5.3)

In which β is the overall affinity constant for $[Cu(BCS)_2]^{3-}$ for a specified pH, β_{max} is the maximal overall stability constant of $[Cu(BCS)_2]^{3-}$, K_a is the acid dissociation constant of BCS and $[H^+]$ is the proton concentration. A β value for $[Cu(BCA)_2]^{3-}$ of $(5.4 \pm 2.7) \times 10^{16}$ M^{-2} has been determined (section 2.3.5) at pH 6.5 [no significant difference was found at pH 7.5 and therefore the same β value has been used at these pH values].

6.17   References

(1)   Gomori, G. *Methods Enzymol. 1* **1955**, 138-146.

(2)   Sato, K. PhD Thesis, Newcastle University, **2004**

(3)   14. Chung, C. T., Niemela, S. L. and Miller, R. H. *Proc. Natl. Acad. Sci. U.S.A.* **1989**, 86, 2172-2175.

(4)   Zhu, H.; Shipp, E.; Sanchez, R. J.; Liba, A.; Stine, J. E.; Hart, P. J.; Gralla, E. B.; Nersissian, A. M.; Valentine, J. S. *Biochemistry* **2000**, *39*, 5413-5421.

(5)   Hall, L. T., Sanchez, R. J., Holloway, S. P., Zhu, H., Stine, J. E., Lyons, T. J., Demeler, B.; Schirf, V.; Hansen, J. C.; Nersissian, A. M.; Valentine, J. S.; Hart, P. J. *Biochemistry* **2000**, *39*, 3611-3623.

(6)   Riddles, P. W.; Blakeley, R. L.; and Zerner, B. *Anal. Biochem.* **1979**, *94*, 75-81.

(7)   Badarau, A.; and Dennison, C. *J. Am. Chem. Soc*. **2011**, *133*, 2983-2988.

(8)   Badarau, A.; and Dennison, C. *Proc. Natl. Acad. Sci. U.S.A.* **2011**, *108*, 13007-13012.

(9)   Xiao, Z.; Donelly, P. S.; Zimmerman, M.; Wedd, A. G. *Inorg. Chem*. 2008, *47*, 4338-4347.

(10)   Xiao, Z.; Brose, J.; Schimo, S.; Ackland, S. M.; La Fontaine S.; Wedd, A. G. *J. Biol. Chem.* **2011***, 286*, 11047-11055.

(11)   Xiao, Z.; and Wedd, A. G. *Nat. Prod. Rep.* **2010***, 27*, 768-789.

(12)   Xiao, Z.; Loughlin, F.; George, G. N.; Howlett, G. J.; Wedd, A. G. *J. Am. Chem. Soc*. **2004**, *126*, 3081-3090.

Appendix A

Figure 1

Apo-subtracted difference spectra for WT-CCS (43 μM) (A), C244S/C246S-CCS (24 μM) (B) and C22S/C25S-CCS (24 μM) (C), in 20mM Tris pH 7.3 containing 200mM NaCl titrated with ~ 0.5 and 1.0 (~0,5, 1.0, 1.5 and 2.0 for WT-CCS) equivalents of Cu(I).
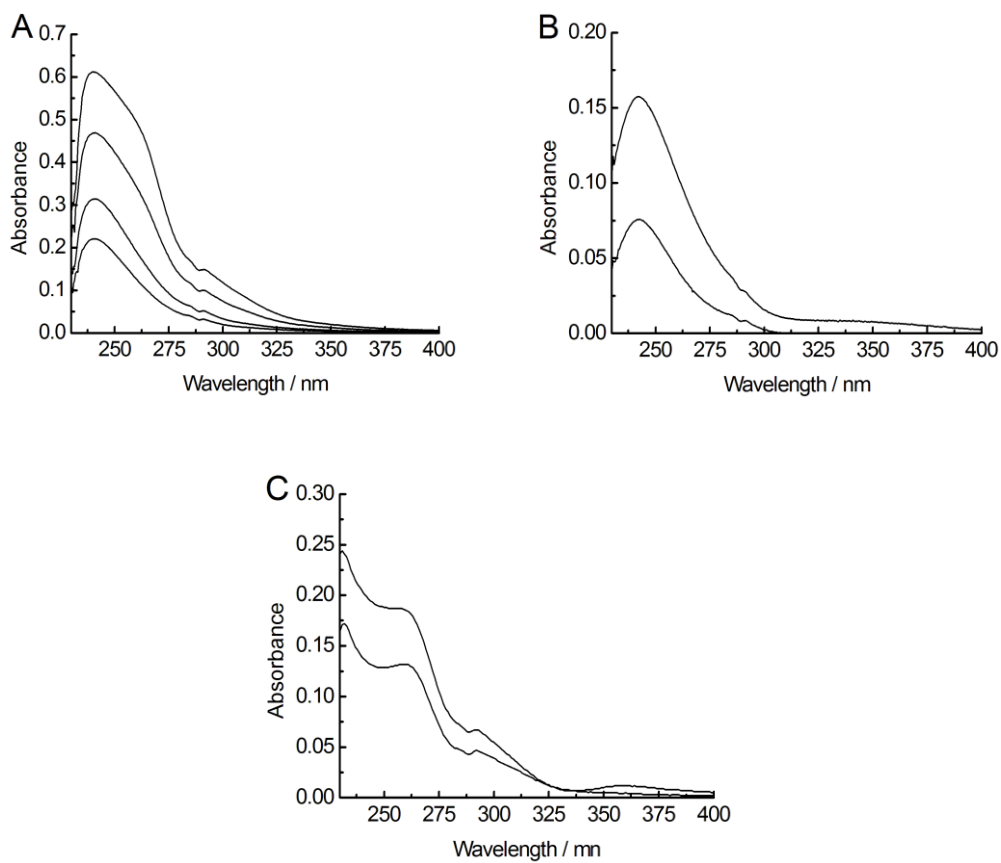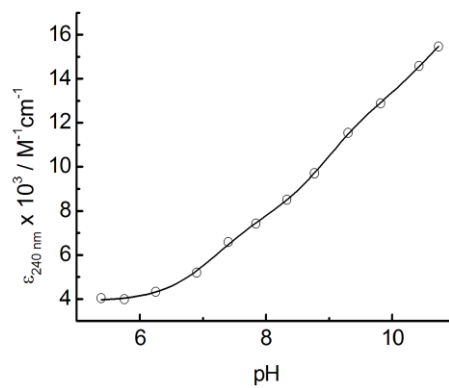
Figure 2

Plot of ε_{240nm} as a function of pH for Arg71Ala apo-D1-CCS. The line shows a fit of the data to equation (3.3) (no variables constrained) giving pK_a's of 7.2 ($\pm$ 0.1) 9.0 ($\pm$ 0.1) and 10.6 ($\pm$0.1) and $\Delta\varepsilon$ values of 3.9 ($\pm$ 0.1) 7.8 ($\pm$0.2) and 12.9 ($\pm$ 0.1) mM cm^{-1}.

*Data acquired by Dr Adriana Badarau

Figure 3

Apo-subtracted difference spectra for Zn-depleted WT-CCS (10µM) in 20 mM Hepes pH 7.5 containing 200 mM NaCl titrated with ~0.4, 0.8, 1.2, 1.6, 2.0, 2.4, 2.8 and 3.2 equivalents of Cu(I).
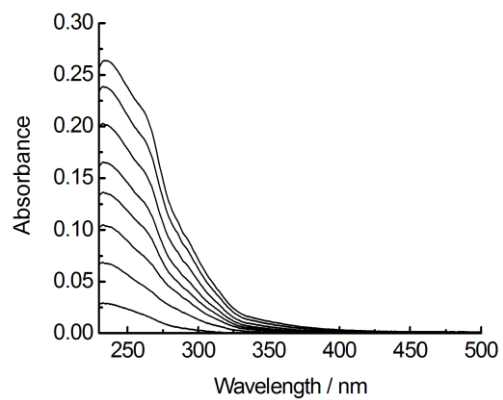
Figure 4

CCS activation of SOD1 assayed by xanthine oxidase WST-1 reduction inhibition. Assay of SOD1 activity for reaction mixtures containing Cu(I)-bound CCS (5 μM) and excess apo-CCS (5 μM) with E,Zn-SOD1 (10 μM) in 20 mM Hepes pH 7.5 containing 200 mM NaCl and 50 μM BCS. Traces for Zn-depleted WT-CCS (magenta), as-isolated WT-CCS (red), C22S/C25S-CCS (green), C244S/C246S-CCS (blue), D1-CCS (cyan) and E,Z - SOD1 in absence of CCS (black) are shown as a function of time with absorbance measured at 450 nm in a 2 mm path-length cuvette.
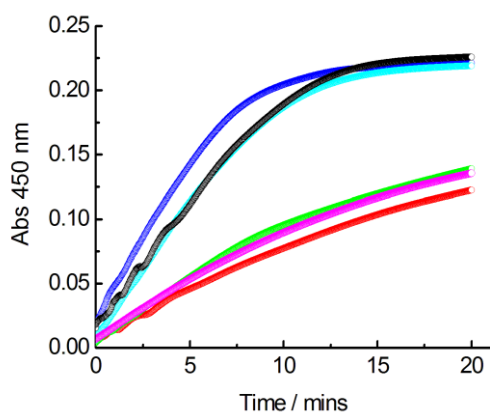
Appendix B

Derivation of equations for Cys pK_a determinations and copper-binding affinities

Derivation 1

Equation for determining pK_a of Cys residues from the pH dependence of the copper-binding affinity.

The binding of copper (Cu) to a protein (P) giving copper-bound protein (CuP) can be expressed as:

$$Cu + P \rightleftharpoons CuP \tag{1}$$

With the equilibrium constant (K_b) expressed as:

$$K_b = \frac{[CuP]}{[Cu][[P]} \tag{2}$$

Since protons H also compete for the copper-binding thiolate of the Cys residues a competing reaction shown below occurs:

$$H^+ + P \rightleftharpoons HP \tag{3}$$

With the equilibrium constant (K_a) expressed as

$$K_a = \frac{[HP]}{[H^+][[P]} \tag{4}$$

Therefore the amount of protein available (P_f), from the total amount of protein present (P_T) where $[P_T] = [CuP]+[P]+[HP]$, to bind copper under a particular pH is dependent on the fraction of ionised thiol residues (α):

$$[P] = \alpha [HP] \tag{5}$$

Which can be expressed as:

$$[P_f] = \frac{[P_T]}{1 + \frac{[H^+]}{K_a}} \tag{6}$$

The K_b at each pH calculated as:

$$K_b = \frac{[CuP]}{[Cu]([P_T]-[CuP])} \tag{7}$$

Therefore the pH dependence of the apparent copper-binding affinity, for a single pK_a dependence can be represented as:

$$K_b = \frac{[CuP]}{[Cu][P]\left(1 + \frac{[H^+]}{K_a}\right)} \tag{8}$$

or

$$K_b = \frac{K_{bmax}}{1 + \frac{[H^+]}{K_a}} \tag{9}$$

where K_{bmax} is the maximal Cu(I)-binding affinity at full ionisation.

For a two proton dependant model, a two pK_a dependence (K_a and K_{a2}) of the Cu(I)-binding affinity, the proportion dissociation can be expressed as:

$$[P_f] = \frac{[P_T]}{1 + \frac{[H^+]}{K_a} + \frac{[H^+]^2}{K_aK_{a2}}} \tag{10}$$

And therefore the pH dependence of the Cu(I)-binding affinity is:

$$K_b = \frac{K_{bmax}}{1 + \frac{[H^+]}{K_a} + \frac{[H^+]^2}{K_aK_{a2}}} \tag{11}$$

Derivation 2

Equation for determining pK_a of Cys residues from the pH dependence of the extinction coefficient at 240 nm (ε_{240nm})

The equation for the binding of a proton (H^+) to a thiolate (S^-) to give a thiol (SH) is:

$$H^+ + S^- \rightleftharpoons HS \tag{12}$$

Therefore, the equilibrium constant for this reaction (K_a) is:

187

$$K_a = \frac{[HS]}{[H^+][[S^-]} \tag{13}$$

Since the proportion of thiol can be represented as Ө the proportion of thiolate is (1-Ө) and so the equation can be represented as:

$$K_a = \frac{\theta}{[1\text{-}\theta][[H^+]} \tag{14}$$

Rearranging the above to represent Ө as a function of $[H^+]$ gives:

$$\theta = \frac{K_a[H^+]}{1 + K_a[H^+]} \tag{15}$$

The overall extinction coefficient at 240nm (ε_{app}), which depends on the proportion of thiol and thiolate, will be as follows:

$$\varepsilon_{app} = \theta(\varepsilon_1 + \varepsilon_0) + (1 - \theta)\varepsilon_0 \tag{16}$$

where ε_1 represents the change in extinction coefficient between the thiolate and the thiol and ε_0 represents the extinction coefficient of the thiolate.

Hence the expression for the change in overall extinction coefficient at 240 nm can be expressed as:

$$\varepsilon_{app} = \frac{\frac{\varepsilon_1[H^+]}{K_a} + \varepsilon_0}{1 + \frac{[H^+]}{K_a}} \tag{17}$$

For a system where three thiol K_a's are considered the following expression is used:

$$\varepsilon_{app} = \frac{\frac{\varepsilon_3[H^+]^3}{K_{a1}K_{a2}K_{a3}} + \frac{\varepsilon_2[H^+]^2}{K_{a1}K_{a2}} + \frac{\varepsilon_1[H^+]}{K_{a1}} + \varepsilon_0}{1 + \frac{[H^+]}{K_{a1}} + \frac{[H^+]^2}{K_{a1}K_{a2}} + \frac{[H^+]^3}{K_{a1}K_{a2}K_{a3}}} \tag{18}$$

Where K_{a1}, K_{a2} and K_{a3} correspond to the three thiol Ka's and ε_1, ε_2 and ε_3 correspond to extinction coefficients for each protonated thiol species.

Derivation 3

Equation for determining the Cu(I)-binding affinities of proteins using the Cu(I) chelators BCA and BCS.

The binding of Cu(I) (Cu) to a protein (P) giving Cu(I)Protein (CuP) can be expressed as:

$$Cu(I) + P \rightleftharpoons Cu(I)P \tag{19}$$

With the equilibrium constant (K_b) expressed as:

$$K_b = \frac{[CuP]}{[Cu][[P]} \tag{20}$$

Likewise the binding of Cu(I) to a Cu(I) ligand (L) which binds Cu(I) as a $Cu(I)L_2$ complex can be expressed as:

$$\beta = \frac{[CuL_2]}{[Cu][L]^2} \tag{21}$$

Where β is the overall equilibrium constant for formation of CuL_2.

Since the total amount of protein (P_t) is:

$$[P_t] = [P] + [CuP] \tag{22}$$

And the total amount of L (L_t) is:

$$[L_t] = [L] + 2[CuL_2] \tag{23}$$

And under the assumption no mixed P-Cu-L heterocomplexes form and that the amount of free Cu (Cu_f) is negligible:

$$[Cu_f] \ll [CuP] + [CuL_2] \tag{24}$$

The equilibrium constant, K_b, can be expressed as:

189

$$K_b = \frac{([Cu]\text{-}[CuL_2])([L]\text{-}2[CuL_2])^2\beta}{([P]\text{-}[Cu]+[CuL_2])[CuL_2]} \qquad (25)$$

Which can be expressed as:

$$[L]^2\text{- }4[L][CuL_2]+ 4[CuL_2]^2\text{- }\frac{K_b([P]\text{-}[Cu]+[CuL_2])[CuL_2]}{([Cu]\text{- }[CuL_2])\beta}=0 \qquad (26)$$

The solution to the equation being:

$$[L]=2[CuL_2]+ \sqrt{\frac{K_b([P]\text{-}[Cu]+[CuL_2])[CuL_2]}{([Cu]\text{-}[CuL_2])\beta}} \qquad (27)$$

In addition the equation can also be expressed as:

$$[P]=\frac{([Cu]\text{-}[CuL_2])([L]\text{-}2[CuL_2])^2\beta}{K_b[CuL_2]}+ [Cu]\text{- }[CuL_2] \qquad (28)$$